NUMERICAL MODELLING OF TWO-PHASE FLOW WITH INTER-PHASE SLIP

by

Amin Hassan Ahmed Baghdadi
B.Sc.(Eng), M.Sc.

Thesis submitted for the degree of
Doctor of Philosophy
in the Faculty of Engineering,
University of London,
and
for the Diploma of Membership
of Imperial College.

Mechanical Engineering Department,
Imperial College of Science and Technology,
London, S.W.7., England.

September, 1979

TO EGYPT

"J' offre mon travail, mon œuvre et ma connaissance
à mon pays où la civilisation a pris naissance" .

ABSTRACT

A numerical prediction procedure, having the acronym "IPSA" (Inter Phase Slip Analyser) is presented and evaluated. The model has been developed for solving the transport equations that govern two-phase flow phenomena. Each conservation law is expressed by a pair of partial differential equations pertaining to each of the interpenetrating continua. The "IPSA" procedure is an iterative one, operating on finite-difference equations connecting the value of variables pertaining to points arrayed on a staggered cartesian grid.

The algorithm can handle one-, two- and three-dimensional spatial distributions of the variables. In this work, the greatest attention has been focussed on one-dimensional problems in order to examine in depth the foundations of the subject.

The predictive power of "IPSA" has been demonstrated by applying it to the solution of two classes of two-phase flows. Firstly, we considered the steady flow of a particulated solid-phase in a suspending fluid medium, with special reference to flows in venturi nozzles. Secondly, we studied the unsteady, stratified flow of two fluids confined in a constant area duct.

A special version of "IPSA" has been developed to account for gravity-stratification phenomena.

The predictions made were compared with available analytical solutions as an assessment of their accuracy; their physical realism was checked by comparison with experimental data.

The predicted results displayed very good agreement with the theory and were in good accord with experimental data. The favourable nature of these comparisons lend support to the belief that the "IPSA" model is a useful engineering design tool.

PREFACE

The work reported in this thesis is the result of my research activities, undertaken in the period 1975-1978, in the Department of Mechanical Engineering, Imperial College, London. During these three years I was involved in the development of numerical procedures for the prediction of fluid dynamic behaviour in both single- and two-phase flow regimes.

During the first semester of my studies I became familiar with the "SIMPLE" (Semi-Implicit Method for Pressure Linked Equations) algorithm (Caretto, et al, 1972). I used the "EASI" (Elliptic Axi-Symmetric Integrator) program (Pun, 1975), which embodied "SIMPLE" in predicting various flow situations with the ultimate goal of mastering the fundamentals of the finite-difference technique that is so basic to the work of the Heat Transfer Section.

Until the end of my first year, I worked on the testing and development of the 2/E/FIX computer code (Pun and Spalding, 1976). I worked closely with Dr. Pun and learned much about the numerical modelling of single-phase flows. I gained much experience while assisting Professor Spalding in testing the "GEMMIX" program by analysing the results obtained from five different models of turbulence; I also had the opportunity to investigate with him flows with high body forces.

For the last two years my research activities have been focussed on the development and validation of a numerical procedure for predicting two-phase flows. This study was carried out initially as a group effort; during this period I had the fruitful opportunity of being supervised by Professor Spalding and had the pleasure to collaborate with Drs. David Tatchell, Ashok Singhal and Mr. Harvey Rosten at CHAM Ltd. (Concentration Heat And Momentum). The "PLANT" (Pipe Line ANalysis; Two-phase) computer code resulted from this joint enterprise. This computer program was constructed with the aim of predicting unsteady stratified flows in under-ocean pipelines. By way of record, it should be noted that the present author's main contribution to this program consisted in developing a numerical technique that takes into account gravity-stratification phenomena. A number of stratified-flow problems were solved and the results were reported in various publications (References from 5 to 7).

The next stage of research was funded by the Science Research Council. Attention was now turned towards the study of solid suspension flows. The investigation involved the transfer of mass and momentum of the dispersed phase of solid particles and the suspending fluid medium, with special reference to the inter-phase slip phenomenon. Various values of gravimetric and density ratios (of particle to fluid) were considered. A parametric study was carried out to examine also the effect of both particle size and

the inter-phase friction coefficient on the pressure, velocity and concentration fields (of the two phases) in different flow geometries.

The sensitivity of the numerical procedure to grid-size and time-increment was thoroughly examined in the course of this work.

Again, it should be recorded here that the code used for two-dimensional calculations was developed by the author with the help of Dr. Urban Svensson (who was, at the time, visiting the Heat Transfer Section as a Research Fellow). The program was a modified version of the 2/E/FIX computer program, adapted for the computations of two-phase flow problems.

* * *

I wish to take this opportunity to acknowledge my debt of gratitude to a number of individuals who directed me in my studies. First and foremost, I am most grateful to my supervisor, Professor Spalding, for his constant and sincere interest; I owe much to his constructive criticism of my research methods and my technical writing. The work presented in this thesis exists largely due to his suggestions and inspirations.

I am also grateful to Dr. Pun who jointly supervised me and to whom I am grateful for throwing so much light on many of my problems. His friendship was of a great help to me throughout my stay. Thanks are due to Dr. Ma for his suggestions and moral encouragement.

I am most obliged to Mr. Peter Dale who provided me with continuous help whenever computing problems arose.

Throughout my study Mr. George Tindall was extremely helpful; he always provided me with an excellent and prompt reprographic service. I am more than thankful to him.

I do appreciate the help and suggestions of my colleagues, post-doctoral fellows and visiting professors. These include: my colleagues who shared the same room with me at various times: Amr Serag El Din, Andrew Pollard, Mohamed El Hadidy and Luen Tong Tam; as well as other students of the section: Alaa El Din Awn, Ayodeji Demuren, Denis Skiadaressis, Vinoth Ramachandra, Tim Maxwell, George Carroll, Ashok Singhal, Parameswaran, Yousif Abrishami and Ebrahim Damangir. Drs. Gordon Mallison, V. Ganesan, A.K. Majumdar, S. Kanbour, Kenjiro Suzuki, M. Sasaki and Professor de Vahl Davis. Thanks are also due to Mr. Bob King for his technical assistance in setting up the demonstration test rigs and for the friendly atmosphere that he kept in the laboratory.

I would like to thank Miss E.M. Archer and Mrs. S. Boot for providing very efficient library services. Thanks are due to Colleen King, Sue Farmiloe, Marguerite Farrell and Maggie Dean for their assistance in administrative work.

I am grateful to Miss C.D.M. Collins for her excellent typing of the Thesis.

Finally, I wish to thank Concentration, Heat and Momentum Ltd., and the Science Research Council, for providing financial support during my studies.

* * *

I would like to extend my gratitude to my parents who offered all possible support. They made a sincere and valuable contribution to every stage of my life; my thankfulness to them cannot be expressed in words. I will always remember Mrs. Zofia and Dr. Adam Ostaszewski who not only provided me with lodging, but gave me invaluable help and constant hospitality.

I cannot express the magnitude of the debt I owe to the man who first inculcated in me a love for science: the late Professor Naguib Bakhoum, God bless his soul.

Finally I wish to thank Dr. Nikos Markatos for his technical assistance and his sincere collaboration in the work.

London

Amin Baghdadi

TABLE OF CONTENTS

	Page No.
ABSTRACT	2
PREFACE	3
TABLE OF CONTENTS	8
NOMENCLATURE	13
1. INTRODUCTION	16
1.1 Desirability of Numerical Prediction for Two-Phase Flows	16
1.2 Objectives of the Study	17
1.3 Two-Phase Flows	18
1.3.1 Classification into Flow Types	18
1.3.2 The Types of Flow Studied	19
1.3.3 Practical Relevance of the Flows Considered	19
1.4 Physical Consideration	20
1.5 The Solution Method Chosen	25
1.6 Review of the Literature	26
1.6.1 Review of Two-Phase Flow Modelling	26
1.6.2 Review of Experimental and Measuring Techniques	30
1.7 Outline of the Thesis	33

		Page No.
2.	MATHEMATICAL FORMULATION	35
	2.1 Introduction	35
	2.2 Governing Transport Equations	35
	2.2.1 Continuity Equations	36
	2.2.2 Momentum Equations	38
	2.2.3 Closure to the Model	40
	2.3 Auxiliary Information	42
	2.4 Inter-Phase Interaction	43
	2.4.1 Momentum Interaction	43
	2.4.2 Inter-Phase Mass Transfer	44
	2.5 Assumption and Modifications	45
	2.6 Closure to Chapter 2	46
3.	THE NUMERICAL SOLUTION PROCEDURE	48
	3.1 Introduction	48
	3.2 Determination of the Finite-Difference Equations	49
	3.2.1 Description of the Finite-Difference Grid	49
	3.2.2 The General Finite-Difference Equation	52
	3.3 The Pressure-Correction Equation	62
	3.4 Description of the "IPSA" Solution Procedure	70
	3.5 The "NEAT" Algorithm	73
	3.6 The "PEA" Technique	74
	3.7 The "SNIP" Procedure	75

		Page No.
3.8	Remarks on the Numerical Procedure	77
	3.8.1 Accuracy of the Solution	77
	3.8.2 Numerical Instabilities	78
3.9	Closure of Chapter 3	81
4.	IMPROVEMENTS TO THE "IPSA" METHOD	82
4.1	Introduction	82
4.2	Description of the "NIPSA" Method	83
	4.2.1 Brief Account and Comparison between "IPSA" and "NIPSA"	83
4.3	The Pressure-Correction Equation	87
4.4	Sequence of the Solution Procedure	89
4.5	Testing the "NIPSA" Method	90
4.6	Closure to Chapter 4	96
5.	DISPERSED-FLOW PREDICTIONS	97
5.1	Introduction	97
	5.1.1 General Background	97
	5.1.2 Purpose of the Chapter	98
	5.1.3 Method of Presentation	99
5.2	Mathematical Description	101
	5.2.1 Equations and Boundary Conditions	101
	5.2.2 Treatment of Inter-Phase and Wall Friction	101
5.3	Prediction for Comparison with Analytical Results	106
	5.3.1 The Acceleration of Particles by a Uniform Free Stream	106
	5.3.2 The Settling of Particles under Gravity	119

		Page No.
5.4	Predictions for Comparison with Experimental Data	129
5.4.1	Single-Phase Flow in a Venturi Nozzle	130
5.4.2	Gas-Particle Flow in Venturi Meters	139
5.4.3	Flow of a Slurry through a Venturi Meter	154
5.5	Parametric Study	163
5.6	Concluding Remarks	185
6.	STRATIFIED-FLOW CALCULATIONS	187
6.1	Introduction	187
6.1.1	General Background	187
6.1.2	Content of the Chapter	187
6.2	Mathematical Description	188
6.2.1	Treatment of Inter-Phase and Wall Friction	189
6.2.2	Two-Variable Adjustments (IPSA-TV)	191
6.3	Predictions for Comparison with Analytical Results	196
6.3.1	Wave Propagation in a Confined Plane Channel	196
6.3.2	Wave Formation in a Plane Channel with One End Closed	221

Page No.

6.4 Prediction for Comparison with Experimental Data 248

6.4.1 Introduction 248

6.4.2 Steady Stratified Flow of Oil and Air in a Horizontal Pipe 249

6.5 Predictions of Flows of Engineering Interest 267

6.5.1 Introduction 267

6.5.2 Transient Flows in Pipes with Inclination and Bends 269

6.6 Concluding Remarks 288

7. CONCLUDING REMARKS 290

7.1 Achievements of the Present Study 290

7.1.1 Numerical Aspects 290

7.1.2 Dispersed-Flow Calculations 291

7.1.3 Stratified-Flow Calculations 292

7.2 Suggestions for Future Work 293

LIST OF REFERENCES 296

APPENDIX A 309

APPENDIX B 311

NOMENCLATURE

SYMBOL	MEANING
A, a	Coefficients in the finite difference equations (FDE)
A_p, a_p	Central coefficient of the FDE
B	Integrated source term
C	Wave speed, also used for the drag coefficient
D	Hydraulic mean diameter
d	Average particle diameter
F_r	Froude number
$f^{\ell d}$	Inter-phase friction coefficient
f^{iw}	Wall-friction coefficient
g	Gravitational acceleration
H	Height of the channel
h	Height of the liquid
N	Number of grid nodes
p	Pressure
P	Reduced pressure
R	Volume fraction
R_e	Reynolds number
R_r	Relative Reynolds number
r	Radial coordinate
S	Source term
t	Time
Δt	Time step

SYMBOL	MEANING
u,v,w	Light-phase velocity components in θ, r and z directions respectively
U,V,W	Velocity components corresponding to the dense phase
V_{SG}	Gas superficial-velocity
V_{SL}	Liquid superficial-velocity
y	Distance measured along the flow pipe
Δy	Length of one grid cell
z	Axial coordinate

GREEK SYMBOLS

α	Pipe inclination
Γ	Exchange coefficient
θ	Tangential coordinate
λ	Courant number
ϕ	General properties
μ	Viscosity
ρ	Density

SUBSCRIPTS

D	Drag
d	Dense phase
E	East neighbour of point P
e	East interface
i	Index denoting either N,S,E,W or n,s,e,w
ℓ	Light phase
N	North neighbour of point P
n	Interface point on line joining P and N

SYMBOLS	MEANING
P	Nodal point
S	South neighbour of point P
s	South interface
W	West neighbour of point P
w	West interface

SUPERSCRIPTS

dw	Wall-dense phase interaction
ℓd	Inter-phase
ℓw	Wall-light phase interaction
*	Guessed values
'	Correction
''	Correction used in stratified flows
→	Indicates vectorial quantities

CHAPTER 1

INTRODUCTION

1.1 DESIRABILITY OF NUMERICAL PREDICTION FOR TWO-PHASE FLOWS

Two-phase flows are of considerable scientific importance and, certainly, of great practical significance; their application is found in mechanical and chemical engineering and in environmental and biological science. They occur in nuclear reactors, boilers, condensers, in air-conditioning and refrigeration equipment, desalination plants, to cite only some instances.

In all these systems, economy of design, optimization of operating conditions and assessment of safety factors require quantitative information. In most cases, experimental studies are expensive and associated with uncertainties that are contingent on the reliability and accuracy of the measuring techniques; not only are there difficulties in conducting experimental research but also it is sometimes impracticable to simulate environmental problems by laboratory experiments, as would be the case with the fall of rain drops, the precipitation of snow or the saltation of a sand storm. It is because of these difficulties in obtaining reliable empirical information that a procedure for predicting such phenomena quantitatively is particularly to be desired.

The non-linearly coupled differential equations associated with the physics of two-phase flows cannot be solved by analytical means, except in very simple flow situations. Among available calculation procedures, those involving the use of numerical techniques are best suited for handling such mathematically complex problems.

1.2 OBJECTIVE OF THE STUDY

The purpose of the contribution is to construct a numerical algorithm capable of predicting two-phase flow phenomena. The study can be thought of as involving the following phases:

(a) To develop a calculation procedure capable of predicting transient two-phase flows.

(b) To validate the numerical accuracy of the solution algorithm by comparing its predictions with known or analytical solutions.

(c) To investigate the physical realism of the different assumptions inherent to the model by comparing its predictions with experimental data available in the literature.

(d) To illustrate further uses of the model by solving problems of significant engineering interest, once the credibility of the solution procedure has been established.

1.3 TWO-PHASE FLOWS

1.3.1 Classification into Flow Types

Two-phase flow is a term covering the interacting flow of matter in two of its three phases: gas, liquid and solid. The main characteristic of two-phase flows is the existence of an interface, the shape of which is very much influenced by the relative motion of the phases. The morphological arrangement of the component phases defines different flow patterns or "flow regimes". In the case of liquid-gas mixtures one distinguishes: droplet, bubbly, slug, annular, as other intermediate flow patterns.

A more general classification depends on whether the pair of phases in concern are "well-separated", "well-intermingled" or exist in an "intermediate" state, that is, between the two previously defined classes. "Well-separated" flows are encountered in the following situations: the breaking of a wave, the slug flow of gas and liquid along a pipe, the drainage of a tank, or the rise of a bubble in a nuclear reactor. "Well-intermingled" phases are found for example when studying: the transport of either snow by wind or sand by water, the bubbly flow of a steam-water mixture and the fluidization phenomena. Two examples of "intermediate" phenomena are: the annular flow of a steam-water mixture together with entrained droplets and wind-blown surf.

1.3.2 The Types of Flow Studied

In this work attention is restricted to two kinds of phase combinations: solid-fluid and gas-liquid. The first kind is studied by reference to the flow of solid particles dispersed in a suspending fluid. As for the second kind, the investigation considers the gravity-stratified flow of a gas and a liquid in plane channels and along circular pipes. It is to be noticed that this choice makes possible a study of the two major categories of two-phase flows, the "well-intermingled" and the "well-separated".

1.3.3 Practical Relevance of the Flows Considered

It is of interest to know the behaviour of the chosen two-phase combinations, since they occur in many practical situations. This is made evident in the list below.

(1) Solid-Suspension Examples

(a) Pneumatic transport along closed tubes.

(b) Separation of dust from gases in a cyclone separator or in an inertia filter.

(c) Sediment deposit in ocean-beds and sediment transport in rivers.

(d) Control of environmental pollution.

(e) Movement of oxide particles in rocket exhaust.

(2) Gas-Liquid Examples

(a) Flow of gas and liquid- condensate in and under - ocean pipelines.

(b) Gas-liquid interaction in distillation columns.

(c) Film condensation in a refrigeration coil.

(d) Breaking of an ocean wave.

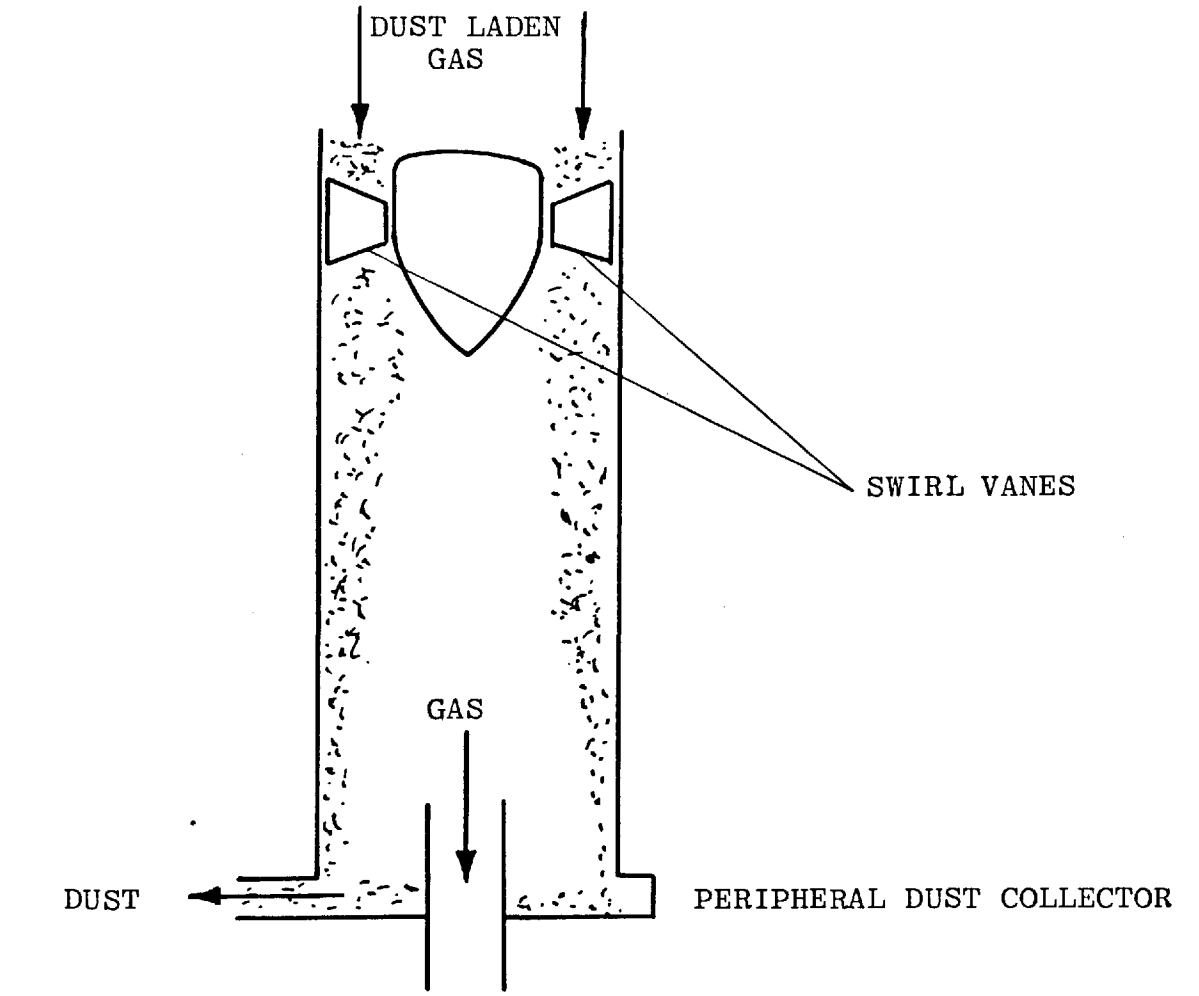
(e) Wind forces acting on the surface of a canal.

Representative samples of both kinds of flow regimes are illustrated in Figures (1-1) and (1-2).

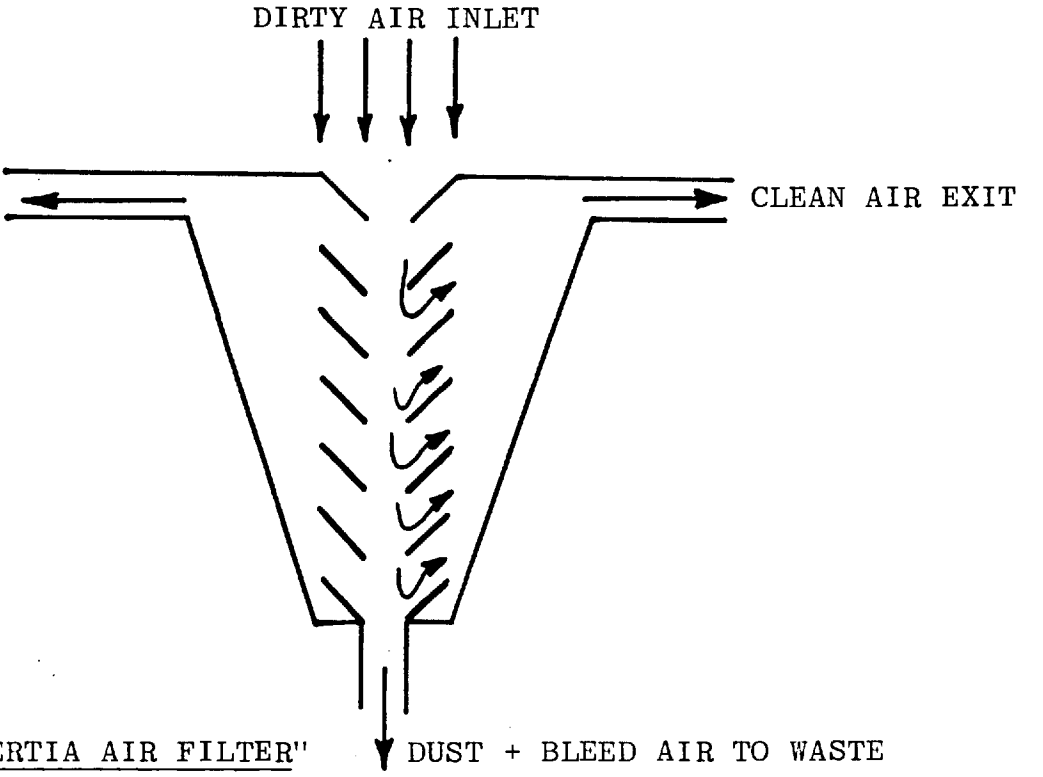
1.4 PHYSICAL CONSIDERATION

The establishment of an adequate algorithm for predicting two-phase flow has been much delayed for a variety of reasons. The main source of difficulty is the intricacy of the exchange processes (of mass, momentum and heat) between the phases. The physically complex mechanism of interaction between the phases introduced much perplexity to its mathematical modelling. The following list reviews the most important source of difficulties associated with two-phase flows.

- The exchange of momentum, heat and mass between the phases may involve: friction, vaporisation and condensation, absorption, and dissolution. The laws of such processes are well known, especially in simple or idealized cases. The prescription of inter-phase transfer laws, which represent the physical input to



"AXIAL-INLET PERIPHERAL-DISCHARGE CYCLONE SEPARATOR"



"INERTIA AIR FILTER"

FIGURE (1-1) SOLID-SUSPENSION APPLICATIONS

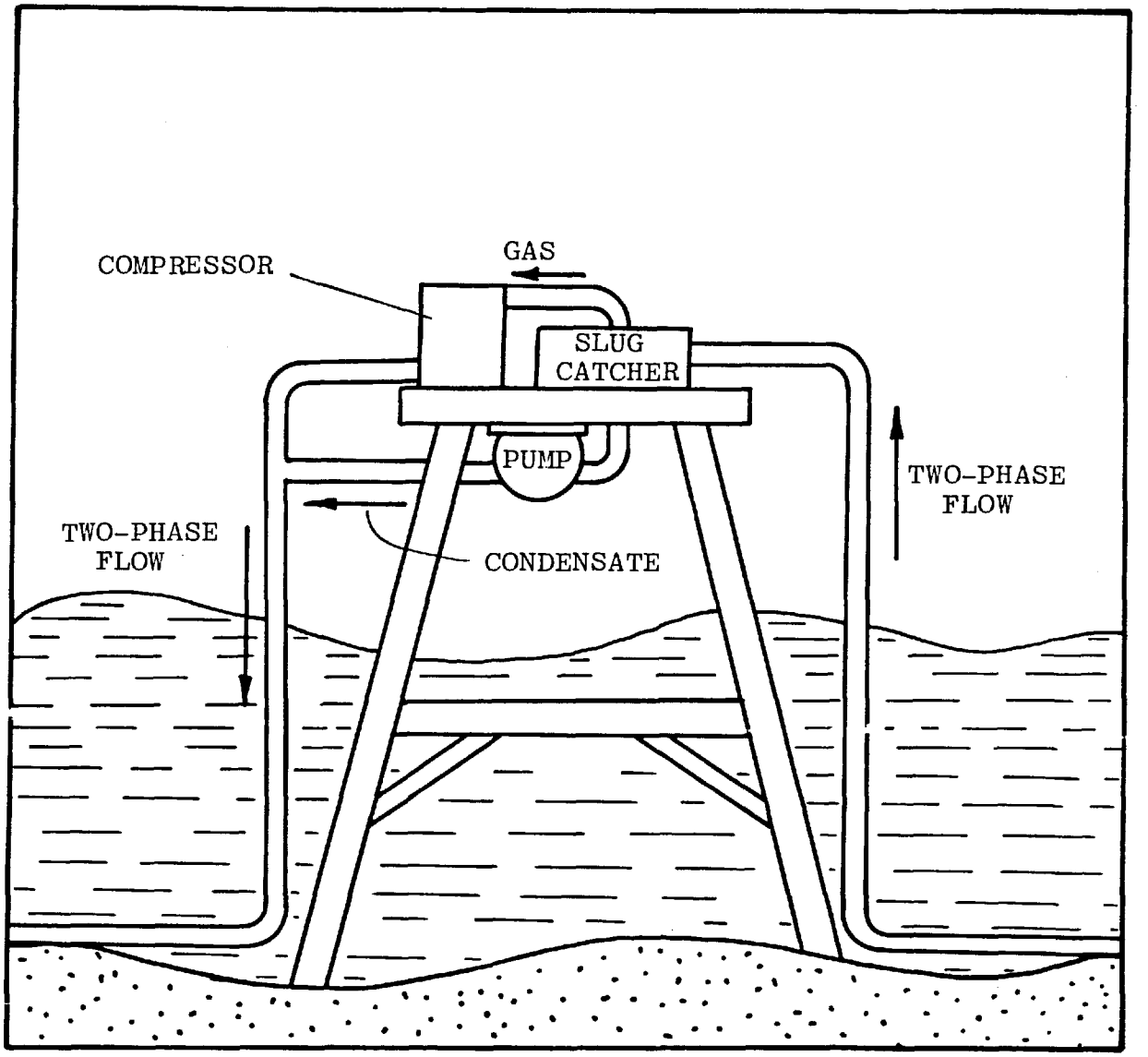


FIGURE (1-2) FLOW OF GAS AND LIQUID-CONDENSATE; A PRACTICAL EXAMPLE: AN INTERMEDIATE COMPRESSOR STATION IN OFFSHORE PIPELINES.

the algorithm, can be performed only speculatively at present.

- The most difficult aspect of all stems from the presence, in general, of inter-phase slip. When developing a model that takes account of the slip, rather than treating the phases as a homogeneous mixture, there are more variables to compute; the problem is not merely quantitative: the point is how to produce an economical algorithm for solving the whole set of equations. It is also worth noting that while a pair of differential equations is used to express the conservation laws, there is only one value for the pressure at each point.

- Density variation, in a gravitational field, entails non-uniform body forces; and the resulting motions tend to equalise these body forces. Problems of this kind, because they involve a second connection between the momentum and species conservation equation (the first connection is that via the continuity), are especially prone to numerical instabilities.

- The surface tension phenomenon is simple for pure liquids; but it is strongly influenced by the interpenetration of the phases. The inclusion of surface tension forces needs special attention

mainly because it requires accurate prediction of the location and curvature of the interface.

- In many cases, the component phases flow at high velocities; under these conditions the flow must be supposed turbulent rather than laminar. In the present context, the quantitative laws of turbulence are different from those in single-phase flows. Before attempting to model numerically such complex phenomena, the mathematical equations governing the transport of turbulence in two-phase flows, must be derived; this task is far from being easy.

- The presence of distributed resistances such as: baffles, tubes, packings and other solid boundaries, often impede the flow of the two-phases. In fact, a solid surface presents a different resistance to a liquid than to a gas; also the no-slip condition at a wall does not hold when the flow of a dispersion of solid particles is considered. Special attention must be given to ascribing physically realistic conditions in the vicinity of any obstacle to the flow.

1.5 THE SOLUTION METHOD CHOSEN

Two-phase flow phenomena are mathematically described by a set of partial differential equations. An equation of the Navier-Stokes type expresses the momentum conservation of each phase. These two equations are interlinked by coupling terms that embody the physical momentum exchange between the phases. Other conservation principles are described by pairs of coupled differential equations that express the different characteristics of the two inter-penetrating continua. The non-linear and coupled equations, associated with the physics of two-phase flow, are intractable except in very simple flow situations. We took recourse to the finite-difference techniques in our search for a general solution to the problem.

A new numerical model has been developed recently by Spalding (1976) for the solution of two-phase flow problems with special reference to the inter-phase slip phenomenon. The model known by the acronym "IPSA" (Inter-Phase Slip Analyser), provides a numerical solution of the governing differential equations using an iterative procedure. This overcomes the difficult problem of solving non-linear equations by analytical means. An important advantage of using codes embodying "IPSA" is their flexibility; a single finite-difference procedure may be employed with relatively minor modifications for a wide range of flow situations. Furthermore they are capable of taking into account, via suitable mathematical models, such physically-important phenomena as turbulence, phase exchange and

chemical reaction.

The numerical model employed in the present work is a "mechanistic" model; the term distinguishes this approach from models applying empirical correlations as their basis and deals mainly with algebraic equations. A mechanistic model is one in which the full governing partial differential equations are solved with as little resort to empirical information as possible.

1.6 REVIEW OF THE LITERATURE

1.6.1 Review of Two-Phase Flow Modelling

The state of the art of modelling two-phase flow with inter-phase slip is reviewed by Hughes et al (1976) and Gidaspow and Solbrig (1976). In these models separate equations of continuity, momentum and energy are written for each phase and the six of them are solved simultaneously. Comparing the system of equations that have appeared, one finds many inconsistencies and discrepancies that put in question the validity of each (c.f. Lyczkowski, 1975; Stuhmiller, 1977 and Banerjee and Hancox, 1978). Various hypotheses have emerged in the modelling of two-phase flow. Despite the difficulty in treating the coupling terms, the pressure gradient term (being the driving potential common to the two phases) was expressed in three different forms in the literature. Accordingly, one may distinguish between three major types of momentum balance, namely:

(i) a momentum balance with a pressure gradient term, ∇P, appearing in only one of the equations;

(ii) a momentum balance for either phase with a gradient of partial pressure in the form: $\nabla(R_i P)$;

(iii) a momentum balance for either phase with a volume fraction weighted pressure gradient appearing as $R_i \nabla P$.

where P is the pressure variable,
R_i is the volume fraction of either phase,
and ∇x is the gradient of the scalar quantity x.

The first assumption was mainly adopted for the dispersed flow of solid particles in a suspending fluid; precisely no pressure drop is included in the solid phase momentum equation, the reason being that a phase can only exert its partial pressure if it is compressible (Rudinger, 1974). This practice was followed by Rudinger and Chang (1969) and Lyczkowski (1975).

Several other authors have suggested the use of partial-pressure momentum equations: Nigmatulin (1967), Pantan (1968), Pai et al (1973) and Roberts and Donelly (1974). In these models the pressure is given a different interpretation, in that it includes a diffusive force arising from the concentration gradients ($P\nabla R_i$); with this

extra force, and in the absence of gravity, such momentum balance cannot represent static-equilibrium. It is with the aim of securing a realistic model that forces of relative nature have to be added to compensate for these induced concentration-gradient effects (compare Harlow, 1974).

Finally, the third category of models, using volume fraction weighted pressure gradients, was shown (by Wallis, 1969 and Harlow and Amsden, 1975) to be adequately applicable to most of two-phase flow problems.

Although, the mathematical formulation of two-phase flow is still debated, most of the researchers have recognized the need to express each conservation law by a pair of differential equations pertaining to each phase. Two different conceptual approaches have been reported, in the literature, for handling the pair of governing equations.

The first approach is based on the concept of two superimposed continua. It is restricted to dispersed flow situations; the conservation equations of the suspending continuum are modified to include extra source terms that take into account the presence of the dispersed phase. This method was proposed initially by Migdal and Agosta (1967) and used by Crowe et al (1975). The mathematical abstraction in this method implies that the source occupies zero volume, which limits the range of its applicability to dilute suspensions.

The second approach is one that considers the coexistence of the two continua with different concentration at different locations in the flow domain. This approach is more general than the first one in that its applicability is not restricted to dispersed flows. Here, the governing equations are solved simultaneously. Models of this type have been described by several authors, among them: Murray (1965); Soo (1967); Anderson and Jackson (1967). Moreover, Piva et al (1978) presented a comparative study with the aim of showing the scope of validity of the above two different approaches.

In the present context, the recent advance in both numerical methods and computer technology, have produced a very useful tool for the solution of the non-linearly coupled differential equations describing two-phase flow phenomena. However, the diversity of the problem has cast doubt even on the possibility of obtaining numerically realistic solutions. In finite-difference techniques, for example, the occurrence of instabilities is an alarming factor. This obstacle may be overcome by the employment of an implicit formulation so as to ensure an implicit coupling between the phases. This practice has been successfully adopted by various authors, e.g. Harlow and Amsden (1975), Baghdadi et al (1977) and Daly (1978), who have reported realistic numerical predictions for two-phase flow problems with inter-phase slip.

Although much attention has been directed towards the study of two-phase flow in recent years, it is apparent from the literature, however, that very little progress has been made.

1.6.2 Review of Experimental and Measuring Techniques

Apart from the usual problems inherent to any measuring method for single-phase flows which has been reported in the works of Katys (1964), Doebelin (1966), Bradshaw (1971) and Considine (1971), further difficulties are encountered due to the interaction between the phases.

In two-phase flows, the simplest method of delineating the different flow regimes is by visual observation. A review of visualisation techniques is given by Hewitt and Taylor (1970). However, the flow speed is often too high for clear observation and one must have recourse to high-speed photography and related techniques. Developments in the photography of two-phase flows are described by Cooper et al (1963). Unfortunately, even with high speed cameras, it is sometimes impossible to define accurately the structure of the flow; the reason is that light is subjected to a complex series of refractions as it passes through the flow and the received image is often confusing and difficult to interpret.

The generally unsatisfactory nature of the visualization techniques has led to a search for a more quantitative way of describing the flow behaviour. Recourse was made to more

sophisticated techniques (that use , for example, X-ray, optical and electrical probes, sampling devices) to evaluate the flow parameters of interest: the pressure-drop, the local concentration of each phase, the local velocity fields and the local temperature of the species.

Hewitt (1972) reviewed the various techniques adopted, and he classified them according to their relevance in the development of the generalized subject of two-phase flow. The statistical measuring techniques were summarized by Delhaye and Jones (1975). The state of the art has been recently reviewed by Delhaye (1976) with special reference to gas-liquid flows.

For the sake of completeness an account of the available measuring techniques for two-phase flows is presented below.

(i) Average Measurements

- X- or γ-rays absorption and photon attenuation techniques are the most currently used for void fraction measurements and can provide detailed information on the flow pattern (Jones and Zuber, 1975).

- The electromagnetic flowmeter, used in single-phase flows, gives a signal proportional to the cross-section averaged velocity. In two-phase flow the given signal is proportional to the area-average velocity of the continuous conducting phase (Charlety, 1971).

- Pressure-drop meters attached to an orifice plate or venturi tube are often used in two-phase flow to measure the gas-quality, defined as the ratio of the particle flow rate to the gas flow rate (Sharma, 1977).

(ii) Point Measurements

- Optical and resistivity probes are used to determine the void fraction at a point; if two probes are used simultaneously one may also measure the time average velocity (DISA, 1977).

- Point values of the velocity may be obtained by making use of hot-film anemometers. Also Laser-Doppler anemometry (LDA) was adapted to two-phase flow measurements; the two-dimensional velocity fields of particulated solid-suspension flows were experimentally determined, using LDA, by Lee and Einav (1972).

- The temperature of each phase can be obtained by the use of phase detecting micro-thermocouples (Delhaye, 1976).

- These methods have been criticized by Delhaye (1976): "Apart from the photon attenuation technique, which has been studied rather extensively, most of the average measuring techniques need to be substantiated by (1) a more rigorous analysis, (2) more systematic experimental studies. Furthermore,

it has been recognized as a consensus that the validity of each technique must be assessed according to the existing flow pattern on the transient aspect of the flow."

A more specific review, relevant to the problems considered in this work, will be provided in Chapters 5 and 6. Particular attention will be paid to the description of the experiments to assess both qualitatively and quantitatively the numerous observations reported. This assessment is important for the present study, since the quoted experiments will furnish firm justification of how realistic the newly developed "IPSA" model is.

1.7 OUTLINE OF THE THESIS

The calculation method developed in this work is for the prediction of unsteady two-phase flows with inter-phase slip. Much attention has been focussed on one-dimensional problems in order to examine in depth the foundations of the subject: its methodology and formulation; such orientation was also favoured by the existence of a few analytical solutions in the literature. The steady, two-dimensional, two-phase flows were investigated in less depth. An overall view of the thesis and its contents is provided below.

The mathematical equations governing the transport of mass and momentum of the co-flowing continua are given

in Chapter 2. In Chapter 3 the above differential equations are transformed to their finite-difference equivalents, and the solution procedure for the resulting set of equations is described. In order to enhance the performance of the algorithm, certain modifications were made; these are presented in Chapter 4.

Chapters 5 and 6 contain the results of the present contribution, together with their comparison with analytical solutions and experimental data; and also an assessment of the calculations with regard to grid-independence. Particularly, the predictions of dispersed flows are given in Chapter 5. As for Chapter 6, the solution of stratified flow problems is presented. In the latter case the gravity force is perpendicular to the main flow direction; the gravity-stratification introduced a new mechanism into the flow process: concentration gradients at the interface produce additional forces on the fluids and wave propagation is likely to be introduced. The effects are incorporated in the calculation scheme and the gravity-wave phenomena are predicted with an accuracy as good as the reduced dimensionality permits.

Concluding remarks are given in Chapter 7 together with a summary of the achievements of the present study, and suitable direction for future work are recommended. The last sections of the thesis contain a list of references cited in the text and appendices that provide supplementary details about the mathematical formulation.

CHAPTER 2

MATHEMATICAL FORMULATION

2.1 INTRODUCTION

The present chapter describes the mathematical formulation of the "IPSA" model. The conservation laws of mass and momentum for two-phase flows are given for each individual phase; the problem specification is completed by the introduction of auxiliary relations and by prescribing appropriate boundary conditions. Following this, the physical hypotheses that describe the interaction between the phases are detailed. Finally, a summary is provided of the approximations involved in arriving at the mathematical description of the problem.

2.2 GOVERNING TRANSPORT EQUATIONS

In two-phase flows the two components coexist with different concentrations at different locations in the flow domain and move with unequal velocities. In order to describe the mass and momentum transports of the two interpenetrating continua, use is made of a pair of differential equations, one for each phase, to express each of the conservation laws.

2.2.1 Continuity Equations

For a three-dimensional transient two-phase flow problem the volumetric continuity equation for the light phase reads:

$$\frac{\partial R_\ell}{\partial t} + \text{div}\,(R_\ell \vec{v}) = S_\ell \quad , \qquad (2.1)$$

for the dense phase it is:

$$\frac{\partial R_d}{\partial t} + \text{div}\,(R_d \vec{V}) = S_d \quad . \qquad (2.2)$$

The mathematical symbols used in the above equations have the following meanings:

t	time;
$\vec{v}$	velocity vector of the light phase, whose components are u,v, and w;
$\vec{V}$	velocity vector of the dense phase, whose components are U,V and W;
R_ℓ, R_d	the volume fractions of the light and dense phases, respectively; the volume fraction is defined as the ratio of the volume occupied by one phase to the total volume;
S_ℓ, S_d	the volumetric source term per unit volume of the light or dense phase, respectively.

The volumetric form, in which both equations (2.1) and (2.2) are written, is nothing more than a particular

adaptation of the "GALA" (Gas And Liquid Analyser) method, Spalding (1974), appropriate to a dimensionless description of the phase volumes.

The source term S_ℓ and S_d represent the volumetric rates of loss or gain due to phase transformation (evaporation and condensation) and they may include compressibility effects as well.

In the special case where there is no phase change and both phases are incompressible,

$$S_\ell = 0 \quad , \qquad \text{and} \qquad S_d = 0 \ .$$

On the other hand, when the light-phase is compressible, its volumetric source will take the form:

$$S_\ell = - \left(\frac{R}{\rho}\right)_\ell \frac{D\rho_\ell}{Dt} \quad , \qquad (2.3)$$

where, ρ_ℓ , the density of the light-phase, is calculated from an equation of state which generally expresses the density as a function of temperature and pressure viz:

$$\rho_\ell = f(p,T) \quad , \qquad (2.4)$$

where,

p is absolute static pressure, and

T is the local absolute temperature of the light-phase

2.2.2 Momentum Equations

The momentum equations for two-phase, transient, three-dimensional flow, in vectorial form, are:

(a) For the light phase

$$\underbrace{\frac{\partial}{\partial t}(R_\ell \rho_\ell \phi_\ell)}_{\text{momentum accumulation}} + \underbrace{\text{div}\{R_\ell(\rho_\ell \vec{v}\phi_\ell}_{\text{convection}} - \underbrace{\Gamma_{\phi\ell,i} \text{ grad } \phi)\}}_{\text{diffusion}}$$

$$= \underbrace{S_{\phi_\ell}}_{\text{source term}} + \underbrace{f_i^{\ell d}(\phi_d - \phi_\ell)}_{\text{inter-phase friction}} - \underbrace{f_i^{\ell w} \phi_\ell}_{\text{wall friction}} \quad , \quad (2.5)$$

where ϕ_ℓ stands for u,v,w and ϕ_d for U,V,W, respectively.

(b) For the dense phase

$$\frac{\partial}{\partial t}(R_d \rho_d \phi_d) + \text{div}\{R_d(\rho_d \vec{V}\phi_d - \Gamma_{\phi d,i} \text{ grad } \phi_d)\}$$

$$= S_{\phi d} + f_i^{d\ell}(\phi_\ell - \phi_d) - f_i^{dw} \phi_d \quad . \quad (2.6)$$

The mathematical symbols not previously defined have the following denotations:

ρ_ℓ, ρ_d — light and dense phase densities;

S_{ϕ_ℓ}, S_{ϕ_d} — source/sink of momentum due to pressure gradients, gravitational forces, virtual masses and rotational accelerations (e.g. centrifugal, coriolis, ... etc.) pertinent to the light and dense phase, respectively;

$\Gamma_{\phi\ell,i}$, $\Gamma_{\phi d,i}$ — "exchange coefficients" in direction i for the light and dense phases, respectively;

$f_i^{\ell d}$ — inter-phase friction coefficient arising from the force exerted by the dense-phase on the light-phase, in direction i;

$f_i^{d\ell}$ — inter-phase friction coefficient arising from the force exerted by the light-phase on the dense-phase, in direction i;

$f_i^{\ell w}$, f_i^{dw} — wall-friction coefficients, caused by the friction between the wall and the light and dense phases respectively, in direction i.

The source terms present on the right-hand side of both sets of momentum equations are given in cylindrical polar coordinates in Table (2-1).

r, θ, z are the radial, tangential and axial coordinates with corresponding velocity components

v,V; u,U; and w,W; g is the gravitational acceleration. It should be noticed in Table (2-1) that there is only <u>one</u> common pressure field for <u>both</u> phases.

The formula $(\rho - \rho_d^*)$ for the buoyancy term in the w and W momentum equations is a consequence of the "reduced-pressure method", Spalding (1976); ρ_d^* is an average value of the density taken over the r-θ planes. The reduced-pressure method is detailed in Appendix A.

2.2.3 Closure of the Model

We have already given eight equations:

(a) three momentum equations for the light phase,

(b) three momentum equations for the dense phase, and

(c) two continuity equations.

However, there are nine unknowns, namely: u,v,w,U,V,W,P, R_ℓ and R_d. An extra equation is therefore needed to close the model. This is provided by the fact that:

$$R_\ell + R_d = 1 \quad , \quad (2.7)$$

which follows from the definition of the volume fractions. Note that (2.7) does not hold in the presence of obstacles in the control volume.

Variable	Source term
v	$- R_\ell \frac{\partial P}{\partial r} + R_\ell \rho_\ell \frac{u^2}{r} + f_r^{\ell d} (V - v) - f_r^{\ell w} v$
u	$- R_\ell \frac{\partial P}{r \partial \theta} + R_\ell \rho_\ell \frac{uv}{r} + f_\theta^{\ell d} (U - u) - f_\theta^{\ell w} u$
w	$- R_\ell \frac{\partial P}{\partial z} - R_\ell (\rho_\ell - \rho_d^*) g + f_z^{\ell d} (W-w) - f_z^{\ell w} w$
V	$- R_d \frac{\partial P}{\partial r} + R_d \rho_d \frac{U^2}{r} + f_r^{d\ell}(v-V) - f_r^{dw} V$
U	$- R_d \frac{\partial P}{r \partial \theta} + R_d \rho_d \frac{VU}{r} + f_\theta^{d\ell}(u-U) - f_\theta^{dw} U$
W	$- R_d \frac{\partial P}{\partial z} - R_d(\rho_d - \rho_d^*) g + f_z^{d\ell}(w-W) - f_z^{dw} W$

TABLE (2-1) SOURCE TERMS FOR THE MOMENTUM EQUATIONS

2.3 AUXILIARY INFORMATION

To complete the mathematical specification of the problem, boundary and initial conditions are needed.

(i) Boundary Conditions

The following physical boundaries will be encountered in the present study:

Inlet

At an inflow boundary the distribution of all quantities must be specified, except that the inlet pressure of an incompressible two-phase flow need not be prescribed.

Wall

At a wall which is stationary and impervious, all the velocity components are zero and the fluxes through the wall are also zero.

Outlet

At the outlet region, in the special case of a fully developed flow, the normal gradients of the transport properties are set to zero and similarly, for both phases, the component of velocity parallel to the exit section is also set to zero. Otherwise, all quantities are prescribed at this boundary, consistently with the governing conservation laws.

Symmetry Planes

At a symmetry plane the normal velocities are set to zero and other variables are prescribed as having zero flux.

(ii) Initial Conditions

In transient problems, the initial fields of the pressure, velocities and other ϕ's must be specified before starting the computations. The initial conditions are dictated by the problem to be solved, they are subject to satisfying volumetric continuity and the condition that R_ℓ and R_d sum to unity.

2.4 INTER-PHASE INTERACTION

2.4.1 Momentum Interaction

Interaction between the two phases arises not only through inter-phase slip; it may result from pressure gradients, which accelerate the two phases at different rates depending on both the density and the volume fraction of the phase.

The inter-phase friction force causing the velocity slip is an internal force for the system as a whole, i.e. the force $F_i^{\ell d}$, exerted by the light phase on the dense phase, is balanced by the equal and opposite force, $F_i^{d\ell}$, exerted by the dense phase on the light phase, that is,

$$F_i^{\ell d} = f_i^{\ell d} \quad (\phi_d - \phi_\ell) \qquad (2.8)$$

and,

$$F_i^{d\ell} = f_i^{d\ell} \quad (\phi_\ell - \phi_d) = - F_i^{\ell d} \quad , \qquad (2.9)$$

the notation being as before (section 2.3) and i stands for θ, r, z (corresponding respectively to u,U; v,V and w,W).

The friction coefficients in equations (2.8) and (2.9) are obtained from empirical correlations, such as those given by Solbrig et al (1976). These empirical formulae depend on the flow regimes and on the properties of coflowing continua.

It is in order to obtain a linearized implicit coupling between the phases that the inter-phase frictional forces were expressed as in equations (2.8) and (2.9). There are precedents for this (compare Harlow and Amsden, 1975).

2.4.2 Inter-phase Mass Transfer

Exchange of mass may take the form of phase transitions or droplet burning. These effects are included as volumetric source terms in the continuity equations; to account for evaporation and condensation effects, an energy equation for the individual fields must be introduced, since the process involves the release

or absorption of latent heat; this will affect in turn both momentum mixing and mass exchange. The process of mass transfer is included in this section for the sake of completeness. For more details on two-phase heat transfer using the "IPSA" method, reference may be made to one of the numerous publications reported by Concentration Heat and Momentum Ltd., for example, the study of heat transfer in a steam generator, reported by Markatos et al, (1978).

2.5 ASSUMPTIONS AND MODIFICATIONS

The main source of difficulty encountered in the study of two-phase flow lies in the lack of information permitting a proper modelling of the field coupling terms. This major difficulty is not connected with the dimensionality of the problem; to minimize the complexity of this study, attention is restricted to the one- and two-dimensional forms of the governing equations. This strategy has a dual purpose. The first is to concentrate on the physical and phenomenological aspects of the flow, without distraction from the variations in lateral directions. The second reason for concentrating on uni-dimensional problems is the availability of analytical solutions in some simple flow situations, which may be used to validate the computational procedure.

The governing equations in their simplified form will be described later in Chapters 5 and 6 for both dispersed and stratified flows, respectively.

In this work no mass exchange is accounted for and the phases are incompressible. Therefore, the "volumetric" continuity equations for light and dense phases, respectively, take the form:

$$\frac{\partial R_\ell}{\partial t} + \text{div}\,(R_\ell \vec{v}) = 0 \qquad (2.10)$$

and,

$$\frac{\partial R_d}{\partial t} + \text{div}\,(R_d \vec{V}) = 0 \qquad (2.11)$$

The inter-phase drag forces are formulated using different assumptions for each type of flow regime. These postulates as well as other auxiliary concepts will be expanded on in Chapters 5 and 6 in the course of studying both dispersed and stratified flows.

2.6 CLOSURE TO CHAPTER 2

The governing equations describing the two-phase flow motion, as two interpenetrating continua, were presented in this chapter. Because of the concern with the relative motion of the two phases, separate equations were written for each phase. The mathematical model can be adapted to the solution of any two-phase flow problem since all the interactive forces may be included as source terms in the equations.

The mathematical problem being posed in this chapter is left to seek a general solution procedure for the governing differential equations. Such a procedure is described in Chapter 3.

CHAPTER 3

THE NUMERICAL SOLUTION PROCEDURE

3.1 INTRODUCTION

In the previous chapter the differential equations which govern the two-phase flow phenomena were presented, as well as the associated boundary conditions and auxiliary relations. The task in this chapter is to present a general numerical solution procedure for these equations, based on a finite-difference implicit scheme, which is adapted to the context of the present governing non-linear, strongly coupled differential equations.

Our approach is a fusion of three newly developed algorithms which we review here in the interest of clarity and completness of the exposition of the present method. The first of these algorithms, "IPSA" (Inter-Phase Slip Analyser, Spalding, 1976) is concerned with the calculation of individual phase velocities and volume fractions pertinent to both the light and dense phases. The hydro-dynamic calculations made,using "IPSA",secure the simultaneous satisfaction of momentum and mass conservation principles throughout the flow domain. The second algorithm embodied is "NEAT" (Nearly-Exact Adjustment of Terms), described in Pratap, Spalding and Tachell (1976). "NEAT" is a line-by-line marching procedure used along a prescribed solution path in solving the finite-difference equations. The third algorithm is known as the "PEA" (Partial Elimination Algorithm),

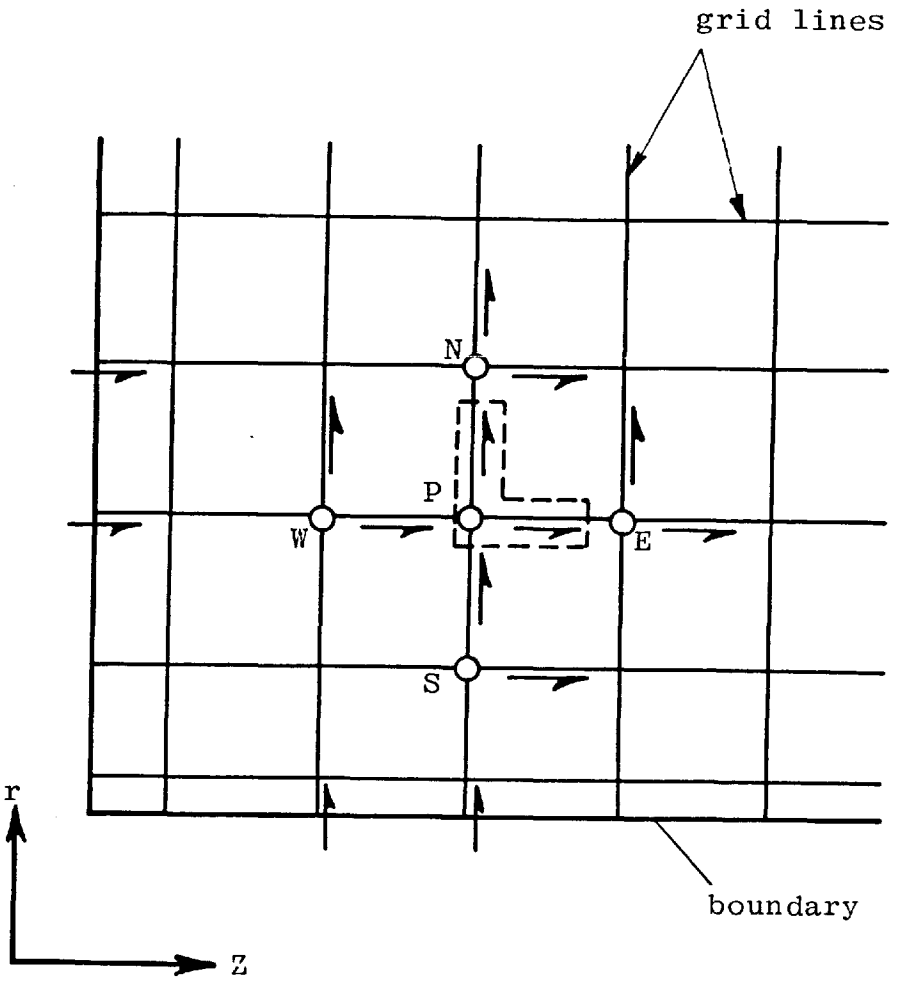
Spalding (1976A); it is a technique which renders the finite-difference equations implicit by eliminating variables which are common between two sets of equations. An assessment of the accuracy and efficiency of the computations is made at the end of the chapter.

3.2 DETERMINATION OF THE FINITE-DIFFERENCE EQUATIONS

3.2.1 Description of the Finite-Difference Grid

The grid distribution consists of a set of orthogonal intersecting lines forming a lattice which covers the whole flow domain. The grid spacing may be non-uniform. With the exception of the velocities, all the dependent and auxiliary variables (i.e. pressure, volume fractions, density and viscosity) are stored at the nodal points of the grid, defined as the points of intersection of the grid lines. The velocity components are calculated at midway positions between the nodes and stored there, each component being displaced in its own direction; the locations are indicated by the arrows in Figure (3-1). The grid arrangement is known as a staggered-grid system. It has two main advantages: firstly, the pressure gradients driving the velocities can be evaluated more conveniently; and secondly, the velocities are directly available for the calculation of convective fluxes.

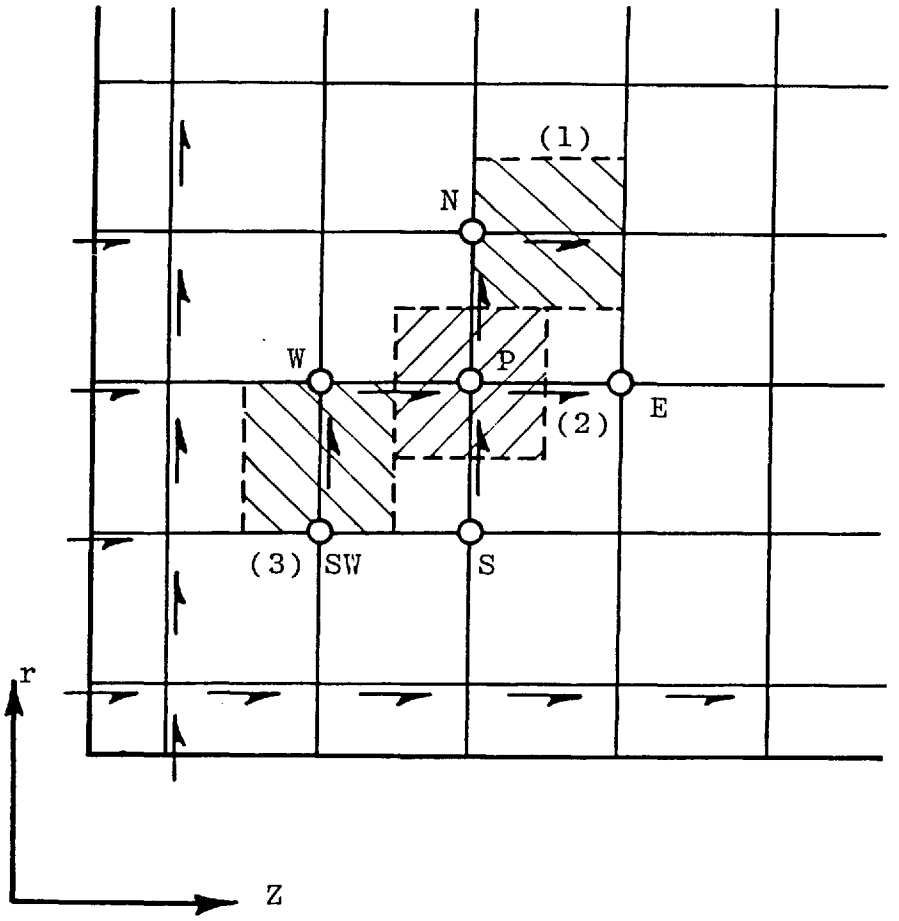
The control volumes for the velocities and the other variables, or their cell boundaries, are defined in Figure (3-2). As indicated in the diagram, a general variable



LOCATION	VARIABLES
O	ϕ , P
→	w , W
↑	v , V

N.B. L-shaped box encloses the velocities indexed by reference to the point P

FIGURE (3-1) STAGGERED LOCATION OF VARIABLES



SYMBOL	CONTROL VOLUME	VARIABLES
(1)	w/W - velocity	w_N/W_N
(2)	grid node	ϕ and P
(3)	v/V - velocity	v_{SW}/V_{SW}

FIGURE (3-2) DEFINITION OF CONTROL VOLUMES

ϕ is stored at the grid nodes; of course ϕ denotes all the dependent variables with the exception of the velocities. Moreover, the notation employed for the staggered-grid arrangement is displayed in Figure (3-3); point P, the central cell node, has four neighbouring nodes called N, S, E and W and the parameters calculated at the faces of the cell boundary lying midway between N, S, E, W and P will be subscripted by n, s, e, w respectively as shown in Figure (3-3).

3.2.2 The General Finite-Difference Equation

The finite-difference equations are obtained by integrating the respective differential equations over the small control volume (known as a cell) surrounding each grid node. The integration procedure is explained with reference to the transport equation written for a general variable ϕ. In two-dimensional polar coordinates, this equation reads:

$$\frac{\partial}{\partial t}(\rho R\phi) + \frac{1}{r}\frac{\partial}{\partial r}\left(\rho rRV\phi - \Gamma_{\phi,r}\, rR\frac{\partial \phi}{\partial r}\right) + \frac{\partial}{\partial Z}\left(\rho RW\phi - \Gamma_{\phi,Z}\, R\frac{\partial \phi}{\partial Z}\right) = S \qquad (3.1)$$

The nomenclature used in this section is the same as in Chapter 2, except that no subscripts are used to distinguish the light phase and the dense phase quantities; ρ stands for density, R for volume fraction, V and W represent the velocities, and ϕ is the property being transported. S is the source of ϕ, and $\Gamma_{\phi,i}$ is the 'exchange' coefficient in the relevant direction.

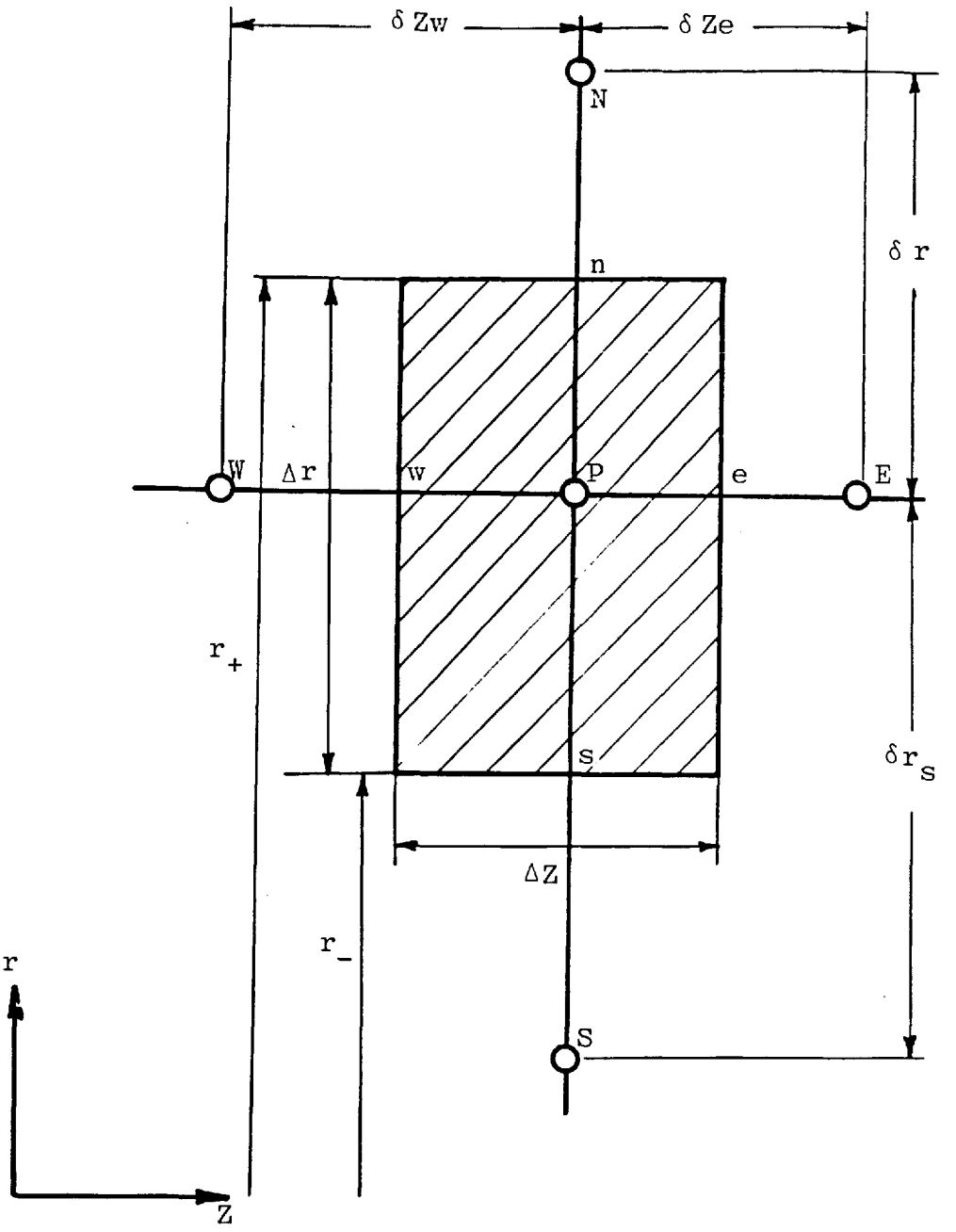


FIGURE (3-3) CELL AND GRID PARAMETERS

The finite-difference formulation of the steady terms of equation (3-1) will be considered first; at the end of this section we turn our attention to the transient term.

As explained, the integration of the steady-state terms is carried out over the cell control volumes. We shall start by the integration of the convective terms of ϕ, followed by the treatment of the diffusion terms, finally the linearization of the source terms will be described.

(a) The r-direction convection term

$$I_1 \equiv \iint_{\Delta VOL} \frac{1}{r} \frac{\partial}{\partial r} (\rho r R V \phi)\, r\, dr\, dZ$$

$$= \iint_{\Delta VOL} \frac{\partial}{\partial r} (\rho r R V \phi)\, dr\, dZ$$

In the above integral the volumes are expressed per unit angular distance (i.e. one radian) since the variations in the θ-direction are neglected.

Using the finite-difference approximations, the above integral may be expressed in the form:

$$I_1 = \{(\rho r R V \phi)_{r+} - (\rho r R V \phi)_{r-}\} \Delta Z$$

$$= (\rho V R C)_{r+} \phi_{r+} - (\rho V R C)_{r-} \phi_{r-}$$

$$= (\rho V R C)_n \phi_n - (\rho V R C)_S \phi_S \quad , \qquad (3.2)$$

where ϕ_n and ϕ_s are values of ϕ at the edges of the interfaces and the terms in round brackets are mass fluxes through the n and s interfaces shown in Figure (3-3). C is the area of the interface.

By using upwind differencing, ϕ_n and ϕ_s are related to ϕ_N, ϕ_P, and ϕ_S, as follows:

$\phi_n = \phi_N$ if the flow is from N to P
i.e. V_n is negative, and

$\phi_n = \phi_P$ if the flow is from P to N
i.e. V_n is positive. (3.3)

Similarly,

$\phi_s = \phi_S$ for positive values of V_s, and

$\phi_s = \phi_P$ for negative values of V_s. (3.4)

Substituting the above relations into equation (3.2) gives:

$$I_1 = \{ |(\rho VRC)_n , 0| + |-(\rho VRC)_s , 0| \} \phi_P + |(-\rho VRC)_n , 0| \phi_N + |(\rho VRC)_s , 0| \phi_S , \quad (3.5)$$

where $|A,B|$ denotes the maximum value of A and B.

(b) The Z-direction convection term

$$I_2 \equiv \iint_{\Delta VOL} \frac{\partial}{\partial Z} (\rho WR\phi)\, r\, dr\, dZ$$

In a similar manner the integral I_2 is expressed in finite-difference form as follows:

$$I_2 = \{ |(\rho WRC)_e , 0| + |(-\rho WRC)_w , 0| \} \phi_P$$

$$+ |(-\rho WRC)_e , 0| \phi_E + |(\rho WRC) , 0| \phi_W \quad . \quad (3.6)$$

(c) The diffusion terms

The diffusion terms are integrated, by analogy with the convection terms, over a given finite-difference cell. However, whilst convection is calculated using upwind differencing, diffusion is calculated using a central difference formula. In other words a general gradient $\frac{\partial \phi}{\partial r}$ is expressed as:

$$\frac{\partial \phi}{\partial r} = \frac{\phi_{r_+} - \phi_{r_-}}{r_+ - r_-} = \frac{\phi_n - \phi_s}{\Delta r} \quad , \quad (3.7)$$

where Δr is the distance between the interfaces, i.e. between n and s as depicted in Figure (3-3).

The same applies to the Z-direction:

$$\frac{\partial \phi}{\partial Z} = \frac{\phi_e - \phi_w}{\Delta Z} \quad , \quad (3.8)$$

here ΔZ is the distance between the other two interfaces which separates the two points e and w.

(d) Treatment and linearization of source terms

The source term S is integrated by assuming it to be constant over the control volume.

Thus, its integral, B, over the control volume is given by:

$$B = \iint_{\Delta VOL} S\, r\, dr\, dZ = \bar{S}\, \frac{(r_+ + r_-)}{2}\, \Delta r\, \Delta Z \quad . \qquad (3.9)$$

Some of the source terms (e.g. inter-phase resistances) are non-linear. Such terms need to be linearized, as follows:

$$S = S^* + \frac{\partial S}{\partial \phi_P} (\phi_P - \phi_P^*)$$

$$= S^* - \frac{\partial S}{\partial \phi_P} \phi_P^* + \frac{\partial S}{\partial \phi_P} \phi_P \quad , \qquad (3.10)$$

$$= S_u + S_p \phi_P \quad , \qquad (3.11)$$

where ϕ_P^* is the value of ϕ_P at the previous iteration; and S^* is the corresponding source term.

The linearization makes the calculation more implicit and improves the stability of the numerical scheme.

(e) Assembly of the coefficients

The integrals of the convection and diffusion terms are now combined and the coefficients of ϕ_P are assembled on the left-hand side to give the following equation:

$$A_P \phi_P = A_N \phi_N + A_S \phi_S + A_E \phi_E + A_W \phi_W + B \quad , \qquad (3.12)$$

equation (3.12) may be abbreviated to:

$$A_P \phi_P = \sum_{i=N,S,E,W} A_i \phi_i + B \quad , \qquad (3.13)$$

where the A_i coefficients represent the convection and diffusion effects of ϕ_i on ϕ_P, i.e. the total mass flux crossing the control volume interface which lies between i and P. The value of the central coefficient A_P in the absence of a source is equal to the sum of the coefficients A_i. In general, however, other contributions are added on. The first of these is the linearized part S_P of the source term from (3.11). Also, due to algorithmic implementation, a readjustment term is needed when the variable ϕ_P is under-relaxed during the course of an iteration (i.e. when ϕ_P is replaced by a weighted combination of its previous value and its present one). A final contribution to A_P results from the transient term as will now be explained.

(f) Treatment of the unsteady term

Upwind differencing is employed to ensure that the time effect propagates only in one direction. All variables are evolving parabolically with time as physically occurring.

The transient procedure adopted is fully implicit in that the neighbouring values and the coefficients A_N, A_S, ... etc., used in the calculation scheme are evaluated at time t_+ (i.e. present time); for notation see Figure (3-4), where the time is considered as another 'coordinate'.

The treatment of the unsteady term, appearing in equation (3.1), is as for the other terms. Integrating over the control volume and using a time increment Δt, the unsteady term becomes:

$$\frac{\{(\rho R\phi)^{J+1} - (\rho R\phi)^{J}\}}{\Delta t} \cdot \Delta VOL \quad , \qquad (3.14)$$

where the superscripts 'J' and 'J+1' denote the values of the variables at time t and $(t + \Delta t)$; ΔVOL is the volume of the finite difference cell.

The term $(\rho R)^{J+1} \cdot \frac{\Delta VOL}{\Delta t}$ is evaluated at the stage J, as available in store, and added to the A_p term; the term $(\rho R\phi)^{J} \frac{\Delta VOL}{\Delta t}$, calculated at the 'old time' t, is added to the source term B (equation (3.12)).

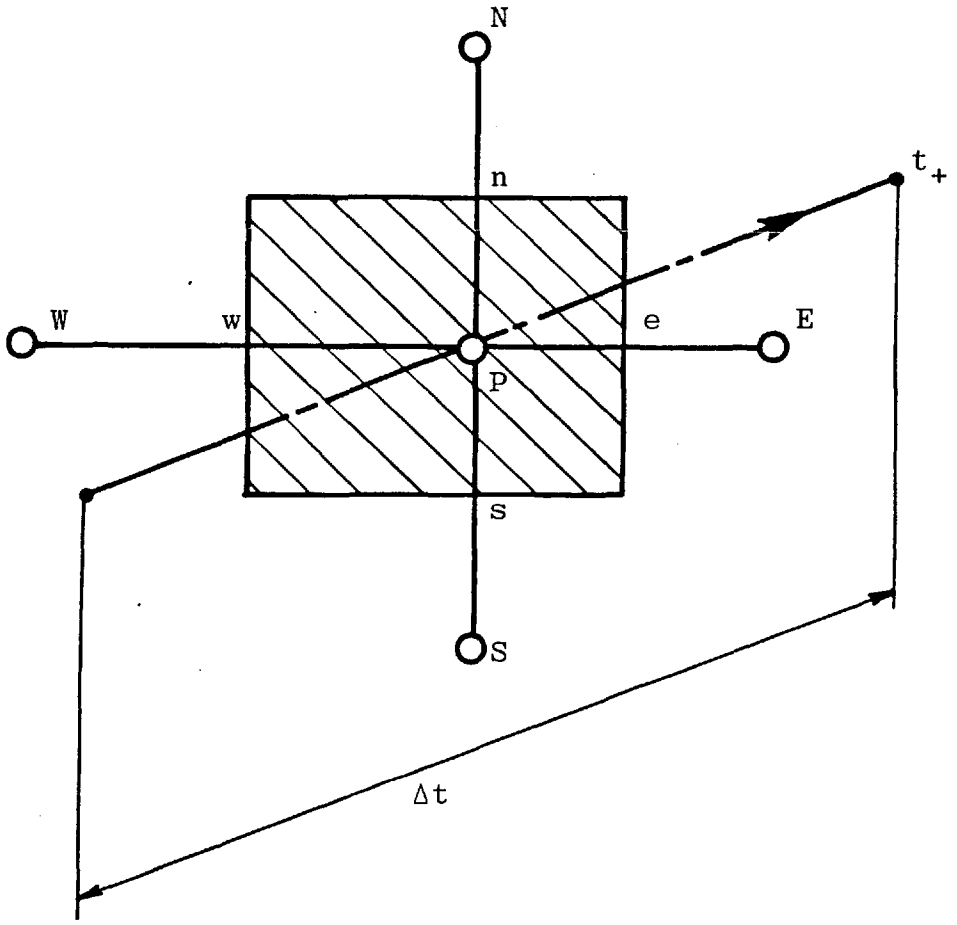


FIGURE (3-4) THE TIME DEPENDENCE REPRESENTED AS A THIRD DIMENSION

(g) General remarks

(i) The general finite-difference equation (3.12) is obtained for a general property ϕ. Extension of this procedure to the integration of the momentum equations is realised by integrating over the control volumes corresponding to the velocity cells and by calculating the required variables at the cell interfaces using appropriate interpolation techniques. One then derives the finite-difference equation corresponding to each of the velocity variables in exactly the same way with ϕ, but replaced with the variable of interest.

(ii) However, to derive the finite-difference form of the continuity equation, the ϕ variable is set to unity; accordingly, the equation describes the transport of the phase concentrations. Moreover, the exchange coefficients are set to zero and the density is removed since we are dealing with volume conservation. This treatment gives different meanings to the coefficients. In this case they express volume fluxes instead of mass fluxes. The finite-difference representation of both of the volumetric equations (2.1) and (2.2) may be written in the form:

$$\sum_{out} a_i (R_\ell)_P = \sum_{in} a_i (R_\ell)_i + s_u \quad , \quad (3.15)$$

and

$$\sum_{out} A_i (R_d)_P = \sum_{in} A_i (R_d)_i + S_U \quad , \quad (3.16)$$

where $\sum_{out} a_i$, $\sum_{out} A_i$ are the central coefficients namely, a_P and A_P.

Unlike in the general ϕ equation (3.13), the central coefficient, A_P, is not the summation of the neighbouring points coefficients. Here it quantifies the volume fluxes leaving the finite-difference cell; to secure this physical requirement of volume conservation, the central coefficient is calculated using a 'downwind' differencing that makes it non-zero only for outflow; the remaining coefficients in equations (3.15) and (3.16) are calculated in an 'upwind' fashion so that they are non-zero only for inflow. As previously discussed, the time dependent terms are included in a_P, A_P and s_u, S_U, the linearised parts of the source term.

3.3 THE PRESSURE CORRECTION EQUATION

The guessed values of the volume fractions, R_ℓ^* and R_d^*, which are the solution of both concentration equations, together with the guessed velocity fields, do not, in general, satisfy the conservation equations. A correction

must be made to these variables to obtain a new pressure field at each cycle of the iteration that tends to reduce the continuity and momentum imbalances; the corrections are meant to eliminate the errors and secure the convergence of the algorithm towards the right solution. A correction variable p' is thus introduced to provide linkage between the volumetric continuity and momentum equations. The putative errors in the calculated volume fractions will be expressed in terms of p'; further, p' itself will be used in adjusting both the velocity and volume fraction fields. The corrected values of V's and R's are employed to compute the pressure field via "SNIP"* (Start with New Integration of Pressure, Spalding, 1976).

(i) Derivation

For simplicity the pressure correction equation is derived using one coordinate dimension, however it will not be difficult to extend the formulation to multi-dimensional situations.

Since the guessed values R_ℓ^* and R_d^* do not sum to unit, a volumetric error at node P (see Figure (3.5)) exists:

$$E_P = R_\ell^* + R_d^* - 1 \quad . \quad (3.17)$$

---

*When "SNIP" is not used the pressure field is adjusted via p' directly so that $P = P^* + p'$.

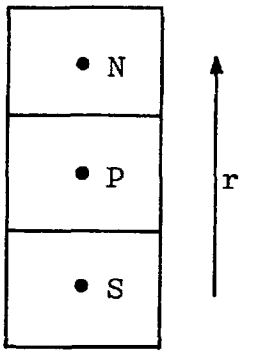


FIGURE (3.5) ONE-DIMENSIONAL REPRESENTATION OF THREE GRID NODES

It is required to calculate R'_ℓ and R'_d, which represent the corrections to R^*_ℓ and R^*_d, so that

$$R'_\ell + R'_d = E_P \quad .$$

The discrepancy, E_P, is eliminated by altering R^*_ℓ and R^*_d at point P by introducing changes to the pressures at S, P, and N; thus,

$$E_P = \left(\frac{\partial R^*_\ell}{\partial P_S} + \frac{\partial R^*_d}{\partial P_S} \right) p'_S + \left(\frac{\partial R^*_\ell}{\partial P_P} + \frac{\partial R^*_d}{\partial P_P} \right) p'_P + \left(\frac{\partial R^*_\ell}{\partial P_N} + \frac{\partial R^*_d}{\partial P_N} \right) p'_N \quad . \quad (3.18)$$

Equation (3.18) may be rewritten, to make the correction variable p'_P its subject, as:

$$- \left(\frac{\partial R_\ell^*}{\partial P_P} + \frac{\partial R_d^*}{\partial P_P} \right) p_P' = \left(\frac{\partial R_\ell^*}{\partial P_N} + \frac{\partial R_d^*}{\partial P_N} \right) p_N' + \left(\frac{\partial R_\ell^*}{\partial P_S} + \frac{\partial R_d^*}{\partial P_S} \right) p_S' - E_P \quad . \quad (3.19)$$

In view of the relative nature of the pressure, the variation of R_P^* associated with an alteration in the pressure, P_P, is equivalent to holding P_P fixed, and inversely altering P_N and P_S. Thus, it follows that,

$$\frac{\partial R_\ell^*}{\partial P_P} = - \left(\frac{\partial R_\ell^*}{\partial P_N} + \frac{\partial R_\ell^*}{\partial P_S} \right) \quad . \quad (3.20)$$

Likewise,

$$\frac{\partial R_d^*}{\partial P_P} = - \left(\frac{\partial R_d^*}{\partial P_N} + \frac{\partial R_d^*}{\partial P_S} \right) \quad . \quad (3.21)$$

The negative sign appearing in equations (3.20) and (3.21) displays the fact that an incremental increase in the pressure at point P will be accompanied by a decrease in the phase volume fractions at locations N and S.

In terms of coefficients, the pressure correction equation (3.19) may be written in the form:

$$a_P \, p_P' = \sum_{i=N,S} a_i \, p_i' - E_P \quad , \quad (3.22)$$

where, by (3.20) and (3.21),

$$a_P = a_N + a_S$$

and

$$\left.\begin{aligned} a_N &= \frac{\partial}{\partial P_N}\,(R_\ell^* + R_d^*) \quad , \\ a_S &= \frac{\partial}{\partial P_S}\,(R_\ell^* + R_d^*) \quad , \end{aligned}\right\} \qquad (3.23)$$

By expanding the derivative $\frac{\partial R}{\partial P_i}$, where R stands for the concentration of either of the two phases at point P, one obtains

$$a_i = \frac{\partial R}{\partial P_i} = \frac{\partial R}{\partial V_i} \cdot \frac{\partial V_i}{\partial P_P} \quad , \qquad (3.24)$$

where V describes the velocity of either phase; here the derivative, $\frac{\partial R}{\partial V_i}$, is evaluated from the continuity equation while $\frac{\partial V_i}{\partial P}$ is computed from the momentum equation.

(ii) Calculation of the Coefficients

- We consider first the term, $\frac{\partial R}{\partial V_i}$, accounting for the variation of the concentration with respect to the velocity.

The continuity equation in its finite-difference form using the same notation as in equation (3.24) reads:

$$R_p = \left(\sum_{in} (RVC)_i + S \right) / \sum_{out} (VC)_i \quad , \qquad (3.25)$$

where C stands for the area of the finite-difference cell.

By differentiating equation (3.25) one obtains:

$$dR_p = \frac{\left(\sum_{in} (RC)_i \, dV_i\right) \left(\sum_{out} (VC)_i\right) - \left(\sum_{in} (RVC)_i + S\right) \sum_{out} C dV_i}{\left(\sum_{out} (VC)_i\right)^2} \qquad (3.26)$$

Hence the variation of R caused by a particular alteration in V is given by:

$$\frac{\partial R}{\partial V_i} = \frac{(RC)_i}{\sum_{out} (VC)_i} \qquad \text{for an inflow velocity} \quad , \qquad (3.27a)$$

or,

$$\frac{\partial R}{\partial V_i} = - \frac{\sum_{in} (RVC)_i + S}{\left(\sum_{out} (VC)_i\right)^2} \cdot C$$

$$= - \frac{R_p}{\sum_{out} (VC)_i} \cdot C \qquad \text{for an outflow velocity} \quad , \qquad (3.27b)$$

where i corresponds to the northern or southern neighbours N and S, of point P. The upwinded values of R are used in both equations (3.27a) and (3.27b).

- We now consider the term $\frac{\partial V_i}{\partial P}$, which is obtained by the differentiation of the finite-difference forms of the momentum equation, i.e.

$$V_P = \sum_{i=N,S} \alpha_i V_i \pm D_P^V (P_P - P_i) + \beta \quad , \quad (3.28)$$

where in terms of earlier notation,

$$\alpha_i = A_i/A_P \quad ,$$

$$\beta = B/A_P \quad ,$$

and

$$D_P^V = C/A_P \quad .$$

Differentiating equation (3.28), the following two values of $\frac{\partial V_i}{\partial P}$, corresponding to the outflow from or the inflow to the cell are obtained:

$$\frac{\partial V_i}{\partial P_P} = D_P^V \quad \text{for an inflow velocity} \quad . \quad (3.29)$$

and,

$$\frac{\partial V_i}{\partial P_P} = - D_P^V \quad \text{for an outflow velocity} \quad (3.30)$$

The coefficients of the pressure-correction are obtained by combining equations (3.27a and 3.27b), (3.29) and (3.30). This being accomplished we now present the correction formulae used in modifying the guessed values of the velocities and concentrations.

(iii) The Correction Formulae

The corrections, V', to the velocities are made by adapting the standard form of the truncated momentum equation, developed by Patankar and Spalding (1972), to the correction of both velocity fields (written at point P), in the following manner:

$$V = V^* + V' \quad , \quad (3.31)$$

where the starred quantities are the guessed ones and the primed are the corrections needed. In terms of the correction variable the above equation may be recast in the form:

$$V = V^* + D_P^V (p'_P - p'_N) \quad . \quad (3.32)$$

The correction formula for the volume fractions may be related to the correction variable p' as follows:

$$R' = \frac{\partial R^*}{\partial P_P} p'_P + \frac{\partial R^*}{\partial P_S} p'_S + \frac{\partial R^*}{\partial P_N} p'_N \quad . \quad (3.33)$$

Substituting $\frac{\partial R^*}{\partial P_P}$ from equation (3.20) into (3.33) one obtains

$$R' = \frac{\partial R^*}{\partial P_N} (p_N' - p_P') + \frac{\partial R^*}{\partial P_S} (p_S' - p_P') \quad ; \quad (3.34)$$

the terms $\frac{\partial R^*}{\partial P_i}$ were evaluated earlier in this section; the modified values of the volume fractions for either phase (at point P) will be:

$$R = R^* + R' \quad . \quad (3.35)$$

3.4 DESCRIPTION OF THE "IPSA" SOLUTION PROCEDURE

The "IPSA" algorithm was developed by Spalding (1976); it was designed for the solution of two-phase flows. In "IPSA", two sets of momentum and continuity equations are considered: one for the light phase and the other for the dense phase. The two sets of momentum equations are solved simultaneously using a single guessed pressure field. The calculated velocity fields are then substituted into the continuity equations and the implied volume fractions are checked for the requirement that

$$R_\ell + R_d = 1 \quad . \quad (3.36)$$

Corrections are then made to the pressure field to remove these errors. The velocity and volume fraction fields are then corrected. The solution of the momentum and continuity equations is repeated iteratively aiming to eliminate the errors and hence securing convergence.

The calculation sequence is briefly outlined in the following steps:

(a) Guess the velocities, concentrations and pressure fields (usually the values in store are employed).

(b) Prescribe initial conditions for all the flow variables at the starting of the solution procedure.

(c) Solve the finite-difference form of the momentum equations, to update the guessed values. The momentum equations are solved simultaneously using "PEA" (Partial Elimination Algorithm).

(d) Calculate the volume fractions R_ℓ and R_d by solving the finite-difference form of the continuity equations. These are solved directly using the "TDMA" (Tri-Diagonal Matrix Algorithm); the description of this algorithm may be found in most numerical analysis texts (e.g. Ames 1969).

(e) Calculate the error in R's as a discrepancy between their sum and unity, i.e.

$$E = 1 - R_\ell^* - R_d^* \quad .$$

(f) Correct the pressure field to annihilate the errors (E's) calculated in the previous step by solving the pressure-correction equation. The pressure field may be directly corrected using the following relation:

$$P = P^* + p'$$

However, if "SNIP" (Start with New Integration of Pressure) is applied a new pressure field is calculated from the momentum equations using the corrected values of the velocities and volume fractions given by equations (3.31) and (3.35); the updated values of the velocities and concentrations will describe the guessed values of the flow variable for the next iteration.

(g) Repeat steps (c) to (f) until convergence (i.e. negligible E's) has been procedure throughout.

(h) Advance in time. At each time step iterate, i.e. repeat steps (c) to (g), until the behaviour of the transient has been studied in as much detail as required.

3.5 THE "NEAT" ALGORITHM

While the overall sequence in which the finite-difference equations are solved is given by "IPSA", "NEAT" describes how each equation is to be solved, over the flow domain, in order to reach the solution in an optimum manner (i.e. in the least number of iterations).

The basic idea in "NEAT" is that attention is shifted from the solution of the finite-difference equations for the whole domain at a time to their solution using a line-by-line marching technique in a predetermined direction. At any particular line, the best available flow information is used to formulate the coefficients in the finite-difference equations; and the solution on that line is obtained to a prescribed degree of accuracy (by iteration on the line) before proceeding to the next line. It is to be noted that all the variables, while using "NEAT", are solved on the same line before proceeding to the next one, unlike the whole field solution approach where each variable is solved on its own for the entire solution domain. The line-by-line procedure therefore interlinks the different variables during the marching procedure.

The direction in which the marching is made, is decided mainly by the flow situation. Usually it is advantageous to march along the predominant flow direction. For example, in a two-dimensional pipe flow problem, the axis of the pipe will be the chosen direction for the march. The flow variables are calculated along lines perpendicular

to the pipe axis. The determination of an appropriate number of "TDMA" solutions on a line is left to the skill and experience of the user. For example, when the flow is elliptic, that is in the absence of a predominant flow direction, the number of iterations on a line is expected to be reduced. This reduction is directly attributable to the downstream effects influencing the upstream condition caused by the recirculating nature of the flow.

3.6 THE "PEA" TECHNIQUE

The central idea in "PEA" (Partial Elimination Algorithm), is to render the finite-difference equations more implicit by eliminating, where needed, the variables which are common to two sets of equations. This is precisely what happens in the momentum equations, due to the inter-phase coupling terms given by equations (2.8) and (2.9). Consider the two sets of momentum equations:

$$a_P v_P = \sum_i a_i v_i + f_r^{\ell d} V_P + B_\ell \qquad (3.37)$$

and,

$$A_P V_P = \sum_i A_i V_i + f_r^{d\ell} v_P + B_d \qquad (3.38)$$

In the above two equations,

$$a_P = \left(\sum_i a_i - S_P + f_r^{\ell d} \right)$$

and,

$$A_p = (\sum_i A_i - S_p + f_r^{d\ell})$$

It is clear that each of the above equations contains both variables v_p and V_p simultaneously. In order to eliminate the velocity of the dense phase from the light phase momentum equation,, and vice versa, these equations may be rewritten, using the "PEA" as:

$$v_p (a_p - f_r^{\ell d} f_r^{d\ell}) = \sum_i a_i v_i + f_r^{\ell d} \sum_i A_i V_i + B_\ell + f_r^{\ell d} B_d \quad ; \quad (3.39)$$

$$V_p (A_p - f_r^{d\ell} f_r^{\ell d}) = \sum_i A_i V_i + f_r^{d\ell} \sum_i a_i v_i + B_d + f_r^{d\ell} B_\ell \quad . \quad (3.40)$$

The use of "PEA" renders the equations more implicit. It enhances the rate of convergence, which otherwise would have been slow because of the interlinkage of the two equations.

3.7 THE "SNIP" PROCEDURE

The "SNIP" (Start with New Integration of Pressure) procedure involves obtaining the pressure distribution by integrating the momentum equations along judiciously chosen paths. If body forces are significant and the numerical scheme is prone to instability, experience shows that these

paths should be along the line of action of these forces.

Here it may be remarked that in the "SNIP" procedure, it is permissible to modify the differential coefficients which represent the variations of velocity with pressure. For example, there is no objection to diminish the differential coefficient of the vertical components of velocity relative to those of the horizontal velocity. By such devices, the induced instability caused by the presence of high body forces can be brought under control.

The pressure field calculated via "SNIP" satisfies at least one set of momentum equations in the direction of the integration path. It is likely to be a better guess than the one resulting from the solution of a Poisson equation for the pressure. When the flow is uni-dimensional "SNIP" gives a better estimation to the pressure field, in that respect "SNIP" exhibits steadier and faster convergence.

The use of "SNIP" may be demonstrated by considering the following finite-difference equation, resulting from the addition of both momentum equations; the subject of the equation being the pressure, one writes:

$$P_N = P_P + \Big(\sum_{i=N,S} A_i V_i + \sum_{i=N,S} a_i v_i + S_V + S_v - A_P V_P - a_P v_P \Big) / (D_P^V + D_P^v) \quad . (3.41)$$

3.8 REMARKS ON THE NUMERICAL PROCEDURE

3.8.1 Accuracy of the Solution

It is important to quantify the accuracy of the numerical solution. The degree of error is assessed by comparing the final finite-difference solutions with exact solutions in known cases, or with experimental measurements. Such comparisons are described in the later chapters of this thesis.

The sources of error in numerical solution procedures are numerous; however, only the truncation error will be presented because of its significant effect on the accuracy of the results obtained.

Truncation Errors

The numerical procedure is based on linearizing the governing differential equations, and integrating them over the flow domain. In the course of discretization procedure and due to the interpolation used between the grid nodes, an error depending on the local grid distribution builds up. The magnitude of this error depends mainly on both the grid size and its distribution. In order to reduce its effect to an acceptable level, it is recommended to use a non-uniform distribution of the finite-difference mesh so as to concentrate nodes in regions of high gradient, and to ensure that the size of the grid is cut down to an extent that

enables it to reach a solution independent of both the grid dimensions and orientation (Baghdadi, Pun and Spalding, 1977).

3.8.2 Numerical Instabilities

In this section a brief review of the causes of numerical instability, and their cure is presented. For more details the reader is invited to refer to one of the following sources: Caretto et al (1971), Roache (1972) and Runchal (1971).

The numercial instabilities, in general, may be attributed to truncation errors,perturbations, boundary conditions and ill-conditioned matrices.

(i) Truncation Errors

These errors are induced, to the numerical solution, because of the finite-difference approximations; if they grow fast enough they lead to an unstable solution. Numerical schemes of explicit type are especially prone to this kind of error. Restrictions on the grid size and the time steps need to be placed for the truncation errors to be kept within harmless bounds.

(ii) Perturbations

The solution procedure, as described in section (3.4), starts by making an initial guess (for steady state), or by prescribing the initial conditions of the flow variables. Since these differ from the expected solution, perturbations

are likely to occur, and when the latter are large instability may prevail. To mitigate the deleterious effects of these perturbations one should select in initializing the variables, a proper guess, i.e. as close to the solution as possible.

(iii) Boundary Conditions

(a) Dirichlet Condition

Here the value of the dependent variable itself is specified on the boundary. This is known to be the most stable of boundary conditions, compare Ruchal (1971).

(b) Von Neumann Condition

In this case the normal gradients are specified at the boundary. If this specification extends to all the boundaries of the domain, then there exists an infinite number of solutions which differ from each other by a constant. Numerical methods fail in this case, because there is no unique solution. Fortunately the problems that we are concerned with never have pure Von Neumann conditions.

(c) Mixed Boundary Conditions

Most of the problems encountered contain a combination of Dirichlet and Von Neumann conditions. Depending on the proportions in which both types of boundary values are mixed, and their relative order of magnitude, numerical instabilities may arise. Two techniques have been tried to eliminate the instability introduced at the boundaries. One consists of an implicit incorporation of

the boundary condition and the other under-relax the effect of the boundary condition on the solution.

The boundary conditions may as well be of the linked type, where more than one dependent variable are supplied indirectly as a function of the space coordindates. This type of boundary condition is treated by using either an implicit incorporation of the boundary condition or by under-relaxation.

(iv) Ill-Conditional Matrices

In general our algorithm is based on solving equations of the type:

$$\phi_i = \sum_j a_{ij} \phi_j + b_i$$

If a_{ij} and b_i are constants, then it can be shown (Varga, 1962) that the above set of equations will converge in an iterative solution procedure if the matrix a_{ij} is diagonally dominant: i.e.

$$\sum_{j,i\neq j} | a_{i,j} | \leq 1 \quad , (3.42)$$

for all i; and, for at least one j:

$$\sum_{j,i\neq j} | a_{i,j} | < 1 \quad . (3.43)$$

In actual practice the coefficients of the finite-difference equations, derived earlier in this section are functions of the dependent variables; no definite criteria exist to ensure the convergence of such equations. However, experience shows that conditions (3.42) and (3.43) are often sufficient for the convergence of the non-linear equations; therefore in the calculation of the coefficients (of the FDE's) we try to fulfil the necessary but not sufficient criteria of convergence given by the above formulae.

3.9 CLOSURE TO CHAPTER 3

In order to familiarise the reader with the "IPSA" method, the basic hypotheses and methodologies, used in developing the numerical model, were highlighted in the present chapter. We are now left with the task of demonstrating the predictive power of the new procedure, based upon the available formulae, in the literature, describing the interactive forces between the phases. This will be the objective of chapters five and six, where the result of the computations will be presented and validated by comparison with analytical solutions and experimental data.

CHAPTER 4

IMPROVEMENTS TO THE 'IPSA' METHOD

4.1 INTRODUCTION

In the previous chapter the solution sequence of the "IPSA" algorithm was presented. In the present chapter a shorter path is followed in reaching the solution of the same set of differential equations (used in "IPSA"). This modified version is given the acronym "NIPSA" (New Inter-Phase Slip Analyser). Although it is based on the pressure-correction idea, however the new formulation has wider applicability since, in the absence of a second phase, the pressure-correction equation reduces to that standardly used for single phase. The novel treatment enhances convergence and reduces both computer time and storage, which are very desirable features for any efficient computational procedure.

A comparison between the original scheme and its modified version is made by devising a simple two-phase test problem, in order to evaluate from different aspects the improvement achieved.

4.2 DESCRIPTION OF THE "NIPSA" METHOD

4.2.1 Brief Account and Comparison between "IPSA" and "NIPSA"

(i) The "IPSA" algorithm focusses attention on the equation:

$$R_\ell + R_d = 1 \quad , \qquad (4.1)$$

as the one which must be satisfied, in order to eliminate the errors arising from the failure of the iterates to satisfy the conservation equations. This leads to a pressure-correction equation as follows:

- Consider the continuity equations in their finite difference form:

$$(R_\ell)_P = \frac{\Sigma a_i (R_\ell)_i + s}{b_i} \qquad (4.2)$$

and,

$$(R_d)_P = \frac{\Sigma A_i (R_d)_i + S}{B_i} \quad ; \qquad (4.3)$$

where a_i, A_i are the inflow coefficients;
b_i, B_i are the outflow coefficients;
s , S are the source terms per unit volume for the light and dense phase respectively.

• By differentiating each of the continuity equations separately, one obtains:

$$(R'_\ell)_P = L_\ell \{\dot{a}_i , \dot{b}_i\}^* \quad , (4.4)$$

and,

$$(R'_d)_P = L_d\{\dot{A}_i , \dot{B}_i\} \quad . (4.5)$$

By adding the above two equations one obtains a relation between $\dot{a}_i$, $\dot{b}_i$, $\dot{A}_i$ and $\dot{B}_i$ and the pressure gradients as follows:

$$\dot{a}_i = L_a \{p'_P - p'_i\} \quad ,$$

$$\dot{b}_i = L_b \{p'_P - p'_i\} \quad , (4.6)$$

etc.

This can be expressed in the form of a correction equation as follows:

$$\gamma_P \; p'_P = \Sigma\gamma_i \; p'_i + E_P \quad , (4.7)$$

where γ_i are the pressure correction coefficients and in fact,

---

*$L_x(\dot{X})$ is equivalent to: a linear function of $\dot{X}$, and $\dot{X}$ is the differentiation of X.

$$\gamma = L_\gamma \{\dot{a}_i, \dot{b}_i, \dot{A}_i, \text{ and } \dot{B}_i\} \quad ;$$

E_P is the error source.

- After solving for the pressure-correction equations, one modifies the velocities and volume fractions for the phases using correction formulae of the type:

$$V' = L_V \{p'_P - p'_i\} \quad , \quad (4.8)$$

$$R' = L_R \{p'_P - p'_i\} \quad . \quad (4.9)$$

(ii) The "NIPSA" method is motivated by <u>overall</u> continuity imbalance. We therefore start by adding the two continuity equations so that:

$$(R_\ell)_P \, \Sigma b_i + (R_d)_P \, \Sigma B_i - \Sigma a_i (R_\ell)_i - \Sigma A_i (R_d)_i - s - S = 0 \quad . \quad (4.10)$$

- By differentiating equation (4.10), and assuming that the variations refer to the velocities only (i.e. we hold the variation in the volume fractions at point P and its neighbouring points) leads to:

$$(R_\ell)_p \Sigma \dot{b}_i + (R_d)_p \Sigma \dot{B}_i = \Sigma \dot{a}_i (R_\ell)_i + \Sigma \dot{A}_i (R_d)_i \quad , \quad (4.11)$$

which is also a relation between $\dot{a}_i, \dot{b}_i, \dot{A}_i$ and $\dot{B}_i$ and the pressure gradients. This implies that all velocities must be adjusted so as to satisfy the total volumetric continuity, while the concentrations are kept fixed (they need <u>not</u> be adjusted).

(iii) The merits of "NIPSA" may be summarized as follows:

- The correction equation reduces to the conventional single-phase one, precisely when either R_ℓ or R_d goes to zero and the other becomes unity.

- Since the concentrations are left unadjusted, there is no need to solve for both R_ℓ and R_d; instead we can solve for <u>either</u> of them and deduce the other from:

  $$R_\ell + R_d = 1 \quad .$$

- It follows from the previous step that <u>only one</u> of the R's needs to be stored.

- Computer time reduction results from reducing the number of equations to be solved, using the matrix-inversion

technique (TDMA), and also by avoiding the adjustment for the concentration fields (practice adopted earlier in "IPSA").

4.3 THE PRESSURE-CORRECTION EQUATION

In this section we present the finite-difference formulation of the novel pressure-correction equation (Spalding, Private Communication, 1978).

The correction variable p' is now based on providing a compensation for the continuity and momentum imbalance, by eliminating the errors in computing the total volumes. With this aim in mind we define an error, Δ_p by the formula:

$$\Delta_p = \{(R_\ell)_p \ \Sigma b_i + (1-R_\ell)_p \ \Sigma B_i\} - \{\Sigma \ a_i(R_\ell)_i + A_i \ (1-R_\ell)_i + s + S\} \quad \cdot (4.12)$$

The volume imbalance, Δ_p, is attributed only to alterations in the velocities v_p and V_p caused by changes in the pressures at nodes S, P, and N (see Figure 3-5); thus by following the same arguments as in the derivation of the correction equation used previously in "IPSA" one may write the modified correction equation at point P in the form:

$$- \left\{\frac{\partial v^*}{\partial P_P} (R_\ell)_P + \frac{\partial V^*}{\partial P_P} (1 - R_\ell)_P\right\} p'_P$$

$$= \sum_{i=N,S} \left\{ \frac{\partial v^*}{\partial P_i} (R_\ell)_i + \frac{\partial V^*}{\partial P_i} (1 - R_\ell)_i \right\} p'_i - \Delta_P \quad . \quad (4.13)$$

Equation (4.13) may be written in the general form:

$$a_P p'_P = \sum_{i=N,S} a_i p'_i - \Delta_P \quad , \quad (4.14)$$

in the same manner as equation (3.22) was deduced from equation (3.19). The finite difference coefficients appearing in equation (4.14) are given by:

$$a_i = \frac{\partial v^*}{\partial P_i} (R_\ell)_i + \frac{\partial V^*}{\partial P_i} (1 - R_\ell)_i \quad , \quad (4.15)$$

and i stands for the points N and S; while

$$a_P = a_N + a_S \quad . \quad (4.16)$$

The differential terms which appear in the coefficients a_i, expressing the effect of pressure on the velocity, are evaluated by using the momentum equations, in the same way as used to derive equations (3.29) and (3.30).

4.4 SEQUENCE OF THE SOLUTION PROCEDURE

The description of the modified solution procedure is indicated as below.

(i) Prescribe the solution domain, and the finite-difference grid.

(ii) Initialise the variables by prescribing an initial guess or specifying the initial conditions at time t = 0.

(iii) Start the calculation by solving the momentum equations, using "PEA" and with guessed values for the pressure.

(iv) Solve only one continuity equation, using the matrix-inversion technique; determine the remaining volume fraction via:

$$R_{\ell} + R_{d} = 1$$

(v) Calculate the errors Δ_p's arising from the total volume imbalance, by solving the pressure-correction equation; use the correction variable to adjust the pressure and velocity fields only; DO NOT ADJUST the R's (they are kept constants).

(vi) Repeat steps (iii) to (v) until Δ_p's attain acceptably low value and convergence is procedured throughout.

(vii) Advance in time. Iterate in each time step, until the behaviour of the transient has been sufficiently studied.

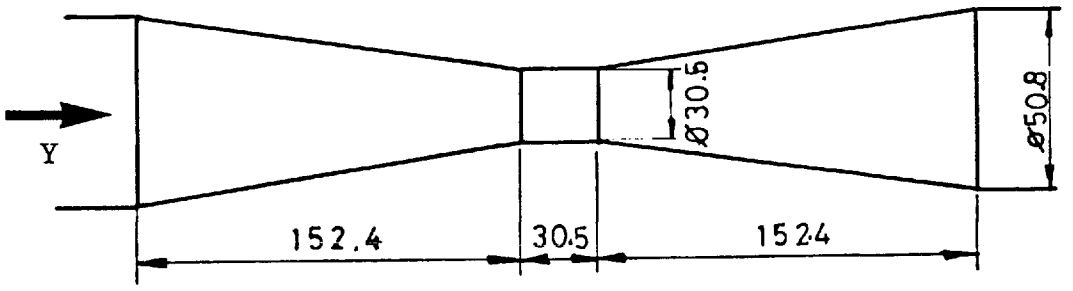
4.5 TESTING THE "NIPSA" METHOD

A test problem is solved to compare between the original solution procedure and its modified version. The results achieved by the innovations are quantified and the flexibility they add to the "IPSA" method is highlighted. The problem chosen, to set the analogy, is the flow of glass particles dispersed in a stream of air in a venturi passage; the configuration is depicted in Figure (4-1). At this stage the problem is regarded only as a means of studying algorithmic properties of "IPSA" and "NIPSA", i.e. attention is restricted to the stability and to the rate of convergence. Other aspects of the results obtained will be subject to an extensive analysis in the following chapters.

Test Case Specification

(i) We consider the one-dimensional flow of solid suspension in a venturi passage, the boundary conditions and flow geometry are shown in Figure (4-1).

(ii) A finite-difference mesh of thirteen grid nodes is used since convergence can be tested using a coarse grid when accuracy is not the main object of the study.



all dimensions in mm.

Data for the Solid Particles:

- density 2480 kg/m^3
- diameter 50 micron

Data for Air:

- density 1.1 kg/m^3
- viscosity 1.8×10^{-5} N.sec./m^2

Boundary Conditions:

- At inlet variables have prescribed values (Dirichlet B.C.)
- At the outlet boundary (located 5 diameters downstream the venturi exit section) the flow is assumed fully developed, i.e. $\frac{\partial \phi}{\partial y} = 0$.

Initial Condition:

- The velocity and concentration fields are chosen as to satisfy volumetric continuity. The pressure field is set to zero everywhere.

FIGURE (4-1) FLOW GEOMETRY AND SPECIFICATION FOR THE VENTURI TEST PROBLEM

(iii) In view of comparing the efficiency of the computation in each case only one step in time was calculated allowing for ten iterations in that time interval. The iterations were stopped when the residuals* (i.e. the remaining errors in the equations) of all the dependent variables, are less than a prescribed convergence criterion, in this case taken to be 10^{-6}.

Discussion of Results

Tables (4-1) and (4-2) describe the results obtained using "NIPSA" and "IPSA" respectively; the following conclusions are drawn.

(a) The same converged solution is reached in six iterations using "NIPSA" as compared to ten for "IPSA"; this represents a saving of 40% in the computations.

---

* In terms of the coefficients in the general finite difference equation the residual source at a node P, R_{Sp}, is defined here as:

$$R_{Sp} = A_p \phi_p - \left(\sum_i A_i \phi_i + B \right) \qquad \cdot(4.17)$$

These residual sources represent the error sources that need to be reduced and eliminated during the successive iterations. They give a good indication of the behaviour of the numerical procedure. The absolute value of the sum of the above algebraic residual source, on the line, are calculated for each dependent variable.

SUM OF ABSOLUTE VALUES OF THE RESIDUALS					
I	v	V	R_ℓ	R_d	p'
1	3.5×10^{-6}	1.9×10^{-7}	1.7×10^{-16}	0	6.2×10^{-17}
2	3.5×10^{-6}	4.6×10^{-6}	4.4×10^{-16}	0	3.5×10^{-17}
3	2.2×10^{-6}	4.0×10^{-6}	5.6×10^{-17}	0	1.4×10^{-16}
4	1.1×10^{-6}	2.3×10^{-6}	2.2×10^{-16}	0	5.8×10^{-16}
5	4.5×10^{-7}	1.0×10^{-6}	1.7×10^{-16}	0	1.7×10^{-16}
6	1.7×10^{-7}	4.1×10^{-7}	0	0	4.0×10^{-16}

* * * FIELD VALUES * * *

IY	YV	v	V	Y	R_d	P
1	0	4.9	4.9	0	1.3×10^{-4}	0
2	6.1×10^{-2}	6.8	6.8	3.1×10^{-2}	1.3×10^{-4}	0
3	1.2×10^{-1}	1.0×10	1.0×10	9.1×10^{-2}	1.3×10^{-4}	-2.0×10
4	1.6×10^{-1}	1.4×10	1.4×10	1.5×10^{-1}	1.3×10^{-4}	-7.3×10
5	1.8×10^{-1}	1.4×10	1.4×10	1.7×10^{-1}	1.3×10^{-4}	-1.3×10^{2}
6	2.0×10^{-1}	1.2×10	1.2×10	1.8×10^{-1}	1.3×10^{-4}	-1.3×10^{2}
7	2.2×10^{-1}	1.0×10	1.0×10	2.1×10^{-1}	1.3×10^{-4}	-1.1×10^{2}
8	2.5×10^{-1}	8.2	8.3	2.3×10^{-1}	1.3×10^{-4}	-7.9×10
9	2.7×10^{-1}	7.0	7.0	2.6×10^{-1}	1.3×10^{-4}	-6.0×10
10	3.0×10^{-1}	6.0	6.0	2.8×10^{-1}	1.3×10^{-4}	-4.0×10
11	3.2×10^{-1}	5.2	5.2	3.1×10^{-1}	1.3×10^{-4}	-4.0×10
12	3.9×10^{-1}	4.9	4.9	3.4×10^{-1}	1.3×10^{-4}	-3.5×10
13	4.9×10^{-1}	4.9	4.9	4.4×10^{-1}	1.3×10^{-4}	-3.4×10
14	5.9×10^{-1}	4.9	4.9	5.4×10^{-1}	1.3×10^{-4}	-3.6×10
15	0			5.9×10^{-1}	1.3×10^{-4}	0

I = Iteration number
IY = Cell index
Y = General variable location(m)
YV = Velocity location(m)

TABLE (4-1) SOLUTION OF THE TWO-PHASE TEST PROBLEM USING "NIPSA" (THE R_d EQUATION IS NOT SOLVED)

SUM OF ABSOLUTE VALUES OF THE RESIDUAL					
I	v	V	R_ℓ	R_d	p'
1	3.5×10^{-6}	1.9×10^{-7}	5.8×10^{-6}	9.6×10^{-14}	9.3×10^{-4}
2	2.7×10^{-4}	8.2×10^{-4}	1.7×10^{-5}	2.8×10^{-13}	5.2×10^{-4}
3	2.2×10^{-4}	7.2×10^{-4}	9.3×10^{-6}	1.5×10^{-13}	3.5×10^{-4}
4	5.9×10^{-5}	1.8×10^{-4}	3.1×10^{-6}	5.1×10^{-14}	1.4×10^{-4}
5	5.8×10^{-6}	2.6×10^{-5}	9.0×10^{-7}	1.5×10^{-14}	4.4×10^{-5}
6	1.1×10^{-5}	3.8×10^{-5}	2.4×10^{-7}	3.9×10^{-15}	1.3×10^{-5}
7	5.6×10^{-6}	2.0×10^{-5}	5.8×10^{-8}	9.6×10^{-16}	3.6×10^{-6}
8	2.3×10^{-6}	7.8×10^{-6}	1.4×10^{-8}	2.3×10^{-16}	9.8×10^{-7}
9	8.0×10^{-7}	2.7×10^{-6}	3.2×10^{-9}	5.3×10^{-17}	2.6×10^{-7}
10	2.6×10^{-7}	8.9×10^{-7}	7.1×10^{-10}	1.2×10^{-17}	6.8×10^{-8}

TABLE (4-2) SOLUTION OF THE TWO-PHASE TEST PROBLEM USING "IPSA"

	SUM OF ABSOLUTE VALUES OF THE RESIDUAL				
I	v	V	R_ℓ	R_d	p'
1	3.5×10^{-6}	1.9×10^{-7}	0	2.7×10^{-20}	6.6×10^{-16}
2	3.5×10^{-6}	4.6×10^{-6}	0	9.5×10^{-20}	3.7×10^{-16}
3	2.2×10^{-6}	4.0×10^{-6}	0	2.7×10^{-20}	5.9×10^{-16}
4	1.1×10^{-6}	2.3×10^{-6}	0	2.7×10^{-20}	4.3×10^{-16}
5	4.5×10^{-7}	1.0×10^{-6}	0	6.8×10^{-20}	5.1×10^{-16}
6	1.7×10^{-7}	4.1×10^{-7}	0	9.5×10^{-20}	2.6×10^{-16}

TABLE (4-3) SOLUTION OF THE TWO-PHASE TEST PROBLEM USING "NIPSA". (R_ℓ IS NOT SOLVED, COMPARE WITH TABLE (4-1)

(b) It is clearly seen that the rate of convergence is accelerated for all the dependent variables, when "NIPSA" is employed. This follows from the promptness in the elimination of the continuity errors, when the novel method is applied, this is manifested in the very small value of the residuals of the p' variable (10^{-16}, already in the first iteration).

(c) Moreover the results reported in Table (4-3) demonstrate that equally good solutions (for the same test problem) are obtained when solving only for the dense-phase volume fraction and calculating R_ℓ from:

$$R_\ell = 1 - R_d \quad , (4.18)$$

unlike the data of Table (4-1) which were obtained by solving for R_ℓ and deducing the value of R_d. This in its turn indicates the versatility of the amended version of "IPSA".

4.6 CLOSURE TO CHAPTER 4

The novel pressure-correction equation, used in the "NIPSA" solution procedure proved its superiority when adapted to the solution of a simple test case. Here only one problem is mentioned in the interest of a clear demonstration. However, the use of the modified "IPSA" method has been extended and efficiently applied to predict a wide variety of problems.

It has to be noted that the amelioration in the new procedure may be attributed to the idea of eliminating global errors, by insisting that a physical law (overall continuity) is satisfied rather than fulfilling a geometrical condition, as is the case in "IPSA". Now that all the theoretical aspects of the model have been demonstrated in the course of the present chapter and the previous one we are left to illustrate the predictive power of the numerical algorithm. This task will be performed in the next two chapters.

CHAPTER 5

DISPERSED-FLOW PREDICTIONS

5.1 INTRODUCTION

5.1.1 General Background

Fluid-particle mixtures belong to the category of dispersions. The suspending fluid media and the discrete cloud of particles are considered here as two inter-penetrating continua. The concentration of particles, in flows of practical interest, varies from extremely low values, where the fluid stream is not affected by the presence of the particles, to sufficiently high values, where the particles occupy a significant fraction of the volume of the mixture and affect therefore the hydrodynamic behaviour of the fluid phase.

When the size of the particles and their concentration are small to the extent that they follow the suspending media (i.e. no slip between the phases), the flow is of the homogeneous type. Such flow situations are encountered when particles are used as tracers to determine local fluid motion. Due to their inertia, the ability of particles to follow rapid changes of the flow velocity may be inadequate and it becomes important to analyse the accuracy with which such particles (of a given size) can be used as tracers in a specific flow. Indeed the flow situation described above,

gives a good example where a theoretical study can assess the accuracy of the measuring techniques.

When the particles affect the fluid flow, a very complex interaction takes place, depending on many factors such as the concentration of the particles, the variety of their sizes and shapes, the agglomeration and inter-particle collision and the heterogeneous particle distribution. The relative importance of the forces acting on the particles, namely: gravity, drag, lift and inertia create different fluid-particle behaviour. The interactive forces are well formulated only in simple cases of very dilute suspension; however, in very dense suspensions, as for the fluidised bed application, the mechanism of the interaction is not yet clearly understood and more fundamental research needs to be carried out before an accurate description of the inter-phase friction forces can be obtained.

In the course of the present work, consideration is given to a wide spectrum of particulate flows. The interaction between the two phases is studied by varying the following parameters: particle size, volume fraction, density ratio and the inter-phase friction coefficients.

5.1.2 Purpose of the Chapter

In the present chapter, a number of illustrative examples of problems which have been solved by use of the "IPSA" model are presented. These descriptions are intended to show how the procedure, which has thus far only been outlined in general terms, can be applied to the solution of

dispersed-flow problems. The illustrative examples have been chosen so as to demonstrate the capabilities of the procedure.

Some of the problems are ones for which analytical or numerical solutions are available: these problems are therefore especially useful as tests of the computational accuracy of the procedure. Other problems are compared with experimental data as an assessment of the physical realism of the predictions. The remainder of the problems are ones which have not been solved before; they demonstrate both the flexibility and the potential of the model. The problems considered as a whole serve as a test of the width of applicability, convergence and economy of the procedure.

5.1.3 Method of Presentation

A uniform format will be adopted for the study of the problems. The motivation for the study and the statement of the objectives will be given initially. These will be followed by "the presentation of the problem"; under this heading we describe the physical situation considered and the information to be obtained. Then the "details of the computations" are given; here we outline the mathematical problem, in terms of the differential equations and the boundary conditions, and indicate how the problem is posed for the numerical solution; moreover, the number of iterations required to obtain a converged solution and the computer time consumed are recorded for

each of the problems. The results are then presented, and finally, a detailed discussion of these results is provided.

In order to keep the presentations as brief as possible, and to avoid needless repetition, it will be useful to mention the following notes which apply to all the descriptions*:

(i) Only new symbols will be defined; otherwise the notation of the previous chapters will be employed.

(ii) In all transient problems, no under-relaxation was used, instead very small time steps were employed to secure stable computations.

(iii) For all steady, one-dimensional problems the transient terms have been used as inertial under-relaxation parameters (Spalding, 1976); i.e. the time increment was progressively increased in each iteration until it reached a very large value which made the transient terms tend to zero and the solution to the steady-state one.

---

*Included in this chapter and the next.

5.2 MATHEMATICAL DESCRIPTION

5.2.1 Equations and Boundary Conditions

The differential equations to be solved are those of volumetric continuity and momentum, previously described in chapter 2. For ease of reference the equations will be written for each of the problems considered together with their boundary conditions (for they are problem dependent features).

5.2.2 Treatment of Inter-phase and Wall Friction

At present, the friction effects are taken into account either by using empirical correlations or by making use of simple expressions based on Stoke's theory. These relations have been widely reviewed by Soo (1967). In this work we shall employ existing formulae in the literature, thus restricting the scope of the present work to the valid range of their applicability, compare Budinger (1976). More general correlations, that may become available from future studies, can be easily incorporated in the numerical algorithm.

(i) Wall friction factors

The fluid-to-wall friction factors are calculated from the same correlations used in single-phase theory, for both the laminar and turbulent flow regimes. The particles are assumed to have negligible wall-effects compared to the

inter-phase frictional forces. For the dilute suspensions, considered in this work, this assumption is quite reasonable. In the case of dense suspensions, the presence of the particles is expected to affect the near-wall region, and an adequate formulation of a wall-friction, valid for the two-phase flow regime under consideration, would be needed.

The wall friction factors are calculated from the following conditions:

(a) <u>For laminar flows</u>

$$f = \frac{16}{(R_e)_\ell} \quad \text{for } (R_e)_\ell \leq 2000, \quad . \quad (5.1)$$

where $(R_e)_\ell$ is the Reynold's number based on the properties of the suspending medium (being the light phase).

(b) <u>For turbulent flows</u>

$$f = 0.079/(R_e)_\ell^{0.25} \quad \text{for } (R_e)_\ell \geq 2800 \quad . \quad (5.2)$$

(ii) Inter-phase friction factor

Two different correlations are employed in the course of this work, to express the inter-phase friction factor as given below.

The first correlation was used by Harlow and Amsden (1975) and is given by

$$f_y^{\ell d} = \frac{6\rho_\ell R_\ell}{d^2}\left(3\,\frac{\mu}{\rho_\ell} + C_D\,|v-V|\,\frac{d}{8}\right) \quad , \quad (5.3)$$

(Viscous drag) (Form drag)

where

μ is the viscosity of the suspending medium

C_D is the drag coefficient, and

d is the particle diameter

The drag coefficient is a function of the Reynold's number based on the slip velocity:

$$R_r = \frac{\rho_\ell |v-V| d}{\mu} \quad . \quad (5.4)$$

One may express C_D as a function of R_r (compare Boothroyd, 1972):

$$C_D = 24/R_r \qquad \text{for } R_r \leq 1 \qquad , (5.5)$$

$$C_D = \frac{24}{R_r}\,(1 + 0.15\,R_r^{0.687}) \quad \text{for } 1 < R_r \leq 1000 \qquad , (5.6)$$

$$C_D = 0.44 \qquad \text{for } R_r > 1000 \qquad . (5.7)$$

In expression (5.3), the particles are assumed to have a perfectly spherical shape with an average uniform diameter, d. The inter-particle forces were neglected, by assuming that the distances between the particles are very large in comparison to their dimensions.

The second correlation employed was derived by Wallis (1969), and used by Shook and Masliyah (1974), it includes the effect of virtual mass and expresses the form drag as a function of the concentration as given below:

$$f_y^{\ell d} = \frac{6\rho_\ell R_\ell}{d^2}\Bigg(\underbrace{R_\ell^{-2.7}\, C_D |v-V|\,\frac{d}{8}}_{\text{Form drag}} + \underbrace{\frac{d^2(3-2R_\ell)}{12R_\ell^2}\,\Big|\frac{V}{v-V}\Big|\,\frac{d(V-v)}{dy}}_{\text{Effect of virtual mass}}\Bigg) \qquad . (5.8)$$

From a comparison of both expressions (5.3) and (5.8) it is worth noting that the smaller the particle diameter the larger is the inter-phase friction coefficient; under these conditions the particles tend to follow the motion of the suspending medium. It may also be noted that expression (5.8) allows for the variation in slip along the flow domain. Thus, it is expected to yield more realistic results for cases where area changes are prominent, as for example in the case of a dispersed-flow in a venturi nozzle.

5.3 PREDICTION FOR COMPARISON WITH ANALYTICAL RESULTS

The credibility of a numerical algorithm is founded upon the accuracy of its predictions. In this section we present an assessment of the accuracy of the calculations obtained using "IPSA" by comparing them with two idealised flow situations of known solutions. The flows considered are listed below:

(i) The acceleration of particles by a uniform-free stream.

(ii) The settling of particles under gravity.

5.3.1 The Acceleration of Particles by a Uniform-Free Stream

There are two advantages in considering the problem of particles-acceleration by a uniform-free stream. The first is that the flow situation has an exact solution: it is therefore possible to establish the accuracy of the numerical solutions with great ease. The second advantage is that, for the free flow considered, the dependent variables depend upon only one space coordinate, as we shall demonstrate below. Thus, predictions can be obtained economically since relatively few grid nodes are required.

(a) Objectives of the study

(i) To demonstrate the feasibility of solving the governing equation (described in section 2) by using the "IPSA" solution procedure.

(ii) To verify the mathematical accuracy of the predictions by comparing them with the analytical solution.

(iii) To show how the accuracy of the predictions depends on the dimensions and distribution of the grid.

(b) Presentation of the problem

(i) Figure (5-1) shows the flow situation considered. The steady flow of solid particles suspended in a free stream of air is studied. At the inlet the co-flowing continua have the following prescribed conditions:

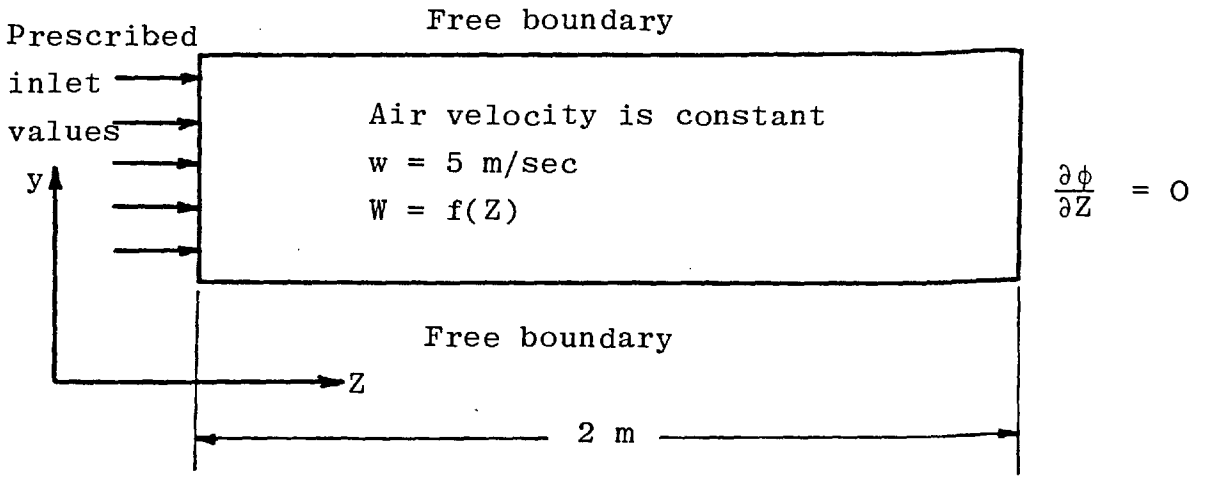
Air-Stream

$w = 5$ m/sec , $v = 0$ and $R_\ell \simeq 1$

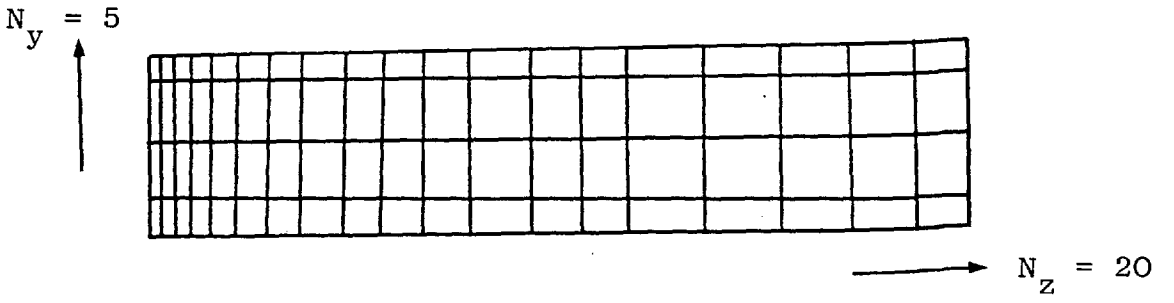
Particles

$W = 1$ m/sec , $V = 0$ and $R_d = 10^{-5}$.

The slip between the phases determines the drag, which is the sole driving force for the particle motion ($g = 0$). For the dilute suspension under consideration the inter-particle forces are neglected. The task is to calculate the particle-velocity distribution as a function of position, for different values of air-to-particle density ratio and for different values of the particle diameter.



(a) THE FLOW GEOMETRY



(b) THE GRID ARRANGEMENT

FIGURE (5-1) FLOW DOMAIN AND BOUNDARY CONDITIONS FOR THE PROBLEM OF PARTICLES ACCELERATED BY A UNIFORM STREAM

(ii) Qualitative description

The particles are expected to be accelerated to the free stream velocity; if the flow field is extended for a large distance from the inlet section, the particles are expected to reach the free stream velocity. It is also anticipated that the mode of acceleration of the particles will be dependent on their inertia (i.e. their size and density-ratio).

(iii) Quantitative description

From theoretical considerations, Morsi and Alexander (1972) gave the particle velocity as a function of position Z and the properties of the two phases, (the flow was assumed to be one-dimensional) as follows:

$$\ln (w-W) + \frac{w}{(w-W)} = \frac{3}{4} \frac{\rho_d}{\rho_\ell} \frac{C_D}{d} z + \ln (w-W(O)) + \frac{w}{(w-W(O))} \quad . (5.9)$$

where W(O) is the inlet velocity of air when z = O.

In equation (5.9) w, the free stream velocity, is not affected by the presence of the particles owing to their very low

concentration. Equation (5.9) is solved by the trial and error procedure, to determine the value of W for the given values of flow properties and particle size.

(c) Details of the computation

(i) Equations to be solved

For the plane flow under consideration, the differential equations are expressed in Cartesian form.

1. Air-stream continuity equation:

$$\frac{\partial}{\partial y}(R_\ell v) + \frac{\partial}{\partial z}(R_\ell w) = 0 \qquad . (5.10)$$

2. Particles continuity equation:

$$\frac{\partial}{\partial y}(R_d V) + \frac{\partial}{\partial z}(R_d W) = 0 \qquad . (5.11)$$

3. Air-stream momentum equations:

(a) in the y-direction

$$\underset{\text{convection}}{\frac{\partial}{\partial y}(R_\ell \rho_\ell v^2) + \frac{\partial}{\partial z}(R_\ell \rho_\ell wv)} = \underset{\text{pressure gradient}}{-R_\ell \frac{\partial P}{\partial y}} + \underset{\text{inter-phase friction}}{f_y^{\ell d}(V-v)} \qquad . (5.12)$$

(b) in the z-direction

$$\frac{\partial}{\partial y}(R_\ell \rho_\ell vw) + \frac{\partial}{\partial z}(R_\ell \rho_\ell w^2) = -R_\ell \frac{\partial P}{\partial z} + f_z^{\ell d}(W-w) \quad . (5.14)$$

4. Particles momentum equations:

(a) in the y-direction

$$\frac{\partial}{\partial y}(R_d \rho_d V^2) + \frac{\partial}{\partial z}(R_d \rho_d WV) = -R_d \frac{\partial P}{\partial y} + f_y^{d\ell}(v-V) \quad . (5.15)$$

(b) in the z-direction

$$\frac{\partial}{\partial y}(R_d \rho_d VW) + \frac{\partial}{\partial z}(R_d \rho_d W^2) = -R_d \frac{\partial P}{\partial z} + f_z^{d\ell}(w-W) \quad . (5.16)$$

Notes on equations:

- The volume fractions have to satisfy the following geometrical condition:

$$R_\ell + R_d = 1 \quad . (5.17)$$

- Due to the absence of gravity forces, the interaction between the phases takes place in the z-direction only (where the slip occurs). Therefore the flow is expected to be uni-dimensional, but the equations

have been solved, in the present context, for a two-dimensional flow domain.

- The inter-phase friction coefficients are calculated by neglecting the viscous drag in equation (5.3), this is the same assumption adopted in the derivation of the analytical solution to the problem, equation (5.9). Thus, $f_y^{\ell d}$ is given by

$$f_z^{\ell d} = \frac{3}{4} \frac{\rho_\ell R_\ell}{d} C_D |w-W| \quad , (5.19)$$

here, C_d, the drag coefficient is given a constant value of 0.44; and

$$f_y^{\ell d} = \frac{3}{4} \frac{\rho_\ell R_\ell}{d} C_D |v-V| \quad . (5.20)$$

(ii) Boundary conditions

- At inlet:

At inlet, all the dependent variables have the following prescribed values:

$w = 5$ m/sec, $v = 10^{-20}$ m/s and $R_\ell \simeq 1.$
$W = 1$ m/sec, $V = 10^{-20}$ m/s and $R_d = 10^{-5}$;

it is to be noted that the v and V velocities are given nearly zero values; by doing so we eliminate the possibility of obtaining indefinite values during the computation (i.e. zero/zero) for

the inlet condition is taken as the initial guess at the start of the calculations.

- At the outlet:

  The gradient of all variables are zero, i.e.

$$\frac{\partial \phi}{\partial z} = 0 \qquad .$$

- Free boundaries:

  At the free boundaries, the normal velocities are set to zero, and the fluxes of other variables are also prescribed to zero.

(iii) Finite-difference grid

Three different finite-difference grids were used, all with uniform cell dimensions in the y-direction:

1. 10 x 5 uniformly distributed also in the z-direction.
2. 12 x 5 non-uniformly distributed in the z-direction.
3. 20 x 5 non-uniformly distributed in the z-direction.

The grid distribution for the 20 x 5 nodes employed is illustrated in Figure (5-1).

(iv) Miscellaneous information

Typical information for a particular computational run is given below.

ACCELERATION OF PARTICLE IN A FREE FLUID STREAM	PERTINENT DATA
Configuration	2-D Plane
Grid	20 x 5
Type of grid spacing	Uniform
Number of iterations	6
Number of TDMA on a line	2
Computational time per grid node per iteration CDC 6600 (sec.)	0.0193

TABLE (5-1) TYPICAL INFORMATION ON A COMPUTATIONAL RUN

(d) Presentation of the results

The particle velocity distribution was obtained both from the analytical solution (5.9) and the present predictions; the predicted values of the particle velocity W at each grid node is given in table (5-2). For ease of reference and in order to evaluate the numerical accuracy of the computations, the theoretical value of W is also tabulated. From the tabulated values it is apparent that the average error in

		PARTICLE-VELOCITY "W"	
Grid number N	Z-distance (m)	Predicted value (m/s)	Theoretical value (m/s)
1	0.	1.	1.
2	0.030	1.27	1.26
3	0.055	1.44	1.43
4	0.095	1.65	1.64
5	0.150	1.85	1.85
6	0.215	2.04	2.06
7	0.290	2.22	2.25
8	0.385	2.41	2.43
9	0.495	2.57	2.60
10	0.605	2.71	2.75
11	0.721	2.84	2.88
12	0.845	2.96	3.00
13	0.980	3.07	3.11
14	1.125	3.17	3.21
15	1.280	3.27	3.31
16	1.445	3.36	3.39
17	1.640	3.46	3.49
18	1.825	3.55	3.56
19	1.917	3.64	3.66
20	2.000	3.64	3.75

TABLE (5-2) GRID-DISTRIBUTION AND THE CORRESPONDING PREDICTED AND THEORETICAL VALUES OF $W(\rho_d/\rho_\ell = 2000,\ d = 5 \times 10^{-4}\ m)$

calculating W does not exceed 1% (the last predicted value of W, at node 20, has not been calculated, instead it is given the same value as the velocity at node 19, i.e. $\frac{\partial \phi}{\partial z} = 0$). It is worth noting that the results obtained were perfectly one-dimensional, in that identical results were obtained along the five nodes in the y-direction for each z location, which support the one-dimensional assumption made in deriving the analytical solution.

(e) Discussion of the results

(i) Effect of particle size and density ratio

Figure (5-2) exhibits the effect of the particle size on the particle velocity. For a fixed density ratio of 2000, the dimensionless particle-to-air velocity ratio, W/w, is plotted against Z for three different values of d, viz. 100, 50 and 25 microns. This graph indicates that the current predictions show a similar trend in each case and they are in perfect agreement with theory (equation (5.9)); it exhibits also the fact that the smaller the diameter of the particles, the quicker they attain the free stream velocity. The effect

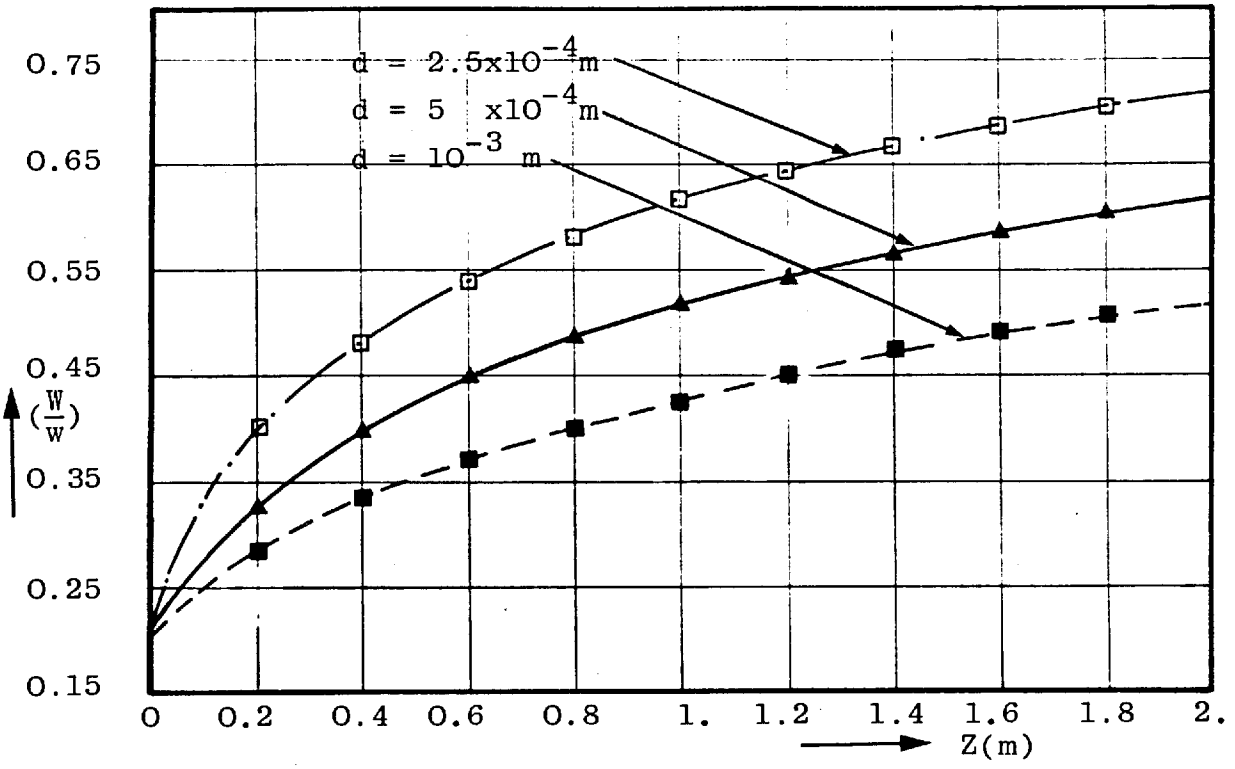


FIGURE (5-2) INFLUENCE OF PARTICLES SIZE ON THEIR ACCELERATION (ρ_d = 2000 kg/m^3)

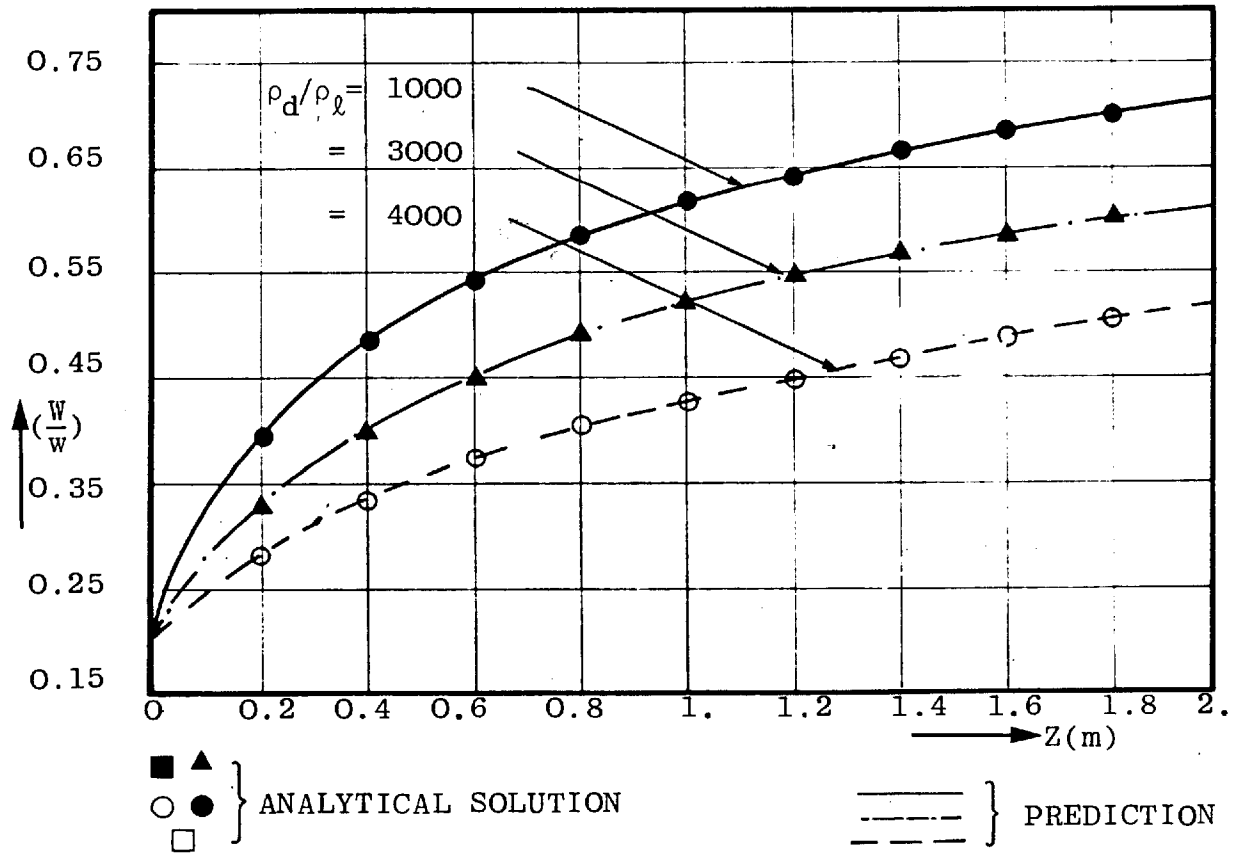


FIGURE (5-3) INFLUENCE OF DENSITY RATIO ON THE ACCELERATION PARTICLES (d = 5 x 10^{-4} m)

of the density ratio on the particles motion is displayed in Figure (5-3). It may be noted that the particles have greater acceleration for the lower density ratios, as should be expected (the fixed parameter being the particle size). The closeness of the results reflects favourably on the predictive power of the numerical procedure.

(ii) Grid-dependence tests

- Effect of the grid distribution

Numerically, it is expected that the use of finer spacings near the inlet, where the velocity gradients are high, will produce more accurate values there; near the outlet the grid size may be increased since the variation in the variables is gradual; however, a very coarse grid will give rise to inaccuracy and possibly instability. Consequently, it was found that the grid expansion ratio* of 1.3 gave the best performance

---

*Expansion ratio = δ_1/δ_2, where δ_1 and δ_2 are the distances separating the two pairs of three consecutive nodes with z-coordinate values of $(Z-\delta_1)$, Z and $(Z + \delta_2)$ respectively.

in terms of accuracy and convergence rate. Such a grid distribution is shown in Figure (5-1).

- The effect of grid size

  Figure (5-4) displays the comparison between the exact solution and the predicted results for three different finite-difference grids. It is seen that the finer the grid spacing employed, the closer are the results to the exact solution.

5.3.2 The Settling of Particles under Gravity

The steady fall of particles under gravity through stagnant air constitutes a simple flow problem. However, it provides a useful testing ground for the present solution procedure in that the problem has an exact solution; thus it is possible to assess the accuracy of the predicted results. As for the previous problem studied, the flow motion is uni-dimensional. However, the mechanism of interaction between the phases is different from the one considered in 5.3.1, in that it is the gravity force that causes the relative motion.

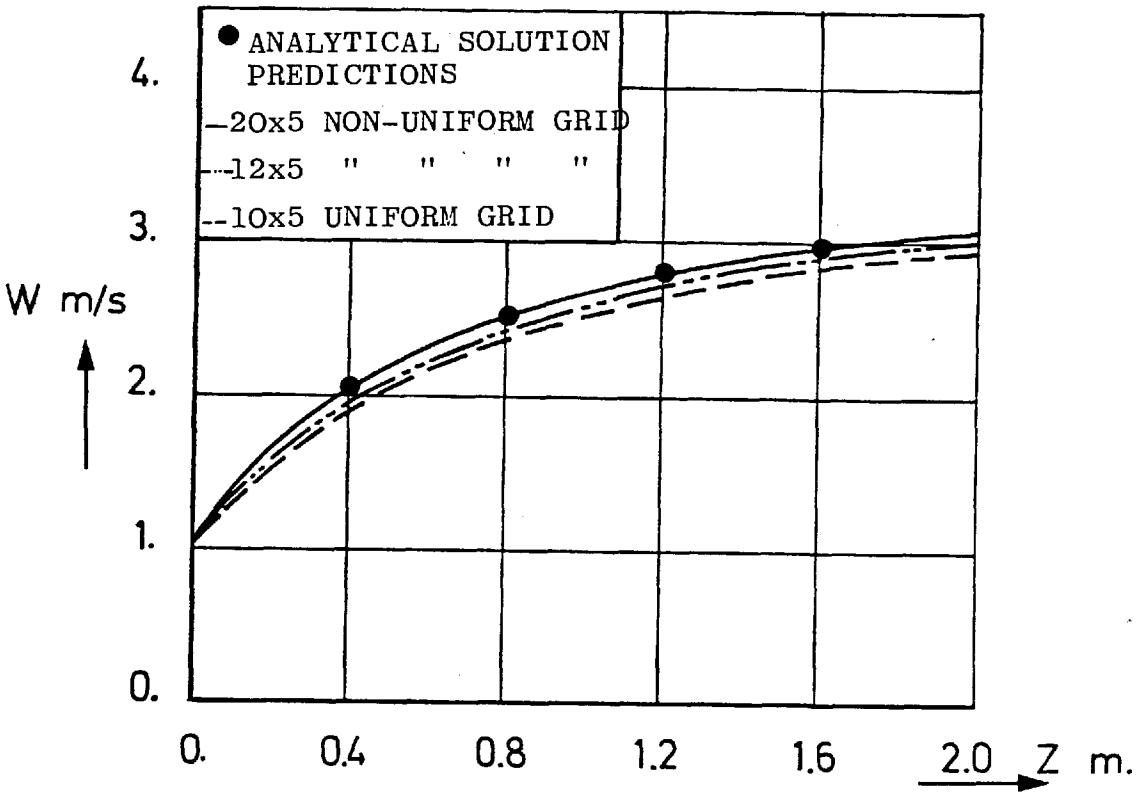


FIGURE (5-4) EFFECT OF GRID REFINEMENT ON THE NUMERICAL SOLUTION (ρ_d/ρ_ℓ = 2000; d = 5 x 10^{-4} m)

(a) Objectives of the Study

(i) To ensure that the gravity-forces have have been correctly formulated.

(ii) To verify the accuracy of the prediction by comparison with the analytical solution.

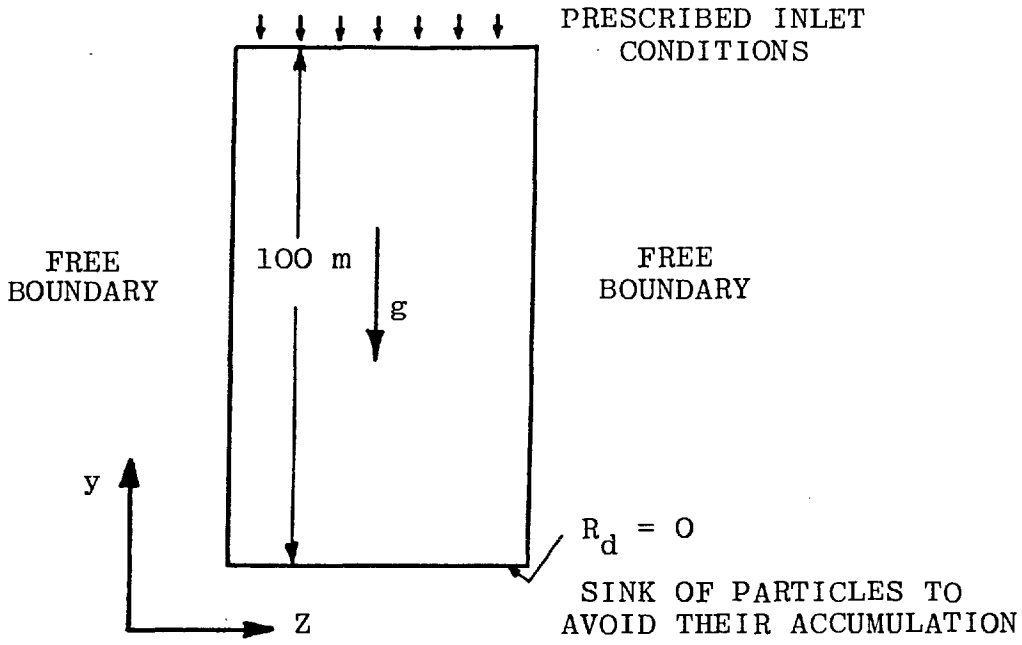
(b) Presentation of the Problem

(i) Statement of the problem

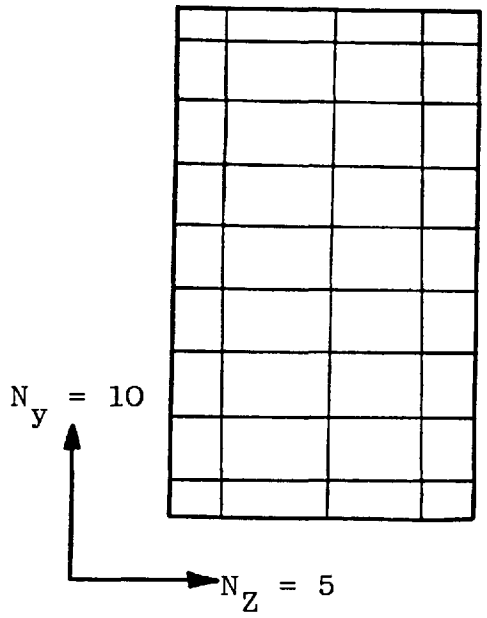
The flow situation is that of a cloud of particles falling through still air under gravity. The flow configuration is depicted in Figure (5-5). The task is to calculate the settling velocity of the particles for different sizes.

(ii) Qualitative description

In the present study, the particles are falling in the negative direction of y; there is no interaction between the air and the particles in the z-direction. The particles accelerate until a steady velocity is reached, when the drag force is balanced by the weight of the particles; this velocity is known as their "settling velocity".



(a) THE FLOW GEOMETRY



(b) THE GRID ARRANGEMENT

FIGURE (5-5) THE FLOW SITUATION FOR THE SETTLING OF PARTICLES UNDER GRAVITY

(iii) Quantitative Description

The settling velocity of the particle may be obtained from theoretical consideration, by making a simple balance of forces on a single moving particle, viz.

$$\rho_d \left(\frac{4}{3} \pi \frac{d^3}{8}\right) g = \frac{1}{2} \left(\frac{\pi d^2}{4}\right) \rho_\ell \; C_D \; V_T^2 \; ;$$

Inertia force — Drag force

where V_T is the settling velocity and is given by:

$$V_T = \sqrt{\frac{4}{3} \frac{\rho_d}{\rho_\ell} g \frac{d}{C_D}} \qquad . (5.21)$$

(c) Details of the Computations

(i) Equations to be solved

The conservation equations for volumetric continuity and momentum (one for each phase) are solved in their two-dimensional steady form as described in sub-section (c) of problem 5.3.1. An extra source term is added to the particle-momentum equation in the y-direction, to account for the gravity effect:

$$S_d^V = R_d (\rho_d - \rho_\ell) g \qquad . (5.22)$$

The above source term was formulated according to the "reduced-pressure" technique described in Appendix A.

- Free boundaries

  At the free boundaries, the normal velocities are set to zero; and the fluxes of other variables are also prescribed to be zero.

(iii) Finite-difference grid

The grid distribution over the flow domain is shown in Figure (5-5). Only five grid nodes are employed in the z-direction, for the flow is one-dimensional: the variation of the variables occurs only along the y-direction, where ten nodes are employed.

(iv) Miscellaneous information

Typical information for a particular computational run is tabulated below.

SETTLING OF PARTICLES UNDER GRAVITY	PERTINENT DATA
Configuration	2-D Plane
Grid	5 x 10
Type of Grid Spacing	Uniform
Number of Iterations	6
Number of TDMA on a line	8
Computational Time per Grid node per Iteration CDC 6600 (sec.)	0.042

TABLE 5-3 TYPICAL INFORMATION ON A COMPUTATIONAL RUN

(d) Presentation of the Results

Figure (5-6) shows the calculated particle-speed versus the y distance (for a particle diameter of 4×10^{-3} m and a density ratio of 1000). It is apparent from the graph that the particles reach the 'settling velocity' very soon after the inlet section. It is this settling velocity that is compared with the theoretical one obtained from the analytical solution (equation (5.21)).

(e) Discussion of the Results

Figure (5-7) presents the calculated settling velocity for different values of particle size. The graph indicates excellent agreement between the theory and the numerical predictions; this may be attributed to the rather simple coupling between the phases, when both the drag coefficient and the relative velocity are constant. In order to evaluate the numerical accuracy of the computations, both the predicted and the theoretical values of the settling velocity are given in table (5-4). The tabulated values demonstrate that the average error in predicting the settling velocity is less than 1%.

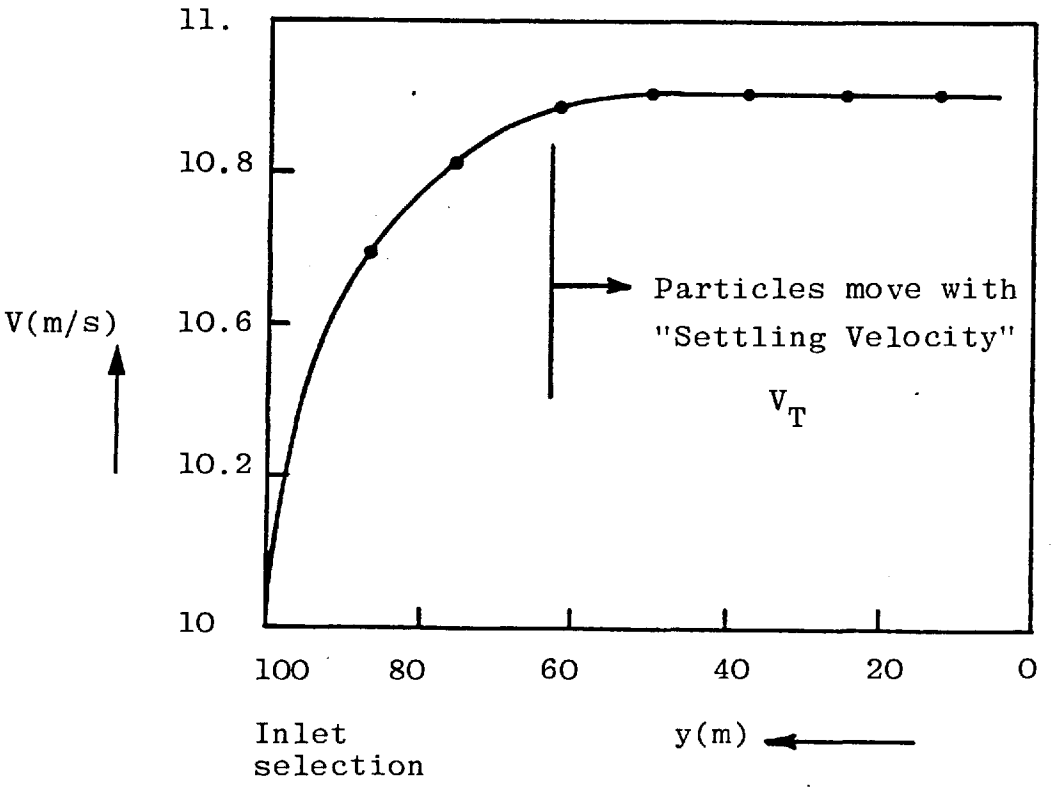


FIGURE (5-6) DETERMINATION OF THE SETTLING VELOCITY FROM THE COMPUTED RESULTS

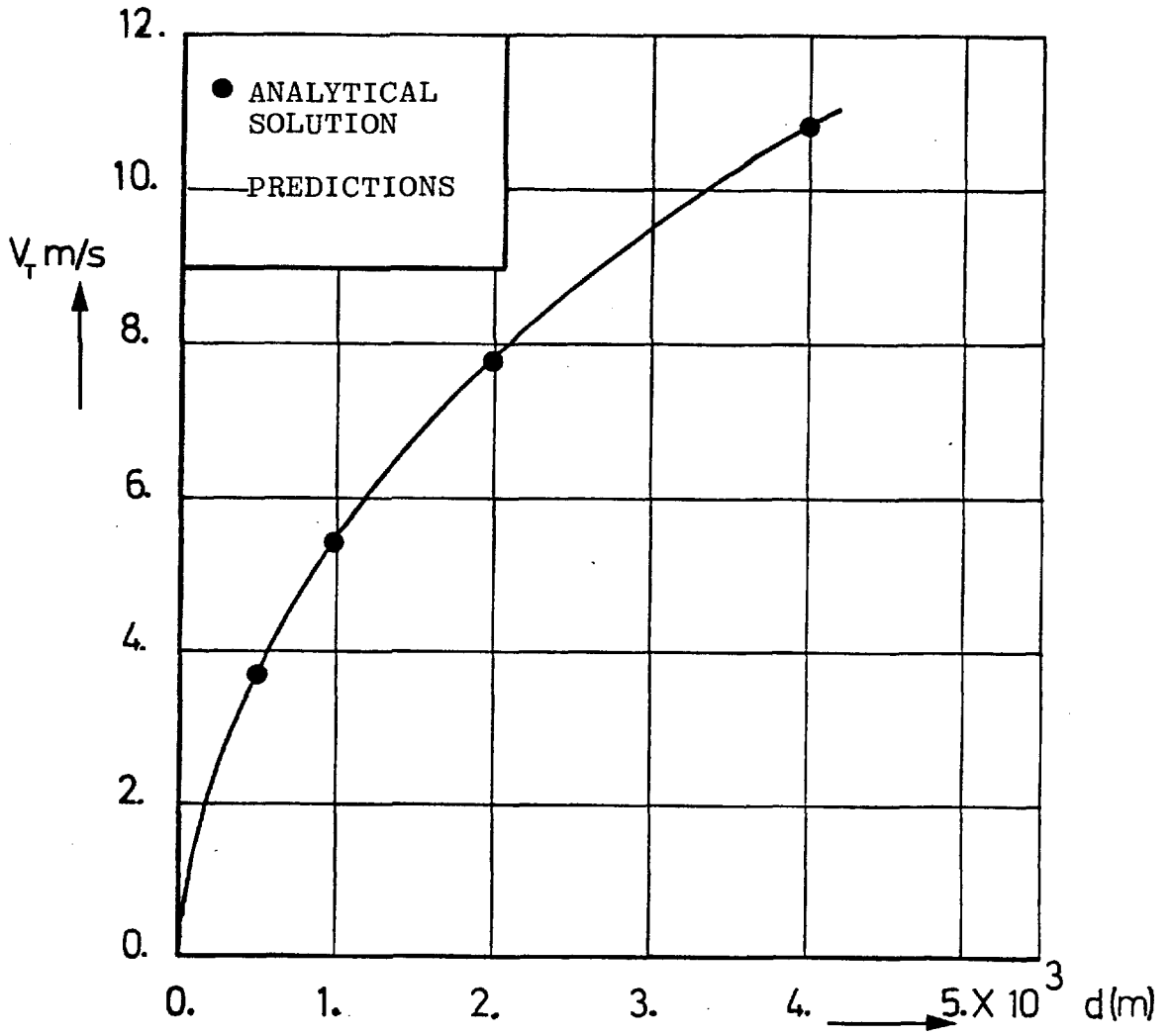


FIGURE (5-7) PARTICLE SETTLING VELOCITY VERSUS DIAMETER

Particle diameter (m)	Predicted value of $\|V_T\|$ (m/s)	Theoretical value of $\|V_T\|$ (m/s)
0.5×10^{-3}	3.76	3.853
1×10^{-3}	5.43	5.449
2×10^{-3}	7.71	7.706
4×10^{-3}	10.90	10.899

TABLE (5-4) PARTICLE SETTLING VELOCITY VERSUS DIAMETER

5.4 PREDICTIONS FOR COMPARISON WITH EXPERIMENTAL DATA

The use of a venturi tube for metering single-phase fluids has been thoroughly investigated and standards have been adopted which allow a high degree of accuracy, compare Jorissen (1951). However, its application to measuring multi-phase mixture appears to have received little attention. The information in the literature on metering two-phase suspensions in venturis is semi-empirical in character; indeed it proposes various phenomenological correlations based on limited experiments, and moreover are of limited applicability.

The gas-particle flow phenomena are so complex that it is too much to expect a closed form analytical solution. Also, the available experimental facilities are confined to a limited number and range of variables (c.f. Boothroyd, 1971). The adaptation of mechanistic models to the solution of such problems seems to be the only plausible and promising approach.

In order to demonstrate the ability of the "IPSA" model to handle such complex features, we have chosen to investigate two typical suspension flows in a venturi. In this section the predictions are compared with the experimental data of Sharma (1977) and Shook et al (1974) who considered, respectively, the flow of glass particles suspended in air and of a lead slurry through a venturi nozzle. As a check of the calculation procedure, the flow of air in a venturi nozzle is considered and the results are compared with the experimental measurements of Sharma (1977).

5.4.1 Single-Phase Flow in a Venturi Nozzle

The problem of the flow of a single-phase (air) in a venturi nozzle serves as a useful test of the solution procedure for the following two reasons. Firstly, one can establish the physical realism of the predictions by comparison with experimental data. Secondly, this is the first problem where the flow is treated as one-dimensional in a variable area duct; therefore the problem provides a check on the assumption of one-dimensionality adopted in the remainder of the problems studied in this thesis.

(a) Objectives of the Study

(i) To compare the predictions with the measurements as an assessment of their realism.

(ii) To study the effect of the grid-refinement and its arrangement on the numerical solution.

(iii) To demonstrate that the area variation is properly incorporated in the computer model.

(iv) To show that no secondary losses, due to recirculation, occur in the case of single-phase phase flow.

(b) Presentation of the problem

(i) Statement of the problem

Figure (5-8) shows the configuration of the venturi nozzle VE2. Air is introduced to the nozzle at the rate of 0.00952 kg/s. For this flow condition, Sharma (1977) has reported experimental measurements for the pressure drop along the venturi meter. The task here is to predict the pressure drop, for the self-same flow, using "IPSA".

(c) Details of the computations

(i) Equations to be solved

In the present problem the conservation equations are written for one phase only, viz:

1. Air-volumetric continuity:

$$\frac{\partial}{\partial y} (R_\ell v) = 0 \qquad . (5.23)$$

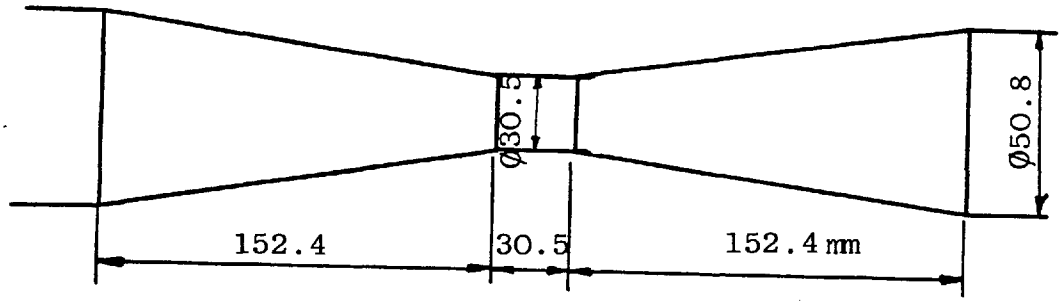
2. Air-momentum conservation equation:

$$\frac{\partial}{\partial y} (R_\rho \rho_\ell v^2) = - R_\ell \frac{\partial P}{\partial y} - f_y^{\ell w} v \qquad . (5.24)$$

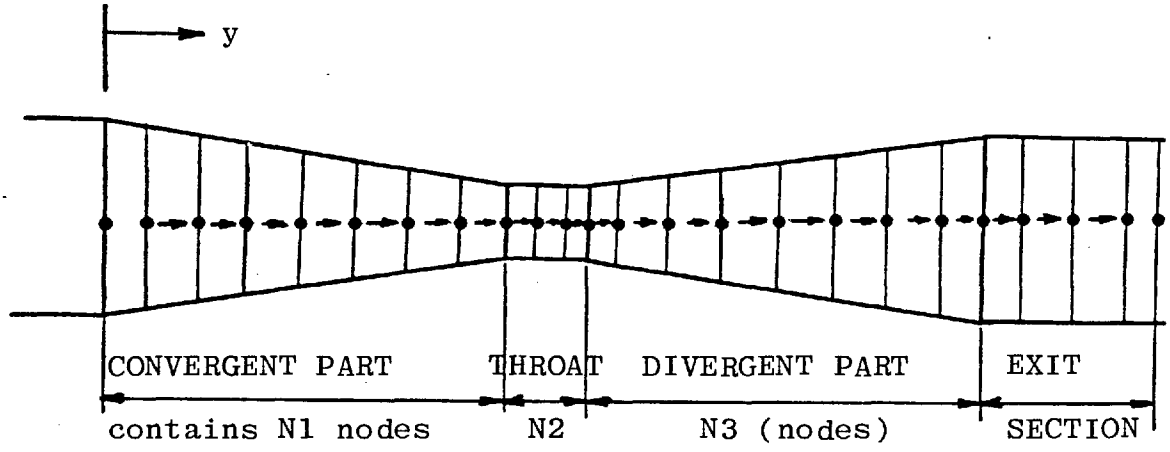
convection ↓ pressure gradient ↓ wall friction

Notes on equations:

- The solution of the second phase is suppressed by setting the central



(a) THE FLOW GEOMETRY



(b) GRID ARRANGEMENT

FIGURE (5-8) THE VENTURI GEOMETRY CONSIDERED: VE2

coefficient of the finite-difference equation, A_p, for both R_d and V to a very large value, say 10^{20}; this is equivalent to setting R_d and V to zero. Under such restriction, the pressure correction equation (4.10) reduces to:

$$\Sigma b_i = \Sigma a_i \quad ;$$

where b_i is the outflow volume from the cell and a_i is the inflow volume to the cell, This implies equality of inflow and outflow which is the continuity principle in single-phase incompressible flows.

- The wall friction factors are calculated from equation (5.2) since the air is in turbulent motion.

(ii) Boundary conditions

- At inlet:

  The inlet velocity is prescribed and is equal to 4.7 m/s.

- At outlet:

  The outlet boundary is located five to ten diameters downstream the venturi exit where fully-developed conditions prevail, i.e. $\frac{\partial v}{\partial y} = 0$.

(iii) Finite-difference grid

In order to examine the effect of grid size on the numerical solution, eight different grids were employed. The distribution of the grid and the number of nodes used are given in Tables(5-6) and (5-7). The grid distribution, along the flow domain, is also depicted in Figure (5-8).

(iv) Miscellaneous information

Typical information on a particular run is given below in Table (5-5).

SINGLE-PHASE FLOW IN A VENTURI NOZZLE	PERTINENT DATA
Configuration	1-D circular and variable cross-section
Grid	45
Type of grid spacing	Non-uniform
Number of iterations	3
Computational time per grid node per iteration CDC 6600 (sec.)	0.0276

TABLE (5-5) TYPICAL INFORMATION ON A COMPUTER RUN

(d) Presentation of the results

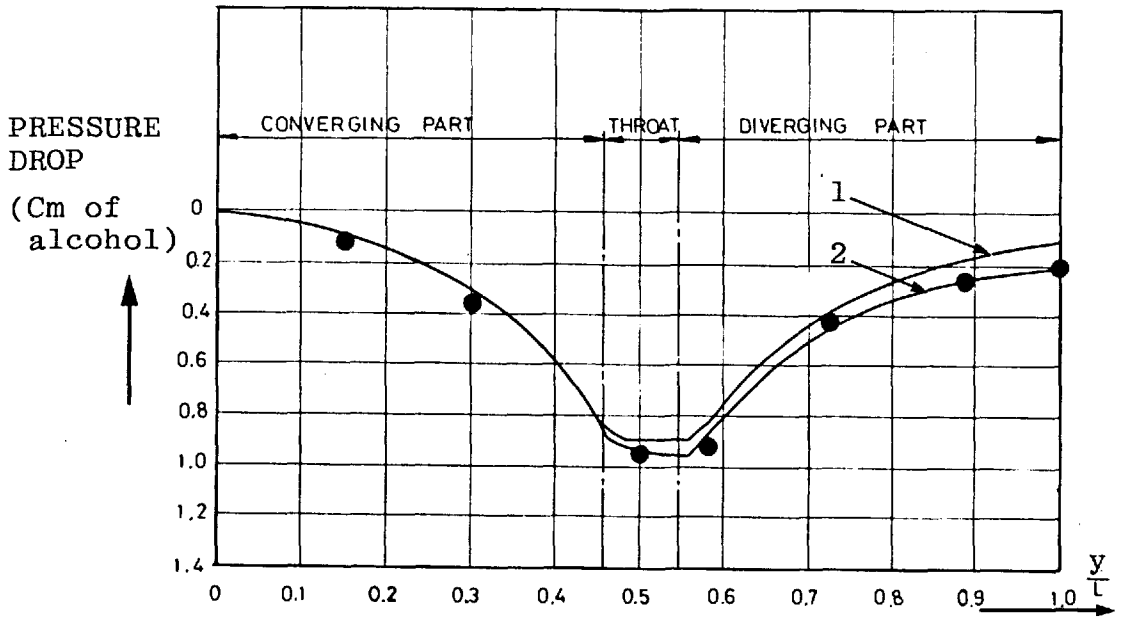
Figure (5-9) shows the experimental value of the pressure drop along the venturi, as well as the predicted values for both inviscid and viscous flow. A non-uniform grid consisting of 45 nodes is employed; the grid distribution is given in table (5-7), run 4.

(e) Discussion of the results

Figure (5-9) shows the predicted pressure variation. The agreement with experimental data is quite satisfactory for inviscid flows. By including the wall-friction a significant improvement is obtained (curve 2). The outcome of the comparison demonstrates the validity of the one-dimensional assumption. No significant discrepancy is observed between the measurements and the predictions, i.e. full account was taken of the frictional and internal losses.

- Grid dependent test

In order to test the grid independence of results the following two sets of runs have been performed. The grid distribution is tabulated below. In tables (5-6) and (5-7) N_1, N_2, N_3 are respectively the number of grid nodes in the convergent part, the throat and the diffuser part of the venturi.



● Measurements —— Prediction: 1 - Inviscid
2 - Viscous

FIGURE (5-9) AIR FLOW IN A VENTURI NOZZLE (RUN 4, SET 2)

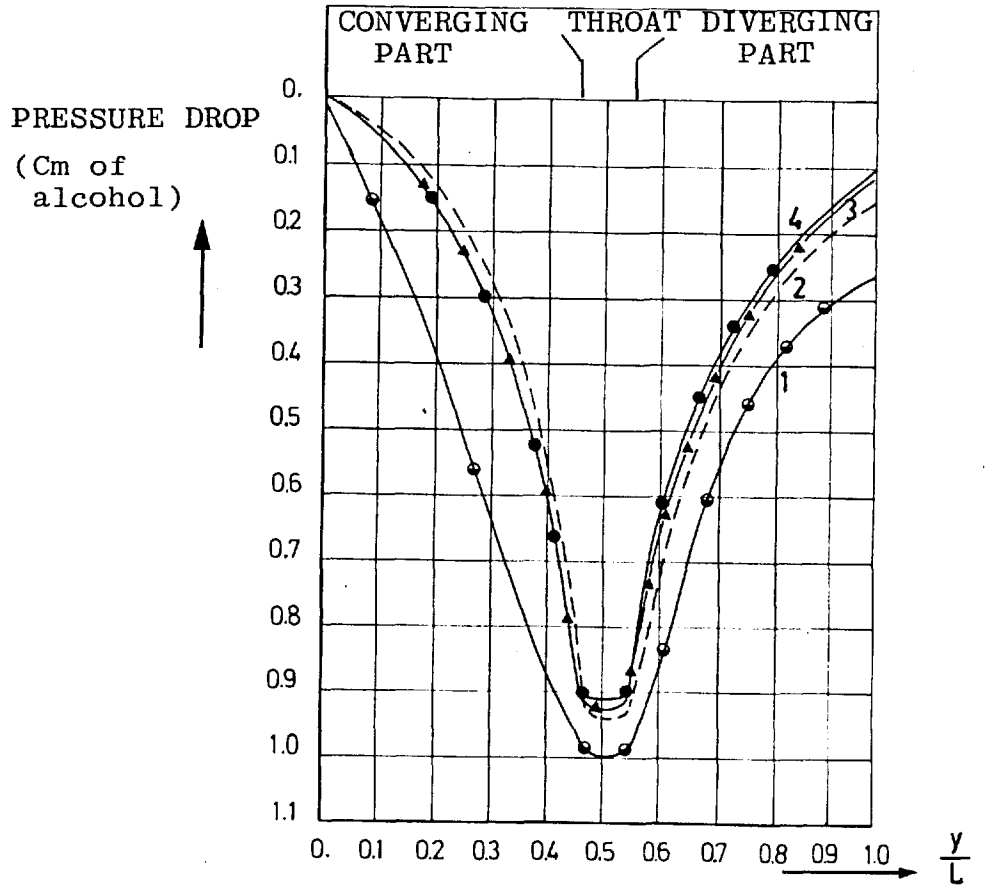


FIGURE (5-10) EFFECT OF GRID REFINEMENT ON THE SOLUTION (RUN 1 to 4, SET 1; TABLE (5-4))

Run No.	N_1	N_2	N_3	$N_1 : N_2 : N_3$	Total No. N
1	4	2	6	2 : 1 : 3	12
2	8	4	12	2 : 1 : 3	24
3	12	6	18	2 : 1 : 3	36
4	16	8	24	2 : 1 : 3	38

TABLE (5-6) RUNS MADE FOR STUDYING THE EFFECT OF THE GRID SIZE (SET 1)

Run No.	N_1	N_2	N_3	$N_1 : N_2 : N_3$	Total No. N
1	10	10	30	1 : 1 : 3	50
2	20	10	20	2 : 1 : 2	50
3	15	5	30	3 : 1 : 4	50
4	20	5	20	4 : 1 : 4	45

TABLE (5-7) RUNS MADE FOR STUDYING THE INFLUENCE OF THE GRID DISTRIBUTION (SET 2)

(i) Effect of grid size

Figure (5-10) illustrates the pressure distribution along the venturi length. Graphs 1 to 4 correspond to runs 1 to 4 of table (5-6). The curves numbered 2, 3 and 4 show how the pressure distribution is influenced by the mesh size. The solution obtained using only twelve grid nodes (curve 1) is excessively inaccurate; but the influence of the refinement of the grid on accuracy appears therefore all the more clearly.

(ii) Effect of grid distribution

To investigate the effect of the grid size on the results, the number of grid nodes was increased while their relative ratio $N_1:N_2:N_3$ was kept constant (in set 1). In set 2 the ratio $N_1:N_2:N_3$ was altered while the total number of grid nodes was kept constant, so as to investigate the effect of the grid distribution on the predictions. It was observed that the more accurate results were obtained from runs 3 and 4 (of set 2).* While run 4 has fewer number of grid nodes than 3 (10% less) it produced the most accurate

*This is because the finer grid spacing was located in the region where "steep" gradients of the variables exist.

results as compared with the measurements (Figure (5-9)). It may be concluded that numerical solution independent of the grid size can be obtained and that substantial economies can be achieved by a proper grid distribution.

5.4.2 Gas-Particle Flow in Venturi Meters

The motivation for the study of the flow of glass-particles suspended in an air stream through venturi meters, stems mainly from the fact that predictions for this flow were obtained by Sharma (1977), who also investigated the problem experimentally. Thus, it is possible to compare our solutions with those obtained by another method (based on the concept of two superimposed continua), and also to assess the physical realism of the computations by comparison with the available experimental data.

(a) Objectives of the study

(i) To investigate the fluid-particle iteration for very high density ratio 1:2480.

(ii) To study the effect of the geometrical configurations in the flow pattern.

(iii) To check the fidelity of the model in its description of the physical process.

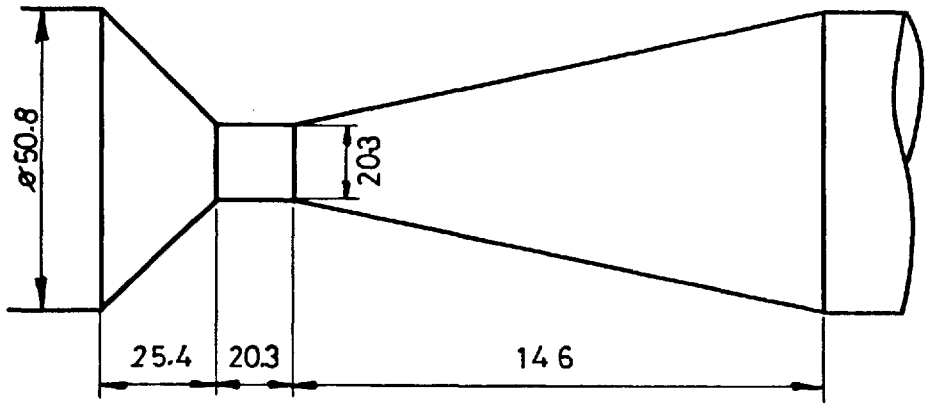
(b) Presentation of the problem

(i) Statement of the problem

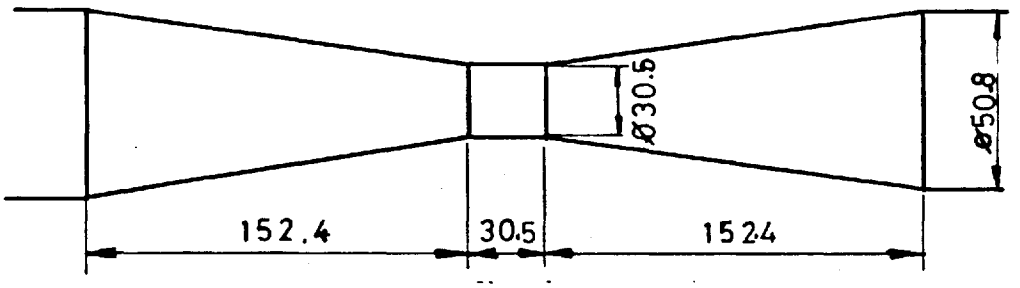
Figure (5-11) illustrates the venturi geometries considered, namely VE1 and VE2. The venturi are set in a vertical position, and the air and the particles flow steadily in the positive direction of y (i.e. against gravity). The task is to calculate the pressure drop along the venturi nozzle for different gravimentric ratios of air to particles.

(ii) Experimental set-up

Sharma (1977) studied the flow of glass particles suspended in an air stream through various venturi meters. He restricted his investigation to vertical positioning and considered two different geometries, namely VE1 and VE2, (see Figure (5-11). A complete schematic diagram of his experimental rig is shown in Figure (5-12)). The flow system consisted of a 2" opaque plastic tube. Only the venturis were made of transparent acrylic material to allow flow visualisation. Air was supplied from a high pressure compressor connected to a large storage tank. Inlet air pressure was controlled by a pressure regulator. The air flow rate was measured



VE 1



VE 2

FIGURE (5-11) THE VENTURI GEOMETRIES CONSIDERED (DIMENSIONS ARE IN mm)

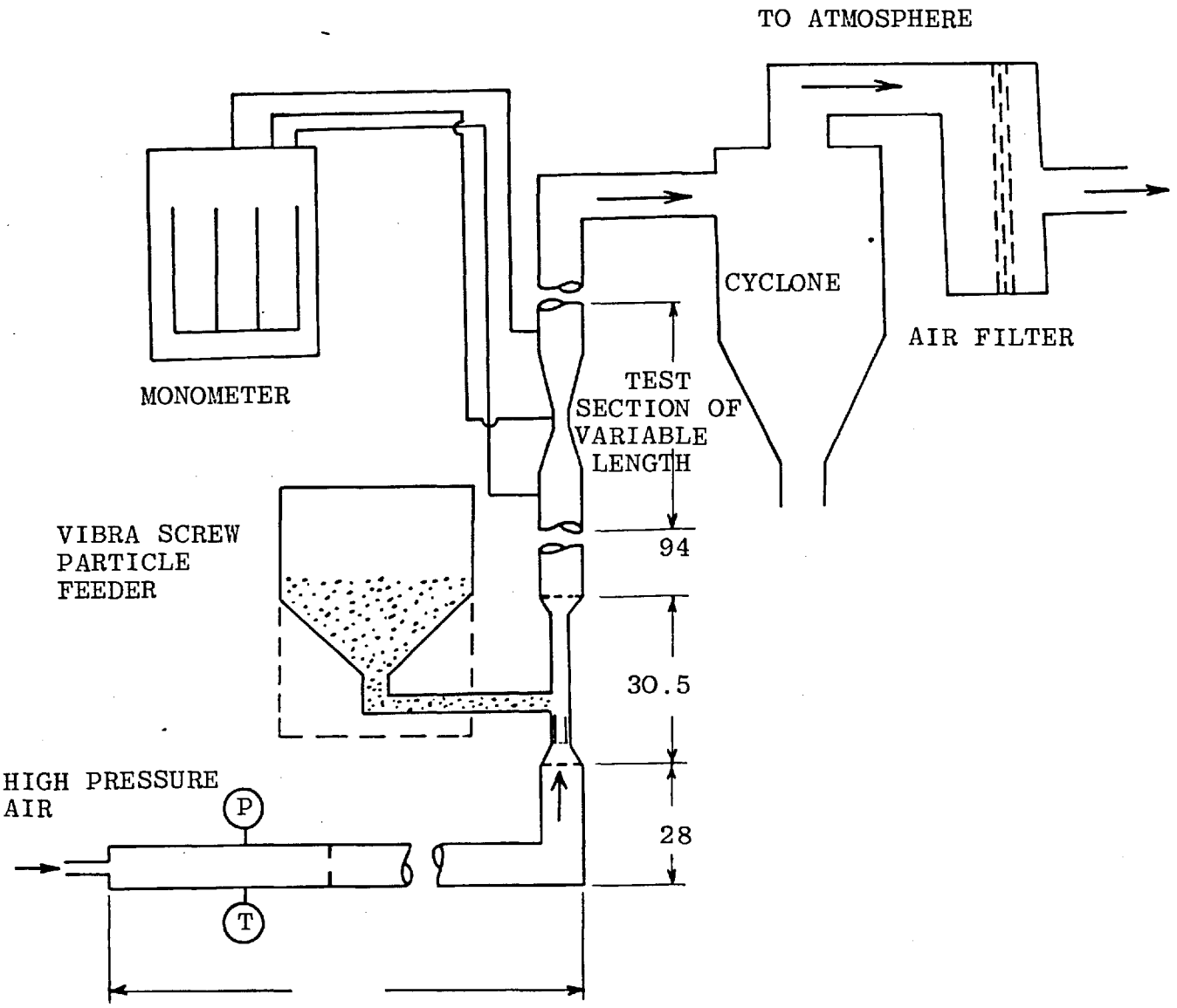


FIGURE (5-12) SCHEMATIC DIAGRAM OF THE EXPERIMENTAL ARRANGEMENT USED BY SHARMA (1977) (DIMENSIONS ARE IN cm)

by an orifice meter. A vibrating screw feeder was used to feed the particles through a fluidized bed mixing section, the mass feed rates of particles were determined by collecting them from the cyclone separator. The air before exhausting to the atmosphere was ducted through a filter box to trap any suspended fine particles. An analysis of the particle size was performed and an average diameter of 20 microns was arrived at. A 24-legs manometer, with methyl alcohol as manometric fluid, was used to measure the pressure differential.

(iii) Reported results

The data reported by Sharma (1977) included:

(a) the experimental measurements of the pressure drop, along the two considered venturi geometries: VE1 and VE2, for different gravimetric ratios of particles to air; the particle-concentration was of the order of 10^{-3};

(b) numerical predictions with a model that simulates the above flow conditions. In fact he used a quasi one-dimensional model, known as CONVAS (CONservative VAriable and Source) which was based on a combined Eulerian-Lagrangian approach.

(c) Details of the present computations

(i) Equations to be solved

1. Gas-volumetric continuity:

$$\frac{\partial}{\partial y}\ (R_\ell v) = 0 \qquad . (5.25)$$

2. Particles-volumetric continuity:

$$\frac{\partial}{\partial y}\ (R_d V) = 0 \qquad . (5.26)$$

3. Gas-momentum conservation equation:

$$\frac{\partial}{\partial y}\ (R_\ell \rho_\ell v^2) = - R_\ell \frac{\partial P}{\partial y} + f_y^{\ell d}\ (V-v) - f_y^{\ell w}\ v$$

↓ convection ↓ pressure gradient ↓ inter-phase friction ↓ wall friction

. (5.27)

4. Particle-momentum conservation equation:

$$\frac{\partial}{\partial y}\ (R_d \rho_d V^2) = - R_d \frac{\partial P}{\partial y} + f_y^{d\ell}\ (v-V)$$

$$- R_d(\rho_d - \rho_\ell)g \qquad . (5.28)$$

↓ Buoyancy force

Notes on equations:

- The volume fractions must sum to unity.
- Wall frictional force appears only in the gas momentrum equation and is calculated from equations (5.1) and (5.2).
- Both variants of the inter-phase friction coefficient defined by equations (5.3) and (5.8) were employed in the present predictions. As will be shown, the choice of the correlation for $f_y^{\ell d}$ does not affect the calculations very much owing to the small particle size which makes the form-drag term predominant in both expressions (5.3) and (5.8).

(ii) Boundary conditions

- At inlet:
  The inlet mass flow rates, as measured by Sharma were used to prescribe the value of the variables at the inlet to the venturi. At this boundary, it was assumed that there is no slip between the air and the glass-particles.
- At outlet:
  The outlet section was taken to be 10 diameters downstream of the venturi exit, where fully-developed conditions were assumed, i.e. $\frac{\partial \phi}{\partial y} = 0$ for all variables.

(iii) Finite-difference grid

A finite-difference grid consisting of 55 nodes was employed. The distribution of the grid along the venturi nozzle was as follows: 20 nodes in the converging part, 5 nodes in the throat, 20 nodes in the diverging section and 10 nodes in the exit section (from the venturi exit to the outlet boundary). The results obtained using this mesh were grid-independent.

(iv) Miscellaneous information

Some further numerical information on the problem is given below.

Gas-particle flow in venturi meters	Pertinent Data
Configuration	1-D circular
Grid	55
Type of Grid Spacing	Non-uniform
Number of iterations	8
Computational time per grid node per iteration CDC 6600 (sec.)	0.0310

TABLE (5-8) TYPICAL INFORMATION ON A COMPUTER RUN

(d) Presentation of the results

Figures (5-13) to (5-18) display the results of the computation and their comparison with both the experimental data and the predictions of Sharma (1977). The graphs exhibit the variation in pressure along both venturi geometries considered (VE1 and VE2), for different gravimetric ratios of particles to air.

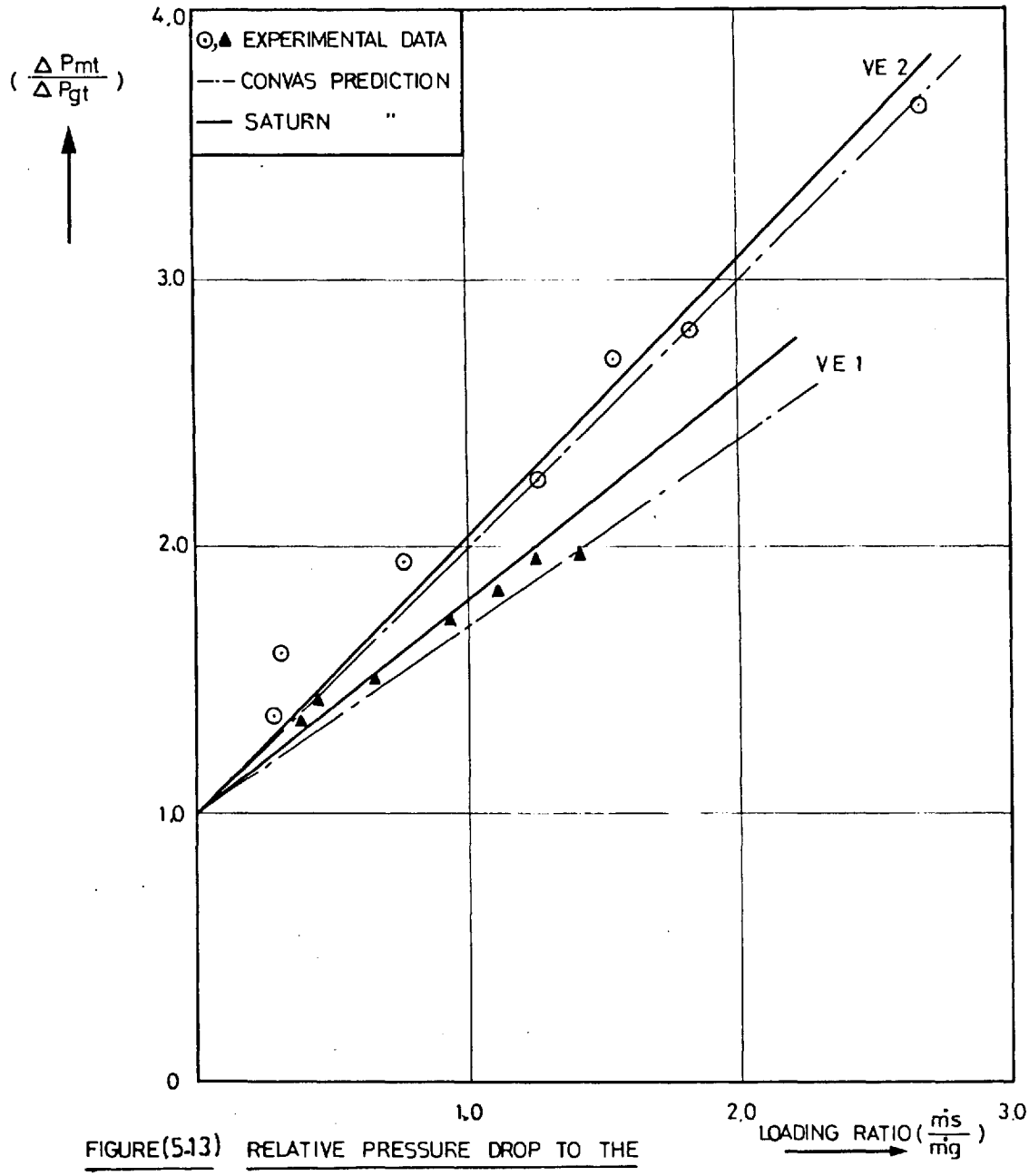
(e) Discussion of the results

Figure (5-13) shows the non-dimensional pressure drop at the throat versus the loading ratio for venturis VE1 and VE2; $\Delta P_{mt}/\Delta P_{gt}$ is the ratio of the pressure drop at the throat for the mixture to the pressure drop due to the gas flow only.

The data for the smaller venturi VE1 show a lower relative pressure drop compared to VE2 for the same loading. This is attributable to the shorter distance between the entrance and the throat with the result that less time is available for the particle to interact with the gas. The experimental points and both "CONVAS" and "SATURN"* predictions indicate a linear

---

"SATURN" (Solid And fluid flow in venTURI Nozzle) which is a version of the "PLANT" code developed for the dispersed-flow predictions.



FIGURE(5-13) RELATIVE PRESSURE DROP TO THE THROAT OF THE VENTURI VERSUS LOADING RATIO

relationship between the loading ratio and the non-dimensional pressure drop. Both predictions are in good accord with the experimental data. However by way of an assessment of the accuracy of both sets of numerical results, we consider the following analysis.

By the use of the least-square technique, the experimental points were joined with the 'best' straight line. The equation for the straight lines representing respectively the experimental, "CONVAS" and "SATURN" results are shown below:

$$\frac{\Delta P_{mt}}{\Delta P_{gt}} = 1 + K_1 \frac{\dot{m}_s}{\dot{m}_g} \quad , (5.29)$$

$$\frac{\Delta P_{mt}}{\Delta P_{gt}} = 1 + K_2 \frac{\dot{m}_s}{\dot{m}_g} \quad \text{and} \quad , (5.30)$$

$$\frac{\Delta P_{mt}}{\Delta P_{gt}} = 1 + K_3 \frac{\dot{m}_s}{\dot{m}_g} \quad . (5.31)$$

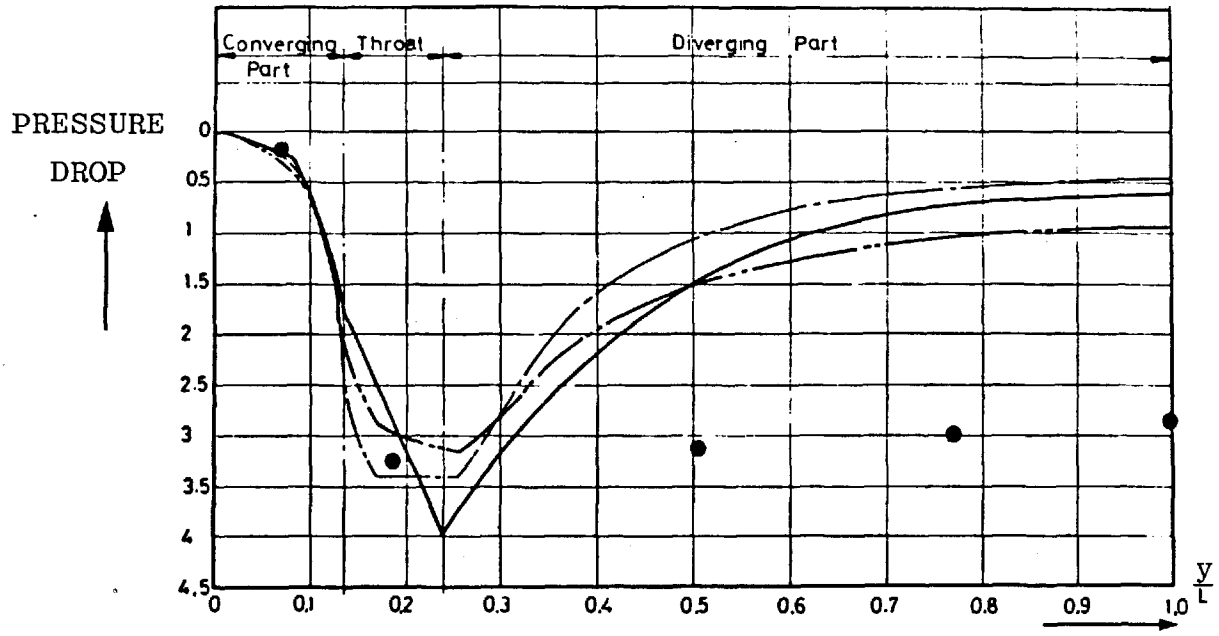
where the values of K_1, K_2 and K_3 for both venturis VE1 and VE2 are tabulated below.

Geometry	K_1 (Exp.)	K_2 ("CONVAS")	K_3("SATURN")
VE1	0.773	0.714	0.801
VE2	1.049	1.001	1.041

TABLE (5-9) THE VALUES OF THE SLOPE K_i FOR DIFFERENT CONDITIONS

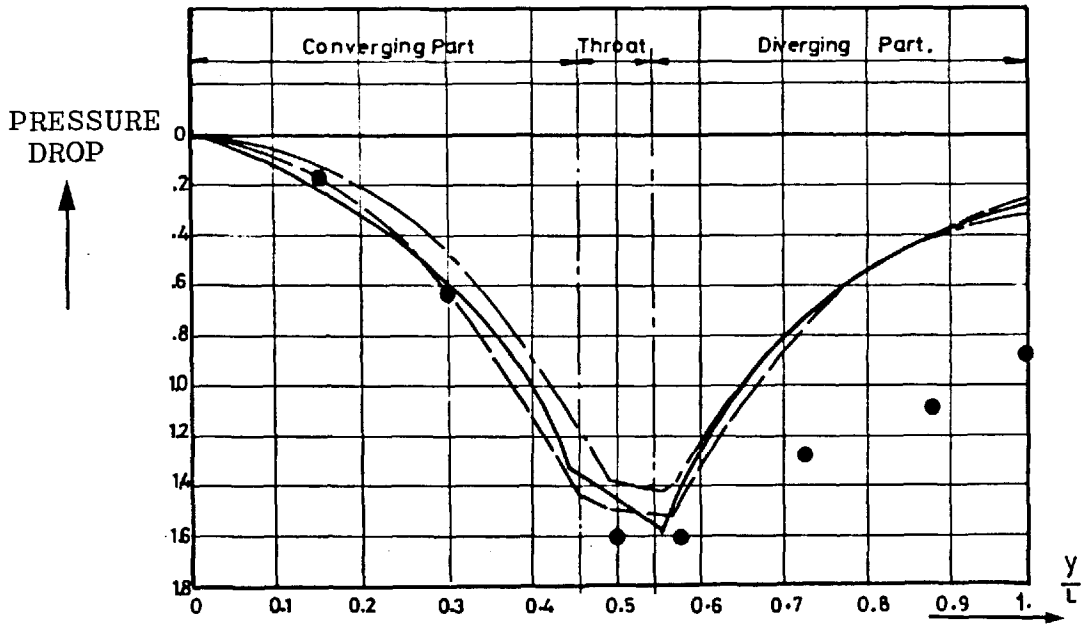
It may be noticed that for both configurations the present calculations give closer agreement with the measurements; this improvement in accuracy is mainly due to the inclusion of the wall-friction effects that "CONVAS" did not take into account.

The pressure drop predictions for the single-phase air flow (section 5.4.1) through the VE2 compared favourably with measured values throughout the geometry. In the case of particulated flow there is good agreement also but only up to the throat; unfortunately the predictions for the diverging part are in marked disagreement with experimental data. This is made painfully clear by Figures (5-14) and (5-15). From these graphs it is apparent that the prediction of the pressure drop shows a slight improvement when "IPSA" is used in conjunction with the Wallis formula (5.8). The large



● Measurements (cm of Alcohol) "IPSA" Predictions —·—·— Using Eq. (5.3)
—— "CONVAS" Prediction —·—·— Using Eq. (5.8)

FIGURE (5.14) VARIATION OF PRESSURE ALONG THE LENGTH OF VE 1 (LOADING RATIO = 0.42)



● Measurements (cm of Alcohol) "IPSA" Predictions — — — Using Eq. (5.3)
—— "CONVAS" Prediction —·—·— Using Eq. (5.8)

FIGURE (5-15) VARIATION OF PRESSURE ALONG THE LENGTH OF VE 2 (LOADING RATIO = 0.29)

discrepancy between the numerical solution and the measured values was attributed, by Sharma (1977), to two-dimensional effects. In fact, Sharma observed (venturis are transparent) that channelling occurs, i.e. the particles tend to concentrate about the centre line in the throat and beyond. In view of this experimental evidence and in order to improve our predictions, we took into account the channelling effect by recourse to the assumption that, due to their high inertia, the particles do not diffuse in the cross stream direction. Thus, the effective flow area of the particles downstream of the converging section, will be considered fixed and equal to the throat area. The computed results obtained are graphed in Figures (5-16) and (5-17). The predictions are now seen in very good accord with the measured values.

It is always tempting to use one-dimensional computations as they are very economical; however one should advisedly be cautious and stop to consider whether it is indeed realistic to suppose a priori that two- or multi-dimensional effects are negligible.

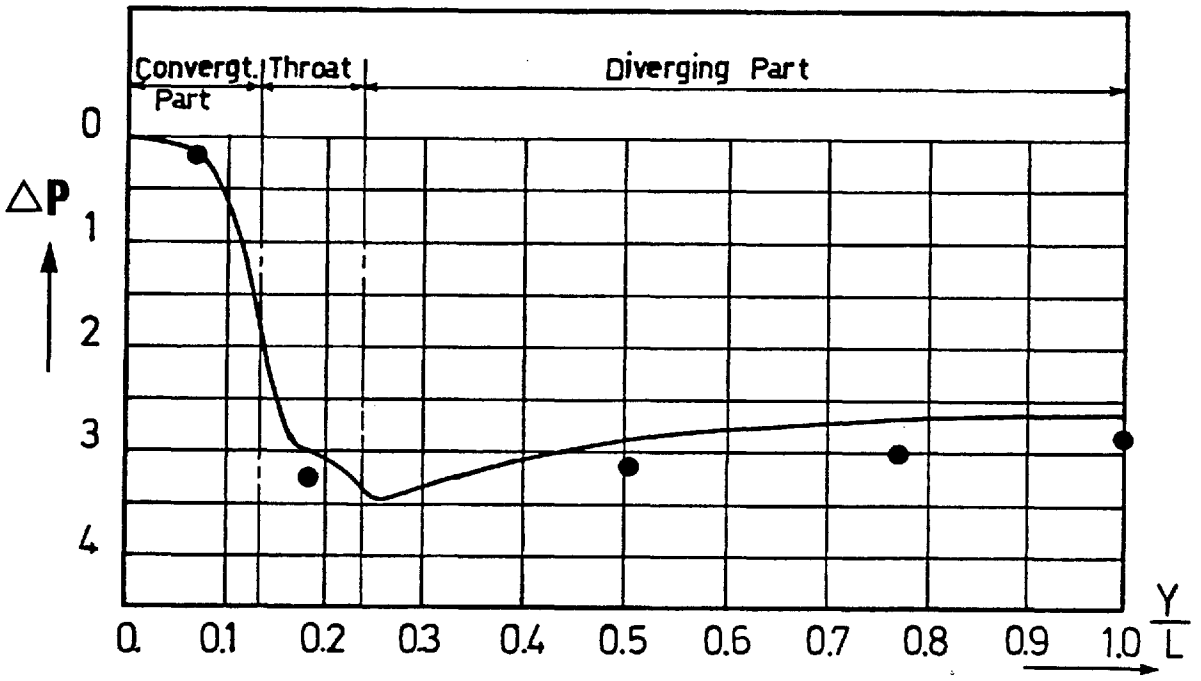


FIGURE (5-16) PRESSURE DROP PREDICTIONS VERSUS MEASUREMENTS, TAKING INTO ACCOUNT 2-D EFFECT; VE 1

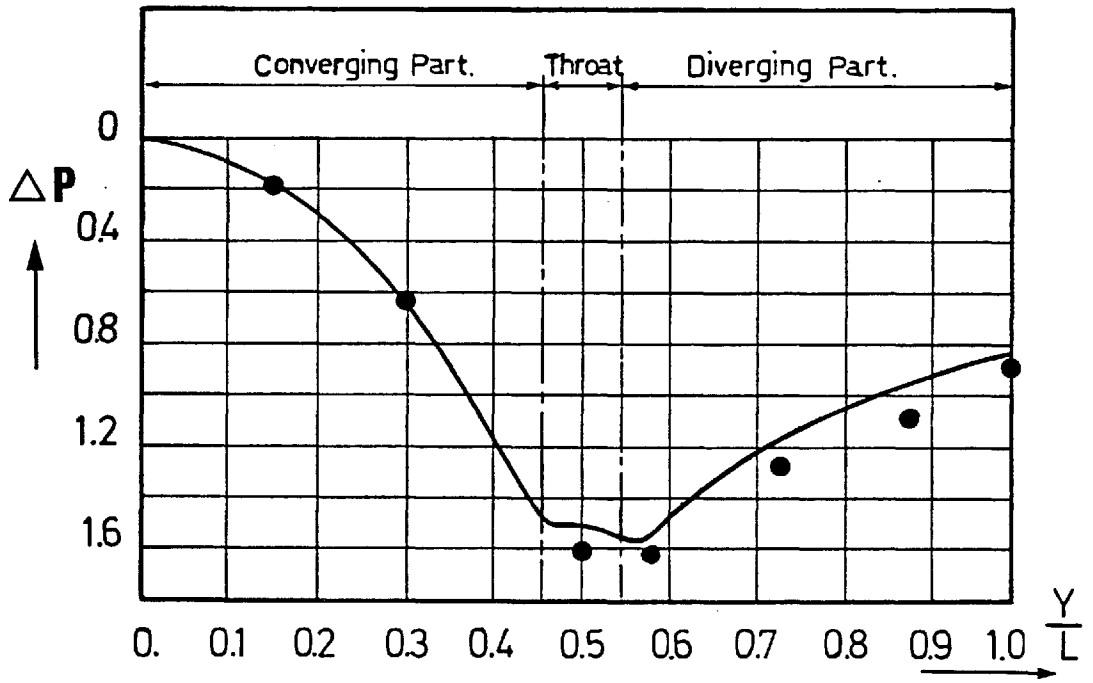


FIGURE (5-17) PRESSURE DROP PREDICTIONS VERSUS MEASUREMENTS, TAKING INTO ACCOUNT 2-D EFFECT; FOR VE 2

5.4.3 Flow of a Slurry Through a Venturi Meter

The flow of a lead slurry through a venturi nozzle is the second problem chosen for the investigation of particle fluid interaction in a variable area duct. The problem is of interest in that it was investigated both theoretically and experimentally by Shook and Masliyah (1974). Thus it is possible to validate the present predictions by comparison with the reported data. In the present problem the lead-particles have an average diameter of 2 mm, i.e. they are 100 times larger than the glass particles considered in problem 5.4.2; this means that the form drag will be much smaller in this case (due to the larger diameter) and that the effect of virtual mass in equation (5.8) will be predominant. Thus, the problem permits as well checking the adequacy of the friction correlations employed in the calculation.

(a) Objectives of the study

(i) To check the adequacy of the friction correlations.

(ii) To study the effect of area variation on the slip between the phases.

(iii) To demonstrate the physical realism of the present prediction by comparison with experimental data.

(b) Presentation of the problem

(i) Statement of the problem

A mixture of water and lead particles is flowing steadily in a vertical venturi.

The specified dimensions and the properties of the flowing slurry are:

Pipe diameter (D)	=	0.0525 m
Throat diameter (D_T)	=	0.0328 m
Length of the convergent part	=	0.05311 m
Length of the divergent part	=	0.1125 m
Water density	=	1000 Kg/m^3
Water viscosity	=	0.001 Ns/m^2
Lead density	=	10920 Kg/m^3
Particle diameter (d)	=	0.002 m

The task is to compute the velocity distribution for both phases and to deduce the discharge coefficient.

(ii) Reported results

Shook et al (1974) made both an experimental and a theoretical investigation for the described problem. They have calculated the discharge coefficient empirically, and used the Runge-Kutta method to solve the one-dimensional equations, governing the flow of the two-phases (they neglected the wall frictional effect). Moreover, they calculated the discharge coefficient C_d (based on their prediction) from the following relation:

$$C_d = \frac{(R_\ell v + R_d V)_1}{\beta^2 \sqrt{\frac{2g(p_1-p_2) + 2g\rho_M(Y_1-Y_2)}{\rho_M(1-\beta^4)}}} \quad , (5.32)$$

where,

subscripts 1 and 2 refer respectively to the inlet section and the throat

β^2 is the ratio of the throat to the inlet area

ρ_M is the mixture density given by:

$$\rho_M = (\rho_\ell R_\ell v + \rho_d R_d V)_1 / (R_\ell v + R_d V)_1 \quad .$$

(c) Details of the computations

(i) Equations to be solved

The equations to be solved are those of volumetric continuity and momentum (one for each phase) in their steady one-dimensional form as described by equations (5.25) to (5.28).

(ii) Boundary conditions

- At inlet:

The variables have the following prescribed values:

Water-velocity = 2.64 m/s

Particle-velocity = 1.93 m/s

Particle-concentration (R_d) = 0.058

It is to be noted that the relative Reynolds number R_r is equal to 14200, thus the drag coefficient, C_D is given a constant value equal to 0.44 (equation (5.7)).

- At outlet:

  Calculations by Shook et al were made only to the throat of the venturi tube. The present calculation considers the outlet boundary from 5 to 10 diameters downstream the venturi exit where fully-developed conditions prevail, i.e.

  $$\frac{\partial \phi}{\partial y} = 0.$$

  The numerical features (computer time, grid, etc.) are much the same as in the previously investigated problem.

(d) Presentation of the results

Figures (5-18) and (5-19a) illustrate the velocity distribution of the lead particles and the suspending medium; the pressure distribution (common to both phases) is shown

in Figure (5-19b). Moreover, the calculated value of the discharge coefficient, C_d (based on the present prediction) is compared with both the theoretical and predicted values given by Shook et al (1974).

(e) Discussion of the results

Figure (5-18) exhibits the variation of the dimensionless particle and fluid velocities with the normalised distance along the convergent part of the venturi. The reported theoretical results of Shook et al (1974) are also presented. The present results are plotted for the two different inter-phase friction formulae (5.3) and (5.8). The current predictions, using the Wallis formula (5.8) indicate that both velocity fields have the correct trends and that the slip velocity increases with distance. The variation in slip is attributed partly to the difference in phase densities and partly to the comparatively large diameter of the particles. In this case the results compare very well with the data of Shook and Masliyah. It is also apparent, from the same figure, that the inter-phase slip is not well accounted for when the friction coefficient is altered to the formula suggested by Harlow and Amsden (5.3). This indicates the influence

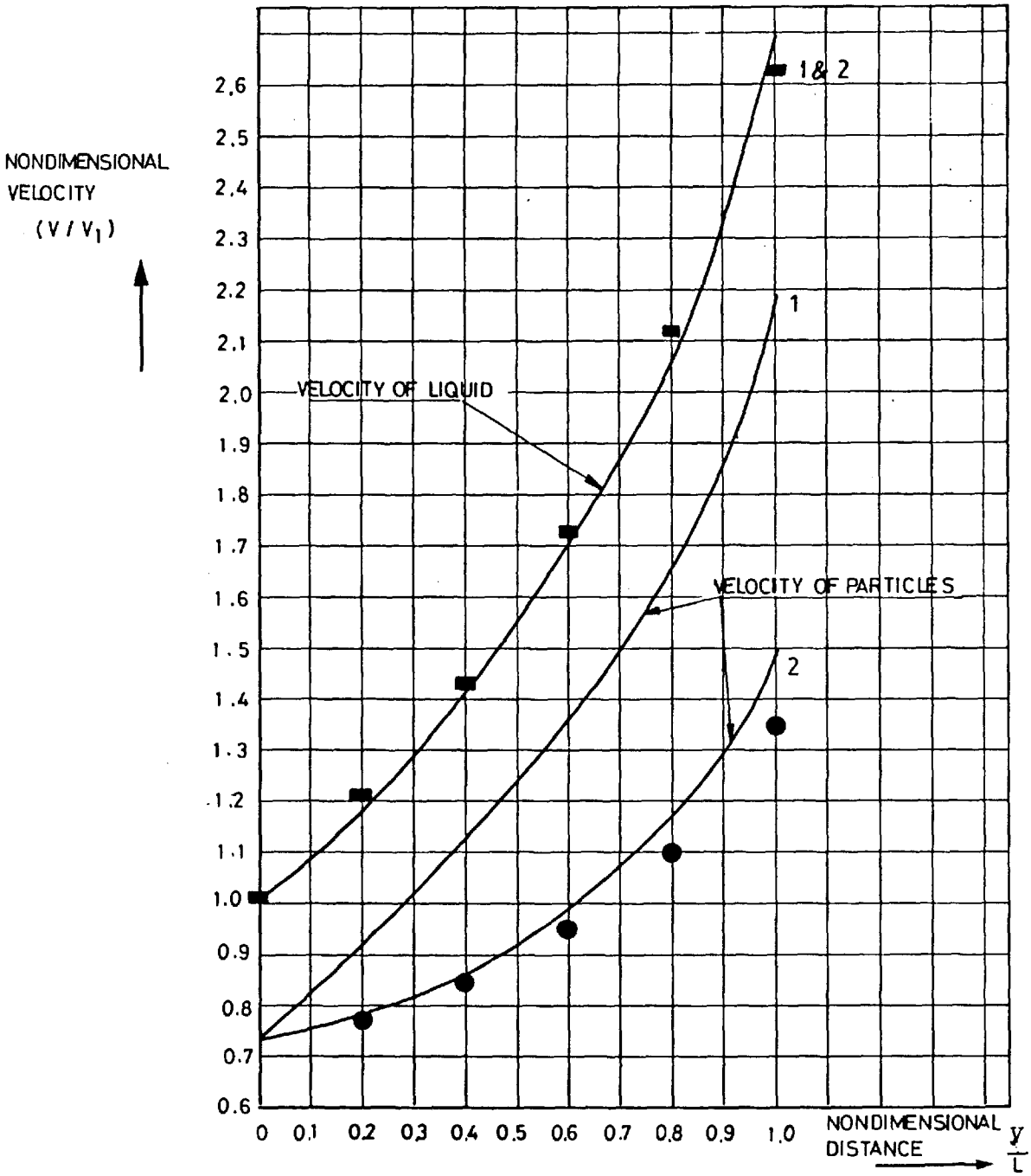


FIGURE (5-18) VARIATION OF FLUID AND PARTICLE VELOCITIES ALONG THE CONVERGING PART OF THE VENTURI NOZZLE (NB: $V_1 = R_d V + R_\ell v$ AT INLET)

of the inter-phase friction correlation on the obtained results. In fact, the expression derived by Wallis simulates faithfully the physical situation by accounting for the added mass effect (Zuber's correction for the effect of other particles).

The hydrodynamic interaction between the phases along the whole length of the venturi is illustrated in Figures (5-19a) and (5-19b). Due to their high inertia, the particles retain their momentum even after passing through the throat. They reach the velocity of the decelerating fluid in the diffuser, and exceed it as depicted in Figure (5-19a). Figure (5-19b) shows the variation in pressure along the venturi. It may be observed that the minimum pressure drop occurs shortly downstream of the throat, a fact that was confirmed by experimental evidence, compare Graczyk (1961).

In order to verify the physical realism of their calculation, Shook et al (1974) evaluated experimentally the discharge coefficient. Its theoretical value was slightly greater than one, namely 1.0861; their experimental study confirmed the fact that the discharge coefficient may exceed unity in the present situation, their reported empirical value was 1.068.

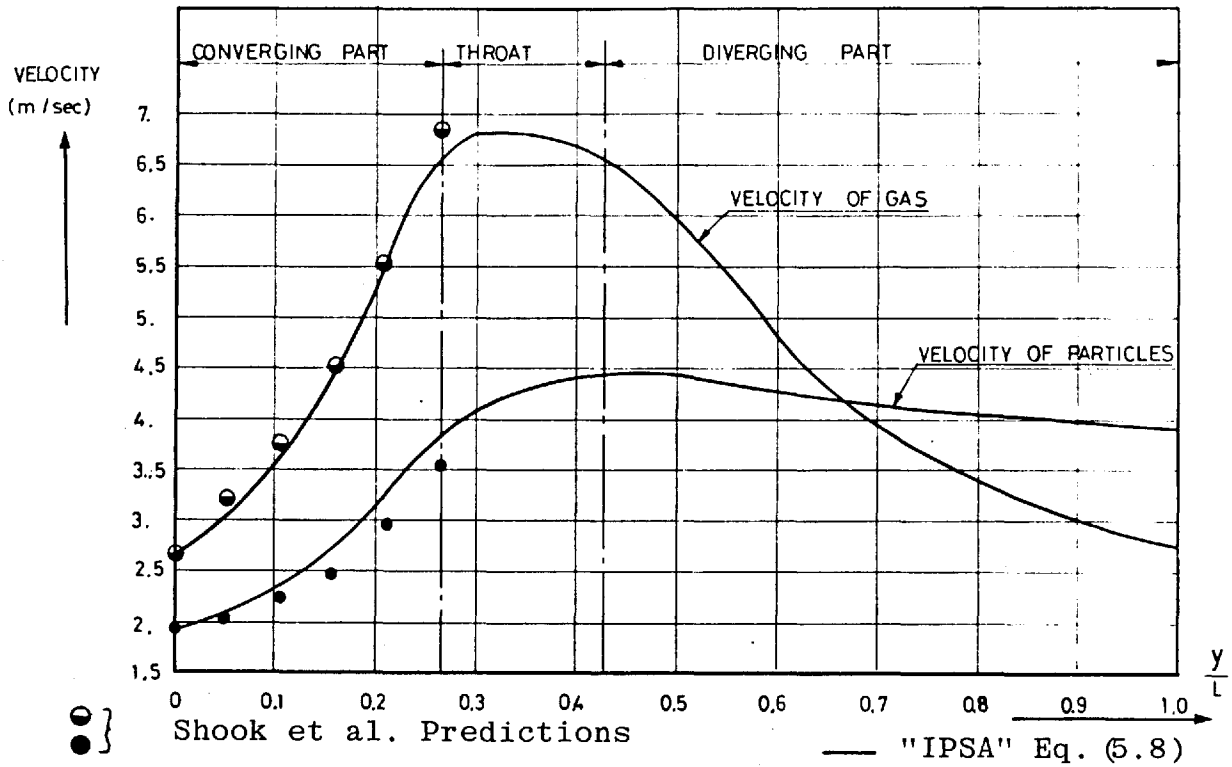


FIGURE (5.19a) VARIATION OF THE FLUID AND PARTICLE VELOCITIES ALONG THE WHOLE LENGTH OF THE VENTURI

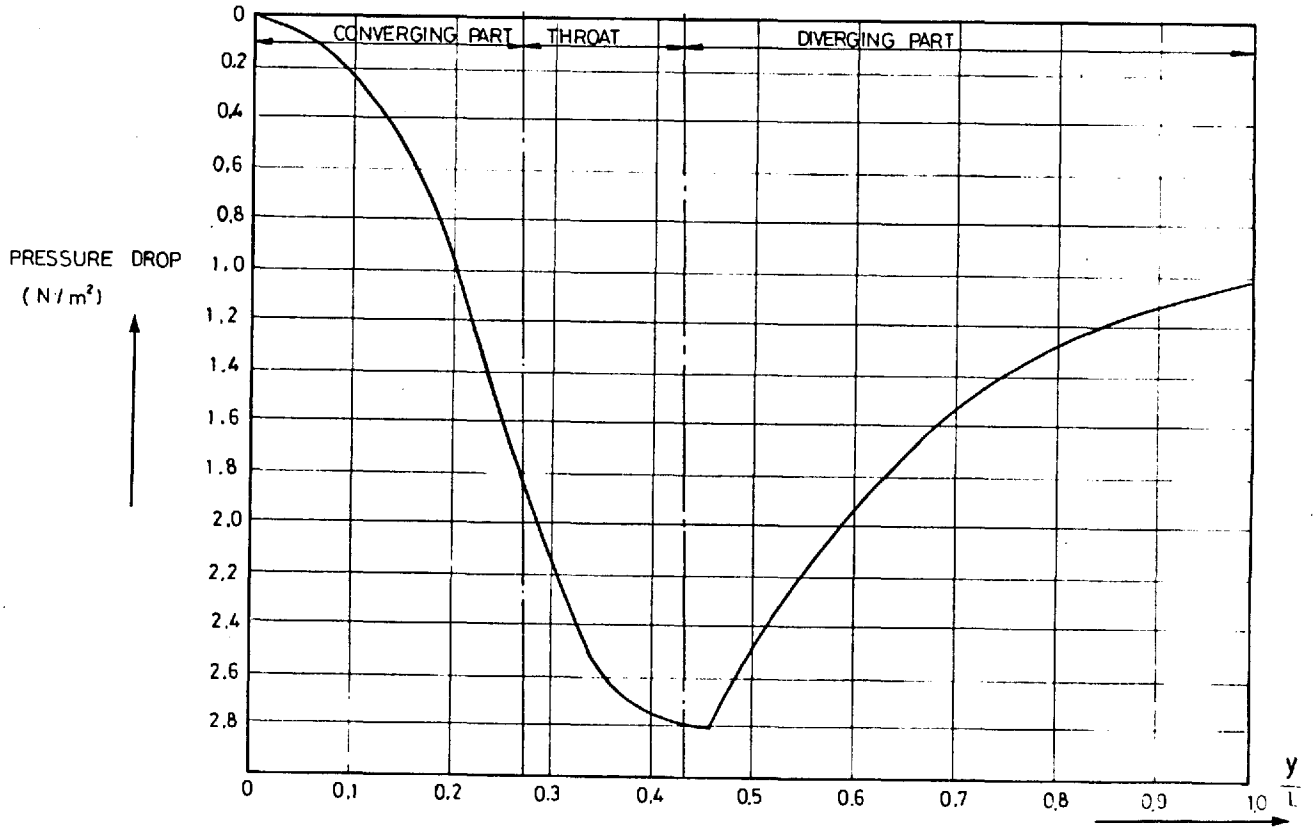


FIGURE (5-19b) PRESSURE DISTRIBUTION ALONG THE VENTURI METER LENGTH

The explanation given was that the increase in the wall friction caused by the presence of the particles is compensated by the effect of the finite inter-phase slip. These observations also indicate the physical realism of the present predictions (using equation (5.8)). The computed value of the discharge coefficient, using "IPSA" was 1.082, which represents an error of only 1% in its calculation.

5.5 PARAMETRIC STUDY

The problems considered previously were solved in order to check the mathematical accuracy of the solution procedure and the fidelity of the model in its description of physical reality. Although comparison of predictions with analytical solutions and experimental data is a good means of checking the credibility of the model, what has been left unsaid in its favour so far is that a larger number of variables and parameters fall under the scope of "IPSA". For example, it is of interest to know the effect of varying the inter-phase friction coefficient on the concentration variation, the slip velocity and the pressure distribution. Also it is important to study the effect of particles size, that being a key parameter, on the flow variables. The present section is devoted to a study of the influence of the various parameters on the flow regime. In this case it is not possible to evaluate our results as no similar study is recorded in the literature.

(a) Objectives of the study

(i) To extend the study to variables that have not been investigated experimentally (because of the difficulty of arranging measurements) such as the concentration and the slip velocity along a venturi nozzle.

(ii) To check the plausibility of the results.

(iii) To demonstrate the potential and the flexibility of the present solution procedure.

(b) Presentation of the study

The parametric study which we are about to describe, considers the flow of glass particles suspended in air along both venturi geometries VE1 and VE2 (Figure 5-11). Firstly, the influence of particle size on velocity and pressure fields is investigated. Then, secondly, we present the effect of altering the inter-phase friction coefficient on the flow variables. Finally, the time response of the particle motion is studied under various flow conditions.

(c) Details of the computations

(i) Equations to be solved

1. Air-volumetric continuity:

$$\frac{\partial R_\ell}{\partial t} + \frac{\partial}{\partial y}(R_\ell v) = 0 \qquad . (5.33)$$

2. Particles-volumetric continuity:

$$\frac{\partial R_d}{\partial t} + \frac{\partial}{\partial y}(R_d V) = 0 \qquad . (5.34)$$

3. Air-momentum conservation equation:

$$\frac{\partial}{\partial t}(R_\ell \rho_\ell v) + \frac{\partial}{\partial y}(R_\ell \rho_\ell v^2) = -R_\ell \frac{\partial P}{\partial y} + f_y^{\ell d}(V-v)$$

momentum accumulation — convection — pressure gradient — inter-phase friction

$$-f_y^{\ell w} v \qquad . \quad (5.35)$$

wall friction

4. Particles-momentum conservation equation:

$$\frac{\partial}{\partial t}(R_d \rho_d V) + \frac{\partial}{\partial y}(R_d \rho_d V^2) = -R_d \frac{\partial P}{\partial y} + f_y^{d\ell}(v-V)$$

$$- R_d(\rho_d - \rho_\ell)g$$

Buoyancy force

. (5.36)

Notes on equations:

- The above equations are expressed in their unsteady forms. For the first two problems considered here, the flow is steady. Thus, the time dependent term is neglected. However, when studying the transient response of the particle motion the full equations are solved.

- The inter-phase friction coefficient is calculated from the Wallis formula (5.8), unless otherwise indicated.

(ii) Initial conditions

Initially, the concentration of both phases is taken as constant along the entire length of the venturi tube. The velocities are inversely proportional to the area. Thus, the concentration and velocity fields satisfy continuity.
A constant slip is also maintained at the start of the computations.

(iii) Boundary conditions

- At inlet:

  All the variables have prescribed values.

- At outlet:

  The outlet section is taken five diameters downstream of the venturi exit where fully-developed conditions are assumed, i.e. $\frac{\partial \phi}{\partial y} = 0$ for all variables.

(iv) Finite-difference grid

A grid consisting of 55 grid nodes was employed for all the problems to be considered. For the transient problem

a time step of 0.001 sec. was selected, since this gave good convergence in the numerical procedure (larger values of the time step have been tried, but the convergence was found to be oscillatory, and for very large values of Δt no convergence was obtained).

(v) Miscellaneous information

For the study of the transient response of particle motion, the information for a typical computational run is tabulated below.

TRANSIENT RESPONSE OF THE PARTICLE MOTION	PERTINENT DATA
Configuration	1-D Circular
Number of grid nodes	55
Grid spacing	Non-uniform
Time step (sec.)	0.001
Number of time steps	300
Number of iterations per timestep*	10
Computational time per grid node per time step CDC 6600 (sec.)	0.0032

TABLE (5-10) INFORMATION ON A TYPICAL COMPUTATIONAL RUN

*For the first seventy time steps 10 iterations were employed; however, the solution was approaching a steady state (as will be discussed later), and only one iteration was needed for the last hundred time steps.

(d) Presentation of the results

The problems considered in this section can be divided into two categories. In the first one we consider the steady flow of air and particles, for different values of the particles size and inter-phase friction coefficient. The second category deals with the transient response of the particles for different flow conditions. The results are not compared with experimental data or analytical solution since none are available. However, the results are discussed with the aim of assessing their plausibility and, at least, their qualitative agreement with currently available knowledge.

(e) Discussion of the results

(i) The influence of particle size

1. Effect on the pressure distribution

Evidently, in any actual sample of particles, the particle size varies over a certain range. In the last section, however, the mass median diameter was used as the best single size with which to represent the whole spread of sizes. In the present section, we will demonstrate the effect of altering the mass median diameter on the pressure distribution; in each case all the particles are

assumed to have a uniform size distribution. The predictions here are made with no slip at inlet between the phases, and the loading ratio is maintained constant. Figures (5-20) and (5-21) show the influence of particle size on the pressure variation for geometries VE1 and VE2 respectively. The graphs indicate that the smaller size particles produce larger pressure drops. It is also to be observed that the minimum pressure drop occurs downstream of the throat (in contrast with single fluid flow). The effect of both particle size and flow boundary becomes apparent when the results depicted in Figures (5-20) and (5-21) are compared.

2. Effect on the velocity distribution

Figure (5-22) shows the effect of varying the particle diameter on both velocity fields. The air stream in the present predictions is not affected by changes in the particle diameter. However, the suspension velocity exhibits a different trend. The figure indicates that the smaller the diameter of the particles, the quicker their response to the flowing air stream. It is also to be observed

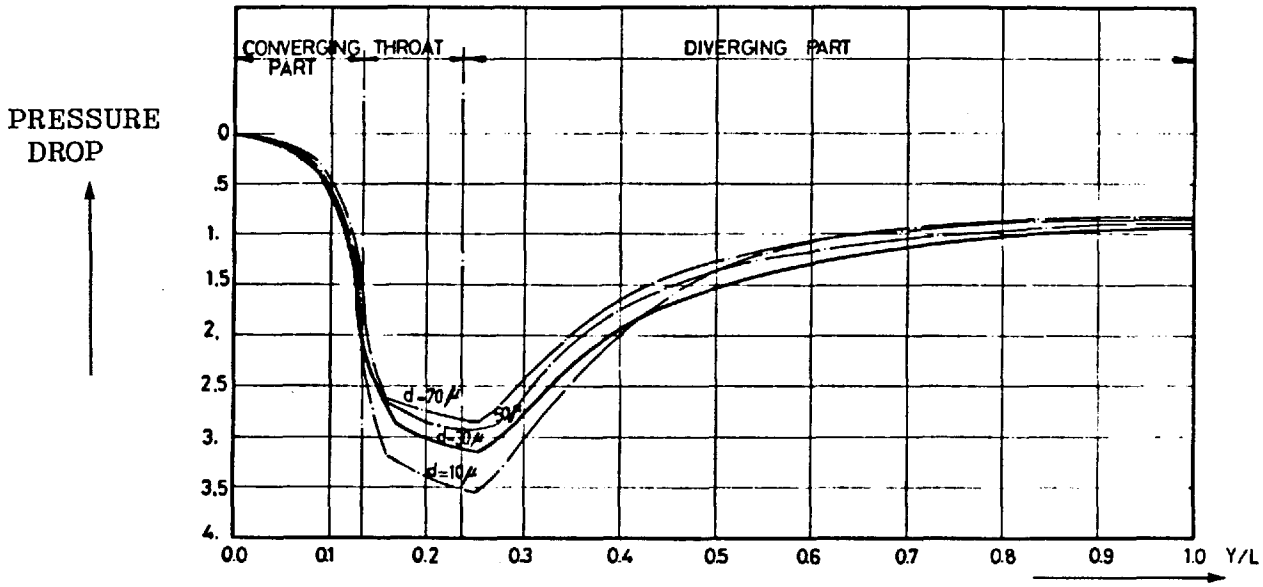


FIGURE (5-20) EFFECT OF VARYING THE PARTICLE SIZE ON THE PRESSURE FIELD; GEOMETRY: VE 1

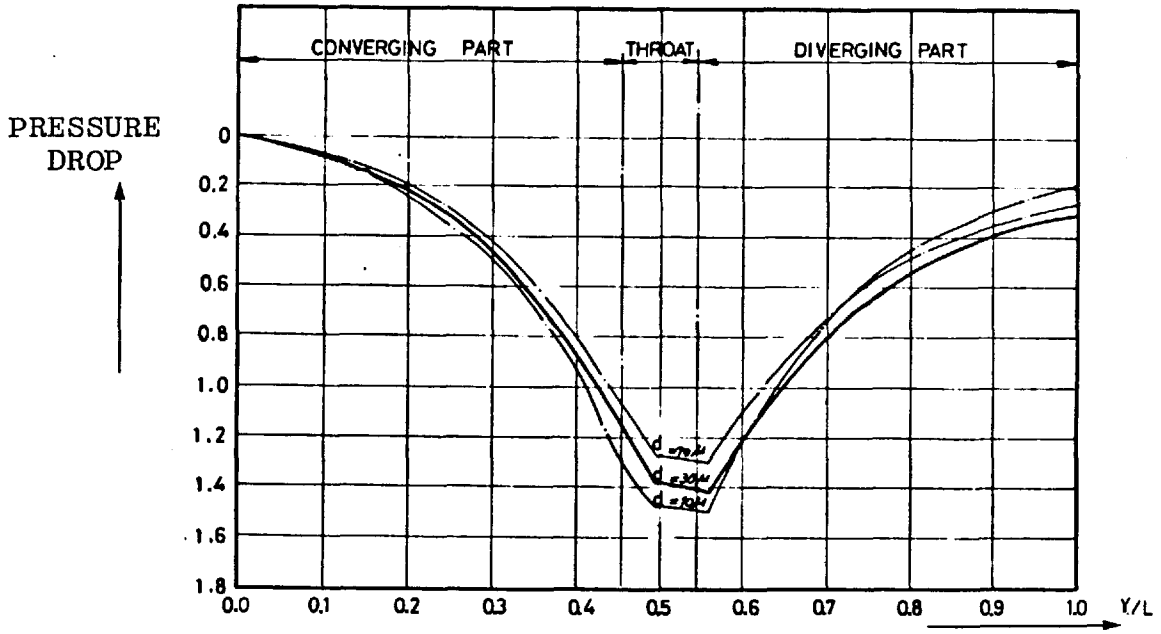


FIGURE (5-21) EFFECT OV VARYING THE PARTICLE SIZE ON THE PRESSURE FIELD; GEOMETRY; VE 2

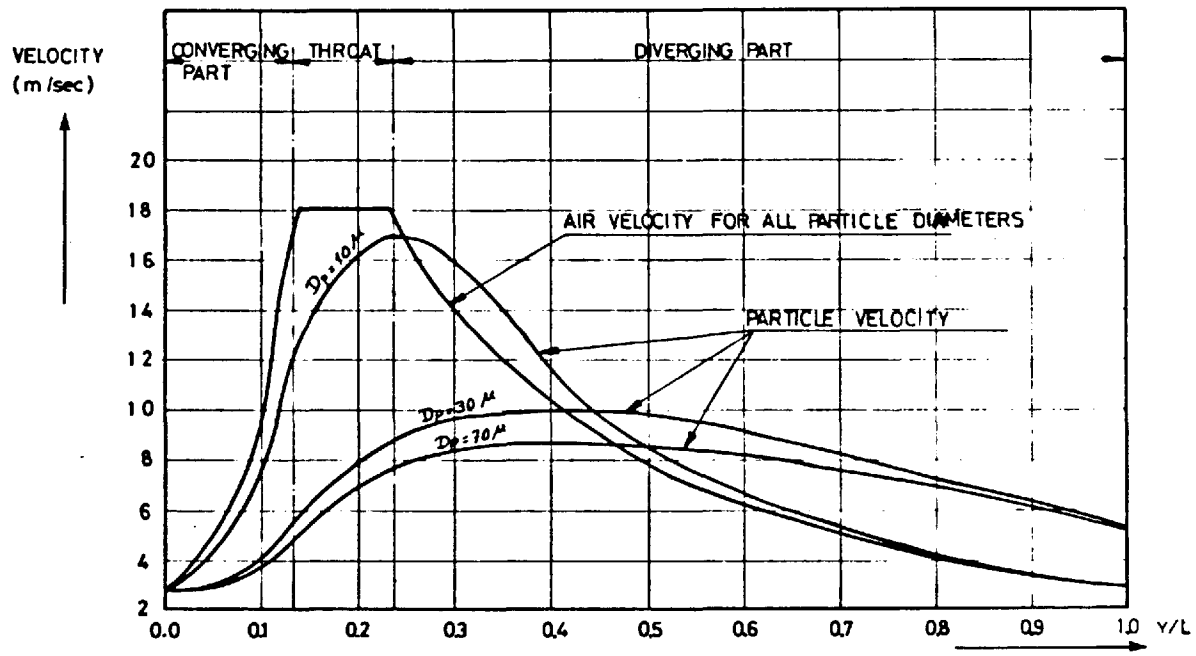


FIGURE (5-22) EFFECT OF VARYING THE PARTICLE SIZE ON THE VELOCITY FIELDS; GEOMETRY: VE 1

that a higher slip between the phases takes place at the throat for the larger particles; this creates an inter-phase frictional force opposing the pressure effects and hence reducing the influence of the latter on the particle motion. It is also to be noticed that the particle velocity exceeds the air velocity in the diffuser part and hence causes the slip to change its direction. Moreover, Figures (5-23) and (5-24) illustrate the different trends in the particle velocity relative to the air stream due to the change in the flow geometry.

(ii) Influence of the inter-phase friction coefficient

In our calculations we have assumed that the inter-phase friction force is expressed by:

$$f_y^{\ell d} = K \quad |v-V| \ (v-V) \ .$$

Here we shall study the effect of varying the parameter K on the two-phase calculations. By assuming an initial slip velocity between the air and the particles

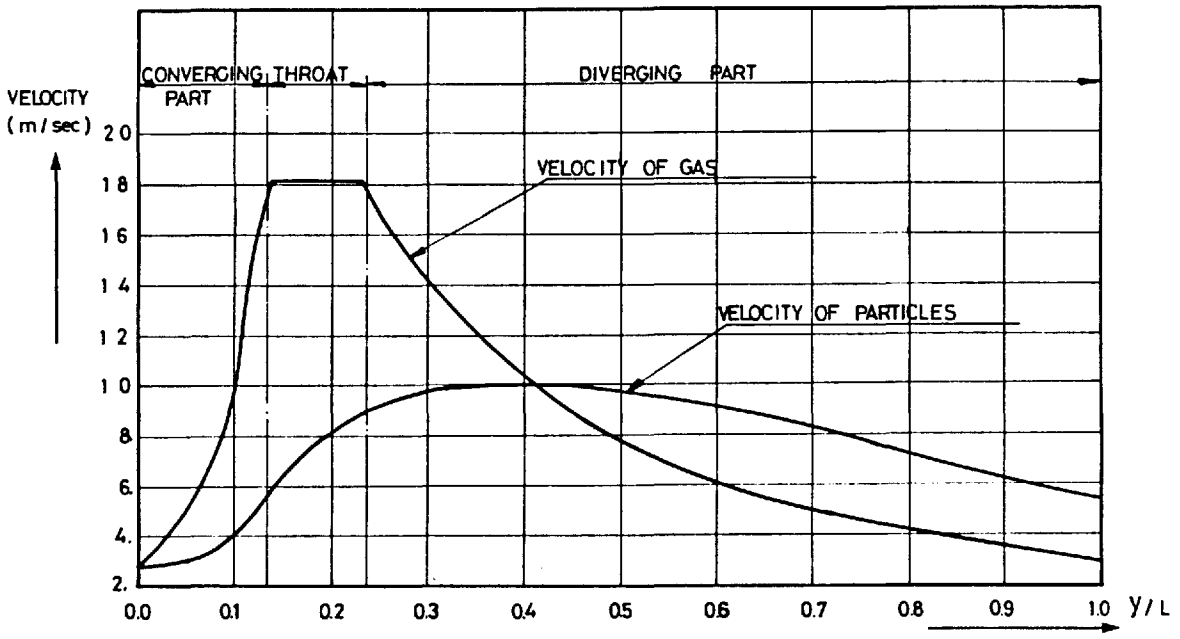


FIGURE (5-23) AIR AND PARTICLE VELOCITY FIELDS; GEOMETRY VE 1

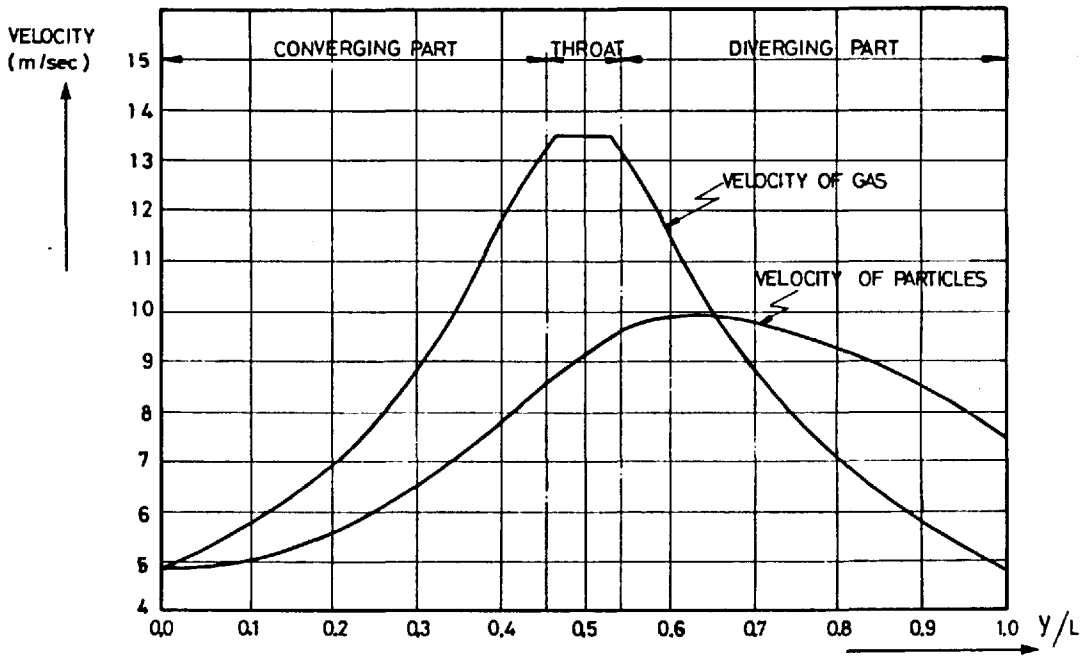


FIGURE (5-24) AIR AND PARTICLE VELOCITY FIELDS; GEOMETRY VE 2

(v = 5 m/s, V = 4 m/s), the velocity fields are computed for three different values of K, namely 10^6, 800 and 200 $N/m^3/m$. The results are plotted in Figure (5-25), (the results relate to the VE2 geometry). It is to be noticed that for the nearly infinite value (10^6) the particles have exactly the same velocity as the air; no slip occurs, i.e. the flow is of the homogeneous type. It is also to be observed that a decrease in K gives the particles an independent hydrodynamic behaviour and the coupling effect is manifested by the appearance of a variable slip velocity. For the lower value of K the change in slip is more significant, c.f. Figure (5-26) (the slip velocity is normalised with respect to the terminal velocity $V_T = d^2 g (\rho_d - \rho_\ell)/18$

= 120 m/sec for this case).

Finally, the influence of K on the concentration of the particles is displayed in Figure (5-27). It is to be observed that for the case of the homogeneous flow, K = 10^6, the concentration, as expected, does not vary along the venturi tube (single-phase

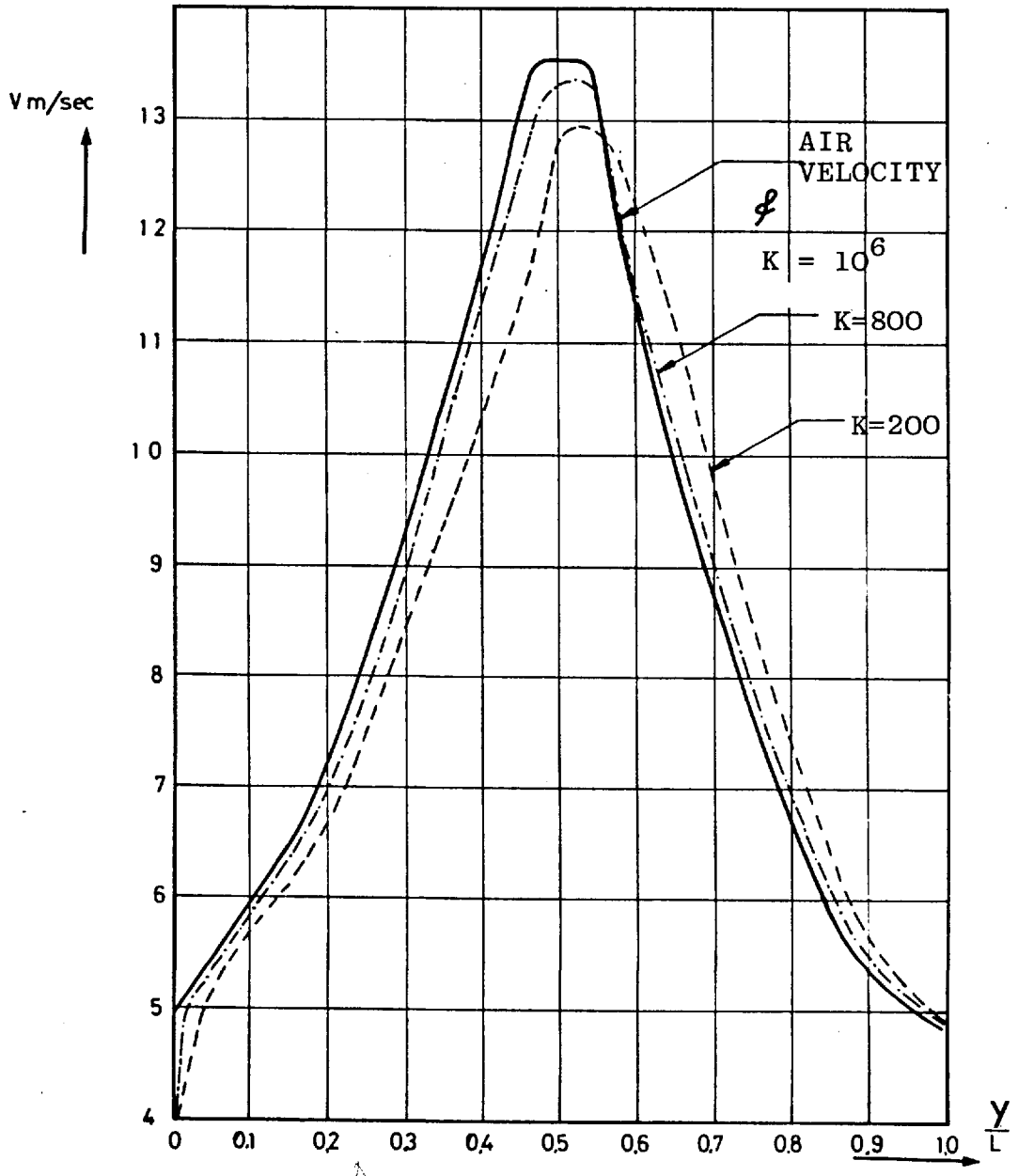


FIGURE (5-25) STEADY-STATE VELOCITY DISTRIBUTION FOR DIFFERENT INTERPHASE FRICTION COEFFICIENT

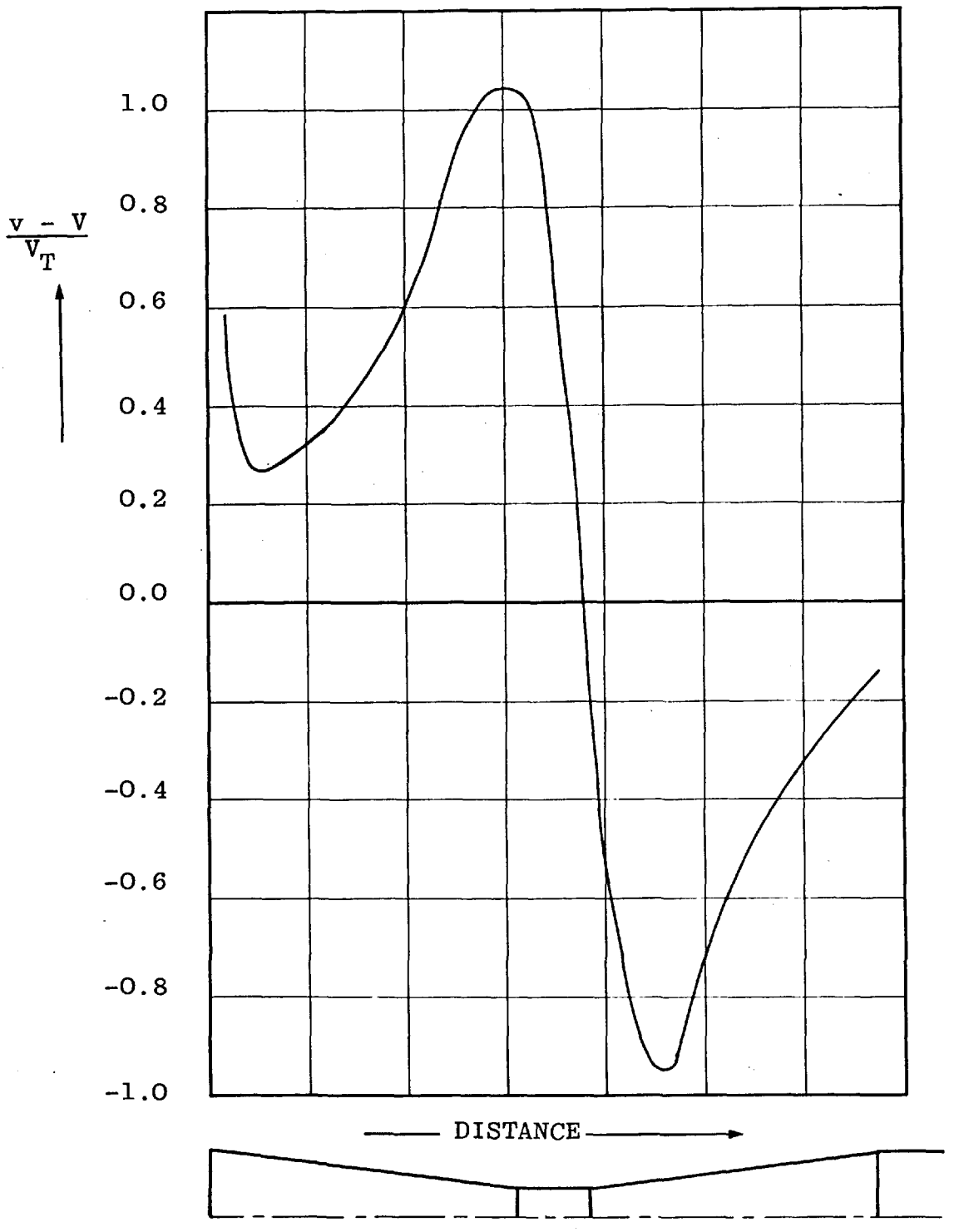


FIGURE (5-26) VARIATION OF THE SLIP VELOCITY ALONG THE VENTURI LENGTH FOR K = 200

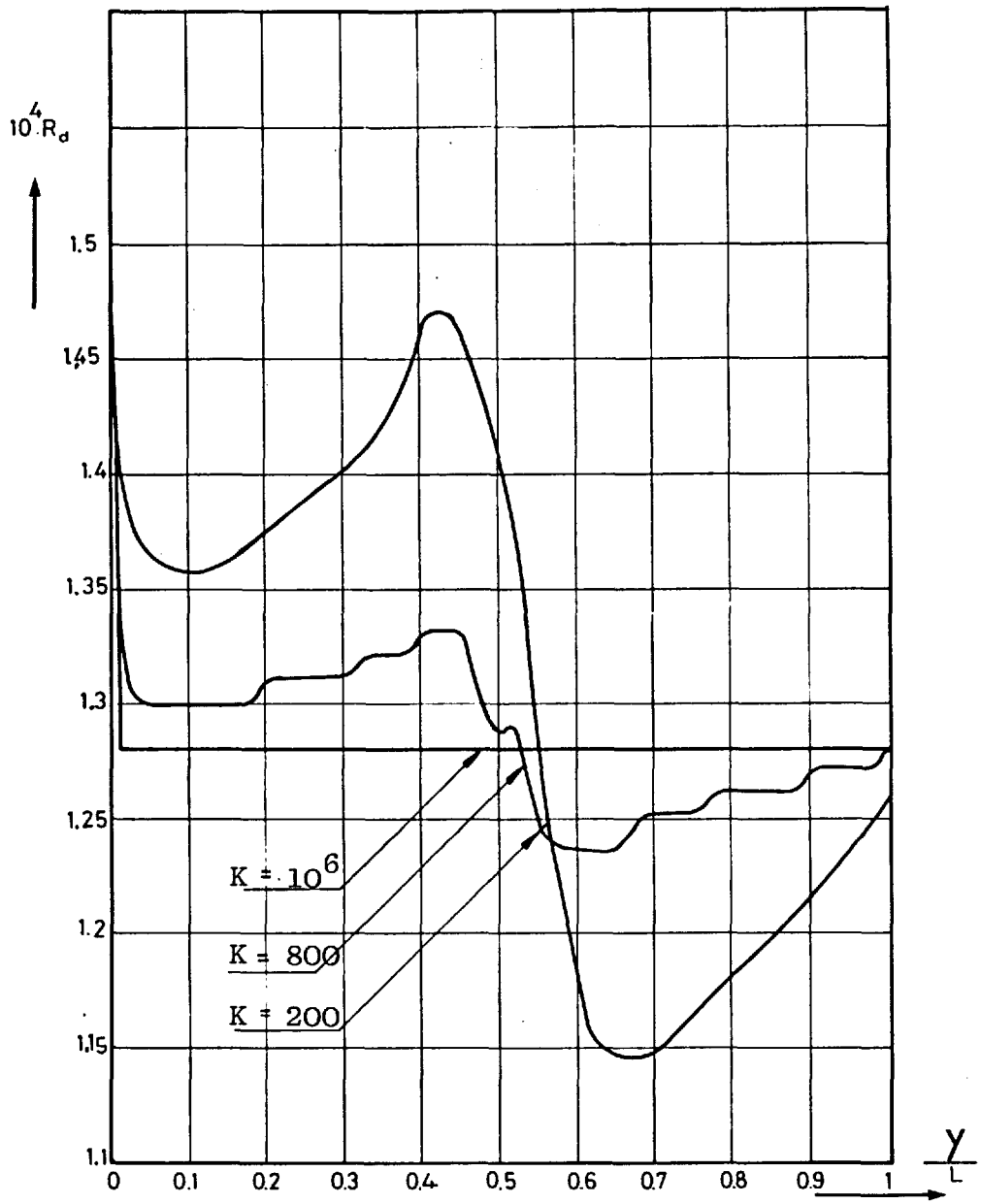


FIGURE (5-27) PARTICLES CONCENTRATION DISTRIBUTION FOR DIFFERENT VALUES OF (K)

flow behaviour). When K decreases, the concentration attains a maximum value near the throat; this fact was confirmed experimentally by visual observation (Sharma, 1977); by comparing the results of Figures (5-26) and (5-27), it is seen that the behaviour of R_d and the slip along the venturi tube exhibits similar trends.

(iii) Transient response of the particle motion

In order to demonstrate the unsteady behaviour of the particles under various conditions we have chosen to investigate the flow variables for two different values of the inter-phase friction parameter, namely K = 200 and 1000 $N/m^3/m$.

For the dilute suspension ($R_d = 1.6 \times 10^{-4}$) under consideration, it was shown that the air velocity is not affected by the changes in particle size. The air velocity is independent of time as demonstrated by Figure (5-28). Figure (5-29) illustrates the influence of the parameter K on the variation in the particle velocity with time. From the definition of K and either from equations (5.3) or (5.8) it is apparent that K is

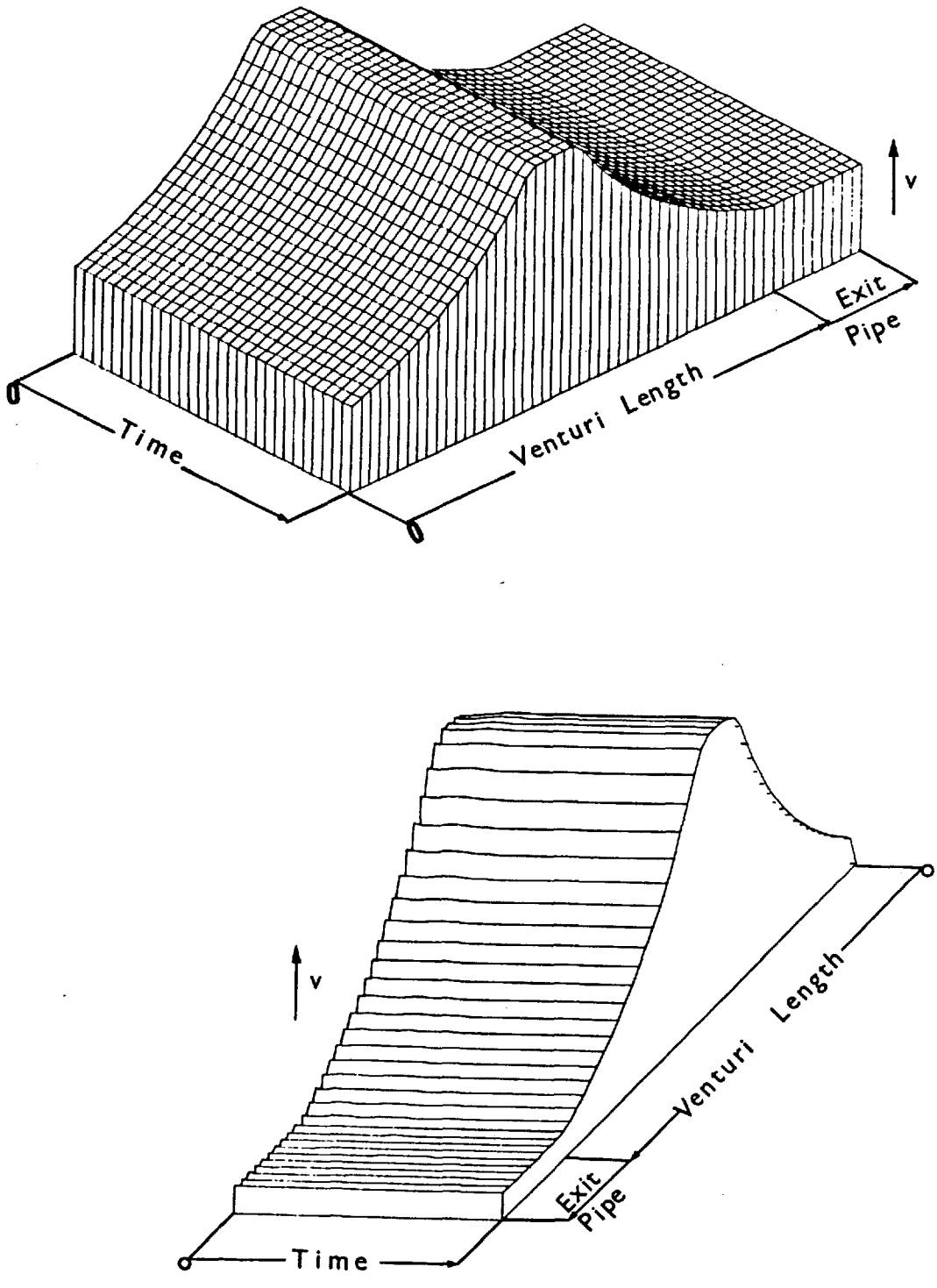
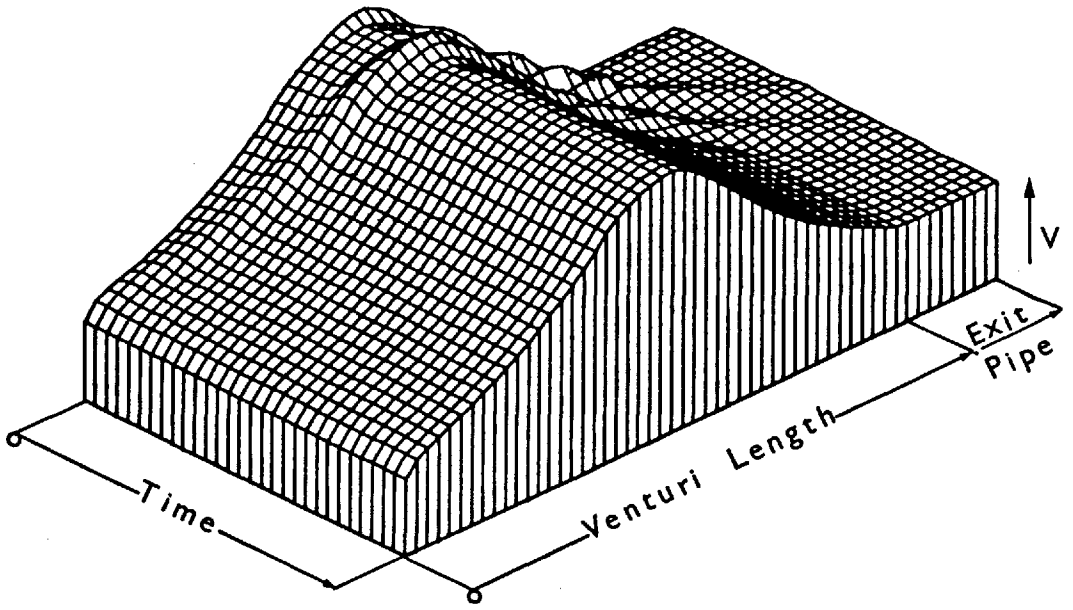
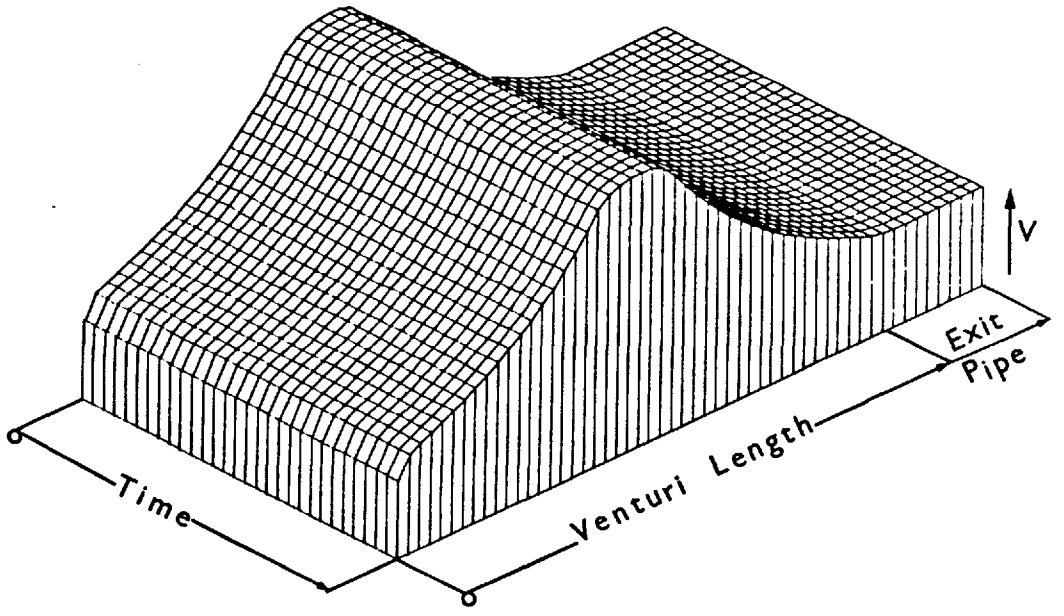


FIGURE (5-28) PERSPECTIVE VIEW OF THE AIR VELOCITY DISTRIBUTION ALONG THE VENTURI TUBE FROM TWO DIFFERENT ANGLES



K = 200



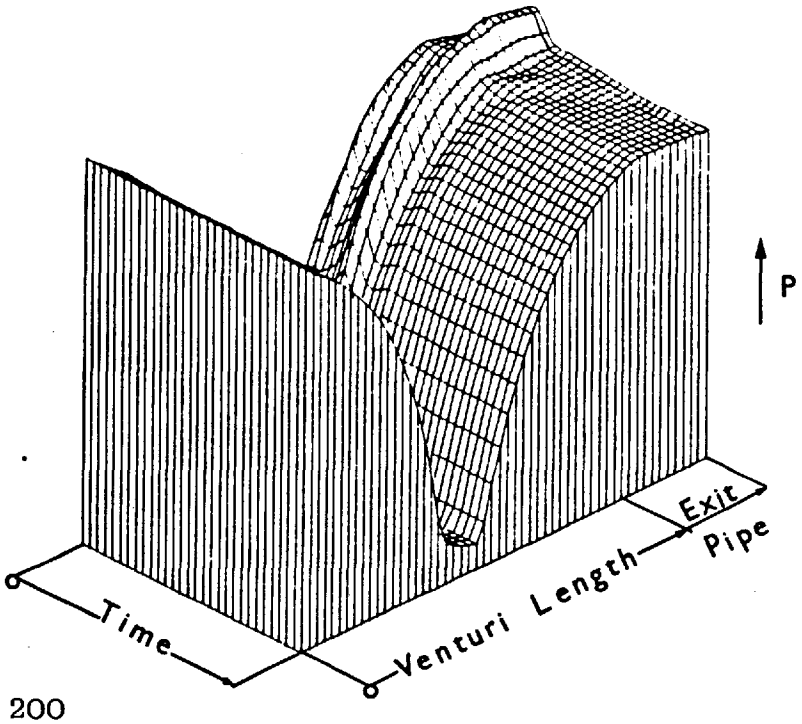
K =1000

FIGURE (5-29) PARTICLE VELOCITY DISTRIBUTION FOR DIFFERENT VALUES OF K

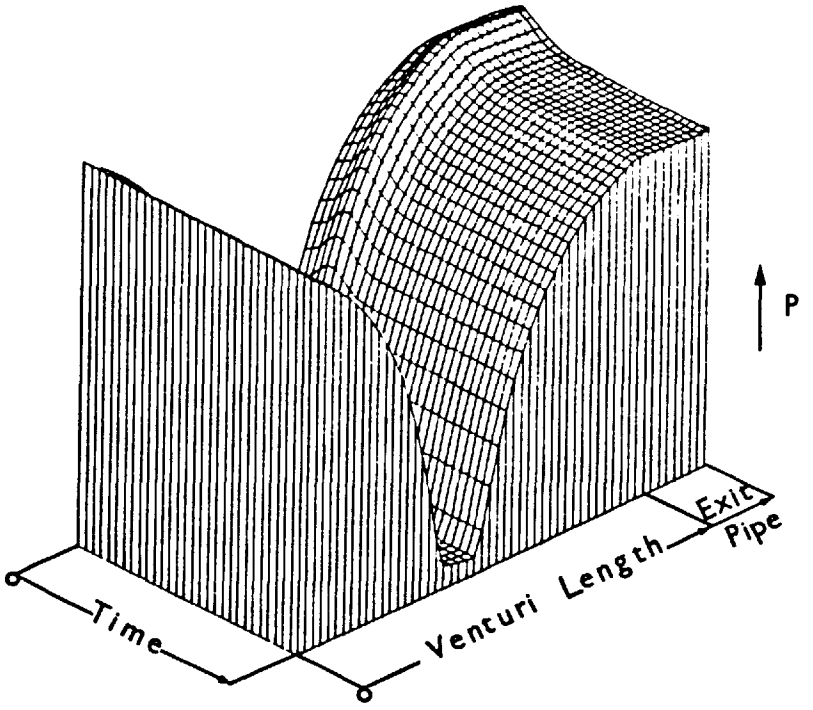
inversely proportional to the diameter of the particles raised to a certain positive power dependent on the Reynolds number. Also, from the same figure, it may be observed that the larger the diameter of the particles (or equivalently, the smaller the K value) the greater is their acceleration; this is particularly noticeable at the diverging section of the venturi. It is clear that large particles take a long time to attain a steady state. The time required for particles to reach an equilibrium position is known as the "relaxation time". For particles accelerating in laminar flows the time constant related to velocity relaxation, denoted t_v, is given (Wallis 1969) by:

$$t_v = \frac{d^2 \rho_d}{18\mu} \quad .$$

The above relation shows that the larger the particle diameters the longer their relaxation time; this confirms our observation, at least qualitatively. Figure (5-30) displays the fact that the larger diameter of the particles the greater their effect on pressure variation.



K = 200

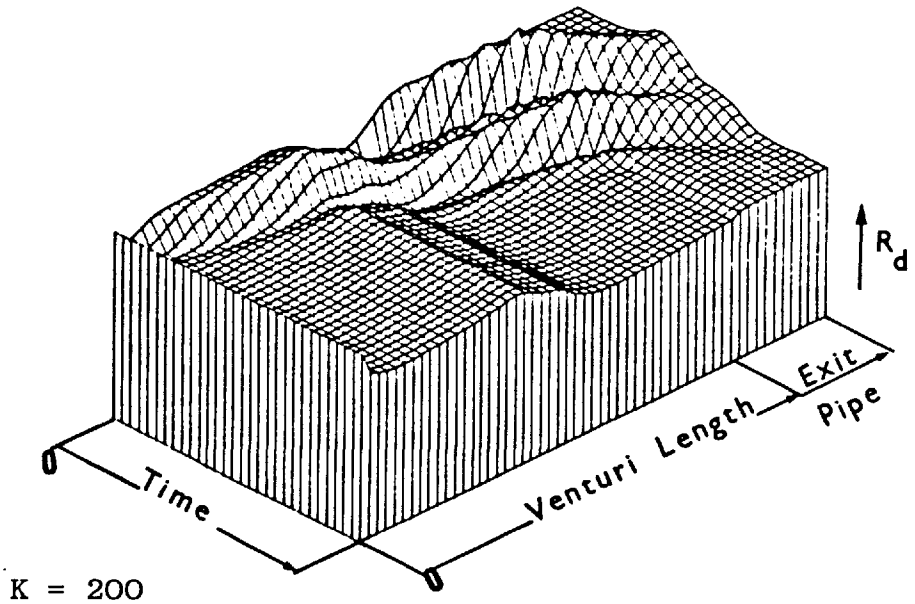


K = 1000

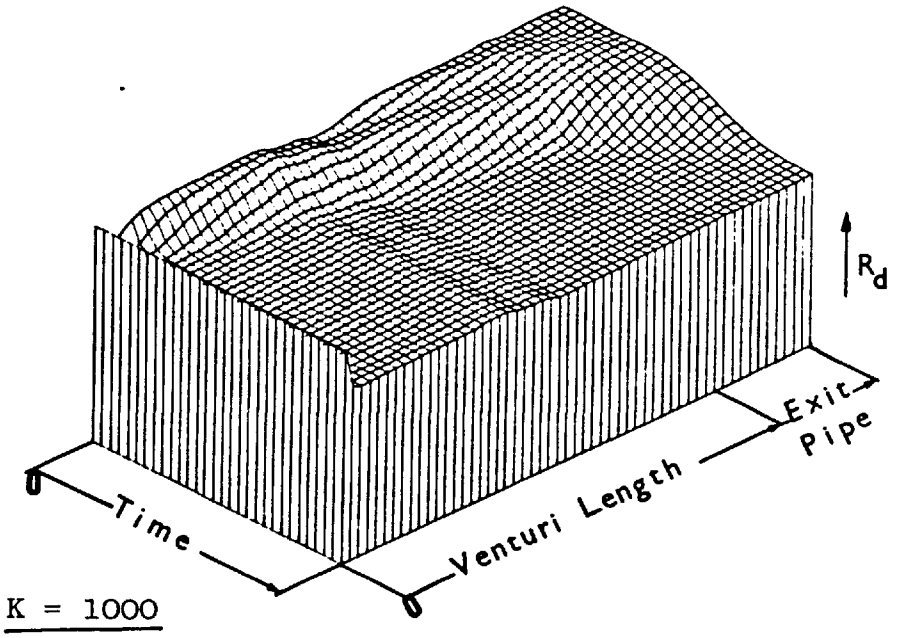
FIGURE (5-30) PRESSURE DISTRIBUTION FOR DIFFERENT VALUES OF K

It is to be noticed that the non-uniform pressure rise, occurring in the diverging part of the venturi, is compensated by a positive drag force (here the particle velocity exceeds the air velocity). This explains the steady behaviour of the air velocity, c.f. Figure (5-29).

Finally, Figure (5-31) represents the variation in the concentration corresponding to two different values of K. It is seen there, that the larger particles have a larger relaxation time and that their presence causes a more significant variation in the concentration than the smaller sized particles. Figures (5-29) to (5-31) demonstrate that the higher the K value the larger the internal friction, i.e. the stronger the coupling. In the limit when K tends to an infinite value (i.e. the particle size is extremely small) the flow tends to homogeneity (with no slip).



K = 200



K = 1000

FIGURE (5-31) THE CONCENTRATION DISTRIBUTION OF THE PARTICLES FOR DIFFERENT VALUES OF K

5.6 CONCLUDING REMARKS

- The results presented in this chapter demonstrate the flexibility of the "IPSA" model in producing accurate and realistic solutions for particulated flows. The investigation also considered certain flow situations which are of scientific and engineering interest and for which no experimental data are at present available. In the latter case, the current predictions seem plausible (they agree qualitatively with what scant theoretical knowledge there is).

- The mathematical difficulties involved in solving the differential equations of two-phase flow have been surmounted. The present predictions although made for simple interactions between the phases (no phase change and no inter-particle forces were accounted for), indicate that the numerical algorithm is stable and yields accurate results as the grid is suitably refined.

- Regarding the economy of the present procedure, comparison was made between the "SATURN" computer code (used in this work) and the "CONVAS" program used by Sharma (1977). Both computer programs are one-dimensional and based on finite-difference iterative procedures. However, the present computer code uses 16448 bytes of core while "CONVAS" requires 32000 bytes. This means that the "SATURN" code needs only about half the storage

employed by "CONVAS". Also, the present program consumes about 80% of the computer time required by the code of Sharma (1977).

• In the next chapter, the predictive power of the present model will be tested by solving the equations for stratified flows. This class of flow belongs to a different category, clearly distinct from the particulated flows, because of the totally different mechanism of interaction occurring among the phases. Evidently this class provides further testing ground for the model and enables us to see how far its versatility stretches.

CHAPTER 6

STRATIFIED-FLOW CALCULATIONS

6.1 INTRODUCTION

6.1.1 General Background

Simultaneous flows of gases and liquids occur in numerous pieces of engineering equipment such as boiler and refrigerator tubes, oil and natural gas pipelines. The stratified flow pattern takes place in approximately horizontal flow passages when the superficial liquid velocity* is below 0.2 m/sec. and that of the gas ranges between 0.6 to 3 m/sec.; depending upon the liquid rate, its flow may be in either laminar or turbulent motion but the gas is normally in turbulent flow.

Due to gravity effects, gradients at the interface introduce additional forces on the fluids, and wave-propagation can thereby be initiated. Any mechanistic model ought to take into account gravity-wave phenomena, since ignoring their effects can lead, in some circumstances, to radically incorrect predictions.

6.1.2 Content of the Chapter

In this chapter the additional terms linking the interface gradient, the pipe inclination and the gradient

---

*The product of the phase velocity and its volume fraction.

in the liquid volume fraction are incorporated; the resulting finite-difference modifications made to the solution procedure in order to obtain accurate and realistic preditions are presented. Accuracy of the solution procedure is checked by comparing predictions with analytical solutions; their physical reality is assessed by comparison with experimental data; finally, the flexibility of the solution algorithm is demonstrated by solving various problems of engineering interest.

6.2 MATHEMATICAL DESCRIPTION

The continuity equations are expressed, in their conventional form, without modifications. On the other hand the momentum equation of the liquid phase will be subject to modifications: new terms will be incorporated to take into account the induced gravity waves.

In its one-dimensional form the gas momentum equation reads:

$$\underset{\substack{\downarrow \\ \text{momentum} \\ \text{accumulation}}}{\frac{\partial}{\partial t}(R_\ell \rho_\ell v)} + \underset{\substack{\downarrow \\ \text{convection}}}{\frac{\partial}{\partial y}(R_\ell \rho_\ell v^2)} = \underset{\substack{\downarrow \\ \text{pressure} \\ \text{gradient}}}{- R_\ell \frac{\partial P}{\partial y}} + \underset{\substack{\downarrow \\ \text{inter-phase} \\ \text{friction}}}{f_y^{\ell d}(V - v)} \underset{\substack{\downarrow \\ \text{wall} \\ \text{friction}}}{- f_y^{\ell w} v} \quad . \quad (6.1)$$

The momentum equation for the liquid phase now becomes:

$$\frac{\partial}{\partial t}(R_d\rho_d V) + \frac{\partial}{\partial y}(R_d\rho_d V^2) = -R_d\frac{\partial P}{\partial y} + f_y^{d\ell}(v - V)$$

$$- f_y^{dw} V - R_d(\rho_d - \rho_\ell)g\cos\alpha\frac{\partial h}{\partial y}$$

$$\downarrow$$

interfacial inclination

$$- R_d(\rho_d - \rho_\ell)g\sin\alpha \qquad , (6.2)$$

$$\downarrow$$

pipe line inclination

where h is the liquid height. (It is a function of its concentration);

α is the angle of pipe inclination;

the other symbols used in equations (6.1) and (6.2) have the same meaning as in chapter 2. The derivation of the extra terms arising from the gravity stratification is given in Appendix B.

6.2.1 Treatment of Inter-phase and Wall Friction

At present, the friction factors are calculated from simple empirical correlations, which are valid for smooth pipes and interface-surfaces. These empirical formulae have been widely reviewed in the work of Solbrig et al (1975); no account of transient effect, has been reported, in formulating the expressions for the friction-factor correlations. In this work we shall employ the existing one-dimensional correlations; they may be easily replaced by more general or

more specific formulae that may become available from future experimental investigations.

(i) Wall Friction Factors

The gas-to-wall and liquid-to-wall friction factors are calculated from the same correlations used in single-phase theory.

(a) For Laminar Flows $R_e \leq 2000$

$$f = \frac{16}{(R_e)_\ell} \quad , (6.3)$$

$$f = \frac{16}{(R_e)_d} \quad , (6.4)$$

$(R_e)_\ell$ and $(R_e)_d$ are the Reynolds numbers based on the light and dense phase properties respectively. The characteristic length used in the Reynolds number expression is the hydraulic mean diameter.

$$D_i = \frac{4 \times (\text{Cross-sectional area of phase i})}{(\text{Wetted perimeter of phase i})}$$

(b) For Turbulent Flows (Blasius Relation)

$$f = 0.079/(R_e)_\ell^{0.25} \quad , (6.5)$$

$$f = 0.079/(R_e)_d^{0.25} \quad . (6.6)$$

The Reynolds numbers are defined as for laminar flow and so is the hydraulic mean diameter; however, these formulae are valid for the range of $R_e \geq 2800$.

(ii) Inter-phase Friction Factor

The interface is assumed to be hydrodynamically smooth and the empirical correlation of Ellis and Gay (1959)* also used by Agrawal et al (1973) is employed in the course of this work:

$$f = 1.293/(R_e)_\ell^{0.57} \qquad \cdot (6.7)$$

The inter-phase friction force per unit volume of the mixture, $F_y^{\ell d}$ may be expressed as being proportional to the square of the relative velocity between the phases, thus:

$$F_y^{\ell d} = \frac{1}{2} \rho_\ell f A'' |v - V|(v-V) \quad ,$$

where A'', the interface area per unit volume, is given by

$$A'' = \frac{\text{contact area between the phases}}{\text{volume of the passage}} \quad .$$

Thus the friction factor, f, is related to the friction coefficient, $F_y^{\ell d}$, through:

$$f_y^{\ell d} = \frac{1}{2} \rho_\ell f A'' | v - V | \quad .$$

6.2.2 Two-Variable Adjustment (IPSA-TV)

The extra terms accounting for the gravity effects are often of a much bigger influence on the heavy-fluid motion than the pressure term, especially when densities differ greatly. Because the concentration gradients, $\frac{\partial R_d}{\partial y}$,

*This correlation is recommended for a laminar flow of the liquid and a turbulent flow of the gas.

are the driving potential for the liquid momentum, rather than the pressure gradients, the new terms bring a new link between V and R_d; consequently the continuity errors are best adjusted by seeking a correction based on R_d, rather than the pressure, or better still on both simultaneously. This fact carried the suggestion of devising a "Two-Variable" adjustment technique suitable for the stratified flow application. The method is detailed in the point below.

(a) The momentum equations (6.1) and (6.2) in their finite-difference forms read:

$$v_P = \sum_{i=N,S} a_i v_i + D^V(P_N - P_p) + b \quad , (6.8)$$

$$V_P = \sum_{i=N,S} A_i V_i + D^V(P_N - P_p) + E^V(h_N - h_p) + B \quad , (6.9)$$

where a_i's and A_i's are the finite-difference coefficients as defined in chapter 3; the source terms are represented by b and B respectively; in addition to the previously defined D^v and D^V terms a new differential term E^V is included in equation (6.9) to account for the rate of change in the liquid-velocity to the liquid-height, $\frac{\partial V}{\partial h}$. Since the height of the liquid is a function of both the position and its concentration, it is possible to express the new term as:

$$E^V (R_N - R_P) + G \quad , (6.10)$$

which is a linearised form suitable for the numerical procedure. In (6.10), R_i represents the liquid volume fraction, this notation will be followed to the end of this section.

(b) For simultaneous satisfaction of the conservation laws, we eliminate the errors using two correction-equations. The correction variables*, p'' and R'', are introduced to correct the driving potential of the velocity fields v and V, namely the pressure and concentration gradients. Following the same reasoning adopted in formulating the pressure-correction equation one may obtain the following two equations.

(i) Gas Correction Equation

$$a_P\, p''_P = a_N\, p''_N + a_S\, p''_S \qquad . (6.11)$$

The coefficients are calculated precisely as for equation (3.22).

(ii) Liquid Correction Equation

$$B_P\, R''_P = B_N\, R''_N + B_S\, R''_S - (a_P\, p''_P - a_N\, p''_N - a_S\, p''_S) \qquad , (6.12)$$

where

$$B_P \equiv B_S + B_N \qquad .$$

---

*p'' is a pressure correction variable exactly as was p'. The extra prime is to refer to the stratified flow situation.

Here the coefficients B_i represent the variation in the height with respect to the concentration. Let h and R be the liquid height and concentration calculated at point P; thus:

$$R_i = \frac{\partial h}{\partial R_{i,*}} = \frac{\partial h}{\partial R_{**}} \quad \frac{\partial R_{**}}{\partial R_{i,*}} \qquad (6.13)$$

In equation (6.13) we distinguish between R_{**} resulting from the solution of the continuity equation and $R_{i,*}$, the guessed value of R_{**} used in the momentum equation. The term $\frac{\partial h}{\partial R_{**}}$ is a function of the geometry; for example, for a plane channel it is constant since R_{**} varies linearly with h. To facilitate its evaluation, the second term is expanded as:

$$\frac{\partial R_{**}}{\partial R_{i,*}} = \frac{\partial R_{**}}{\partial V_i} \cdot \frac{\partial V_i}{\partial R_{i,*}} \qquad . \quad (6.14)$$

By adopting the same practice as in chapter 3, for calculating the finite-difference coefficients; the term, $\frac{\partial R_{**}}{\partial V_i}$, is derived from the continuity equation and the term $\frac{\partial V_i}{\partial R_{i,*}}$ is computed via the momentum equation.

The correction equations (6.11) and (6.12) are solved iteratively and the resulting correction variables p'' and R'' will be used in adjusting

the field values of the velocity and the concentration as usual (chapter 3 and 4). However, because of the appearance of new terms accounting for the concentration gradients, the liquid velocity fields are corrected using a new form of the truncated momentum equation, thus:

$$V_P = V_P^* + \hat{D}^V(p''_P - p''_N) + E^V(R''_P - R''_N) \qquad . (6.15)$$

(c) The calculation sequence when using IPSA-TV is briefly outlined in the following steps:

(i) Prescribe the solution domain and the finite-difference grid.

(ii) Prescribe initial conditions for all the flow variables at time t = 0.

(iii) Solve the momentum equations using R_* values.

(iv) Solve the continuity equations to obtain R_{**} values.

(v) Eliminate the errors $(1-R_{\ell,**} - R_{d,**})$ by setting up and solving equations for the corrections p'' and R''.

(vi) Correct the velocity and concentration fields.

(vii) Repeat steps (iii) and (vi) until convergence is secured.

(viii) Advance in time, while iterating in each time step until the transient has been sufficiently studied.

6.3 PREDICTIONS FOR COMPARISON WITH ANALYTICAL RESULTS

The prediction of wave motion in stratified, two-phase flows is of great practical interest; for example, wave-motion in pipelines transporting mixtures of gas and liquid is of considerable importance. In the present section two idealised flows, for which analytical solutions are available, are used to validate the IPSA-TV solution procedure. The problems considered are:

(i) Wave-propagation in a confined plane channel;

(ii) Wave-formation in a plane channel which has only one end closed.

Both these problems are examples of transient, one-dimensional stratified, two-phase flows.

6.3.1 Wave-Propagation in a Confined Plane Channel

The interest in solving the problem of the wave-propagation in a closed channel stems mainly from the fact that there exists an exact solution for the frictionless motion. Thus, for the case of inviscid flow, it is possible to assess the accuracy of the numerical predictions. Moreoever, the effect of friction is studied here without reference to analytical solutions since none are available. The flow situation is also of particular interest in that it permits an exclusive test for the simulation of "dynamic wave propagation" in stratified flow regimes.

The layout of the study comprises: the statement of the objectives, the presentation of the problem, the details of the computation, the presentation of the results and then the discussion.

(a) Objectives of the study

(i) To evaluate the accuracy of the computed results by comparing them with the exact solution that is available only for frictionless motion.

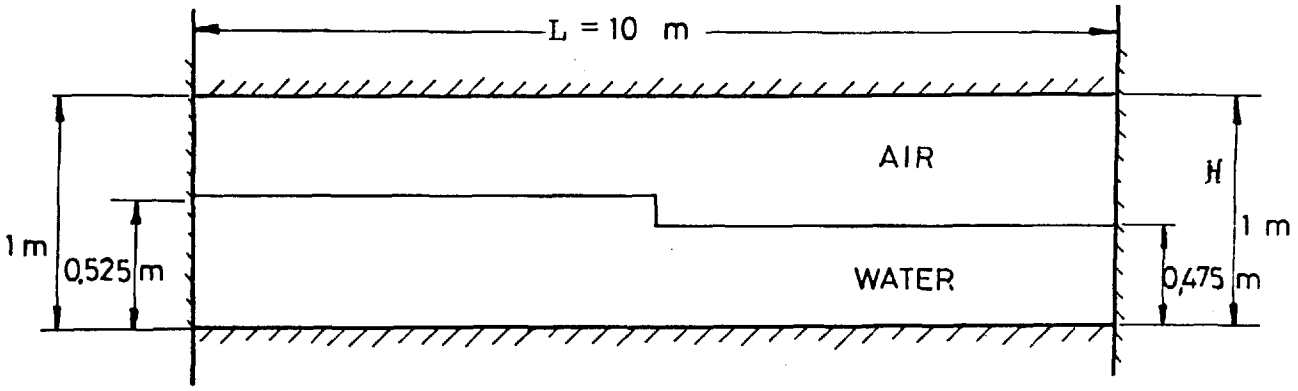
(ii) To examine the effect of friction with especial reference to the inter-phase friction at the air-water interface.

(iii) To investigate the sensitivity of the numerical procedure to grid and time-step refinement.

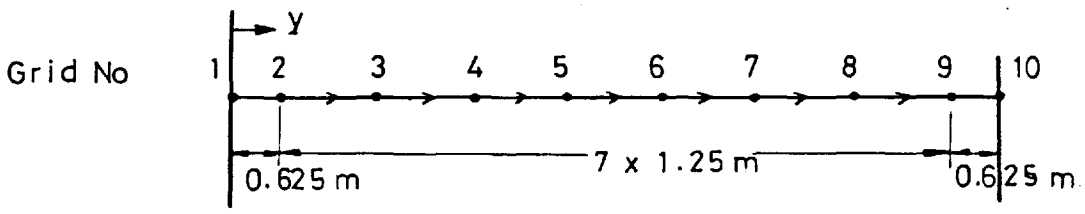
(b) Presentation of the problem

(i) Statement of the problem

The flow situation is shown in figure (6-1). At the initial instant (t = 0), both fluids (water and air) are stationary, and the interface has a discontinuity at the mid-section of the channel. As a result of the initial gradient in the liquid-height a wave is expected to travel in both directions, from the mid-section, and will be reflected from both ends. The problem is to compute the wave-speed by



(a) THE FLOW GEOMETRY



(b) THE GRID ARRANGEMENT

FIGURE (6-1) THE CLOSED-CHANNEL INITIAL-DISCONTINUITY PROBLEM

means of a one-dimensional analysis of the transient response of the flow.

(ii) Qualitative description

The flow situation under consideration is analogous to a shock-tube problem owing to the fact that a finite discontinuity is propagated, by both the compression and the rarefaction wave fronts, in opposite directions. In the absence of friction, the air-water interface will continue to "slosh", with a fixed frequency.

(iii) Quantitative description

The speed, C, at which the wave travels is obtained from theoretical considerations (small amplitude waves, Wallis (1969)) viz.

$$C = \sqrt{\frac{(\rho_d - \rho_\ell)\, gH}{\left(\frac{\rho}{R}\right)_d + \left(\frac{\rho}{R}\right)_\ell}} \quad ; \quad (6.16)$$

in deriving the above formula for the wave-speed, the motion was assumed to be frictionless.

(c) Details of the present computations

(i) Equations to be solved

1. Gas-volumetric continuity:

$$\frac{\partial R_\ell}{\partial t} + \frac{\partial}{\partial y}\,(R_\ell v) = 0 \quad . \quad (6.17)$$

2. Liquid-volumetric continuity:

$$\frac{\partial R_d}{\partial t} + \frac{\partial}{\partial y} (R_d V) = 0 \qquad . (6.18)$$

3. Gas-momentum conservation equation:

$$\frac{\partial}{\partial t} (R_\ell \rho_\ell v) + \frac{\partial}{\partial y} (R_\ell \rho_\ell v^2) = -R_\ell \frac{\partial P}{\partial y} + f_y^{\ell d} (V-v)$$

↓ momentum accumulation; ↓ convection; ↓ pressure gradient; ↓ inter-phase friction

$$- f_y^{\ell w} v \qquad . (6.19)$$

↓ wall friction

4. Liquid-momentum conservation equation:

$$\frac{\partial}{\partial t} (R_d \rho_d V) + \frac{\partial}{\partial y} (R_d \rho_d V^2) = -R_d \frac{\partial P}{\partial y} + f_y^{d\ell} (v-V)$$

$$-f_y^{dw} V - R_d (\rho_d - \rho_\ell) g \cos \frac{\partial h}{\partial y} \qquad . (6.20)$$

↓ gravity force due to interfacial inclination

Notes on equations:

- The volume fractions must satisfy the geometrical condition, viz.

$$R_\ell + R_d = 1 \qquad .$$

- For the inviscid flow computations, frictional forces, both at the air-water interface and the channel surfaces, are neglected.

- When frictional effects are taken into account:

  (1) the wall friction factors will be deduced (equations (6.3) and (6.4)) by analogy with single-phase flow which is the existing situation near the wall boundaries;

  (2) the inter-phase friction factor will be calculated from the empirical correlation (6.7) developed by Ellis and Gay (1959) and from a theoretical formula derived in the course of this work as will be detailed later in this section.

(ii) Initial conditions

- for the concentrations

$R_d\ (y,0) = 0.525$; $R_\ell\ (y,0) = 0.475$ for $y \leq 5$ m

$R_d\ (y,0) = 0.475$; $R_\ell\ (y,0) = 0.525$ for $y > 5$m

- for the velocities

$V\ (y,0) = v(y,0) = 0.$

(iii) Boundary conditions

- at y = 0

$$\frac{\partial R_d}{\partial y}(0,t) = \frac{\partial R_\ell}{\partial y}(0,t) = 0.$$

$$V(0,t) = v(0,t) = 0.$$

- at y = L

$$\frac{\partial R_d}{\partial y}(L,t) = \frac{\partial R_\ell}{\partial y}(L,t) = 0.$$

$$V(L,t) = v(L,t) = 0.$$

The above differential equations are transformed to their finite-difference equivalents and the resulting set of equations are solved using the "IPSA-TV" algorithm (section 6.2.2).

(iv) Finite-difference grid

In order to examine the effect of grid size on the numerical solution, five different grids, containing respectively 10, 20, 30, 40 and 50 nodes were employed. The grid distribution along the flow domain, for a grid consisting of 10 nodes is illustrated in Figure (6-1).

(v) Time step

The time increment employed, Δt, was related to the grid size, Δy, and the wave speed, C, via the Courant number, λ, defined by

$$\lambda \equiv C/(\frac{\Delta y}{\Delta t}) \quad .$$

The effect of the time step on the numerical prediction was studied by considering four different values of the Courant number namely: 0.2, 0.6, 1.2 and 2.0; in each case the grid size was maintained constant.

(vi) Miscellaneous information

Typical information on a particular run is given below in Table (6-1).

WAVE MOTION IN THE CONFINED CHANNEL	PERTINENT DATA
Configuration	Plane
Number of grid nodes	50
Type of grid spacing	Uniform
Grid size per unit length of the channel	0.02083
Time step Δt (sec.)	0.02
Courant number	0.2
Number of time steps	330
Number of iterations per time step	20
Computational time per grid node per time step CDC 6600 (sec.)	0.031

TABLE (6-1) TYPICAL INFORMATION ON COMPUTATIONAL RUN

(d) Presentation of the results

Computations have been performed both with and without friction (fluid-to-fluid and fluid-to-solid). The behaviour of the system, for the case of zero friction, is illustrated in Figure (6-2). The depicted results are typical examples of liquid-height, pressure and velocity distributions; they confirm the qualitative description of the problem, in that two disturbances propagate in opposite directions from the centre of the pipe which is apparent from both concentration and pressure distributions. It is also to be noted that both fluids move in opposite directions and that the product of the velocity and the concentration of each of the phases is constant (volumetric continuity satisfaction), as indicated from the velocity distribution plots.

In order to evaluate from different aspects the results obtained, a detailed analysis is provided below.

(e) Discussion of the results

(i) Frictionless flow

In this section predictions are obtained using a grid of 50 nodes and a time step of 0.02 seconds. The numerical accuracy

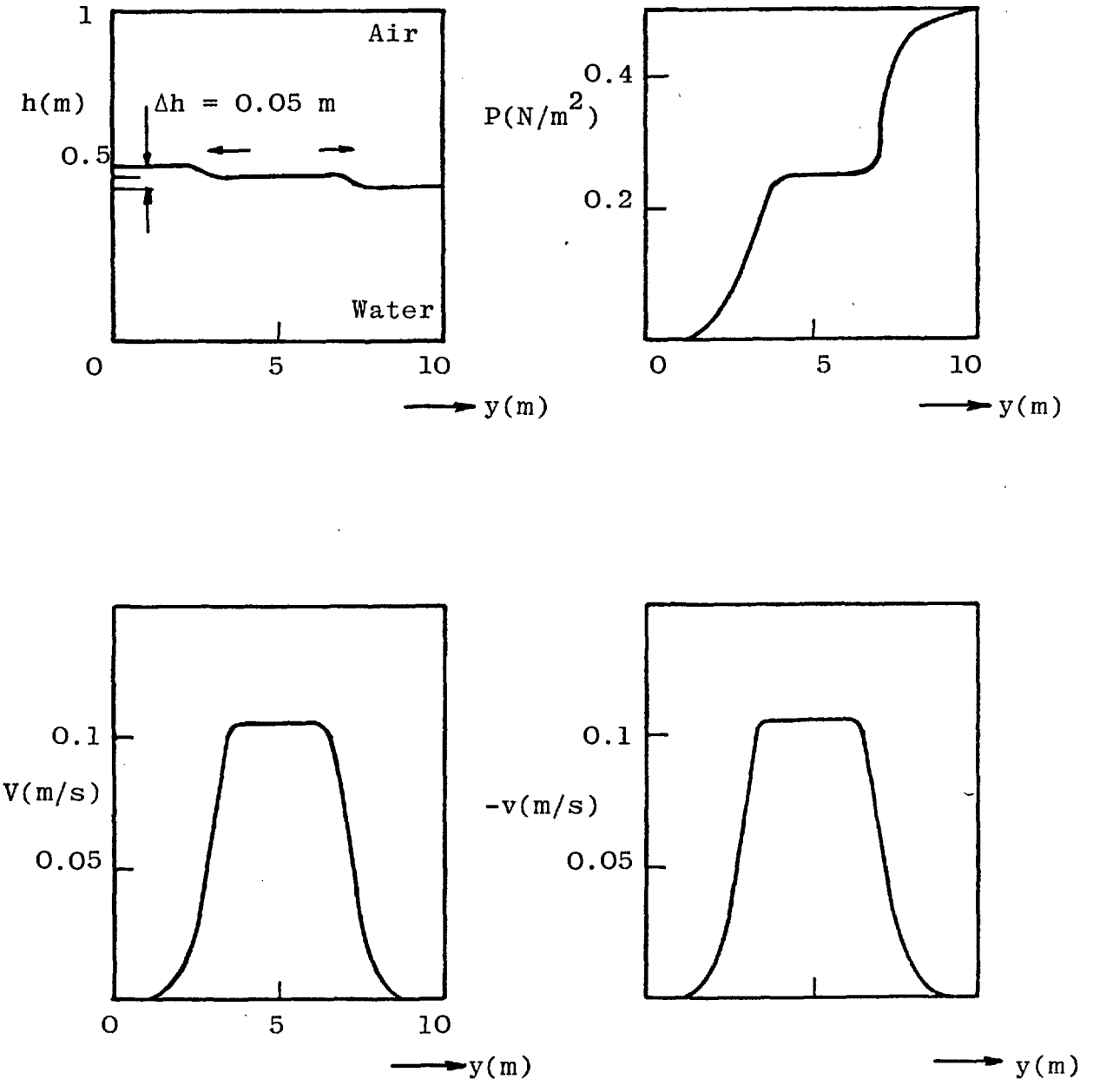


FIGURE (6-2) VOLUME FRACTION, PRESSURE AND VELOCITY DISTRIBUTIONS OF TWO PHASES AT TIME t = 1 sec., USING 50 GRID NODES

of the results is assessed by comparison with the exact solution.

Figure (6-3) shows the predicted positions of the air-water interface, at time intervals of half a second. For ease of comparison against the analytical results, the theoretical locations of wave fronts (calculated from equation (6.16) are presented as a dotted line, in each diagram. It can be seen that the sharp discontinuity is "smeared" over several grid intervals; this numerical-diffusion behaviour may be mitigated by using either floating grids or particle tracking techniques, compare Wolfshtein (1968). In the present prediction the smearing effect was substantially reduced by using a fine grid (50 grid nodes). For quantitative comparison, the wave speed is deduced from the following relation:

$$\text{Computed wave speed} = \frac{\text{Half length of the channel}}{\text{Time required for interface to flatten}} .$$

The computed wave speed is 2.203 m/sec.; while the theoretical value, calculated from (6.16), is 2.21 m/sec.; thus the error in calculating the wave speed is only

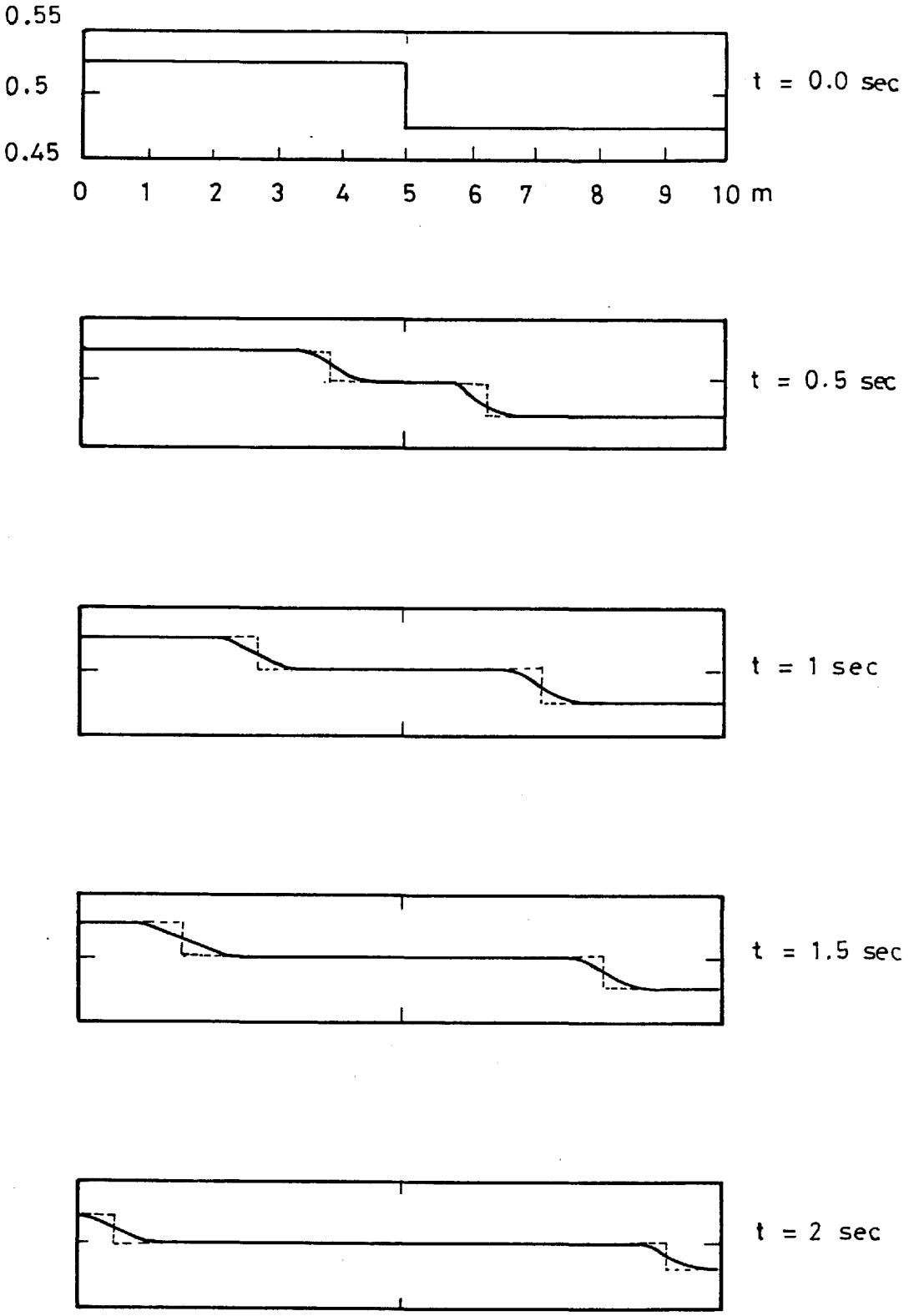


FIGURE (6-3) LIQUID LEVELS PREDICTED FOR THE CONFINED CHANNEL

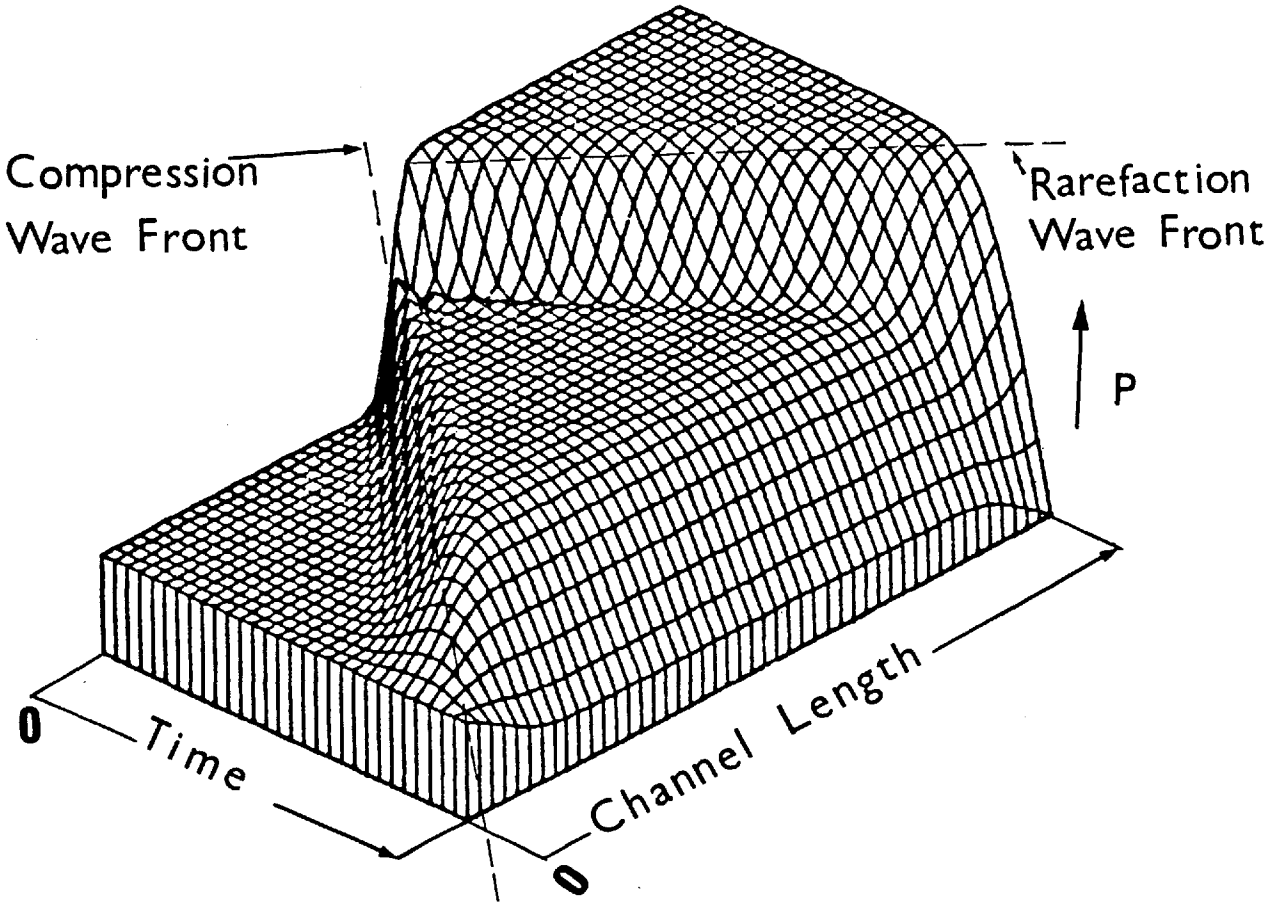
0.32 percent; the results of the prediction are shown to be in excellent agreement with the theory of wave propagation.

Moreover, the calculated pressures and liquid heights, as functions of time and distance, are shown in Figures (6-4) and (6-5). While Figure (6-4) represents a quarter period, Figure (6-5) shows a complete cycle of the wave formulation. Other noteworthy points are the following:

- The pressures are higher in the regions of lower liquid levels and vice versa; these opposite driving forces will keep both fluids in a counter-current motion.
- After about 2.2 seconds (which is approximately quarter-cycle time), pressure and liquid level are nearly uniform all along the channel.

These observations further support the phyical realism of the numerical computations.

Finally, the water-velocity distribution as a function of time and position is illustrated in Figure (6-6). It is to be noted that the water-velocity is zero



- PRESSURE DISTRIBUTION

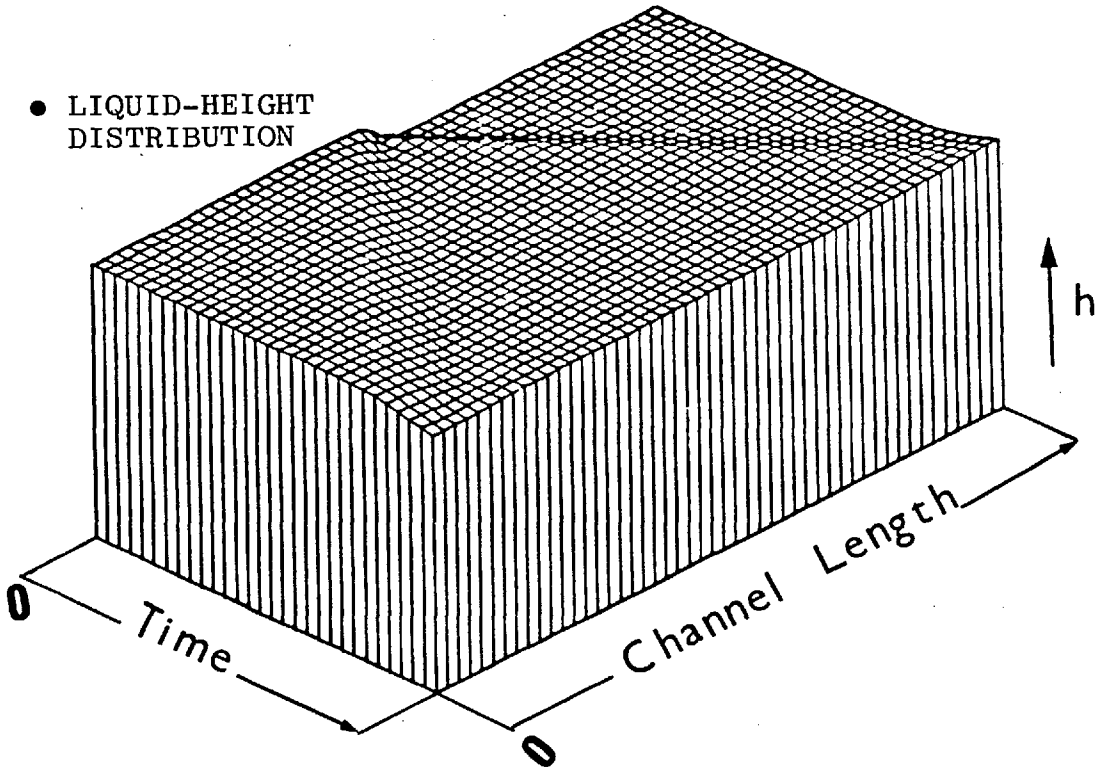


FIGURE (6-4) PREDICTION FOR A QUARTER CYCLE

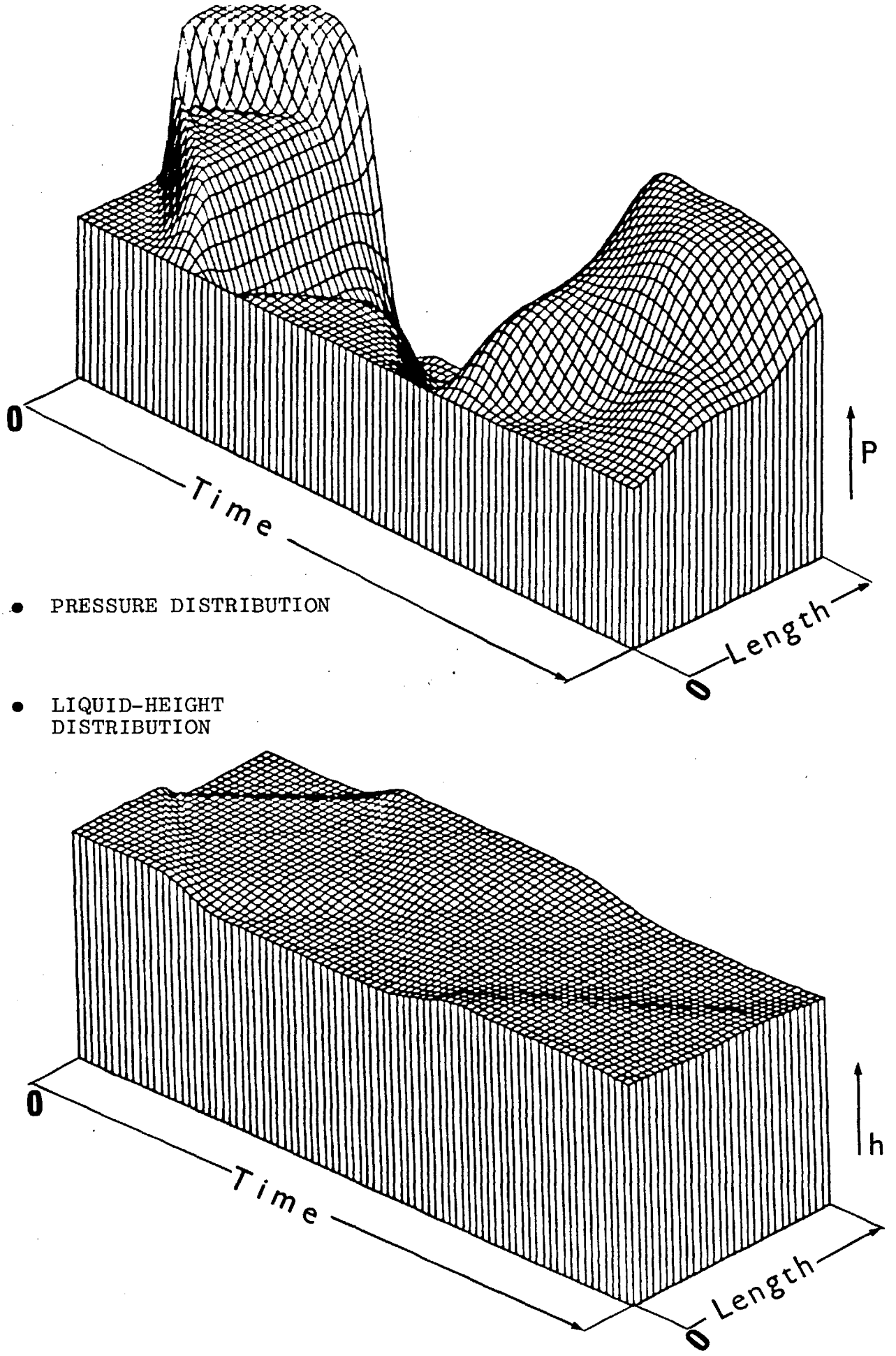


FIGURE (6-5) PREDICTION FOR A COMPLETE CYCLE

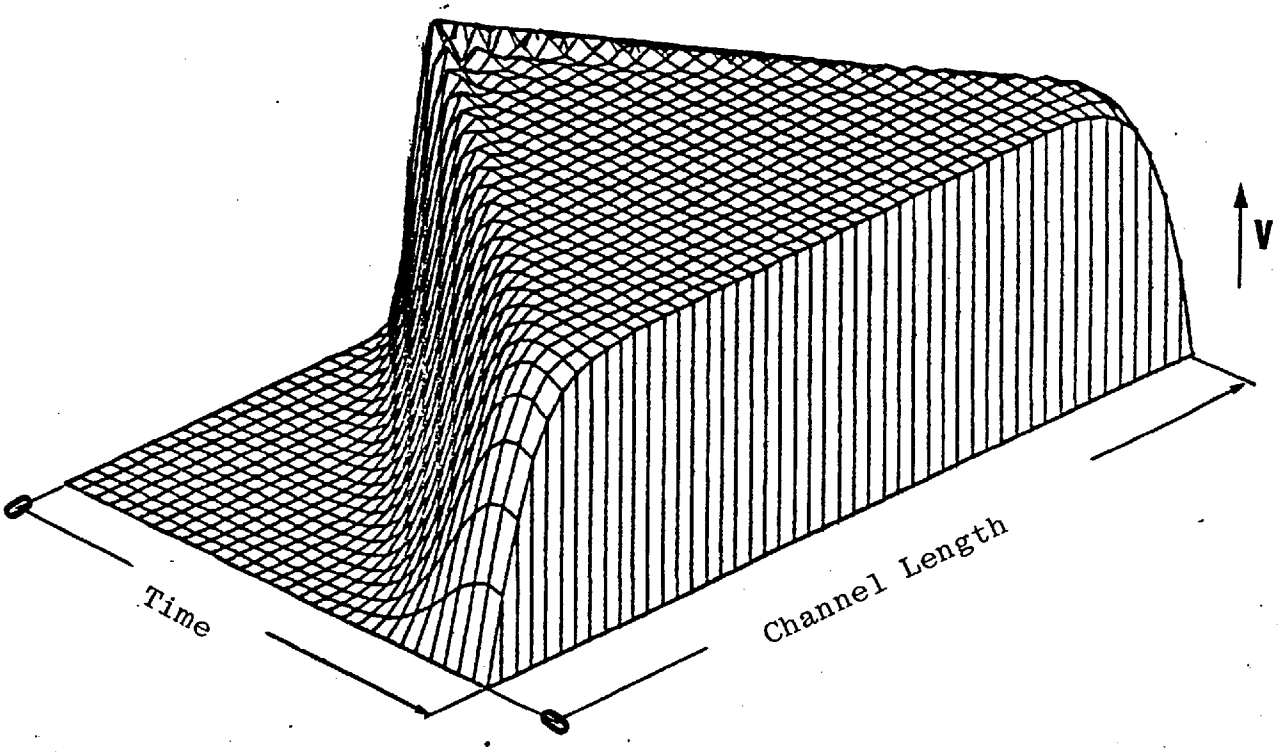


FIGURE (6-6) LIQUID-VELOCITY DISTRIBUTION OVER A QUARTER CYCLE

at both ends and that it gradually reaches its maximum value at the location of the two wave fronts where the concentration gradients are maximum, compare with Figure (6-4) The concentration and velocity profile, would be represented by step functions; the "smearing" in both profiles is caused by the false-diffusion effects which are prominent even when, as in the present situation, no "physical diffusion" and no source terms are present in the process analysed.

(ii) Friction effects

- Computations have also been performed with the inclusion of the friction effects both at the air-water interface and at the channel surface. The wall friction factors are deduced by analogy with single-phase flow which is the existing situation near the wall boundaries.

- The inter-phase friction force is calculated using the empirical correlation developed by Ellis and Gay (1959):

$$F_y^{\ell d} = \tfrac{1}{2}\,\rho_\ell A'' f\,|v - V|\,(v - v)$$
$$= f_y^{\ell d}\,(v - V) \qquad , (6.21)$$

where

$$f = 1.293/(R_e)_\ell^{0.57}$$

The above correlation implies that the interfacial forces are only dependent on the gas properties (light-phase), and is restricted to laminar-liquid/turbulent-gas flow patterns. Nevertheless, the Ellis and Gay assumption is valid when, for example, the inertia forces caused by the light-phase are predominant; however, in the extreme conditions where the forces due to the heavy phase are predominant or, as in the present, when both phases are in laminar flow, the Ellis and Gay correlation becomes inappropriate. It is mainly these restrictions that motivated the derivation of a new expression for the inter-phase friction coefficient, $f_d^{\ell y}$.

- In deriving our proposed friction coefficient we restrict our attention to the laminar flow of both phases. The flow situation is simulated by an electrical analogue circuit as shown in Figure (6-7), where the driving potential for both fluids is presented by the two EMF sources. The current i stands for the resulting velocity vector and the electrical equivalent conductance of the circuit is given by:

$$\frac{1}{K} = \frac{1}{K_\ell} + \frac{1}{K_d} \qquad ; (6.22)$$

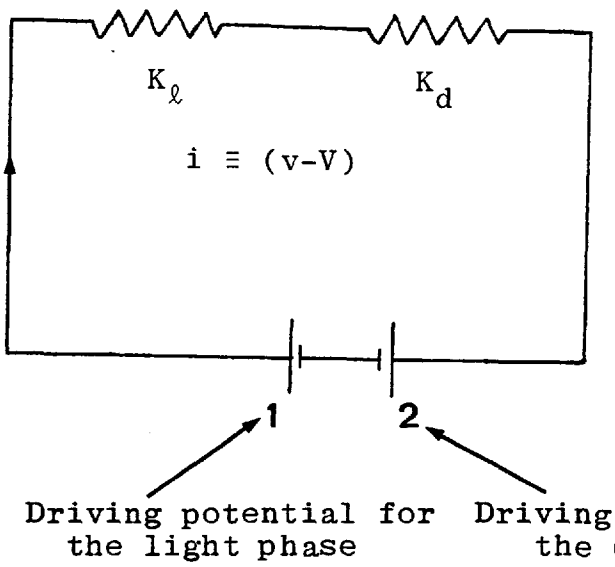


FIGURE (6-7) THE ELECTRICAL ANALOGUE CIRCUIT

K_ℓ and K_d are the representative impedance for the light and dense phases respectively. These are defined as:

$$K_i = \tfrac{1}{2} (f\rho R)_i \quad |v-V| \quad \frac{A_{int.}}{VOL} \qquad . (6.23)$$

Equation (6.23) expresses the impedance of the phase i which stands for either ℓ or d;

$A_{int.}$ is the interface area and,

VOL is the volume.

For a plane channel and laminar flow the friction factor is calculated from:

$$f_i = \frac{24}{(R_r)_i} \qquad , (6.24)$$

where $(R_r)_i$ is the relative Reynolds number, given by:

$$(R_r)_i = \frac{\rho_i |v - V| h_i}{\mu_i} \quad , (6.25)$$

where h_i is the height of phase i, related geometrically to its concentration, and

μ_i is the corresponding phase viscosity.

Substituting from equations (6.19) and (6.21) into (6.18) one may deduce the friction coefficient, $f_y^{\ell d}$, corresponding to the equivalent impedance of the circuit as:

$$f_y^{\ell d} = \frac{12\ R_\ell R_d \mu_\ell \mu_d}{H(R_\ell \mu_\ell + R_d \mu_d)} \quad . (6.26)$$

Equation (6.26) displays the fact that no inter-phase friction is present if only one phase is flowing. It expresses the drag function, $f_y^{\ell d}$, in terms of the properties of both phases and their geometrical inter-relation as implicitly given by the use of the phase volume fractions and the height, H, of the channel. A further advantage of using equation (6.26) is the linearity of the source term that procures steadier convergence for the numerical scheme (by comparison with correlation

(6.7)). Finally the derivation may be extended to turbulent flow applications by redefining the friction factors and the corresponding phase impedances.

- The computations made for the viscous flow differed slightly from the inviscid results. Predicted velocities and volume fractions were identical, at least up to two significant digits, for the first 1¼ cycles. The purpose of making this study was not to validate the predictions since no source of comparison is available. The ultimate aim however was to compare between the suggested empirical formula and the theoretical one developed in this section. When applied to the actual flow situation depicted in Figure (6-1), both formulae gave identical results. The value of the friction coefficient, $f_y^{\ell d}$, according to the present approach is 1.1×10^{-4} Kg/(sec.m^3), while it takes an average* value of 3×10^{-4} Kg/(sec.m^3) when using the empirical relation. Although the final solution reached is identical, nevertheless the

---

*The average value is calculated over a complete cycle of the wave motion (where the velocity is a function of time and position).

author favours the use of equation (6.26) for calculating the inter-phase frictional force when a laminar to laminar interface is in question. This is partly due to the restrictions imposed in the empirical correlation (6.7) (that implies a turbulent motion of the gas), and partly because the use of equation (6.26) provides a linear coupling between the phases which is desirable in that it procures steadier convergence for the numerical procedure.

(iii) Grid-dependence tests

In order to examine the grid independence of the numerical predictions, the following two sets of runs were performed.

Run No.	No. of Grid Modes (N)	Time Step (Δt) Seconds	Courant No.
1	10	0.100	0.2
2	20	0.050	0.2
3	30	0.033	0.2
4	40	0.025	0.2
5	50	0.020	0.2

TABLE (6-2) RUNS MADE FOR STUDYING THE EFFECT OF THE GRID SIZE (SET 1)

The Courant number, λ, defines a non-dimensional time relating the wave speed C to the grid dimension Δy and the time step Δt through:

$$\lambda = C/(\frac{\Delta y}{\Delta t}) \quad . \quad (6.27)$$

For stability and when no under-relaxation is used, it is necessary that $\lambda \leq 1$, compare Roache (1972). It may be noted from Table (6-2) that the Courant number is kept constant.

Run No.	No. of Grid Nodes (N)	Time Step (Δt) Seconds	Courant No.
1	30	0.033	0.2
2	30	0.100	0.6
3	30	0.200	1.2
4	30	0.330	2.0

TABLE (6-3) RUNS MADE FOR STUDYING THE EFFECT OF THE TIME STEP (SET 2)

In this set, the number of grid nodes is fixed, and the time step Δt is progressively increased.

(a) Effect of grid size

For quantitative comparisons of results, the percentage error in the computed wave speed has been calculated for each run, as follows:

$$\% \text{ Error in Wave Speed} = \frac{\text{Theoretical Value} - \text{Computed Value}}{\text{Theoretical Value}} \times 100 \quad . \quad (6.28)$$

The variation of error with the number of grid nodes used is presented in Figure (6-8). As expected the error reduces with increasing number of grid nodes. It may be noted that for $N \geq 30$, the error is almost negligible. A qualitative illustration of two interfaces, predicted respectively by using 10 and 50 grid nodes is displayed in Figure (6-9); it is clearly seen that the smearing effect is substantially reduced by the use of a fine grid.

(b) Effect of time step

In the first two runs of set 2 (Table (6-3)), the convergence of the solution procedure is satisfactory; i.e. residual errors, for all dependent variables,

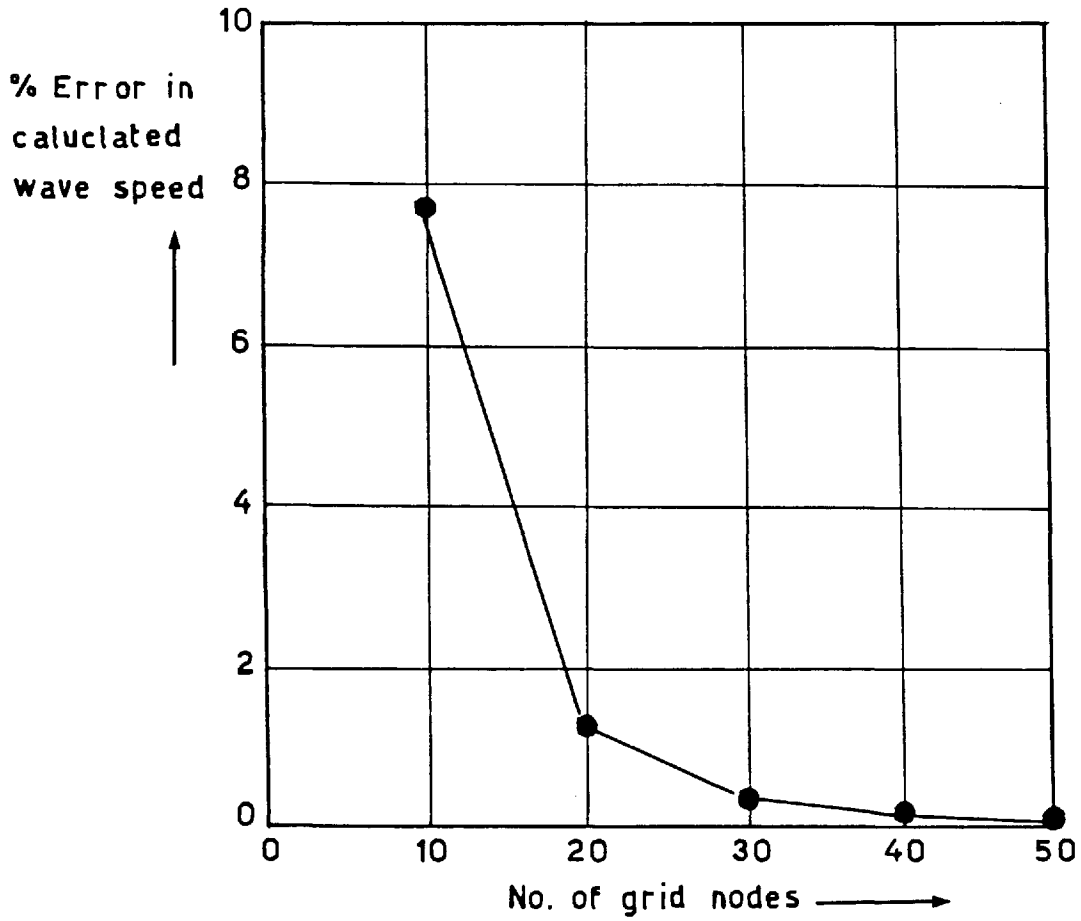


FIGURE (6-8) EFFECT OF GRID REFINEMENT IN THE CLOSED-CHANNEL INITIAL-DISCONTINUITY PROBLEM.

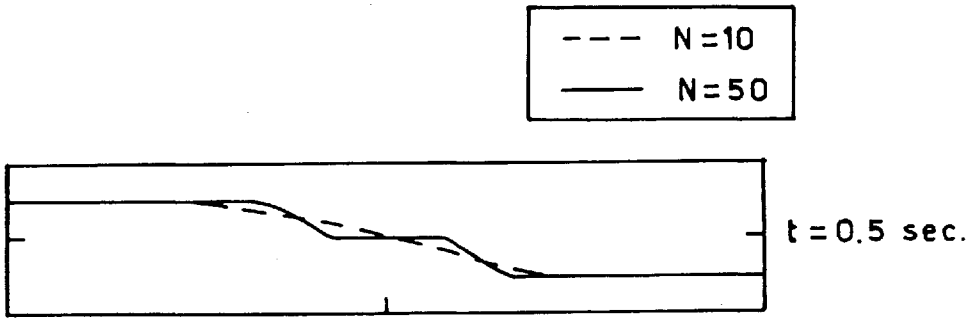


FIGURE (6-9) INTERFACE POSITION, AT t=0.5 second, PREDICTED BY USING N=50 AND N=10 GRIDS.

diminish with increasing number of iterations during each time step, in almost a monotonic manner and reduce to values lower than the preassigned limits. The rate of convergence is found to be practically the same for both the runs. For the last two runs, the solution did not converge. This suggests that under-relaxation factors may be necessary for using larger time steps. At present, it is preferable not to have any under-relaxation parameter in the code. Thus from the above test, it can be inferred that the use of 30 grid nodes and a Courant number of 0.6 leads practically to grid-independent results.

6.3.2 Wave Formation in a Plane Channel with One End Closed

The problem of the wave formation in a plane channel with one end closed is another example of gravity-waves in two-phase flow. In the present problem, there is no initial discontinuity in the air-water interface; instead the discontinuity is expected to build up with time, thus giving insight into the mechanisms of wave formation and propagation in stratified flow regimes. The problem is also of interest in that the flow situation has an exact solution; it is

therefore possible to establish the accuracy of the numerical solution procedure.

(a) Objectives of the study

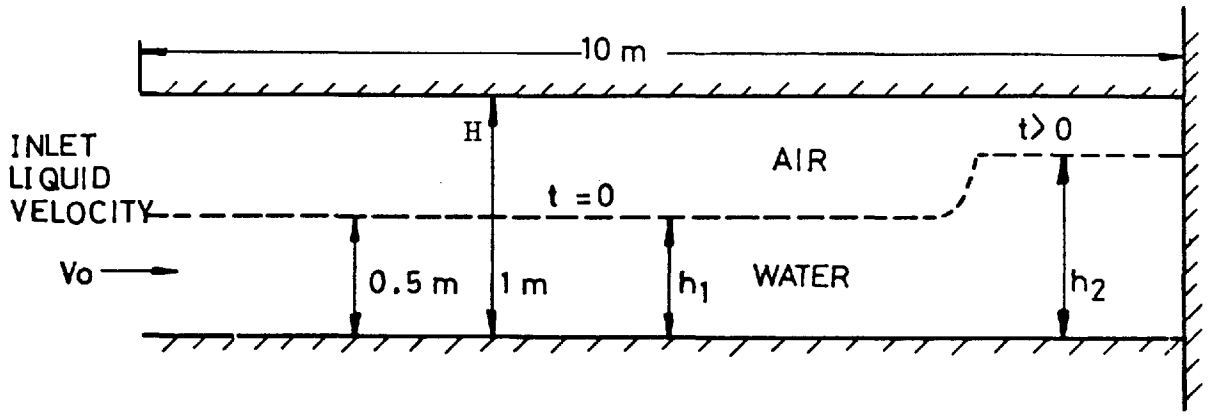
(i) To check the numerical accuracy of the computed results for different flow conditions (inlet water velocity, V_o and the initial liquid-height, h_1).

(ii) To demonstrate that when the grid size is small enough and the time step is properly selected, the numerical predictions become effectively independent of the cell dimension and the time increment employed in the computations.

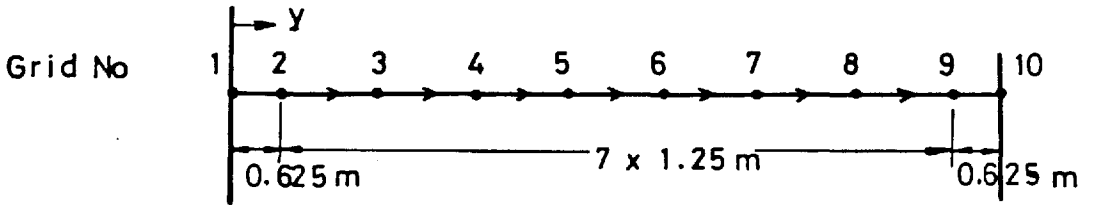
(b) Presentation of the problem

(i) Statement of the problem

The flow geometry and the grid distribution are shown in Figure (6-10). The motion is assumed to be frictionless. Initially, at t = 0, the air-water interface is horizontal and the two fluids are moving with uniform and equal velocities in opposite directions. At the entrance to the channel, a constant flux of water is maintained from t = 0 onwards. The outlet section of the channel is suddenly closed at t = 0 (and remains so for t > 0); as a result, a surge wave builds up and



(a) THE FLOW GEOMETRY



(b) THE GRID ARRANGEMENT

FIGURE (6-10) PLANE CHANNEL WITH ONE END CLOSED

propagates upstream towards the open end. The task is to compute the wave-speed by a one-dimensional analysis of the transient response of the flow.

(ii) Qualitative description

The instantaneous closure of the channel outlet is expected to bring to rest the water immediately adjacent to the closed end; the kinetic energy thus lost is transformed into potential energy; consequently, the water level begins to rise at the closed end. Successive layers of water are brought to rest progressively. In this manner a gravity wave is formed and is expected to travel at a speed, C.

(iii) Theoretical analysis

The quantitative description of the problem is obtained from theoretical considerations. Shortly after the sudden closure of the channel, the generated wave reaches a steady-state condition and propagates with a constant speed; this steady-state flow condition is analysed below, following Streeter and Wylie, (1969).

For the control volume shown in Figure (6-11), the continuity relation per unit width is given by:

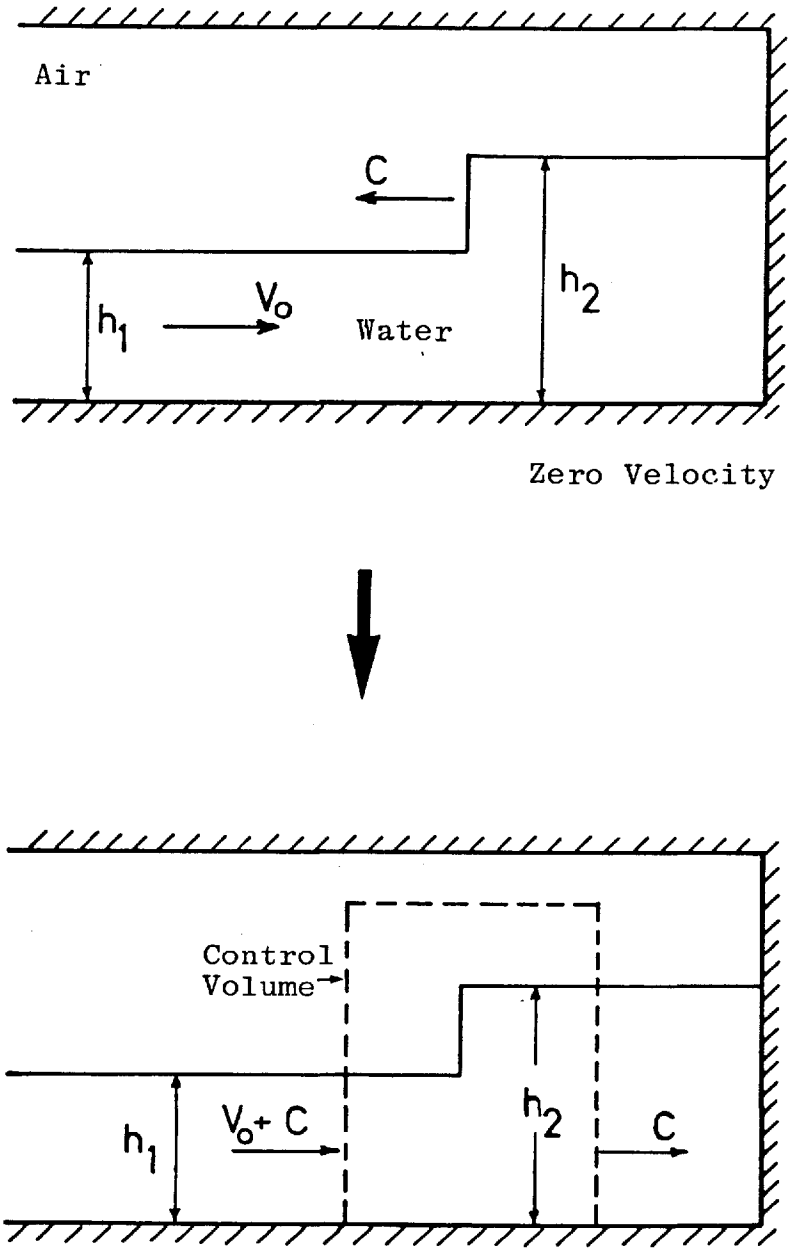


FIGURE (6-11) SURGE WAVE REDUCED TO STEADY-STATE CONDITION BY SUPERPOSITION OF SURGE VELOCITY C

$$\frac{h_2}{h_1} = 1 + \frac{V_o}{C} \quad , (6.29)$$

and the momentum equation per unit mass yields,

$$V_o + C = \sqrt{gh_1}\{\frac{h_2}{2h_1}(1 + \frac{h_2}{h_1})\}^{\frac{1}{2}} \quad . (6.30)$$

It is to be noted that, in deriving the above equations, the inertia and the momentum of the air were neglected in comparison with those of the water. In order to determine the wave speed, C, and the liquid height, h_2 (for given V_o and h_1), C can be eliminated from equations (6.29) and (6.30) to give:

$$(\frac{h_2}{h_1})^3 - (\frac{h_2}{h_1})^2 - (1 + 2F_r)\frac{h_2}{h_1} + 1 = 0 \quad , (6.31)$$

where F_r is the Froude number defined according to:

$$F_r \equiv \frac{V_o^2}{gh_1} \quad . (6.32)$$

Equation (6.31) is a third order algebraic equation in h_2/h_1, it has three real roots for all positive values of h_1 and all subcritical velocities (i.e. for $F_r < 1$ or $V_o < C$). Only the positive root having a value greater than unity is relevant to the present situation. Negative

and fractional roots are not realistic here since they imply a decrease in the water level ($h_2 < h_1$) which contradicts continuity, equation (6.29). Having obtained the ratio of liquid heights, $\frac{h_2}{h_1}$, C is determined from equation (6.29).

(c) Details of the present computations

(i) Equations to be solved

1. Gas-volumetric continuity:

$$\frac{\partial R_\ell}{\partial t} + \frac{\partial}{\partial y}(R_\ell v) = 0 \qquad . (6.33)$$

2. Liquid-volumetric continuity:

$$\frac{\partial R_d}{\partial t} + \frac{\partial}{\partial y}(R_d V) = 0 \qquad . (6.34)$$

3. Gas-momentum conservation equation:

$$\frac{\partial}{\partial t}(R_\ell \rho_\ell v) + \frac{\partial}{\partial y}(R_\ell \rho_\ell v^2) = - R_\ell \frac{\partial P}{\partial y} \qquad . (6.35)$$

momentum accumulation — convection — pressure gradient

4. Liquid-momentum conservation equation:

$$\frac{\partial}{\partial t}(R_d \rho_d V) + \frac{\partial}{\partial y}(R_d \rho_d V^2) = - R_d \frac{\partial P}{\partial y} - R_d(\rho_d - \rho_\ell)\, g \cos\alpha \frac{\partial h}{\partial y} \qquad . (6.36)$$

gravity force due to interfacial inclination

Notes on equations:

- The volume fractions must satisfy the geometrical condition, viz.

$$R_\ell + R_d = 1 \qquad . (6.37)$$

- Wall and inter-phase friction are neglected in that the analytical solution is available only for inviscid flow.

(ii) Initial conditions

At t = O:

- Water-height (which is uniform along the channel) = h_1 m
- Water-velocity (" " ") = V_o m/sec
- Air-velocity (" " ") = $-V_o$ m/sec

(iii) Boundary conditions

- At Inlet:

  The velocities and concentrations are prescribed:

  for air, $v(O,t) = -V_o$ and $R_\ell\ (O,t) = 1 - \frac{h_1}{H}$

  for water, $V(O,t) = V_o$ and $R_d\ (O,t) = \frac{h_1}{H}$

- At the closed end:

  Both fluids have zero velocity and the concentration gradients at the wall are set to zero.

The above differential equations are transformed to their finite-difference equivalents and the resulting set of equations are solved using the "IPSA-TV" algorithm (section 6.2).

(iv) Finite-difference grid

In order to examine the effect of grid size on the numerical solution, four different grids, containing respectively 10, 20, 30 and 50 nodes, were employed. The grid distribution along the flow domain is shown in Figure (6-10) for a grid consisting of 10 nodes.

(v) Time step

The time increment employed, Δt, was related to the grid size, Δy, and the wave speed, C, via the Courant number, λ, defined by

$$\lambda \equiv C/(\frac{\Delta y}{\Delta t}) \quad .$$

In order to secure steady convergence, it is recommended that $\lambda \leq 1$, compare Roache (1972). Accordingly, the time step was chosen so as to make the ratio $\frac{\Delta y}{\Delta t}$ greater than the wave speed, C.

(vi) Miscellaneous information

Typical information on a particular computational run is tabulated below.

WAVE FORMATION IN A PLANE CHANNEL WITH ONE END CLOSED	PERTINENT DATA
Configuration	Plane
Number of grid nodes	50
Grid spacing	uniform
Grid size per unit length of the channel	0.02083
Time step (sec.)	0.02
Courant number	0.2
Number of time steps	200
Number of iterations per time step	20
Computational time per grid node per time step CDC 6600 (sec.)	0.0333

TABLE (6-4) TYPICAL INFORMATION ON A COMPUTATIONAL RUN

(d) Presentation of the results

Three different sets of computaions were made. The initial liquid-height, h_1, was given the values 0.6, 0.5 and 0.4 metres respectively for data sets 1, 2 and 3. In each set the fixed inlet water-velocity, V_o, was altered to take values between 0.2 and 1 m/sec.

The results of the three sets of computations performed are presented in Tables (6-5), (6-6) and (6-7). It is to be noted that all the predicted wave-speeds in the forementioned tables were obtained by employing 50 grid nodes and a time step of 0.02 seconds, so that the ratio $\Delta y/\Delta t$ is kept constant at a value of 10.4 m/sec. Moreover, the percentage error in calculating the wave-speed is given by

$$\% \text{ Error} = \frac{(\text{Theoretical value of C}) - (\text{Predicted value of C})}{\text{Theoretical value of C}} \times 100$$

Finally, the Courant number is calculated as follows:

$$\lambda = \text{Theoretical value of C} \times \frac{\Delta y}{\Delta t} \quad .$$

(e) Interpretation of the results

The purpose of this section is to demonstrate how the wave speed may be calculated from the computed results.

Figure (6-12) exhibits the calculated liquid levels for the whole channel at different time intervals, corresponding to the case where $h_1 = 0.5$ m and $V_o = 1$ m/sec. (A grid of 50 nodes and a time step of 0.02 seconds were employed.) The graph indicates that the wave front builds up in different modes during a transition period

SET 1

V_o (m/sec)	Froude Number	Predicted value of C	Theoretical value of C	% error in calculating C	Courant Number
0.2	0.007	2.107	2.381	11.4	0.229
0.4	0.027	2.118	2.340	9.0	0.225
0.6	0.061	2.162	2.302	6.0	0.221
0.8	0.109	2.174	2.261	3.8	0.217
1.0	0.173	2.179	2.245	2.0	0.216

TABLE (6-5) RESULTS OBTAINED FOR h_1 = 0.6 m

SET 2

V_o (m/sec)	Froude Number	Predicted value of C	Theoretical value of C	% error in calculating C	Courant Number
0.2	0.008	1.930	2.167	10.9	0.208
0.4	0.032	1.972	2.125	7.3	0.204
0.6	0.073	2.013	2.087	3.5	0.200
0.8	0.131	2.009	2.053	2.2	0.197
1.0	0.204	2.019	2.023	0.2	0.194

TABLE (6-6) RESULTS OBTAINED FOR h_1 = 0.5 m

SET 3

V_o (m/sec)	Froude Number	Predicted value of C	Theoretical value of C	% error in calculating C	Courant Number
0.2	0.010	1.735	1.934	10.3	0.186
0.4	0.040	1.801	1.892	4.8	0.182
0.6	0.092	1.840	1.855	1.0	0.178
0.8	0.163	1.818	1.823	0.3	0.175
1.0	0.255	1.807	1.808	0.1	0.174

TABLE (6-7) RESULTS OBTAINED FOR h_1 = 0.4 m

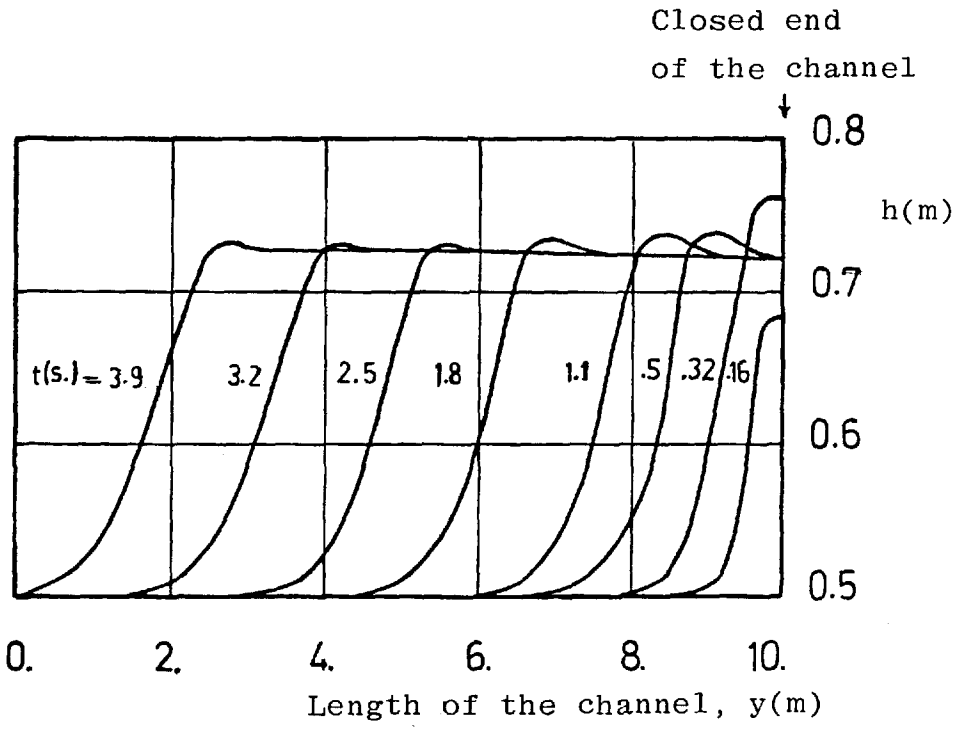


FIGURE (6-12) LIQUID LEVELS AT DIFFERENT TIME (N.B. y AND h ARE PLOTTED TO DIFFERENT SCALES)

of approximately one second, and thereafter the wave travels steadily (a state of equilibrium between the inlet flow rate and the rise in the liquid level is maintained) with a constant speed, C.

The wave speed, C, is obtained by division of the distance travelled by the wave front, Δy_{wave}, to the time taken to reach that location, i.e.

$$C = \Delta y_{wave} / t \quad .$$

At any time, t, the location of the wave front, B, corresponds to the point A where the liquid is brought to rest, as depicted in Figure (6-13). In the particular example shown, C equals 2 m/sec.

Figure (6-14) shows the calculated wave-speed versus time. It is apparent, from the graph, that the propagation speed reaches a steady value after approximately one second. It is this steady value of the wave speed, that is compared with the theoretical one obtained from the analytical solution.

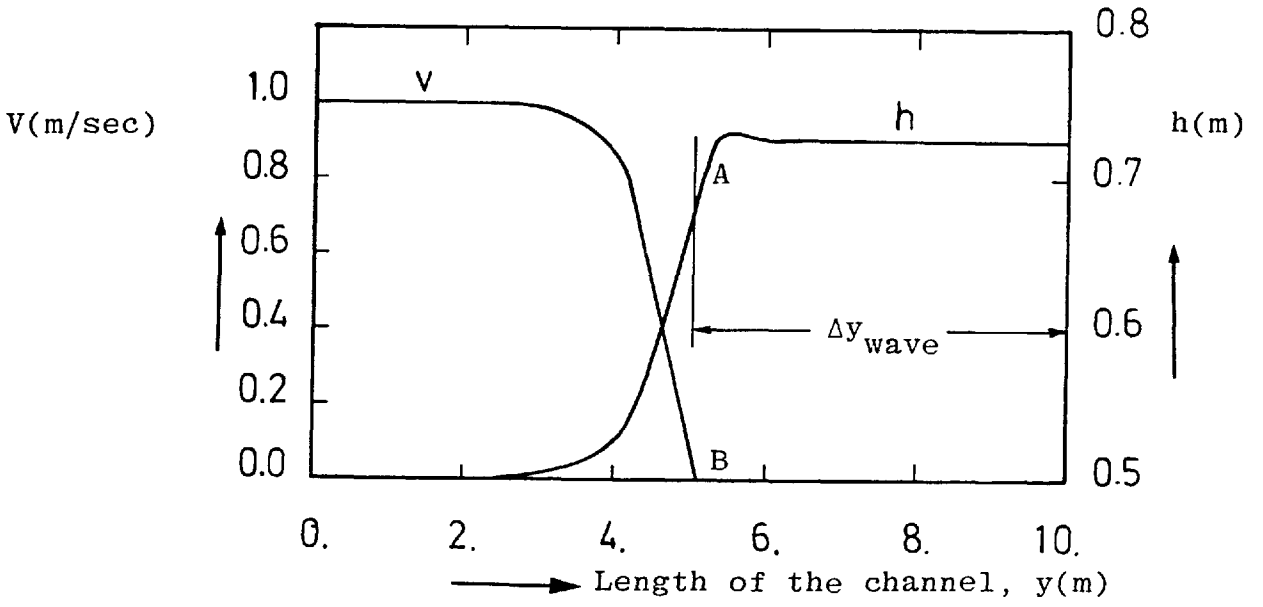


FIGURE (6-13) WATER-HEIGHT AND VELOCITY VARIATIONS ALONG THE CHANNEL (t = 2.5 sec.)

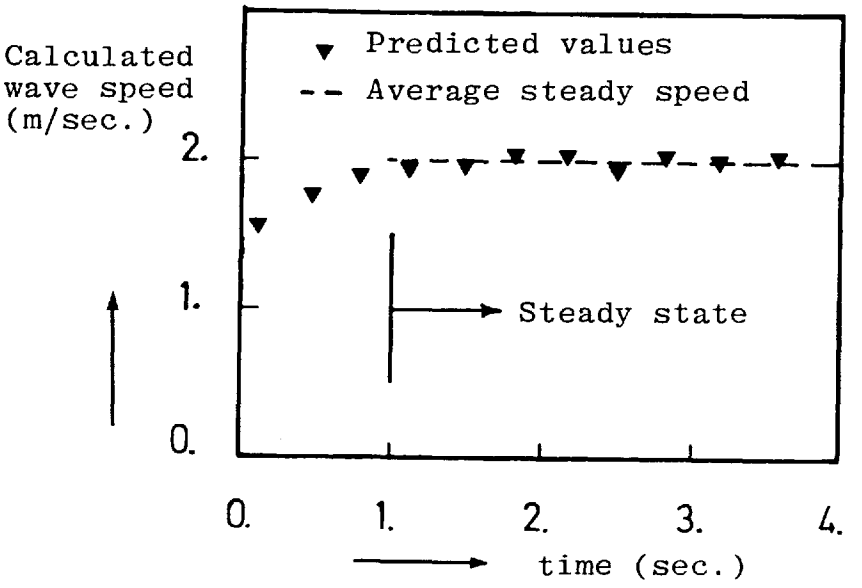


FIGURE (6-14) PREDICTED WAVE SPEED VERSUS TIME

(f) Discussion of the results

(i) Effect of the Froude number

The results given in Tables (6-5) to (6-7) indicate that the wave-speed is dependent on the initial conditions (h_1 and V_o), for example C varies inversely with V_o.

The ratio between the initial liquid-momentum to the gravity force is expressed by the Froude number, V_o^2/gh_1. It is apparent from the tabulated results that an increase in the Froude number, either by reducing the initial liquid-height, h_1, or by increasing its initial velocity, V_o, yields more accurate predictions of the wave-speed. This may be attributed to the larger momentum changes associated with the increase in Froude number, as shown in Figure (6-15). The wave front configuration has been plotted, at time t = 1 sec., for h_1 = 0.4 m and for two values of V_o, namely 1 m/sec and 0.2 m/sec. It may be observed that for the higher value of V_o the liquid-accumulation creates a steep wave front much closer to a step disturbance than that for the lower value. Since the theory assumes a step disturbance in deriving equations (6.29) and (6.30), it

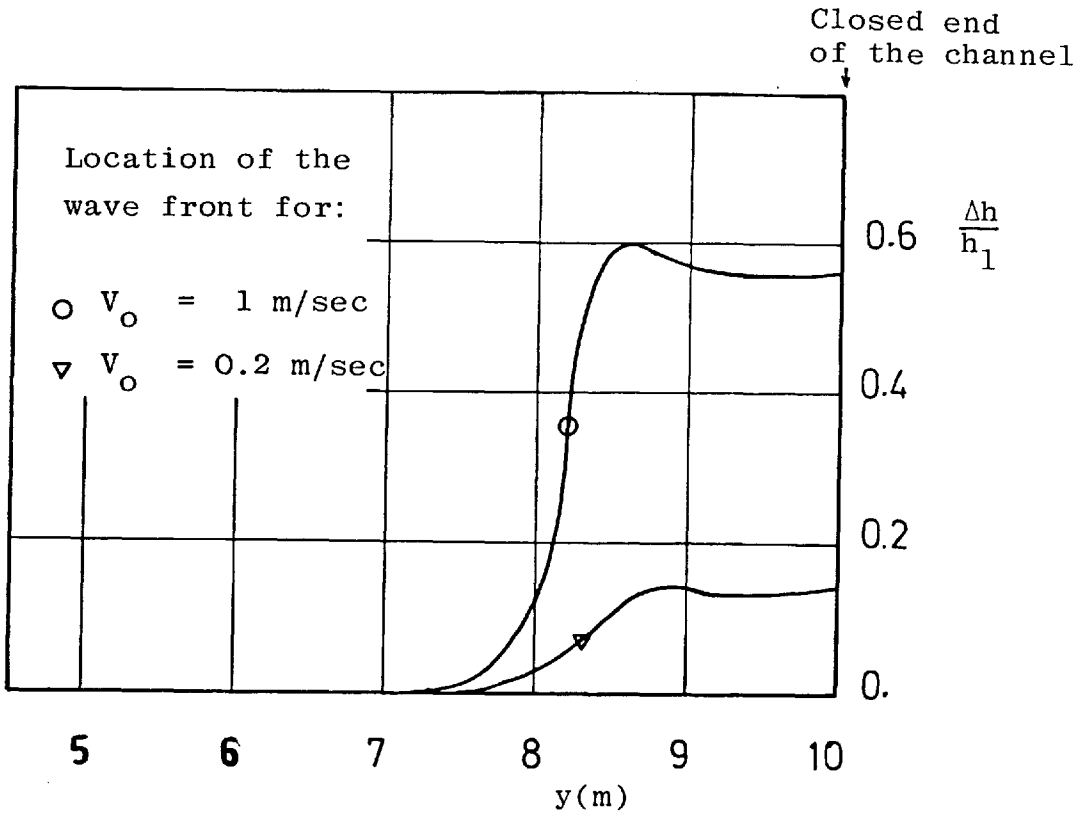


FIGURE (6-15) WAVE FRONT CONFIGURATIONS
(t=1 sec; h_1= 0.4 m) N.B. $\Delta h = h - h_1$

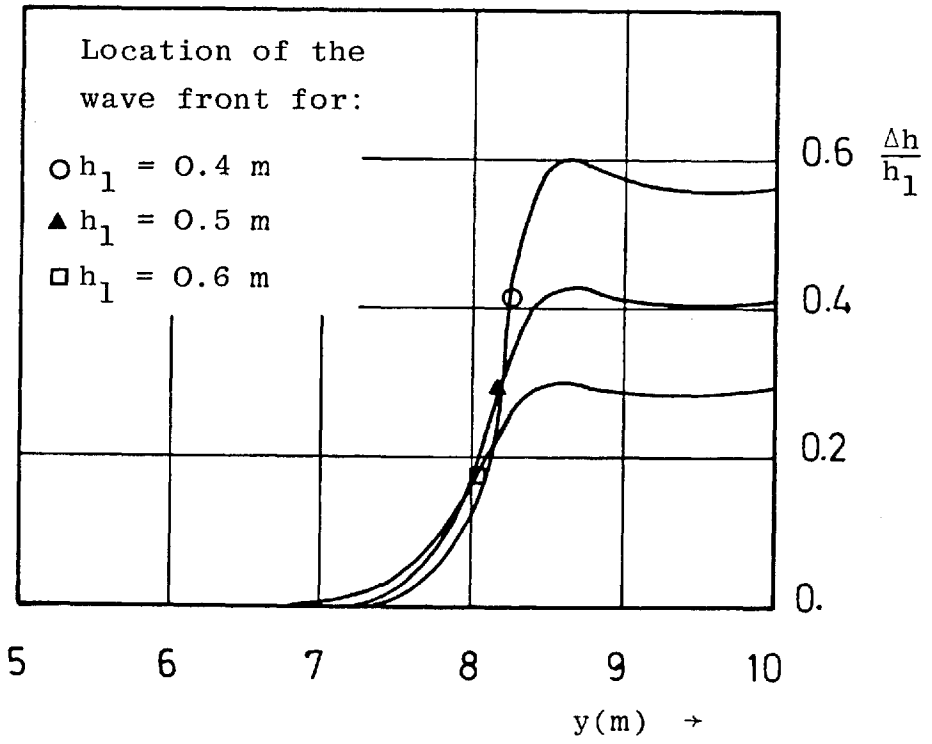


FIGURE (6-16) WAVE FRONT CONFIGURATIONS
(t=1 sec; V_o = 1 m/sec)

is to be expected that the computed wave-speed for the case where V_o = 1 m/sec will be in better agreement with the theory.

It is also noted that for the lower value of V_o there is a larger amount of smearing in the wave front; this is caused mainly by the numerical false diffusion, which represents an additional fictitious diffusive effect that leads to a degeneracy in the accuracy of the computations. The percentage error in predicting the wave-speed is presented in Table (6-7); this error amounts only to 0.1% for V_o = 1 m/sec and is of about 10% for V_o = 0.2 m/sec. In the latter case, the accuracy of the results may be improved by employing a finer mesh size, as will be demonstrated later in this section.

In the above-mentioned example, the value of the Froude number was altered through changes in the value of V_o, while h_1 was maintained constant. Now, consider the increase in the Froude number by reducing h_1 at a constant value of V_o.

Three cases are studied for V_o = 1 m/sec and h_1 equal to: 0.6, 0.5 and 0.4 metres respectively. Figure (6-16) depicts the dimensionless rise in the water level (above its initial height), after a time interval of one second, versus the channel length, for the three cases considered. The results confirm the earlier deductions from Figure (6-15), in that the larger the Froude number (or the lower the value of h_1) the steeper is the resulting wave front. Once again, it is to be noted that the less smearing of the wave front there is, the more accurate the predictions are.

For the three sets of flow conditions presented in Tables (6-5) to (6-7), the error in computing the wave-speed is shown in Figure (6-17) as a function of the initial liquid velocity for the different value of h_1. As observed earlier, the error decreases with increasing Froude number.

(ii) Effect of grid-size

- In order to examine the grid-dependence of the numerical results, four runs have been performed, these are given in Table (6-8) below.

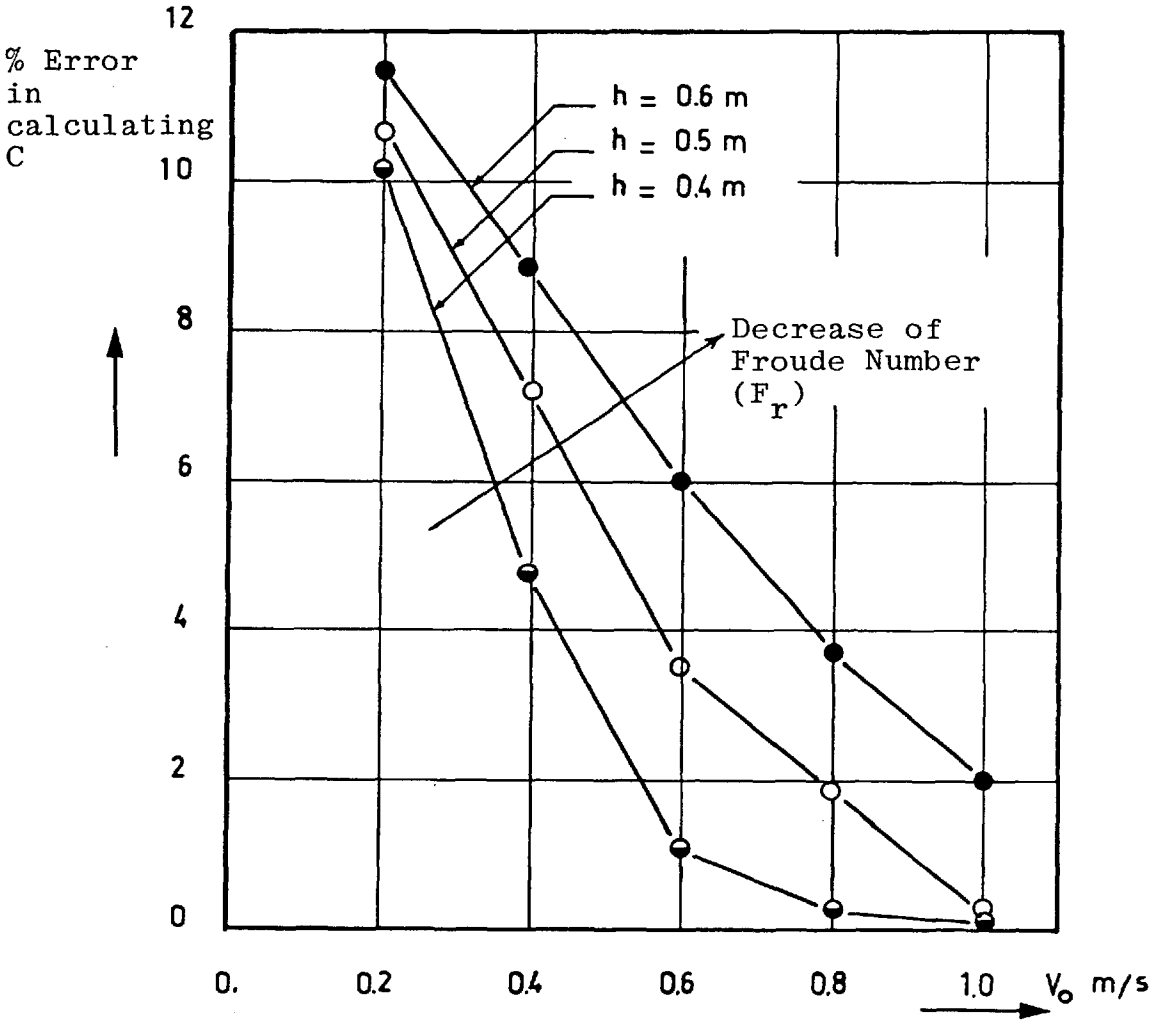


FIGURE (6-17) PERCENTAGE ERROR IN CALCULATING C FOR DIFFERENT VALUES OF F_r

Run No.	No. of Grid Nodes (N)	Time Step Δt Seconds	Courant Number
1	10	0.1	0.2
2	20	0.05	0.2
3	30	0.033	0.2
4	50	0.02	0.2

TABLE (6-8) RUNS MADE FOR STUDYING THE EFFECT OF GRID SIZE (h_1 = 0.5 m; V_o = 1 m/sec)

It may be noted that in each case the Courant number has been kept constant.

Figure (6-18) presents the variation of the error in the computed wave-speed with the number of grid nodes. As expected, the error reduces with increasing number of grid nodes. Figure (6-19) displays the wave front, after two seconds; the results were obtained by using 10, 20 and 50 grid nodes respectively. It is clearly seen that the "smearing" is substantially reduced by the use of a finer grid.

- In an attempt to reduce the effect of false diffusion in the case where h_1 = 0.4 m and V_o = 0.2 m/sec, the number of grid nodes has been increased to 150

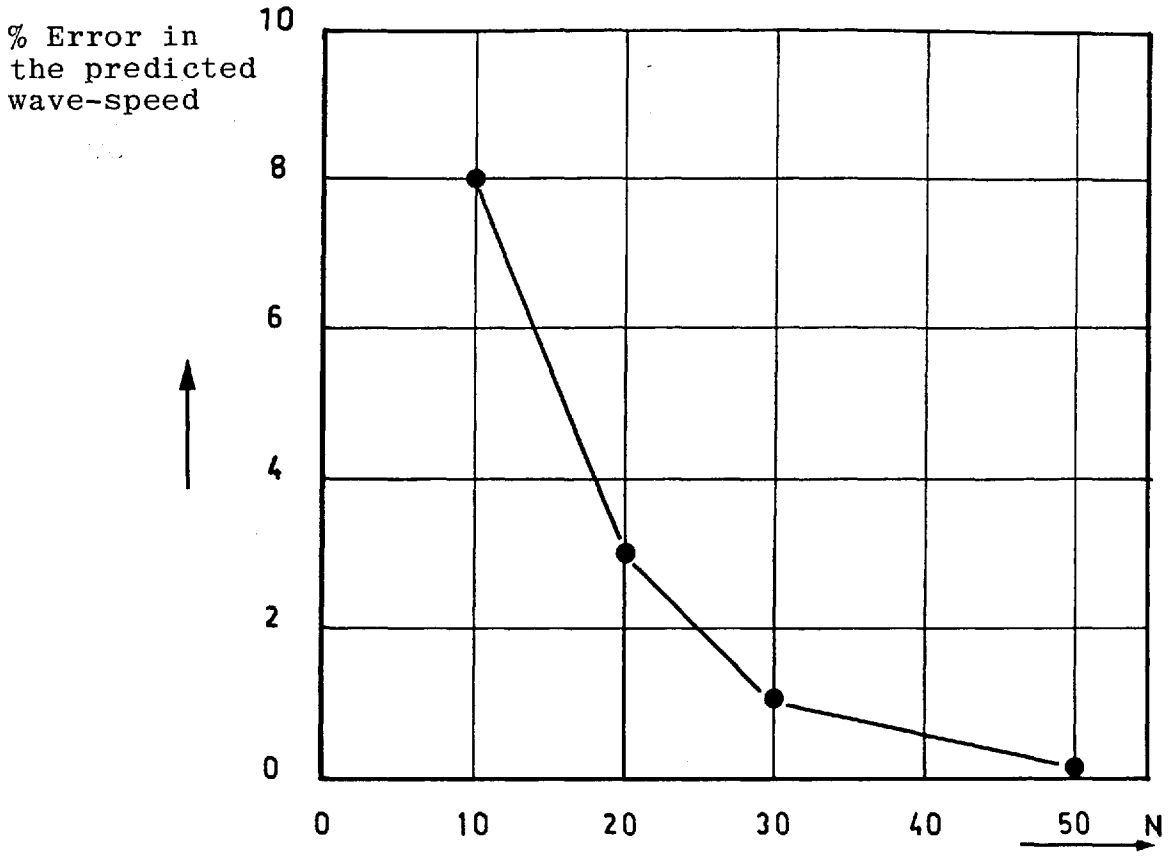


FIGURE (6-18) EFFECT OF GRID REFINEMENT IN THE CLOSED END CHANNEL PROBLEM

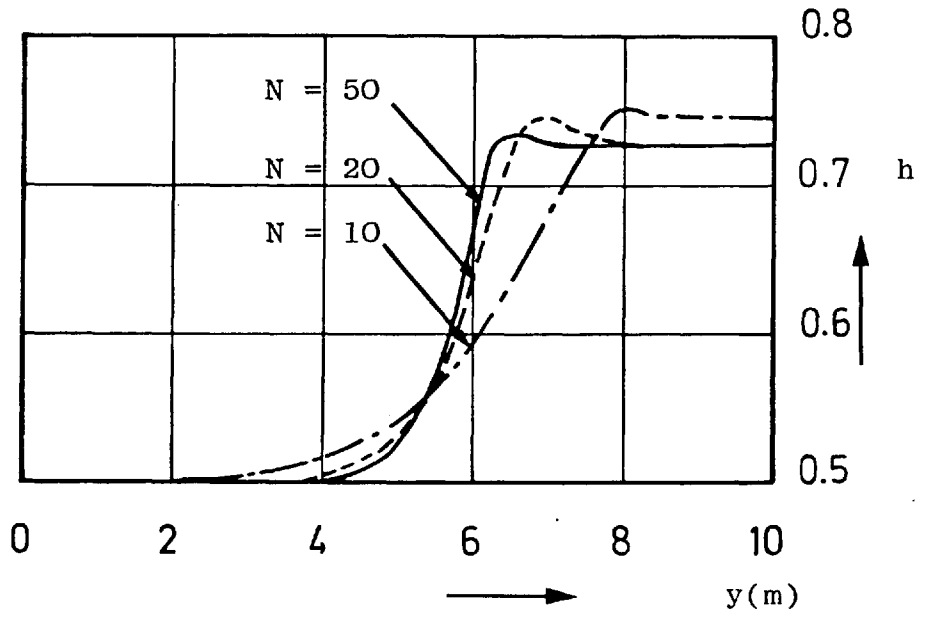


FIGURE (6-19) WAVE FRONT CONFIGURATION, AT t = 2 sec. PREDICTED USING: 10, 20 AND 50 GRID NODES

and the time step was reduced to maintain a constant value of the Courant number. The predicted wave front, after a period of one second, is illustrated in Figure (6_20) for N = 50 and 150 nodes respectively. The graph indicates that for the finer grid, the shape of the wave is closer to a step disturbance and that the wave has travelled a larger distance in the same time interval (i.e. its speed has increased due to a reduction of the false diffusion). A comparison of the error in the computed wave-speed, in both cases, reveals that the tripling of the number of grid nodes (from 50 to 150) leads to a reduction in the error (of the predicted wave-speed) from 10% to 6.5%. This modest improvement in the accuracy was achieved at the cost of a three-fold increase in the computing time. This in turn suggests that the use of finer grid is not the most economical way of reducing the effects of false diffusion. There are other available methods for mitigating these effects; they involve the use of stream-function coordinates for, at least, the concentration equation. These methods

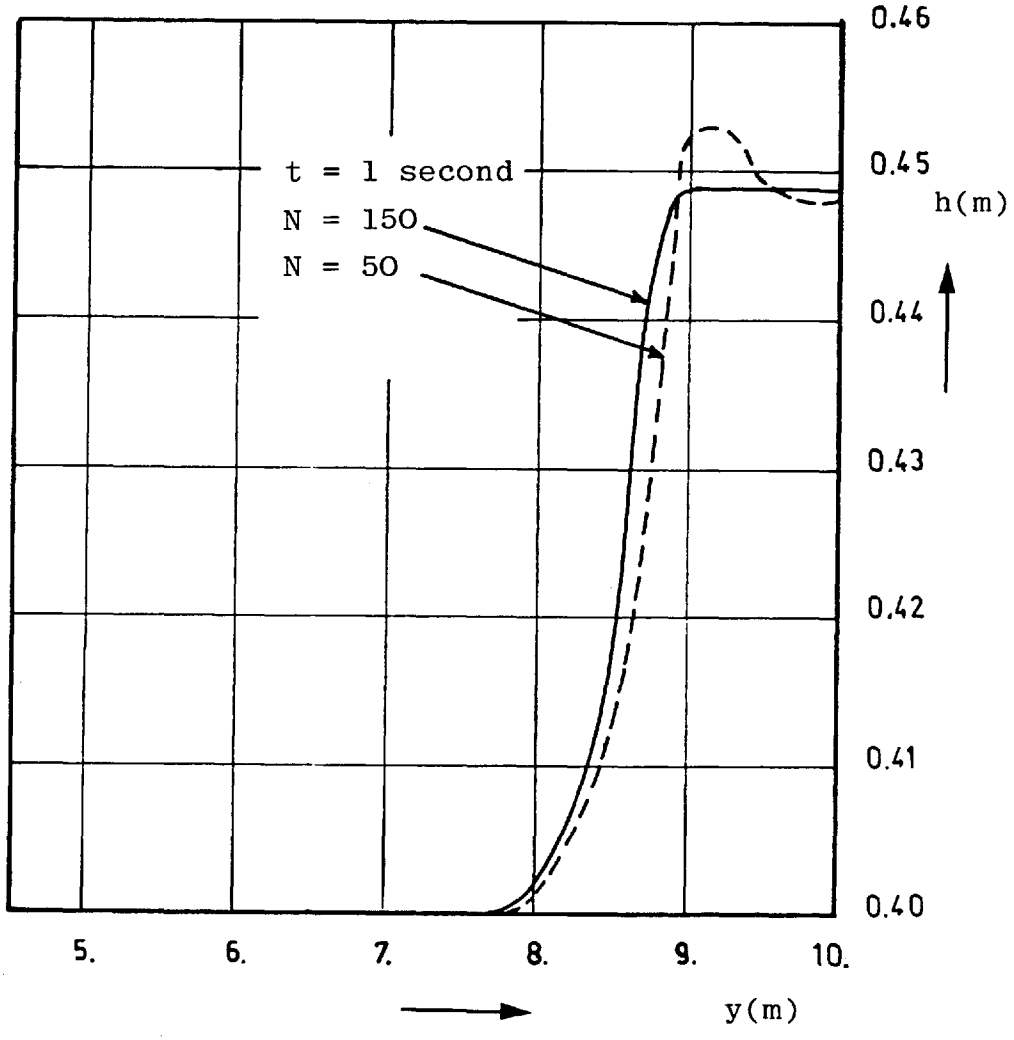


FIGURE (6-20) EFFECT OF GRID REFINEMENT ON THE WAVE CONFIGURATION (h_1 = 0.4 m; V_o = 0.2 m/sec.)

have not been employed in the present study and are left for future investigations.

(iii) Qualitative presentation of the results

Figures (6-21) to (6-23) present perspective views of the computed variables. Figure (6-21) shows the build-up of the wave front, for the case where h_1 = 0.5 m and V_o = 1 m/sec, viewed from various angles. For the same initial conditions, the velocity fields for both air and water are depicted in Figures (6-22) and (6-23) respectively. The air, having an initial velocity equal to $-V_o$, accelerates nearly to rest; on the contrary the water decelerates to stagnation as it reaches the closed end of the channel.

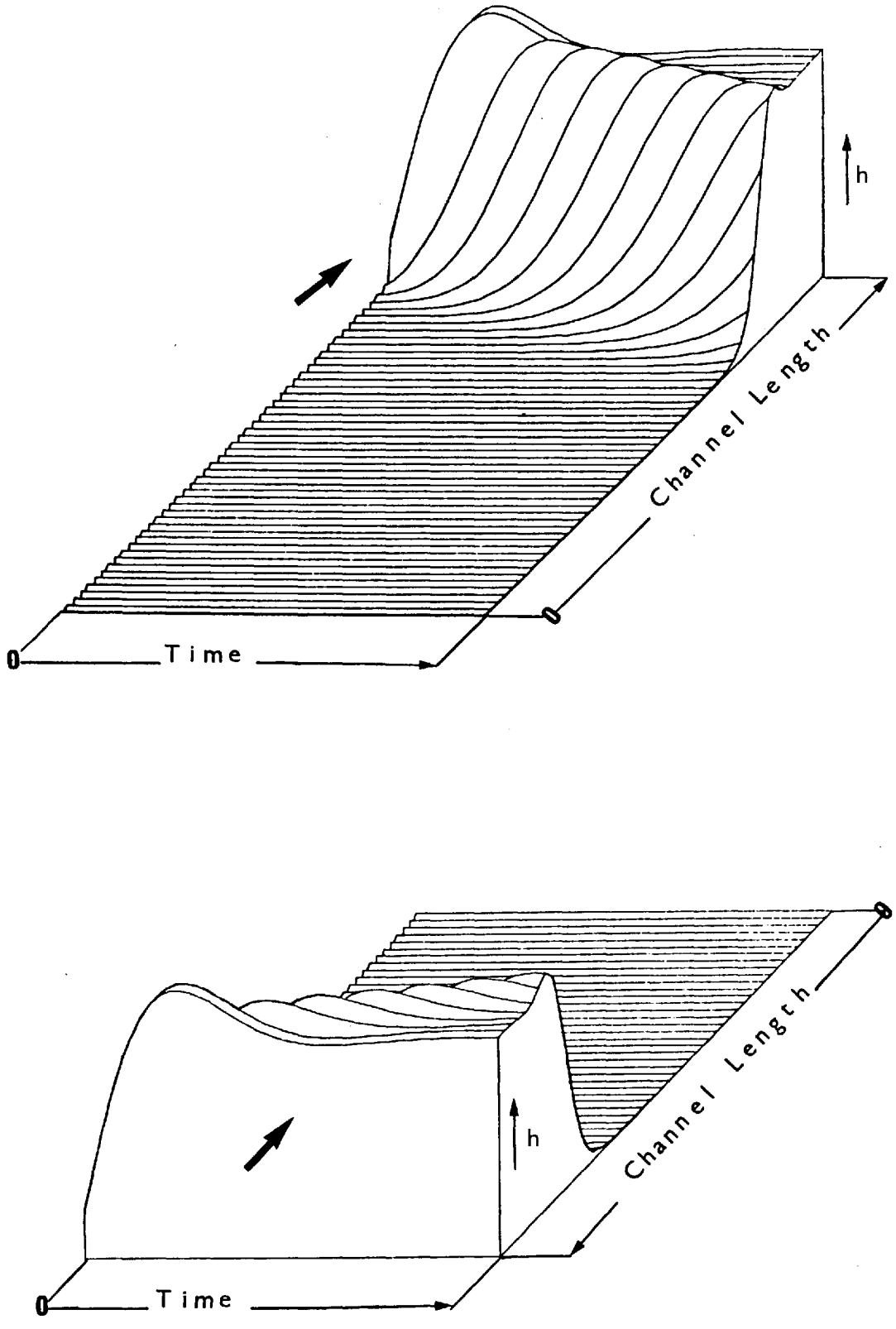


FIGURE (6-21) THE BUILD-UP OF THE WAVE FRONT AS SEEN FROM DIFFERENT VIEWS (h_1 = 0.5 m AND V_o = 1.0 m/sec.)

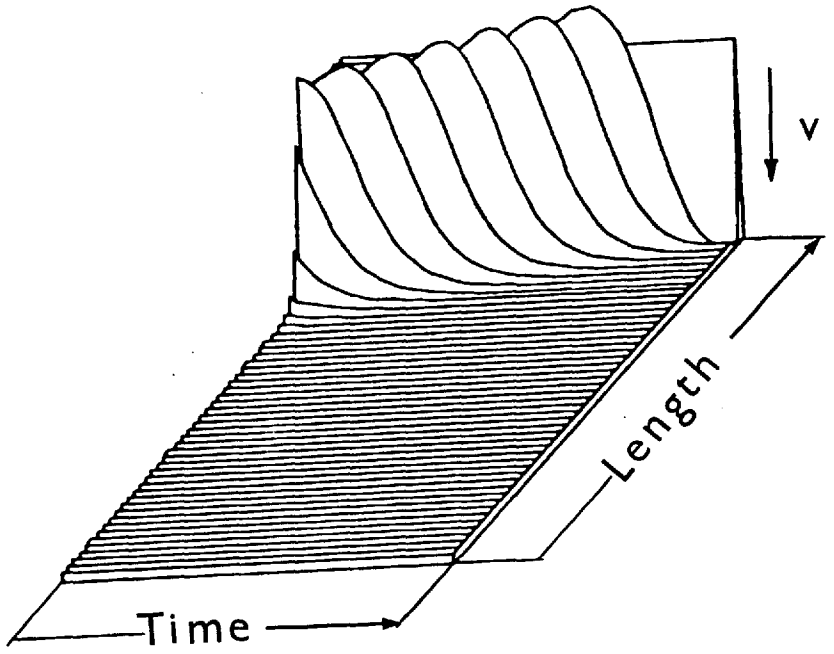


FIGURE (6-22) GAS VELOCITY DISTRIBUTION IN THE CLOSED-END CHANNEL PROBLEM

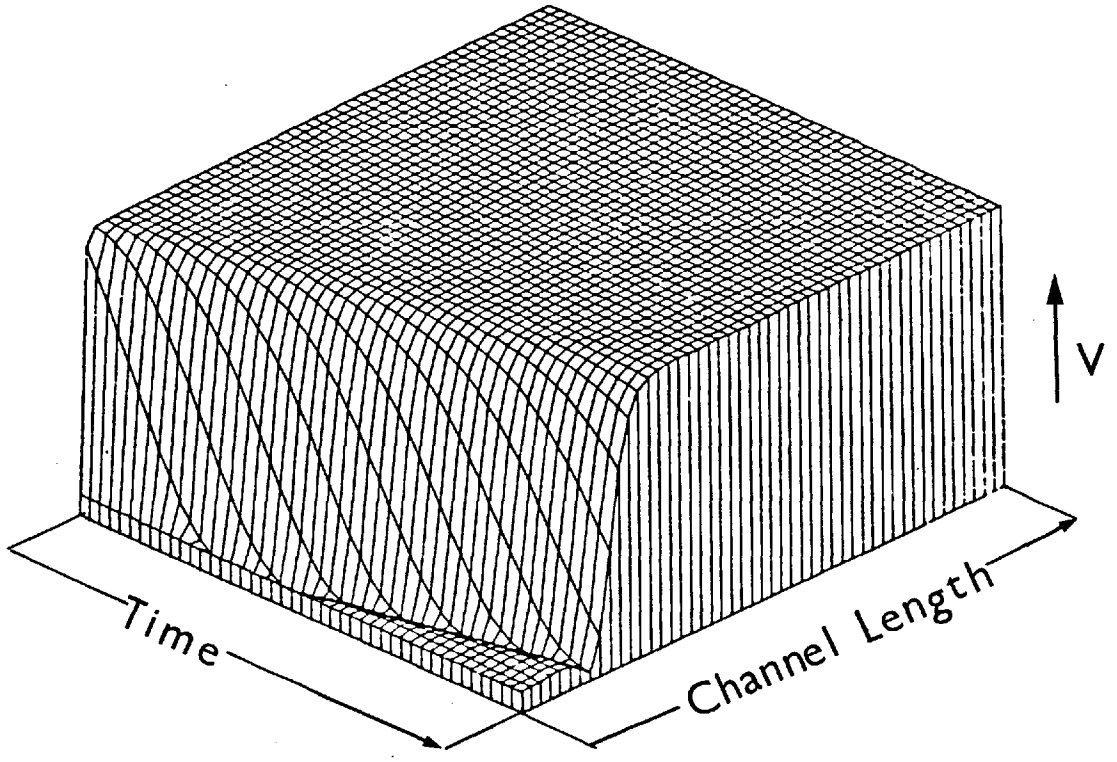


FIGURE (6-23) LIQUID VELOCITY DISTRIBUTION IN THE CLOSED-END CHANNEL PROBLEM

6.4 PREDICTION FOR COMPARISON WITH EXPERIMENTAL DATA

6.4.1 Introduction

Prediction of the two-phase flow characteristics is based largely on empirical correlations. The most widely used, that of Lockhart and Martinelli (1949), has been modified by several researchers (e.g. Bertuzzi et al, 1956 and Baroczy, 1965), however errors up to fifty percent have been reported in their applications. These correlations are related completely to the flow-pattern, and are based on flow visualisation. More recently, mechanistic approaches have been used successfully to predict pressure drop, hold-up, and other parameters for horizontal stratified gas-liquid flows in pipelines and conducts. Etchells (1970), Govier and Aziz (1972) and Agrawal et al, (1973) proposed the calculation of the frictional pressure drop for laminar-liquid/turbulent-gas stratified flow from friction factors, based on single-phase flow, properly adapted to the geometrical configuration of the cross-sectional area of the pipe. In the present section, the investigation of two-phase concurrent stratified flow in a pipe is carried out, and the resulting predictions are compared with the experimental data reported by Agrawal et al, (1973). Special attention is given to frictional effects between the fluids and the pipe wall as well as the interfacial shear forces.

(b) Presentation of the problem

(i) Statement of the problem

Figure (6-24) illustrates the flow geometry considered. Both air and oil are flowing steadily in the same direction. The air is in turbulent motion while the oil is in laminar motion; the air-oil interface is smooth and horizontal. The fluid properties and the pipe dimensions are as follows:

Liquid (oil) density	=	814.67 kg/m^3
Liquid viscosity	=	5.06×10^{-3} Ns/m^2
Gas (air) density	=	4.13 kg/m^3
Gas viscosity	=	1.8×10^{-5} Ns/m^2
Pipe diameter (D)	=	0.02576 m
Pipe length	=	30 m

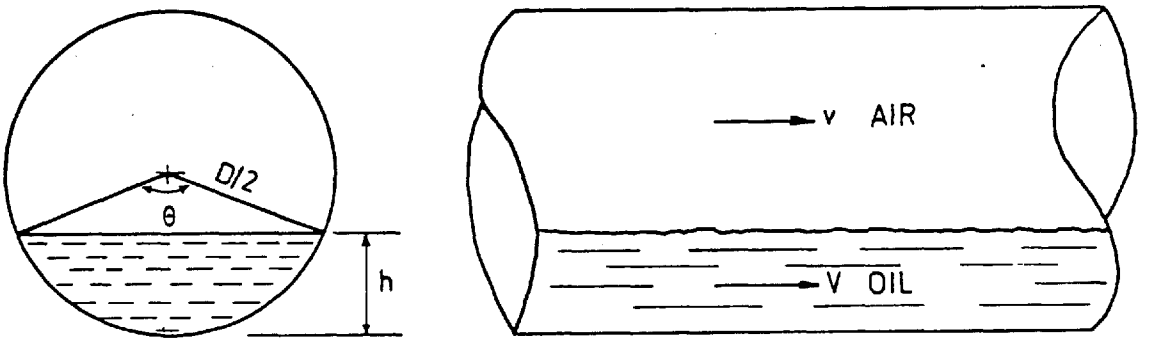
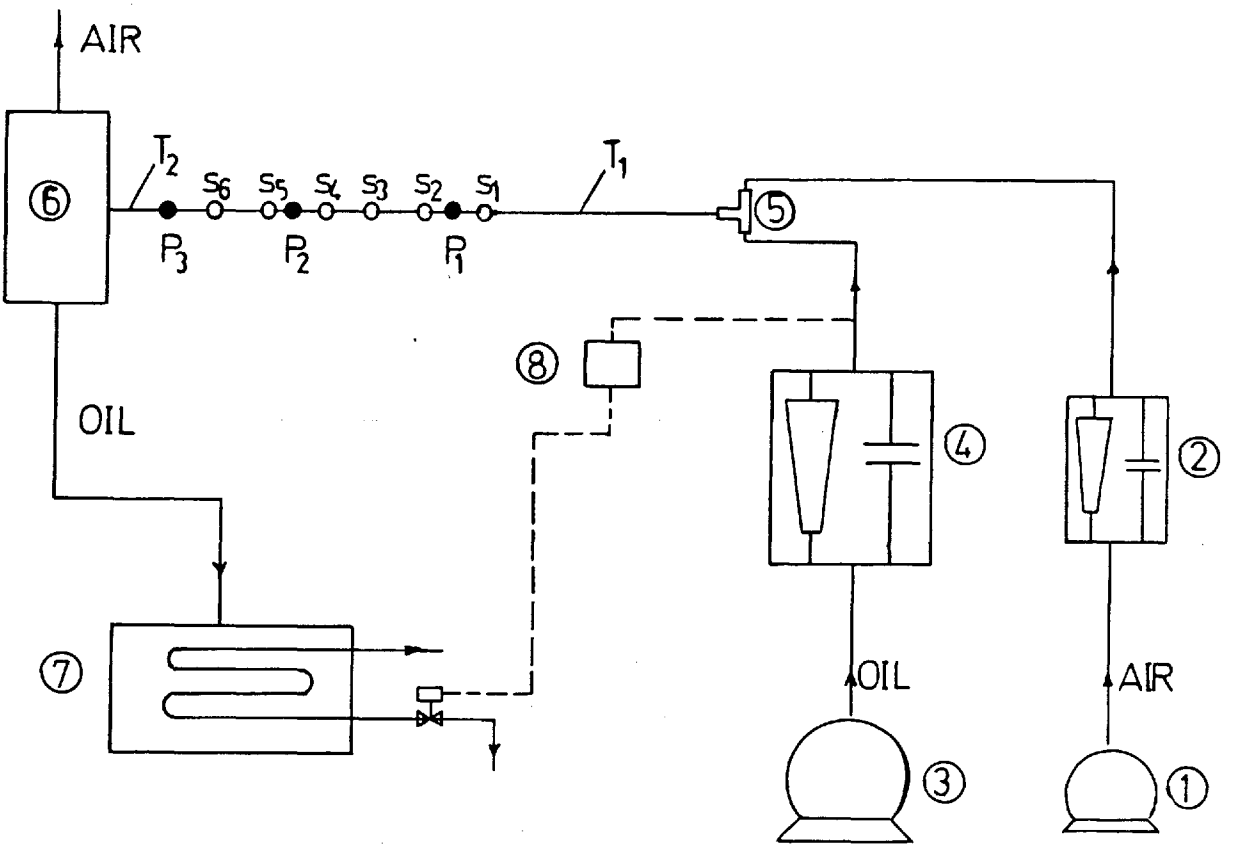


FIGURE (6-24) GEOMETRY AND NOTATION FOR THE STRATIFIED FLOW CONSIDERED

The task is to calculate the pressure drop and the volume fractions for known superficial velocities of the two phases.

(ii) Experimental arrangements

The geometry shown in Figure (6-24) respresents only a part of the experimental apparatus devised by Agrawal et al (1973). A schematic diagram of the major components that constitute the flow loop is shown in Figure (6-25). The test loop consisted of a clear acrylic tubing mounted on a trestle, supported every two feet by rubber cushioned blocks and levelled to within 1/16 inch. Air was supplied by a compressor and oil was introduced by means of a pump, the amount of both fluids was measured using rotameters and orifice meters. The two components were mixed in a simple T-junction, because the method of introducing the two streams does not affect the resulting two-phase flow patterns providing that the "Calming Zone" is of sufficient length, compare Govier and Aziz (1972); all the taping points were thus located down-stream the calming zone. The two phases, after leaving the test section, entered a gas-liquid separator where the gas left the



1. Compressor.
2. Gas metering (rotameter and orifice meter).
3. Pump.
4. Oil metering (rotameter and orifice meter).
5. Mixing chamber.
6. Gas-oil separator.
7. Storage tank plus heat exchanger.
8. Temperature controller.

P_1, P_2, P_3	Pressure taps
T_1, T_2	Thermometers
S_1, S_2, ..., S_6	Capacitance-type volume fraction sensor

FIGURE (6-25) SCHEMATIC FLOW DIAGRAM OF THE FLOW LOOP OF AGRAWAL ET AL.

system and the oil is returned to the pump through a storage tank with an internal heat exchanger to control the temperature and regulate the pressure of the flow.

Pressures were measured using water manometers. The oil volume fractions were measured using capacitance-type sensors, mounted directly in the flow line and causing no disturbance to the oil stream; the resulting signals were recorded and continuous monitoring of the liquid volume fraction was obtained, to a calibrated accuracy of 1.2%.

(iii) Reported results

The data reported by Agrawal et al (1973) includes:

(a) pressure drops, and
(b) average liquid volume fractions;

the paper also describes the results of several calculation methods developed by the authors and several other researchers. The data have been presented in two sets, identified by the fixed values of liquid superficial-velocity, V_{SL} (which is the product of liquid velocity and volume fraction). These values are

V_{SL} = 0.202 ft/sec and 0.046 ft/sec. respectively. In each case, the gas superficial-velocity is varied to obtain data for a number of flow conditions.

(c) Details of the computations

(i) Equations to be solved

1. Gas-volumetric continuity:

$$\frac{\partial}{\partial y} (R_\ell v) = 0 \qquad . (6.38)$$

2. Liquid-volumetric continuity:

$$\frac{\partial}{\partial y} (R_d V) = 0 \qquad . (6.39)$$

3. Gas-momentum conservation equation:

$$\underset{\text{convection}}{\frac{\partial}{\partial y} (R_\ell \rho_\ell v^2)} = \underset{\text{pressure gradient}}{- R_\ell \frac{\partial P}{\partial y}} + \underset{\text{inter-phase friction}}{f_y^{\ell d} (V-v)} - \underset{\text{wall friction}}{f_y^{\ell w} v} \qquad . (6.40)$$

4. Liquid-momentum conservation equation:

$$\frac{\partial}{\partial y} (R_d \rho_d V^2) = - R_d \frac{\partial P}{\partial y} + f_y^{d\ell} (v-V) - f_y^{dw} V - R_d (\rho_d - \rho_\ell) g \cos \alpha \frac{\partial h}{\partial y} \qquad . (6.41)$$

Notes on the equations:

- The volume fractions must satisfy the geometrical condition, viz.

$$R_\ell + R_d = 1 \qquad . (6.42)$$

- The wall- and interface-friction forces are calculated, from empirical correlations as given in section 6.2.3. For the circular cross-section used, the hydraulic mean diameter for the gas-phase is given by:

$$D = \frac{4 \times (\text{Cross-sectional area of the gas phase})}{\text{Wetted perimeter}} .$$

From geometrical relations, see Figure (6-24), one obtains:

$$D_\ell = 2\pi D \, R_\ell / (2\pi - \theta + 2 \sin \tfrac{\theta}{2}) \qquad . (6.43)$$

Likewise, the liquid hydraulic mean diameter, D_d, is given by:

$$D_d = 2\pi D \, R_d / \theta \qquad . (6.44)$$

Moreover, the inter-phase area per unit volume, A'', used in the calculation of $f_y^{\ell d}$ (equation (6.7)) is given by:

$$A'' = 4 \cos \tfrac{\theta}{2} \, / \, \pi D \qquad . (6.45)$$

- In the case of a circular pipe, the height of the liquid free surface above the bottom of the pipe, h, is related to the liquid volume fraction through the following two parametric relations:

$$h = \frac{D}{2} (1 - \cos \frac{\theta}{2}) \quad , (6.46)$$

and,

$$\theta - \sin \theta = 2\pi R_d \quad . (6.47)$$

For a certain value of R_d, the corresponding value of θ is calculated, from the latter equation, by using the Newton-Raphson technique and then the liquid height is deduced.

(ii) Boundary conditions

At inlet:

The values of the concentrations and the velocities are prescribed for both phases, so as to specify known values of the superficial velocity of the air and the oil that correspond to the measured ones.

At outlet:

At the outlet section, fully developed conditions prevail; thus the gradients of all dependent variables are set to zero or $\frac{\partial \phi}{\partial y} = 0$.

(iii) Finite-difference grid

An important feature of this problem is the fully developed nature of its flow (downstream of the calming zone). Thus, for computations only one metre of the pipe length is considered. A finite-difference grid consisting of 10 nodes is employed. The grid distribution is identical to the one illustrated in Figure (6-10).

(iv) Miscellaneous information

Typical information on a computational run is provided below.

STEADY STRATIFIED FLOW OF OIL AND AIR IN A PIPE	PERTINENT DATA
Configuration	Circular pipe
Grid nodes	10
Type of grid spacing	Uniform
Grid size per unit length of the pipe	0.125
Number of iterations	13
Computational time CDC 6600 (sec.)	0.1855
Computational time per grid node, CDC 6600 (sec.)	0.01855

TABLE (6-9) TYPICAL INFORMATION OF A COMPUTATIONAL RUN

(d) Presentation of the results

For the first set of flow conditions (V_{SL} = 0.202 ft/sec.), the pressure drops and the average liquid volume fraction, E_L, are presented in Figures (6-26) and (6-27). In each diagram, the experimental data, the present predictions and the spread of the other reported predictions are shown. Similarly, Figures (6-28) and (6-29) present the results for the second set of flow conditions (V_{SL} = 0.046 ft/sec.).

(e) Present prediction technique

For the simultaneous determination of the average liquid volume fraction, E_L, and the pressure drop, a trial and error procedure is adopted. A value of E_L, is first assumed. The pressure drop ($\partial P/\partial y$) and the liquid-surface inclination ($\partial h/\partial y$) are then determined (knowing both liquid and gas superficial velocities). These calculations are repeated for a set of different values of E_L. The final solution, obtained by interpolation, is the one which corresponds to $\partial h/\partial y = 0$.

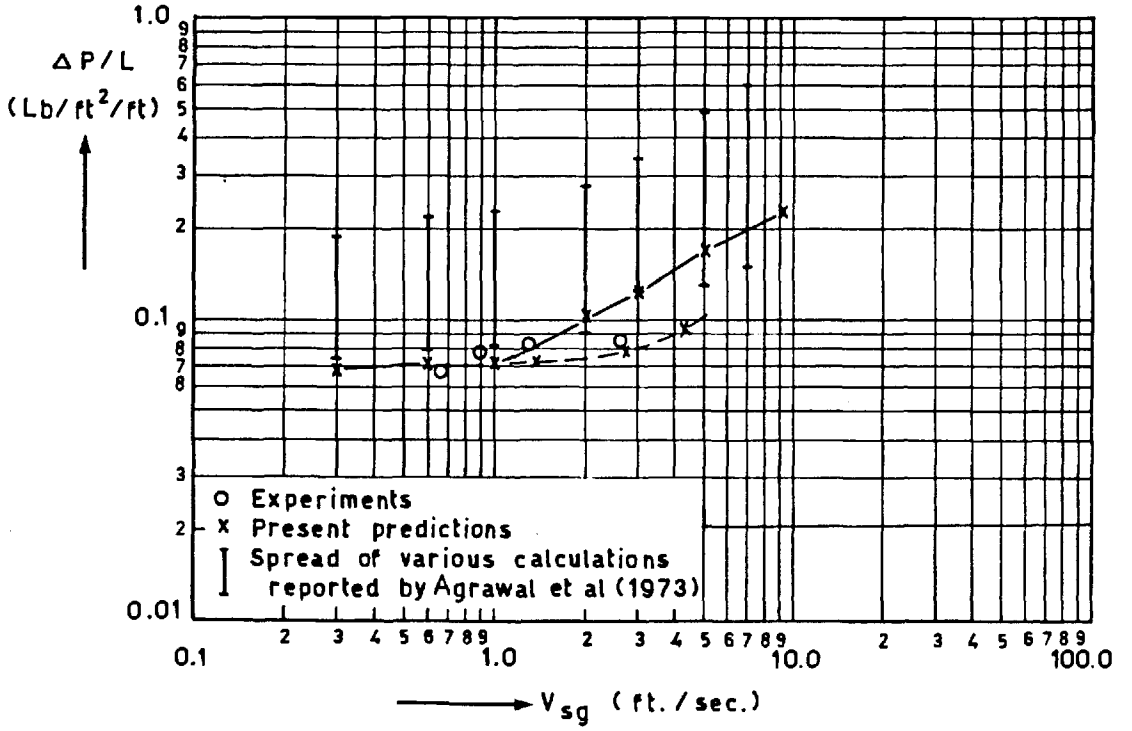


FIGURE (6.26) EXPERIMENTAL AND CALCULATED PRESSURE DROPS ; FOR SUPERFICIAL LIQUID VELOCITY , V_{SL} = 0.202 FT / SECOND. —x— RESULTS OBTAINED BY TRIAL & ERROR ; --x-- RESULTS USING THE MEASURED VALUE OF E_l AS AN INPUT.

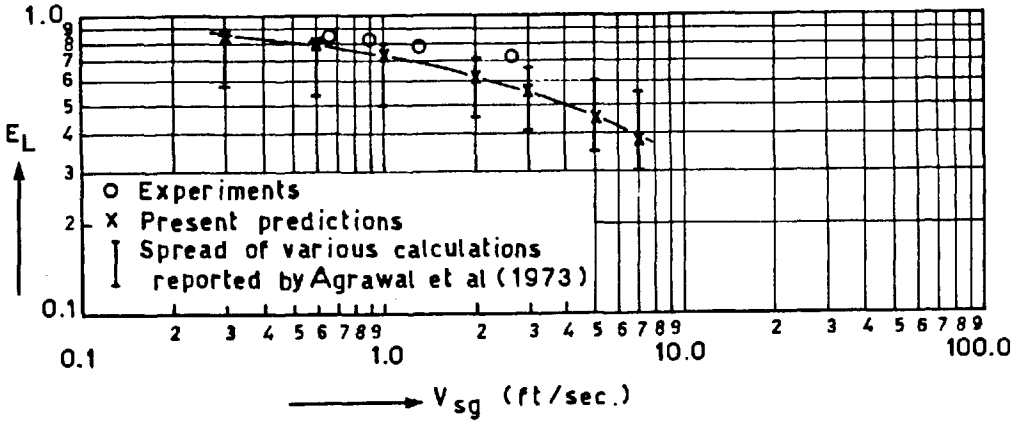


FIGURE (6.27) EXPERIMENTAL AND CALCULATED LIQUID-VOLUME FRACTIONS FOR SUPERFICIAL LIQUID VELOCITY , V_{SL} = 0.202 FT / SECOND.

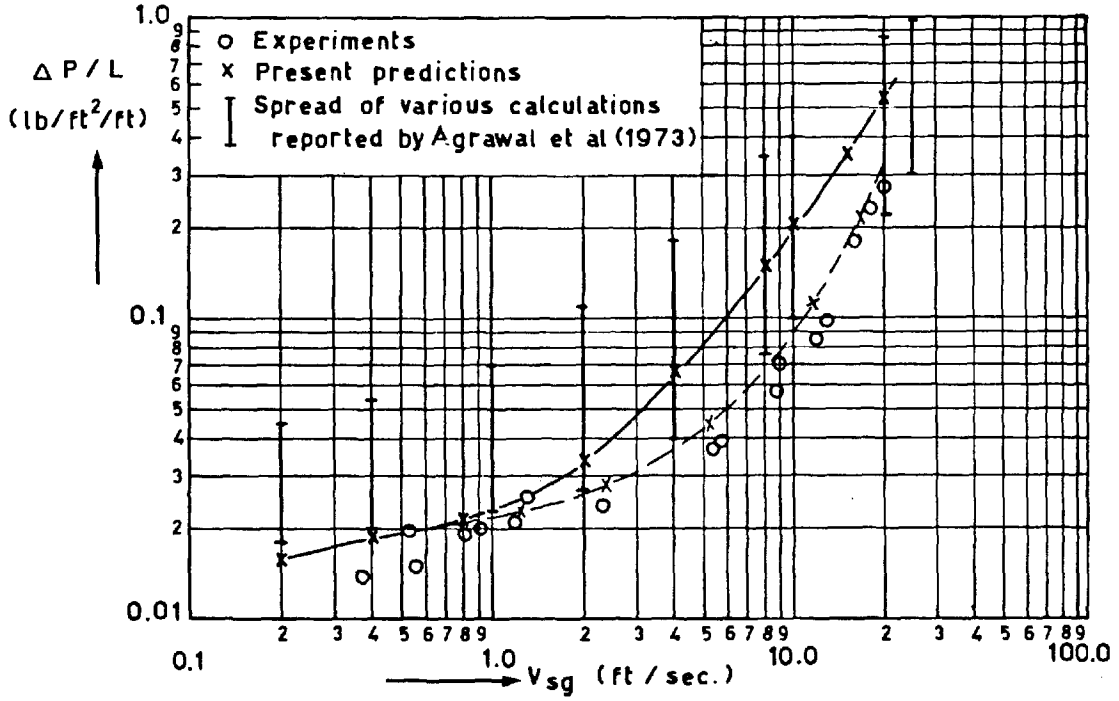


FIGURE (6-28) EXPERIMENTAL AND CALCULATED PRESSURE DROPS, FOR SUPERFICIAL LIQUID VELOCITY, V_{SL} = 0.048 FT/SECOND —x—RESULTS OBTAINED BY TRIAL AND ERROR---x--RESULTS USING THE MEASURED VALUE OF E_l AS AN INPUT.

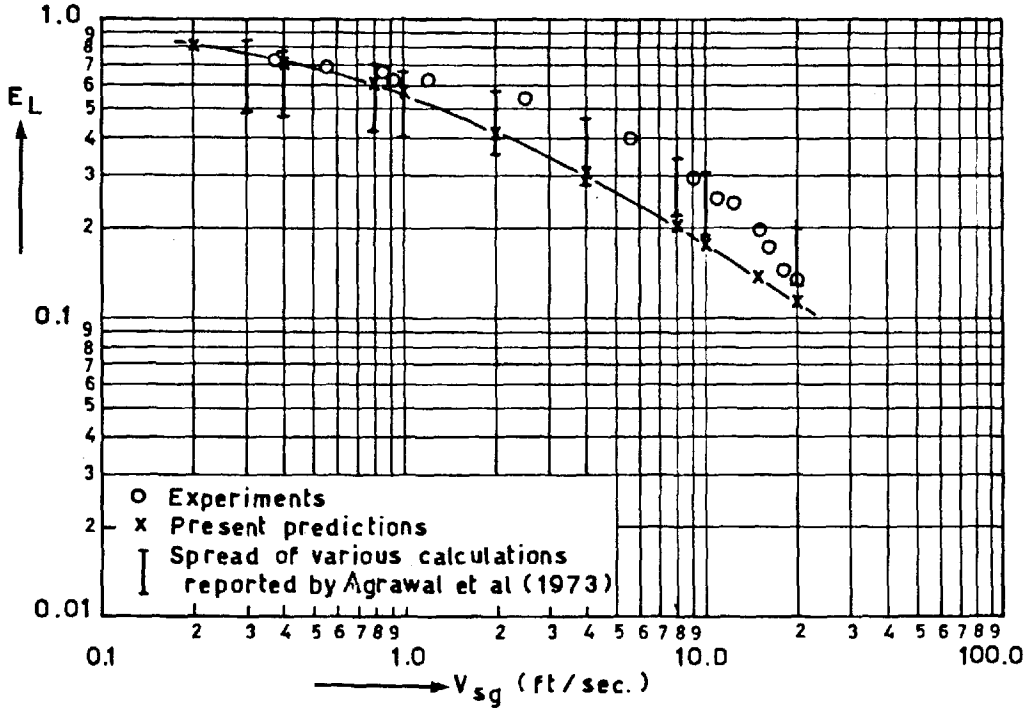


FIGURE (6-29) EXPERIMENTAL AND CALCULATED LIQUID-VOLUME FRACTIONS, FOR SUPERFICIAL LIQUID VELOCITY, V_{SL} = 0.048 FT/SECOND.

(f) Discussion of the results

(i) Results obtained using the trial and error procedure

Figures (6-26) to (6-29) indicate that the predictions based on the trial and error procedure adopted, of the pressure drops and average volume fractions have the correct trends in each case. The agreement with experimental data is quite good, particularly at low gas flow rates. In general the calculated pressure drops are higher and the liquid volume fractions are lower than the respective experimental values. This discrepancy refers partly to the interpolation method used in conjunction with the trial method, and partly to the empirical uncertainties. For example if the chosen value of E_L is less than the corresponding experimental value we shall obtain a value of the liquid concentration equal to $R_d - \Delta R$, where ΔR is the positive error in calculating the value of R_d; this will lead to an over-estimated value of the gas concentration, namely $R_\ell + \Delta R$. Since at a certain flow condition the superficial velocity of the two phases is specified, then the actual air velocity will be decreased by Δv where:

$$v - \Delta v = \frac{V_{SG}}{R_\ell + \Delta R} \qquad . (6.48)$$

Conversely the oil velocity is increased by ΔV

$$V + \Delta V = \frac{V_{SL}}{R_d - \Delta R} \qquad . (6.49)$$

These under- and over-estimations cause an increase in the predicted value of the pressure as follows:

$$\Delta P \propto (\rho_\ell R_\ell v^2 + \rho_d R_d V^2) - \{\rho_\ell (R_\ell + \Delta R)(v - \Delta v)^2 + \rho_d (R_d - \Delta R)(V + \Delta V)^2\}$$

The proper values — guessed values

. (6.50)

Neglecting the incremental terms of the second order and using equations (6.48) and (6.49) one obtains

$$\Delta P \propto \Delta R \left[\rho_\ell R_\ell v^2 \left(\frac{2}{R_\ell + \Delta R} - 1\right) + \rho_d R_d V^2 \left(\frac{2}{R_d - \Delta R} + 1\right)\right],$$

which may be approximated to,

$$\Delta P \propto \Delta R \left[\rho_\ell v^2 (2 - R_\ell) + \rho_d V^2 (2 + R_d)\right] \qquad . (6.51)$$

This shows that an error, ΔR, in calculating the volume fractions leads to an over-estimation of the corresponding value of ΔP proportional to the product of that error and a weighted average of both oil and air momenta.

(ii) Refinement of the predictions

In order to refine the quality of the predicted results, instead of guessing a value for E_L we take its measured value (so as to dispel any doubt in the evaluation of E_L) and accordingly we calculate the pressure drops. When this method is employed, the results of the pressure drops show closer agreement with the experimental data reported by Agrawal et al (1973) than the one obtained via the trial and error procedure; see Figures (6-26) and (6-28). The discrepancy between the measurements and the current predictions is not attributed to an error in calculating E_L; it arises from the uncertainties associated with the formulation of the friction correlations. These correlations represent a physical input to the numerical algorithm, they may be replaced by more accurate formulae in future compuations whenever these will be

available. At present, we are limited to examining the effects of varying the friction coefficients on the solution.

(iii) Investigation of the frictional effects

The relative effectiveness, of the gas-wall ($f_y^{\ell w}$), liquid-wall (f_y^{dw}) and the inter-phase ($f_y^{d\ell}$) friction coefficients, is studied by performing compuations in which one coefficient is reduced to half its normal value while the other two remain unchanged. These tests have been carried out for V_{SL} = 0.046 ft/sec., and the following two values of the superficial gas velocities: V_{SG} = 13.12 ft/sec; and 1.31 ft/sec.

The calculated results are presented in the following tables.

RUN NO.	FRICTION COEFFICIENT	PRESSURE DROP 0.1lb/ft^2/ft (EXP. VALUE)	AVERAGE LIQUID VOLUME FRACTION 0.23 (EXP. VALUE)
1	Standard values	0.275	0.150
2	$f_y^{d\ell} = \frac{1}{2} f_y^{d\ell}$ standard	0.273	0.178
3	$f_y^{\ell w} = \frac{1}{2} f_y^{\ell w}$ standard	0.183	0.170
4	$f_y^{dw} = \frac{1}{2} f_y^{dw}$ standard	0.260	0.114

TABLE (6-10) EFFECT OF VARYING THE FRICTION COEFFICIENTS, V_{SG} = 13.12 ft/sec.

RUN NO.	FRICTION COEFFICIENT	PRESSURE DROP 0.024 lb/ft^2/ft (EXP. VALUE)	AVERAGE LIQUID VOLUME FRACTION 0.6 (EXP. VALUE)
1	Standard values	0.028	0.51
2	$f_y^{d\ell} = \frac{1}{2} f_y^{d\ell}$ standard	0.028	0.56
3	$f_y^{\ell w} = \frac{1}{2} f_y^{\ell w}$ standard	0.024	0.55
4	$f_y^{dw} = \frac{1}{2} f_y^{dw}$ standard	0.018	0.44

TABLE (6-11) EFFECT OF VARYING THE FRICTION COEFFICIENTS, V_{SG} = 1.31 ft/sec.

From these tables, the following observations are made:

(a) The reduced inter-phase friction does considerably improve the calculated liquid-volume fraction, its effect on pressure drops is only marginal.

(b) The reduction in gas-wall friction brings in a more significant improvement for the calculated pressure drops than for the liquid volume fraction values.

(c) The reduction of liquid-wall friction worsens the results of the liquid volume fractions.

By performing this exercise, we have demonstrated that agreement between theory and experiment can be improved by altering the correlations.

6.5 PREDICTIONS OF FLOWS OF ENGINEERING INTEREST

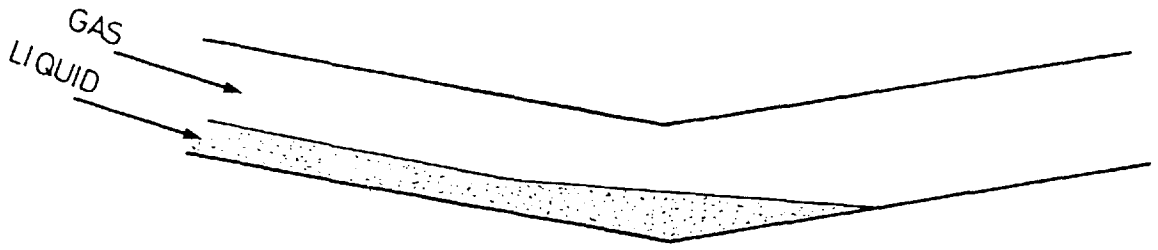
6.5.1 Introduction

The problems considered previously have been compared with analytical results and experimental data to test the credibility of the model and the solution procedure. In this section we demonstrate the flexibility of the model, by applying it to the solution of various flows of engineering interest. The flow of gas and oil condensate in under-ocean pipe lines is studied because of its practical relevance. This flow is characterised by the slug formation. The mechanism of slug formation is not well understood. What is evident is that slugs will tend to form at any dip in a nearly horizontal section of the pipe, and that formation will involve the following sequence of events, illustrated in Figure (6-30):

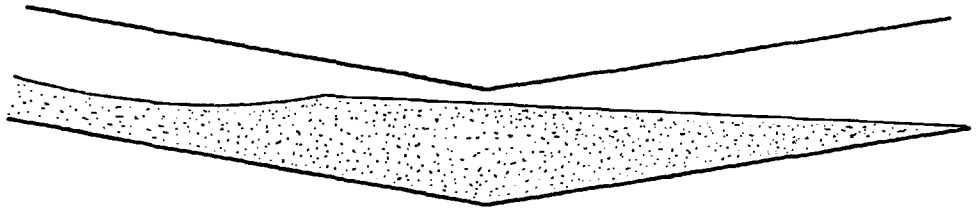
(i) If the pressure drop in the pipe is insufficient to carry the liquid up to the upward-inclined section, liquid will build up at the bottom of the dip (Figure(6-30a)).

(ii) The liquid will build up to block (or nearly to) the pipe (Figure (6-30b)).

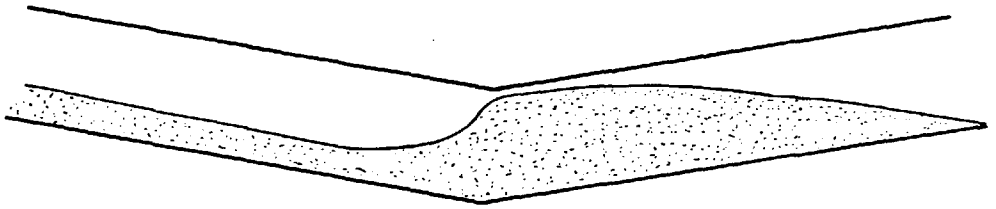
(iii) As the liquid blocks the pipe, the gas pressure upstream the dip will build up, until the upstream pressure is sufficiently high to force the liquid



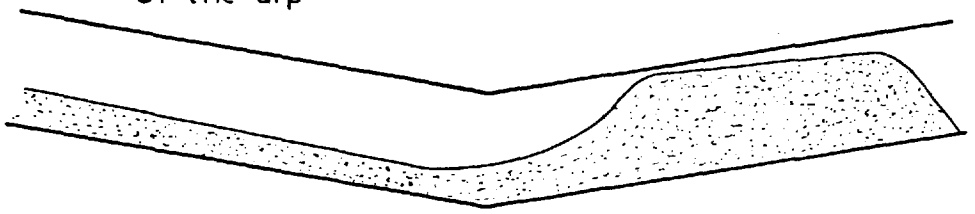
(a) Liquid builds up in the dip



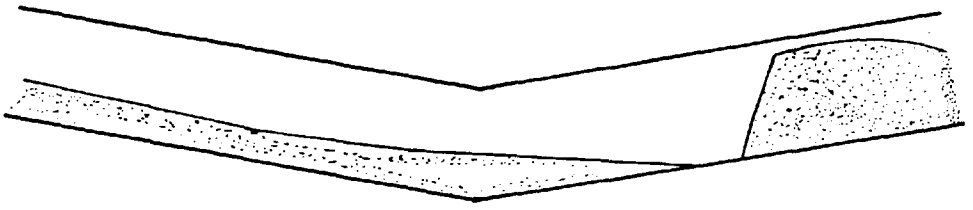
(b) Liquid nearly blocks the pipe; gas pressure builds up behind the blockage



(c) The gas pressure forces a liquid 'slug' out of the dip



(d) The slug continues to move downstream



(e) The dep begins to fill again

FIGURE(6-30) ILLU STRATION OF THE LIKELY MECHANISM OF SLUG FORMATION AT A V-SHAPED DIP IN A PIPE

collected in the dip, to move along the pipe as a slug (Figure (6-30c)).

(iv) The slug then continues downstream. The dip begins to fill up behind the slug, and the process is repeated.

The slug formation involves a complex interaction of gas and oil hydrodynamics; waves are expected to form in the stratified flow upstream of the dip as a consequence of the unsteady "gulping" occurring at the dip. Thus, the present case combines the critical aspects of gravity stratification encountered in the course of the previously studied problems of sections 6.3 and 6.4.

6.5.2 Transient Flows in Pipes with Inclinations and Bends

By extending the predictions to flow conditions where the transient behaviour is easy to anticipate, one may verify the predictions at least qualitatively. This fosters confidence in the present procedure and demonstrates its flexibility. It is with this aim in mind that we have chosen to analyse the transient response of stratified flows in V-bends and inclined pipes.

The study of the present problem is laid out below, in the same pattern as for the previously discussed problems.

(a) Objectives of the study

(i) To demonstrate that the solution procedure gives plausible solutions for the transient behaviour in pipes with a V-shaped dip.

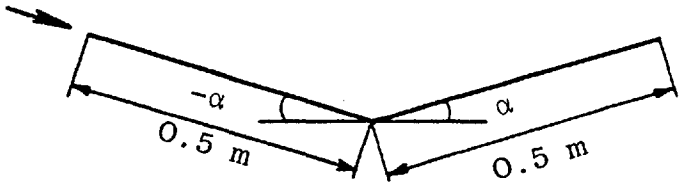
(ii) To examine the effect of the grid-refinement and the choice of the time increment on the amplitude, the phase angle and the period of the transient phenomenon.

(b) Presentation of the problem

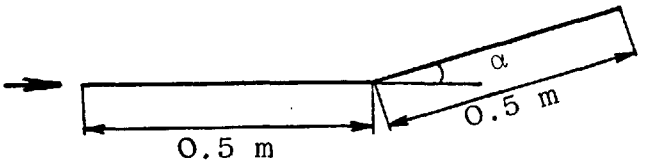
(i) Statement of the problem

The transient flow of oil and air in inclined pipes and bends, of different constructions, is analysed. The geometries considered are shown in Figure (6-31). The angle of inclination is taken as a parameter and its influence on the transient phenomenon is studied.

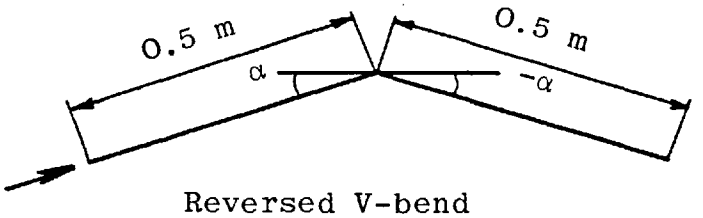
The fluid properties and the pipe diameter are the same as in problem 6.4.2. Initially, the velocities and the concentrations are given uniform values along the pipe. At the



V-bend

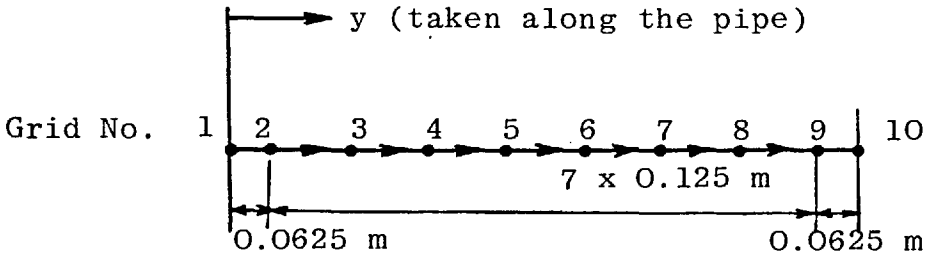


Inclined pipe with one horizontal side



Reversed V-bend

(a) Geometries considered



(b) Grid arrangement

FIGURE (6-31) THE INCLINED PIPE GEOMETRIES CONSIDERED

inlet section a constant influx of air and oil is maintained from t = 0 onwards. At the outlet the liquid-height is kept constant and the velocities are allowed to vary.

(c) Details of the computations

(i) Equations to be solved

1. Gas-volumetric continuity:

$$\frac{\partial R_\ell}{\partial t} + \frac{\partial}{\partial y} (R_\ell v) = 0 \qquad . (6.52)$$

2. Liquid-volumetric continuity:

$$\frac{\partial R_d}{\partial t} + \frac{\partial}{\partial y} (R_d V) = 0 \qquad . (6.53)$$

3. Gas-momentum conservation equation:

$$\underset{\substack{\downarrow \\ \text{momentum} \\ \text{accumulation}}}{\frac{\partial}{\partial t} (R_\ell \rho_\ell v)} + \underset{\substack{\downarrow \\ \text{convection}}}{\frac{\partial}{\partial y} (R_\ell \rho_\ell v^2)} = \underset{\substack{\downarrow \\ \text{pressure} \\ \text{gradient}}}{-R_\ell \frac{\partial P}{\partial y}} + \underset{\substack{\downarrow \\ \text{inter-phase} \\ \text{friction}}}{f_y^{\ell d} (V-v)} \underset{\substack{\downarrow \\ \text{wall} \\ \text{friction}}}{- f_y^{\ell w} v} \qquad . (6.54)$$

4. Liquid-momentum conservation equation:

$$\frac{\partial}{\partial t}(R_d \rho_d V) + \frac{\partial}{\partial y}(R_d \rho_d V)^2 = - R_d \frac{\partial P}{\partial y} + f_y^{d\ell}(v-V)$$

$$- f_y^{dw} V - R_d(\rho_d - \rho_\ell) g \cos \alpha \frac{\partial h}{\partial y}$$

↓

gravity force due to interfacial inclination

$$- R_d(\rho_d - \rho_\ell) g \sin \alpha \quad . \quad (6.55)$$

↓

pipe line inclination

Notes on equations:

- The concentrations must sum to unity in order to satisfy the geometrical condition.
- The wall- and inter-phase-friction factors are calculated in exactly the same manner as in problem 6.4.2.

(ii) Initial conditions

At t = 0:

- Oil-concentration (which is uniform along the channel) = 0.265
- Oil-velocity (which is uniform along the channel) = 0.0529 m/s
- Air-velocity (which is uniform along the channel) = 2.28 m/s

It is to be noted that the oil is in laminar motion while the air flow is turbulent.

(iii) Boundary conditions

- At inlet:

  The velocities and concentrations are prescribed: for air, $v(0,t) = 2.28$ m/s and $R_{\ell}(0,t) = 0.735$, for oil, $V(0,t) = 0.0529$ m/s and $R_d(0,t) = 0.265$.

- At outlet:

  At the exits of all the bends dealt with in this section, the concentrations are fixed while the velocities are allowed to vary with time. This implies that, at the outlet sections, the liquid-height is constant, which is equivalent to fixing the liquid driving potential at a specified level; this may be achieved by connecting the outlet of the pipe to a large reservoir of fixed liquid-level.

(iv) Finite-difference grid

In order to examine the effect of grid size on the predicted results, three different grids, containing respectively 10, 20 and 30 nodes were employed. The grid distribution along the pipe is

illustrated in Figure (6-31) for a grid consisting of 10 nodes.

(v) Time step

For a 10 node grid, different values of the time increment Δt were tried. It was found that a steady rate of convergence was secured when $\Delta t = 0.25$ sec, for all values of $\alpha \leq 2^{o}$. However, to maintain the same rate of convergence when $\alpha = 10^{o}$, Δt was reduced to a value of 0.025 sec. This may be attributed to the larger changes in the properties associated with the steeper pipe-inclinations. In other words, the sequence of event is much more rapid when $\alpha = 10^{o}$, which needs a smaller march in time to enable a proper detection of the transient behaviour.

Once the above values of Δt were selected, the value of Δt corresponding to a grid of N nodes is given by:

$$\Delta t_{N} = (\Delta t_{10} \cdot \frac{10}{N}) \quad ,$$

where Δt_{N} is the time increment corresponding to a grid of N nodes.

(vi) Miscellaneous information

Finally, some characteristic features, of the 1^{o}-bend problem, are tabulated below:

FLOW IN A 1^{o}-BEND	PERTINENT DATA
Configuration	Circular
Grid nodes	20
Grid size per unit length of the bend	0.0556
Type of grid spacing	Uniform
Time step Δt(sec.)	0.125
Number of time steps	1000
Number of iterations per time step	20
Computational time CDC 6600 (sec.)	597
Computational time per grid node per time step CDC 6600 (sec.)	0.0298

TABLE (6-12) TYPICAL INFORMATION ON A COMPUTATIONAL RUN

(d) Presentation of the results

(i) For V-bends

Figures (6-32) to (6-36) display the predicted results for the V-bend configurations considered. For ease of reference the relevant pipe geometry is sketched in each figure. The time variation of liquid-flow rate at outlet, normalised with respect to the inlet volume flux, is shown in each diagram.

(ii) For bends having one side horizontal

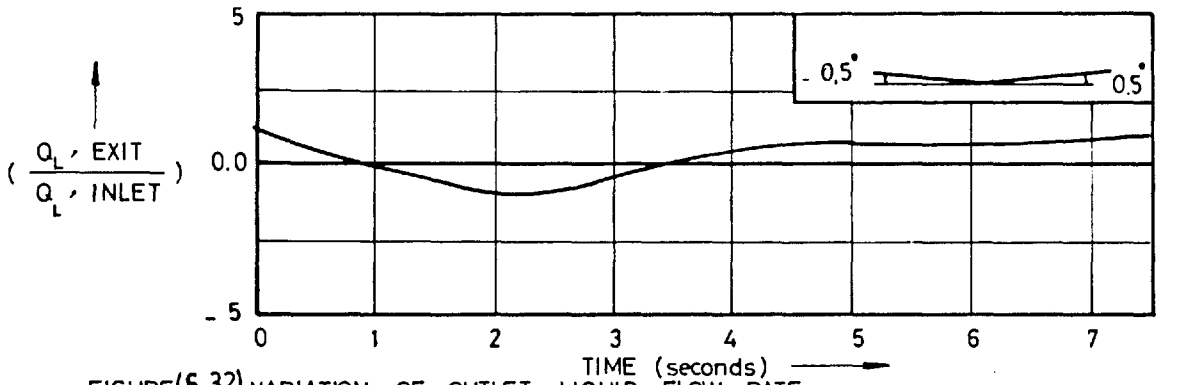
Figures (6-37) and (6-38) display the time variation in liquid-height along the pipe length, for both cases when α equals 1^{o} and 10^{o} respectively.

It is to be noticed here that the results obtained are considered grid-independent when the reduction in the grid size does not cause any alteration to the obtained solution. The dependence of the solution, on both grid size and time step employed, will be shown later in this section.

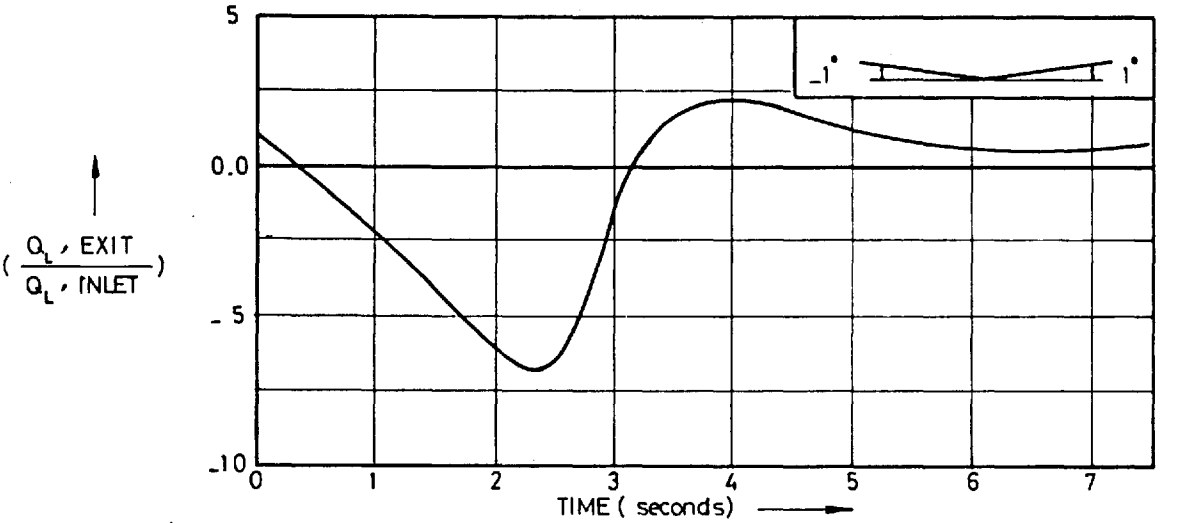
(e) Discussion of the results

(i) V-bends

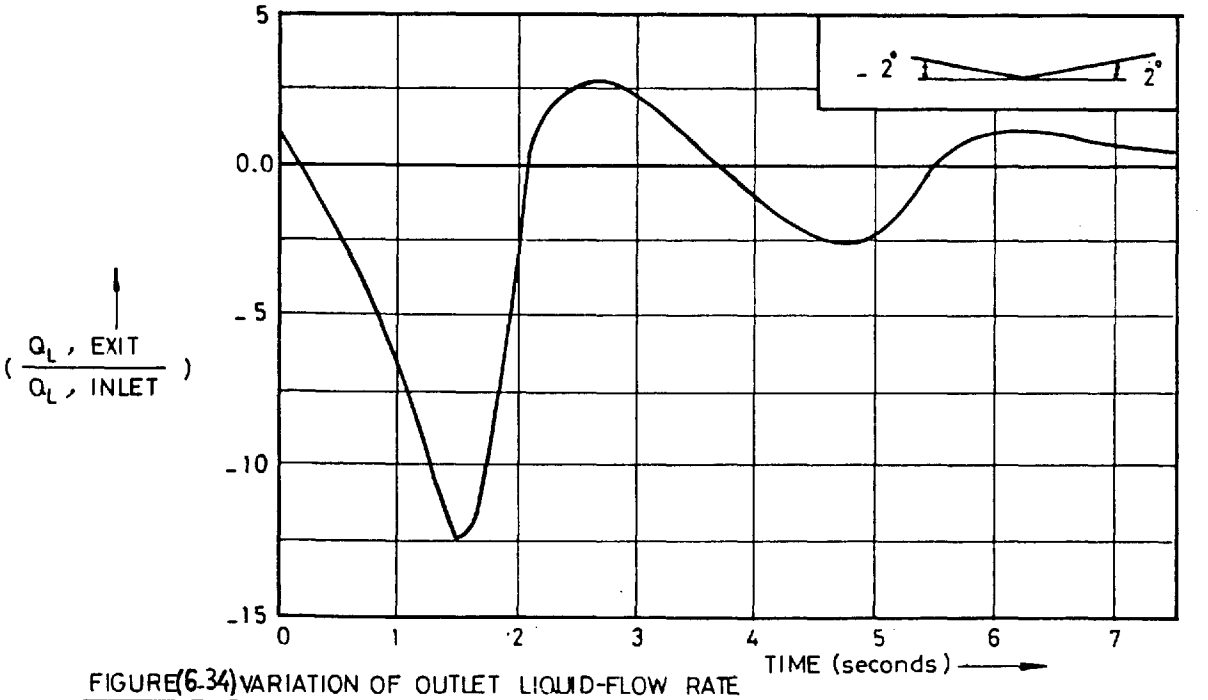
Figure (6-32) exhibits transient behaviour in the outlet flow rate for a shallow V-bend (symmetrically inclined to the horizontal, $\alpha = 0.5^{o}$); for steeper V-bends the results are illustrated in Figures (6-33) and (6-34)



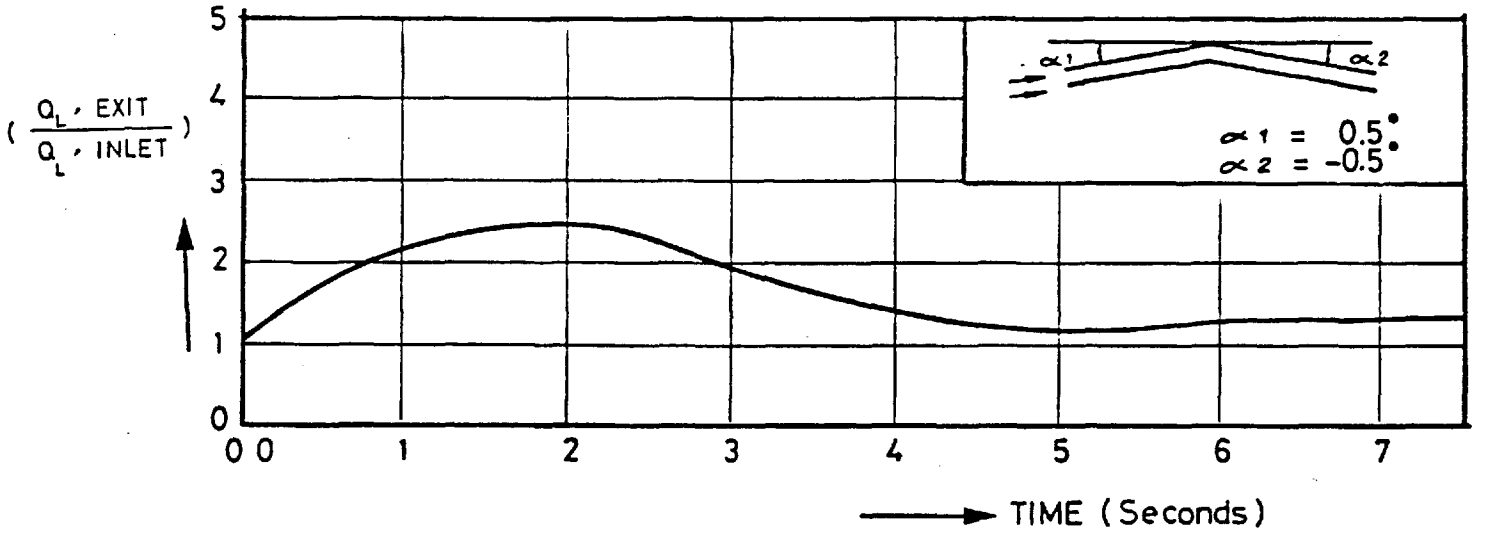
FIGURE(6-32) VARIATION OF OUTLET LIQUID-FLOW RATE



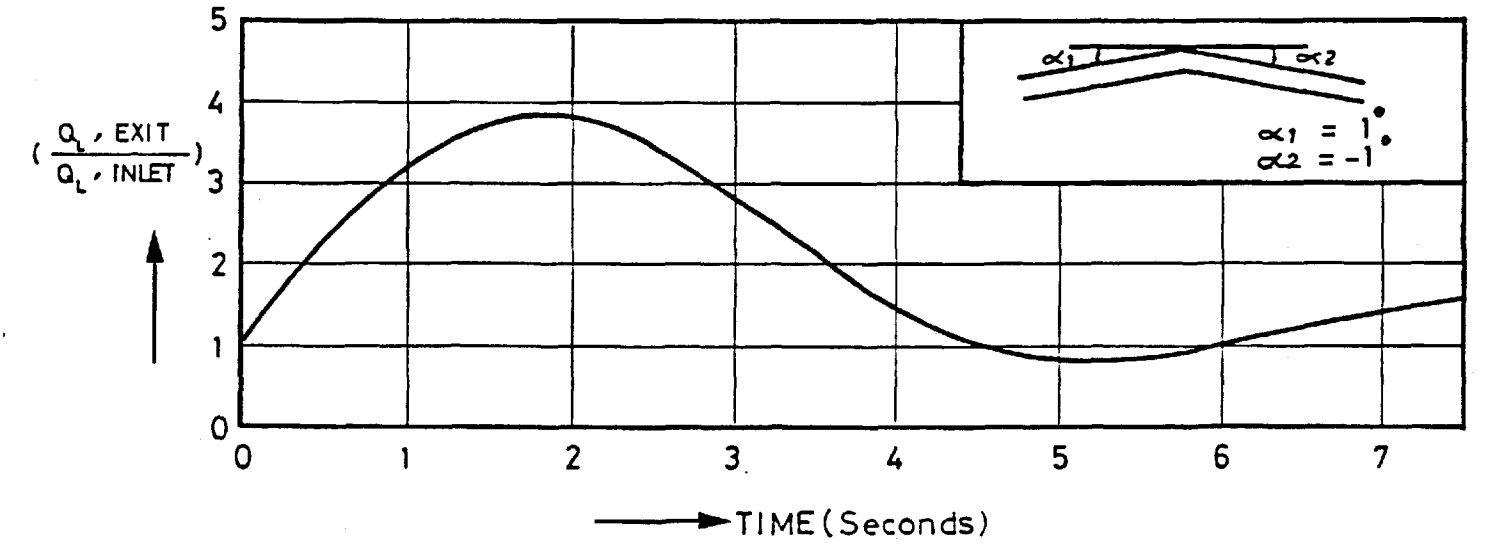
FIGURE(6-33) VARIATION OF OUTLET LIQUID- FLOW RATE



FIGURE(6-34) VARIATION OF OUTLET LIQUID-FLOW RATE



FIGURE(6-35) VARIATION OF OUTLET FLOW-RATE OF LIQUID



FIGURE(6-36) VARIATION OF OUTLET FLOW-RATE OF LIQUID

where $|\alpha| = 1^{o}$ and 2^{o} respectively. It is noticed that the steeper the bend, the larger the amplitudes and the smaller the period of the fluctuations, i.e. the transients are more severe in sharp angle bends. If the bends are reversed as shown in Figures (6-35) and (6-36) the results obtained exhibit trends opposite to those of Figures (6-32) and (6-33) respectively.

(ii) Bends having one side horizontal

We now consider the transient occurring in two bends having half of their length horizontal and the other half inclined at either 1^{o} or 10^{o} (to the horizontal). Figures (6-37) and (6-38) display the time variation in liquid height along the pipe length, for both cases. Figure (6-38) shows how strong the transient is, for steeper bends pipe; the sequence of events is more distinguished here: the maximum liquid level develops first near the bend, then it is shifted towards the outlet and finally settles in the near-bend region. For the 1^{o}-pipe bend the same sequence of events may be visualised by examining Figure (6-39), where the time variation in the liquid height is presented for

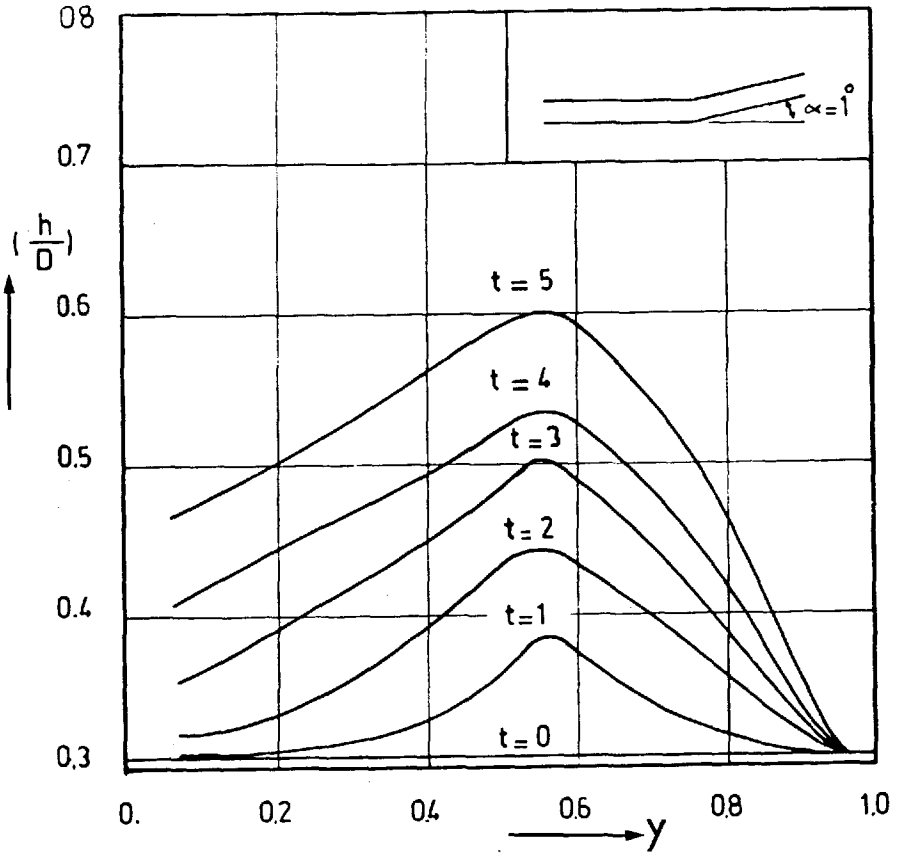


FIGURE (6-37) LIQUID LEVELS AT DIFFERENT TIMES IN A 1° V-BEND

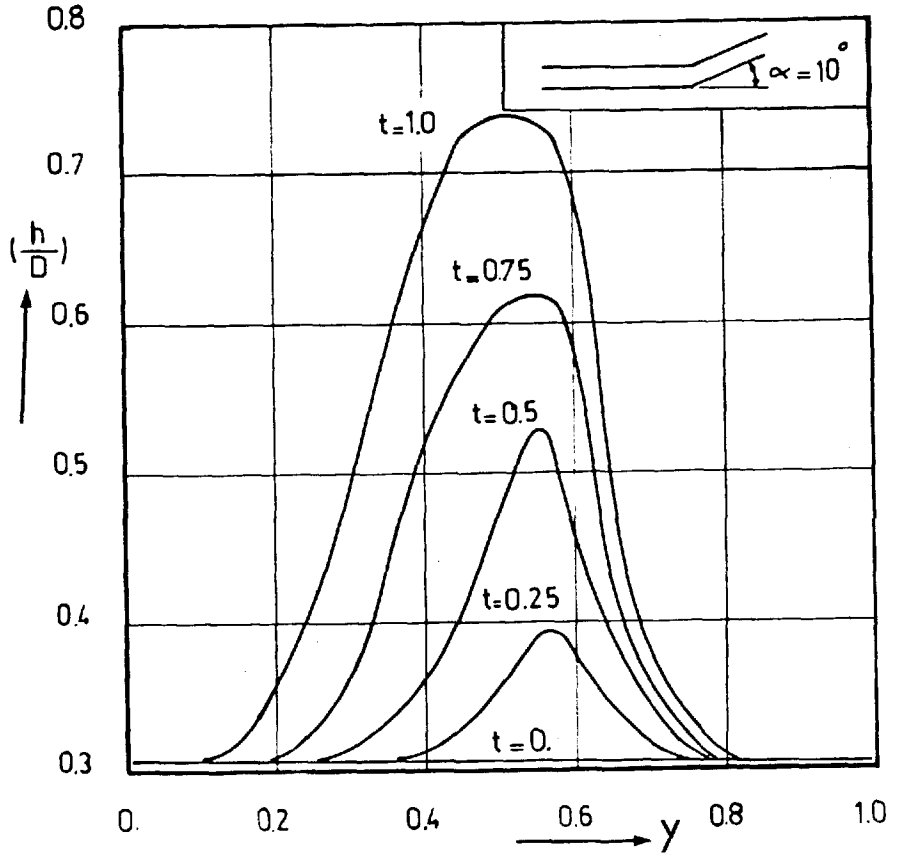


FIGURE (6-38) LIQUID LEVELS AT DIFFERENT TIMES IN A 10° V-BEND

a time period of 15 seconds. For the same span of time the corresponding velocity distribution is depicted in Figure (6-40). By comparing the last two figures one notices that the velocity of the liquid is lower in the region of higher liquid levels, as expected.

- Grid-dependence tests

  (a) Effect of the Grid Size on the Amplitude and Phase of the Transients

  For the two bends with one side horizontal, Figures(6-41) and (6-42) exhibit the effect of grid refinement on the amplitude of the fluctuations at different time intervals. Figure (6-41) shows that the error in predicting the maximum value of the liquid-height increases with time. By doubling the number of grid nodes from N = 10 to N = 20 (N.B. when N = 30, no significant changes occurred and the results were much the same as for N = 20), the change in liquid-height, after one second, was about 2.3%; however, after five seconds the error grew and reached a value of 9% (as shown in Figure (6-41)). The effect of reducing the mesh size is not only manifested in the evaluation of liquid-height but it does introduce a discernable lag in the phase angle as

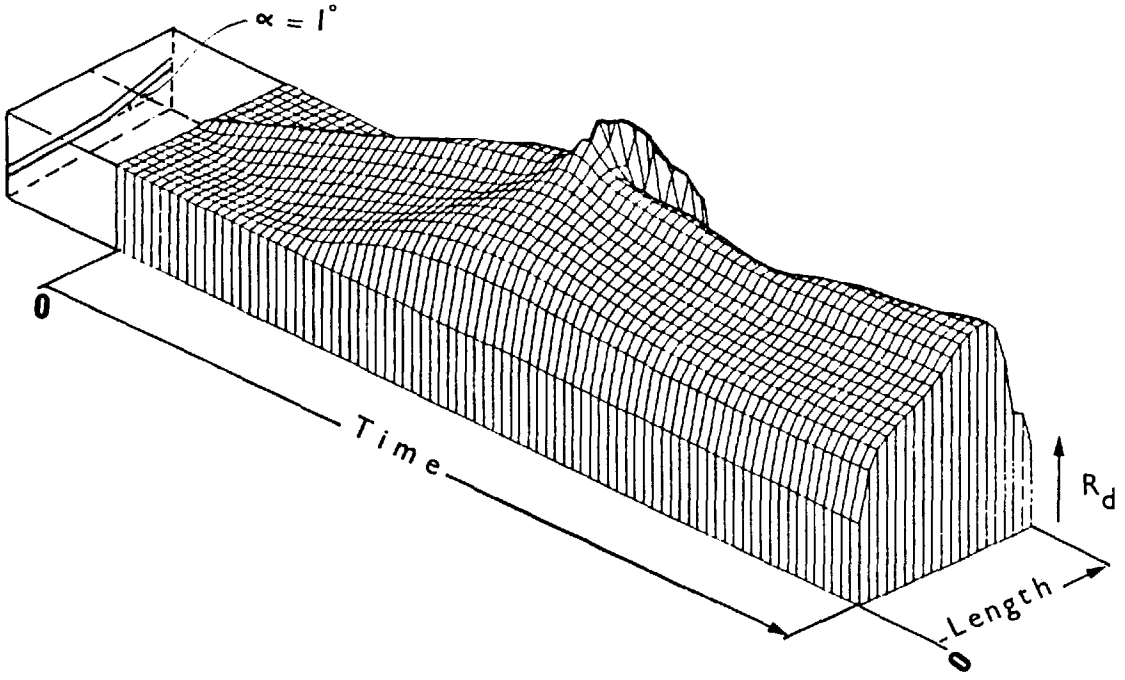


FIGURE (6-39) VARIATION OF LIQUID CONCENTRATION IN A 1^{o} V-BEND

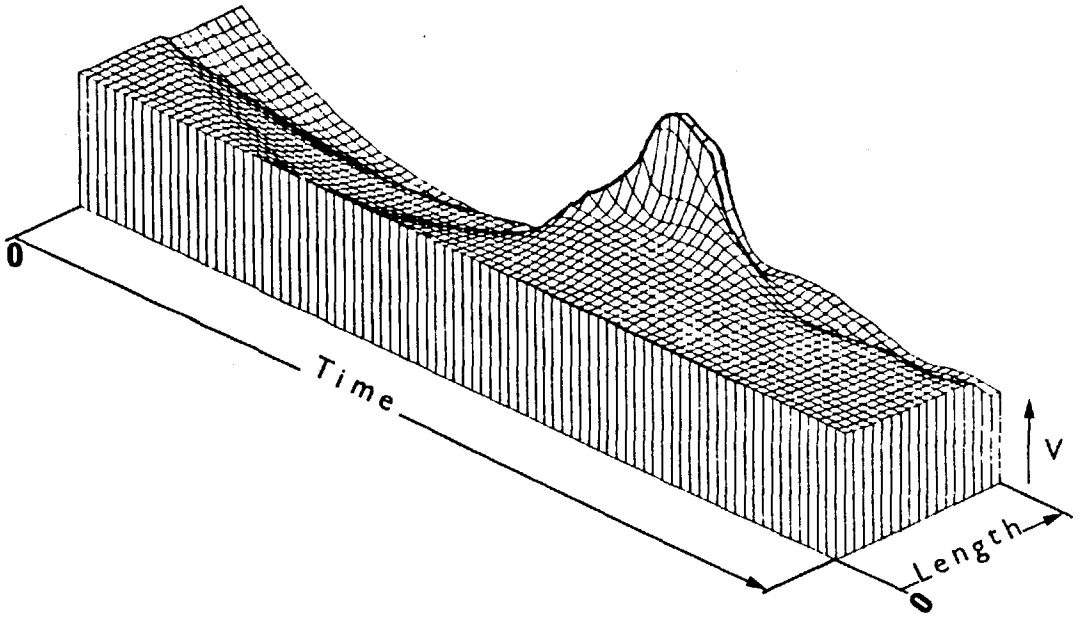


FIGURE (6-40) PREDICTED VELOCITY DISTRIBUTION IN A 1^{o} V-BEND

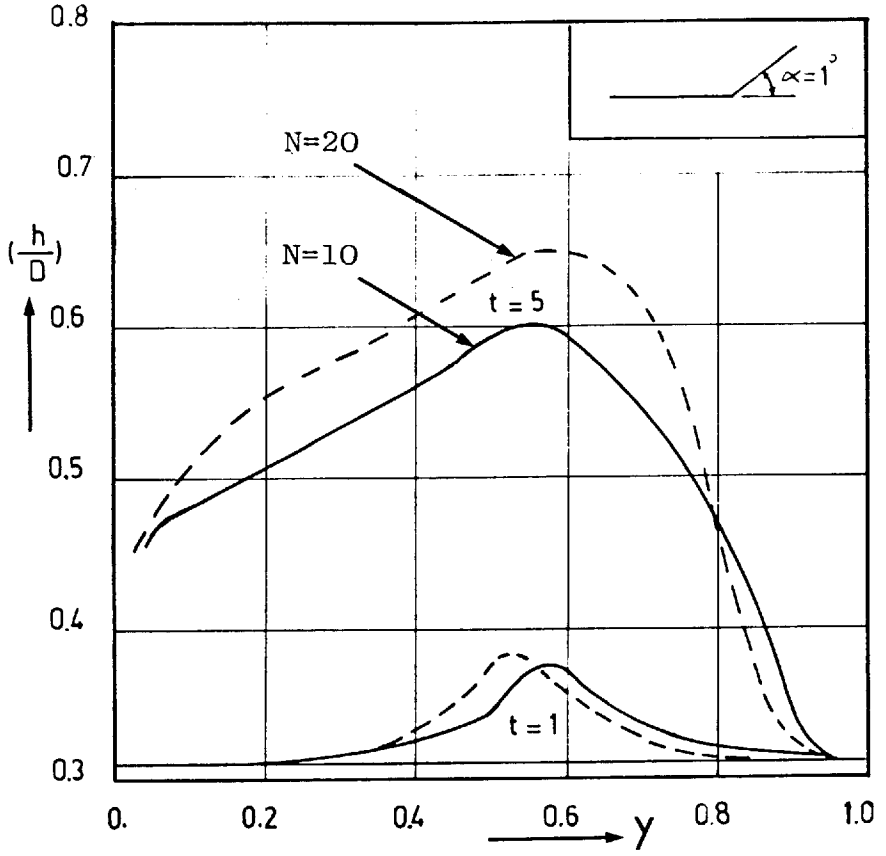


FIGURE (6-41) EFFECT OF GRID REFINEMENT ON THE AMPLITUDE FOR 1° V-BEND, AT DIFFERENT TIMES

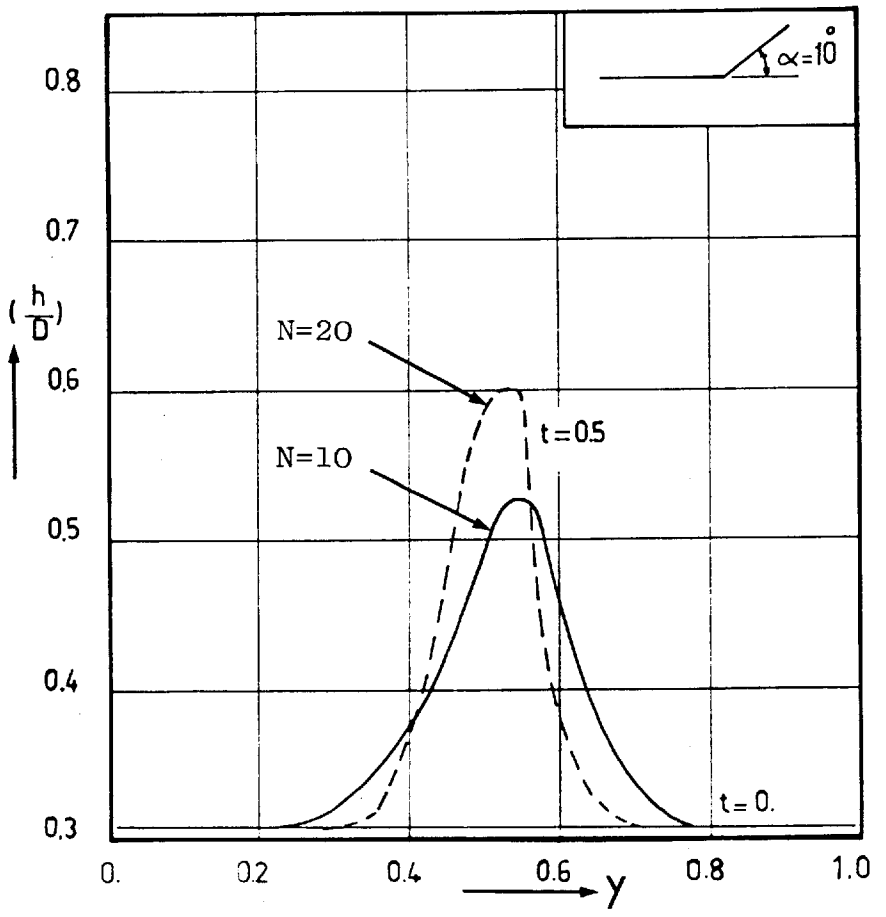


FIGURE (6-42) EFFECT OF THE GRID REFINEMENT ON THE AMPLITUDE, FOR 10° V-BEND, AT DIFFERENT TIMES

well as a diminution in the smearing of the wave front. Despite the magnification in the discrepancy, due to the stronger transient behaviour in the steeper bend, Figure (6-42) confirms the same observations.

(b) Effect of the Grid on the Period of the Transients

Figure (6-43) illustrates the transient behaviour of the non-dimensional outlet flow rate ($\alpha = 1^{o}$); the calculations were performed using two different mesh sizes: N = 10 and N = 20 (for N = 30 the results are practically the same as N = 20). The discrepancy in computing the minimum flow rate is as high as 50%; however, the periodicity of the transient is reduced by 8.5% when using a fine grid arrangement.

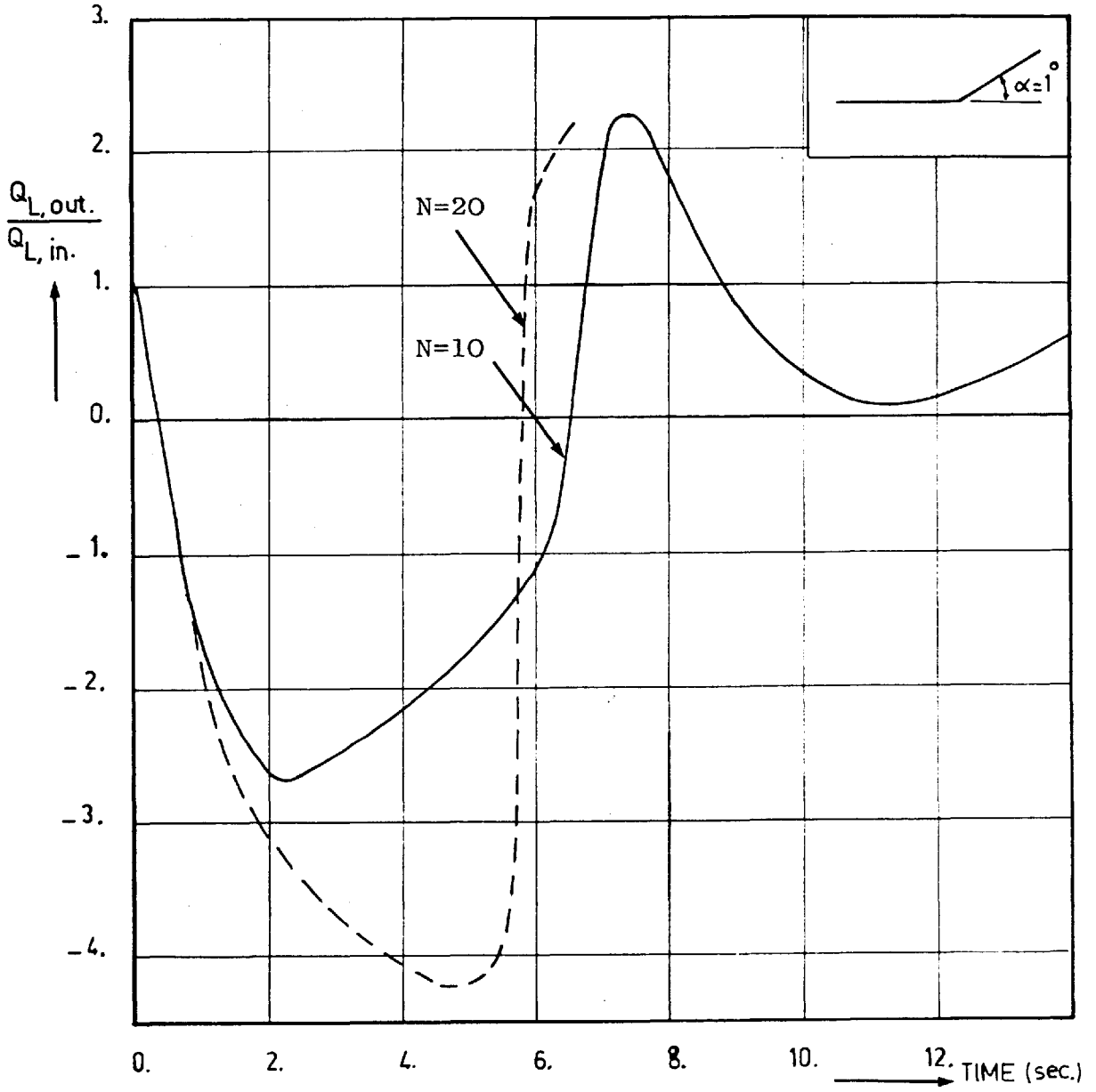


FIGURE (6-43) EFFECT OF GRID REFINEMENT ON THE PERIOD OF THE TRANSIENT

6.6 CONCLUDING REMARKS

- The results shown in this chapter demonstrate that the "IPSA" model produces accurate and realistic solutions for flows involving wave-propagation, and for stratified flows in pipes; the method also gives plausible solutions for the transient behaviour in pipes with a V-shaped dip.

It is worth emphasising that the solutions to all the problems were obtained with the same procedure, "IPSA-TV"; in each case, the sequence of operations outlined in sub-section 6.2.2 was followed without deviation.

- The numerical algorithm is stable, and yields results which converge to the solution of the differential equations as the grid and time step are suitably refined.

- In the assessment of the accuracy of the predictions, it is important to distinguish between two major kinds of error. One is computational: it arises from the various practices involved in the reduction of the differential equations to algebraic ones, and in the solution of the latter. The other major kind of error results from the inadequacy of our knowledge of the basic physical processes, which is reflected in our inability to make the differential equations described the real processes. Errors of the latter kind are of course absent from the predictions of idealised flow situations of section 6.3, so these may be regarded as tests of the computational accuracy alone. However, when frictional effects are taken into account, it is likely that the success or failure of the procedure to

predict the behaviour of the flow rests mainly on the validity of the physical hypotheses on which the friction-coefficients are based. In order to accept the results for viscous flows, with the same confidence as for the inviscid ones, more comparison with experiment and, perhaps, modifications to the theory, must be made.

With regard to the "false diffusion", which is the major contributor to computational errors, the findings of the studies described in this section suggest that the use of finer grids is sufficient to reduce the errors; however, a better remedy, that of using floating grids, was proposed in order to eliminate the "false diffusion".

- Regarding the economy of the present procedure, no comparison with the behaviour of other numerical procedures has been made, since the problems considered in this chapter have not been solved previously with a general computational procedure such as the one described here; however, the computing times for the cases studied in the course of this work were not excessive. This claim should not, however, be taken to imply that we are complacent about the speed of convergence presently attainable; at this early stage of the development much attention was given to the study of the algorithmic features of the procedure, and the optimisation of the method is left for future development.

CHAPTER 7

CONCLUDING REMARKS

The major objective of this thesis, that of providing a calculation procedure for two-phase flow phenomena, may be said to have reached a successful conclusion; in so far as the predictions obtained by "IPSA" for dispersed and stratified flows were shown in the course of this work to be numerically accurate and physically realistic. Below, a synoptic view is offered of how the "IPSA" model was validated and, lest this appears too self-congratulatory, we briefly survey the horizon for the many problems left undone.

7.1 ACHIEVEMENTS OF THE PRESENT STUDY

7.1.1 Numerical Aspects

1. Improvements were introduced to the basic version of "IPSA", in order to enhance its performance. The modifications, as presented in chapter 4, resulted in substantial improvement in the convergence rate and in an appreciable reduction in computer time.

2. A two-variable correction procedure, known as "IPSA-TV", was developed(and presented in chapter 6)to enable the solution of

stratified flows. This special version of "IPSA" took full cognizance of the gravity stratification effects. It was shown to produce realistic and accurate results when compared with both shallow-water theory and experimental data.

By reason of these results it may be concluded that the method of computation is stable, and that it produces results which will converge to the solution of the differential equations as the grid and time step are suitably refined.

7.1.2 Dispersed-Flow Calculations

Various fluid-particle problems have been solved. The predictions obtained in chapter 5 indicate that the newly developed algorithm can handle such mathematically complex situations. The following conclusions can be drawn:

1. The mathematical model is well posed and produces realistic and accurate solutions.

2. The study was restricted to dilute suspensions where a rather weak interaction between the phases is in evidence. Despite this, the existing alternatives of the inter-phase friction coefficient (equations (5.3) and (5.8)), were found to be questionable. This may be viewed as a warning for anyone intending to attempt the solution of dense suspension:

the major uncertainties relating to the inter-phase transfer still need to be cleared by means of experimental studies.

3. In the limit, when the dispersed phase has been neglected, the "IPSA" model reduces to a single-phase algorithm capable of predicting single fluid behaviour.

7.1.3 Stratified-Flow Calculations

The scope of the "IPSA" model is not inherently restricted to dispersed flows and indeed this point was proved by a modification of the algorithm for the study of stratified flows. Some computational models reported in the literature are applicable to only one or other of the two classes of two-phase flows considered here. The stratified flow calculations have been presented in chapter 6, the results lead to the following conclusions:

1. The model has been shown to predict correctly wave-motion on a stratified interface, and pressure drop and the hold-up in a steady stratified pipe flow. The truthfulness of the model has been demonstrated by the excellent agreement of its predictions with both analytical solutions and experimental data.

2. The model has been shown to predict unsteady motions, leading to slug formation in V-bend flows. The results were seen to be qualitatively plausible.

7.2 SUGGESTIONS FOR FUTURE WORK

Numerical models of fluid flow and heat transfer processes are well established for homogeneous phases, now they are under active development for the separated and interspersed phases. The present study is only a step in this direction but the goal is still far away. Many two-phase phenomena of importance await even their first inspection and present virgin territory for exploration. It is therefore useful at the close of this thesis, to look to the future so as to plan the next steps and to assess likely obstacles.

The recommendations for future work are listed below:

1. Numerical Problems

   (i) The incompletely-solved problems of single-phase numerical analysis spread their influence in the two-phase area such as:

   - The need to mitigate or better still eliminate the influences of numerical diffusion by appropriate choice of grid

configuration* and finite-difference formulation.

- The need to preserve order and flexibility in the associated computer codes, as the complexity of their physical content increases.

(ii) The difficulty in prescribing the wall boundary conditions implies an extensive study, in order to understand the mechanism of interaction between the phases and the wall boundaries. The development of wall functions valid for two-phase calculations is a desideratum.

2. Physical Problems

(i) The search for realistic and universal turbulence models is one of the most important and difficult tasks to achieve, in view of the numerous difficulties that are still encountered in single-phase flow modelling.

(ii) Multi-phase flows exhibit physical processes of their own; each of these defines a flow regime that is distinguishable from the others by specific interaction mechanism.

---

* The use of a floating grid system is one possible way.

For example, liquid-gas mixtures may exhibit: droplet, bubble, slug, annular or even other flow regimes, the prescription of inter-phase transfer laws at present can be performed only speculatively. This is another area that needs further research.

(iii) A framework of experimental studies is urgently needed in order to improve the available empirical correlations which hitherto have not taken into account transient effects. Also they are needed as an indisputable means of verifying the physical realism of any postulates proposed by the methodologists.

REFERENCES

1. AGRAWAL S S, GREGORY G A & GOVIER G W (1973)
"An Analysis of Horizontal Stratified Two-Phase Flow in Pipes".
The Canadian Journal of Chemical Engineering, vol.51, pp 280-286, June 1973.

2. AMES WF (1969)
Numerical Methods for Partial Differential Equations
Nelson and Sons Ltd., 1969.

3. ANDERSON T B & JACKSON R (1967)
"A Fluid Mechanical Description of Fluidized Beds".
Ind. Eng. Chem. Fundamentals, vol.6, pp 527-534

4. ATKINSON B, KEMBLOWSKI Z & SMITH J M (1967)
"Measurements of Velocity Profile in Developing Liquid Flows".
A.I. Ch. E. Journal, vol. 13, no. 1, pp 17-20, 1967

5. BAGHDADI A H A & ROSTEN H I (1977)
"Progress Report No. 1: The PLANT Code for One-Dimensional, Two-Phase Pipe-Line Calculations".
CHAM Report 1580/1

6. BAGHDADI A H A, ROSTEN H I & SINGHAL A K (1977)
"Progress Report No. 3: The PLANT Code for One-Dimensional, Two-Phase Pipe-Line Calculations".
CHAM Report 1580/3.

7. BAGHDADI A H A, ROSTEN H I, SINGHAL A K & TATCHELL D G (1977)
"Modelling of Slug Formation in Under-Ocean Pipe-Lines".
CHAM Report 1580/4.

8. BAGHDADI A H A, PUN W M & SPALDING D B (1977)
"A Few Case Studies with the CHAMPION 2/E/FIX Computer Code".
Imperial College, London, Mechanical Engineering Department, Heat Transfer Section Report No. HTS/TN/77/8, 1977.

9. BAGHDADI A H A, ROSTEN H I, SINGHAL A K, SPALDING D B, TATCHELL D G (1978)
"Finite-Difference Predictions of Waves in Stratified Gas-Liquid Flows".
ICHMT Seminar 1978, to be published by Hemisphere, 1979.

10. BANERJEE S & HANCOX W T (1978)
"Transient Thermohydraulics Analysis for Nuclear Reactors".
International Heat Transfer Conference, vol. 6, pp 311-337, Toronto 1978

11. BAROCZY C J (1965)
"A Systematic Correlation for Two-Phase Pressure Drop". Chem. Eng. Progr. Symposium, Ser. No. 64, 62, 232, 1965.

12. BERTUZZI A F, TEK M R & POETTMANN F H (1956)
"Simultaneous Flow of Liquid and Gas through Horizontal Pipe".
Petro. Trans., 207, 17, 1956.

13. BOOTHROYD R G (1971)
Flowing Gas-Solids Suspensions.
CHAPMAN and HALL Ltd., 1971.

14. BRADSHAW P (1971)
An Introduction to Turbulence and its Measurement.
Pergamon Press, 1971.

15. CARETTO L S, GOSMAN A D & SPALDING D B (1971)
"Removal of an Instability in a Free Convective Problem".
Imperial College, London, Mechanical Engineering Department, Heat Transfer Section Report No. EF/TN/A/35, 1971.

16. CARETTO L S, GOSMAN A D, PATANKAR S V & SPALDING D B (1972)
"Two Calculational Procedures for Steady, Three-Dimensional Flows with Recirculation".
Imperial College, London, Mechanical Engineering Department, Heat Transfer Section Report No. HTS/72/5, 1972.

17. CHARLETY P (1971)
"Ebullition du Sodium en Convection Forcée".
These de Docteur-Ingenieur, Faculté des Sciences de l'Universite de Grenoble, 1971.

18. CONSIDINE D M (1971)
Encyclopedia of Instrumentation and Control.
McGraw-Hill, 1971.

19. COOPER K D, HEWITT G F & PINCHIN B (1963)
"Photography of Two-Phase Flow".
UKAEA, Report No. AERE-R 4301

20. CROWE C T, SHARMA M P & STOCK D E (1975)
"The Particle-Source-In-Cell (PSI-Cell) Model for Gas-Particle Flows".
ASME Paper No. 75 WA/HT.25, 1975.

21. DALY B J (1978)
"Numerical Studies of Multi-Phase Flow in a Pressurised Water Reactor".
ICHMT Seminar, 1978, to be published by Hemisphere, Washington.

22. DELHAYE J M & JONES O C (1975)
"Measurement Techniques for Transient and Statistical Studies of Two-Phase, Gas-Liquid Flows".
ASME Paper 75-HT-10, 1975.

23. DELHAYE J M (1976)
"Measurement Techniques for Studies of Two-Phase Gas-Liquid Flows".
Proceedings of NATO Advanced Study Institute, August 1976, Istanbul, Turkey, Edited by Kakaç S and Mayinger F, Hemisphere Publication 1977.

24. DISA (INFORMATION DEPARTMENT) (1977)
"Type 55-S Two-Phase Flow Equipment", (Point Measuring of Void Fraction).
DISA Elektronik A/S DK-2740 Skovlunde, Denmark, 1977.

25. DOEBELIN E O (1966)
Measurement System, Application and Design.
McGraw-Hill, 1966.

26. ELLIS S R & GAY B (1959)
"The Parallel Flow of Two Fluid Streams:Interfacial Shear and Fluid-Fluid Interaction".
Trans. Inst. Chem. Eng., 37, 2, 1959.

27. ETCHELLS A W (1970)
"Stratified Horizontal Two-Phase Flow in Pipe".
Ph.D. Thesis, Univ. Delaware, 1970.

28. GIDASPOW D & SOLBRIG C (1976)
"Transient Two-Phase Flow Models in Energy Production".
Two-Phase Flows and Heat Transfer Proceedings of NATO Advanced Study Institute, Istanbul, Turkey, Edited by Kakaç S and Verziroglu T N, Hemisphere Publication, 1976.

29. GOVIER G W & AZIZ A (1972)
The Flow of Cómplex Mixtures in Pipes.
Van Nostrand Reinhold Company, 1972.

30. GRACZYK C (1961)
"The Application of the Venturi Tube to the Measurement of the Rate of Coal-Dust Transported by Air".
Acta Imeko, vol. 4, p.251.

31. HARLOW F H (1974)
"Round Table Discussions: Modelling of Two-Phase Flow".
5th International Heat Transfer Conference, Tokyo.
Proc. in Heat Transfer, Vol. VII, pp. 163-168.

32. HARLOW F H & AMSDEN A A (1975)
"Numerical Calculation of Multiphase Fluid Flow".
J. of Computational Physics, 17, 19-52, 1975.

33. HEWITT G F & HALL TAYLOR N S (1970)
Annular Two-Phase Flow.
Pergamon Press, Oxford, 1970.

34. HEWITT G F (1972)
"The Role of Experiments in Two-Phase Systems with Particular Reference to Measurement Techniques".
Progress in Heat and Mass Transfer, Vol. 6, pp.295-343.

35. HUGHES E D, LYCZKOWSKI R W, McFADDEN J H & NIEDERAUER G F (1976)
"An Evaluation of State-of-the-Art Two-Velocity Two-Phase Flow Models and their Application to Nuclear Reactor Transient Analysis".
Electric Power Research Institute, Report EPRI NP-143.

36. JONES O C & ZUBER N (1975)
"The Interaction between Void Fraction Fluctuations and Flow Patterns in Two-Phase Flow".
Int. J. Multiphase Flow, 2,273-306, 1975.

37. JORISSEN A L (1951)
"Discharge Measurement by Means of Venturi Tubes".
Transaction of ASME, vol. 73, p. 403.

38. KATYS G P (1964)
Continuous Measurement of Unsteady Flow
Pergamon Press, 1964.

39. LEE S L & EINAV S (1972)
"Migration in a Laminar Suspension Boundary Layer Measured by the Use of a Two-Dimensional Laser-Doppler Anemometer".
Int. Progress in Heat and Mass Transfer, vol. 6, pp. 385-403, 1972.

40. LOCKHART R W & MARTINELLI R C (1949)
"Proposed Correlation of Data for Isothermal Two-Phase, Two-Components Flow in Pipes".
Chem. Eng. Progr. 45, 39, 1949.

41. LYCZKOWSKI R W (1975)
"Transient Propagation Behaviour of Two-Phase Flow Equations".
15th National Heat Transfer Conference, San Francisco, 1975.

42. MARKATOS N C G (1974)
"The HELIOS Computer Program".
CHAM Ltd., Report No. 1030/1.
Bakery House, 40 High Street, Wimbledon, London, SW19 5AU.

43. MARKATOS N C G, MOULT A, PHELPS P J & SPALDING D B (1978)
"The Calculation of Steady, Three-Dimensional Two-Phase and Heat Transfer in Steam Generator". ICHMT Seminar 1978, to be published by Hemisphere 1979.

44. MIGDAL D & AGOSTA V D (1967)
"A Source Flow Model for Continuum Gas-Particle Flow".
Transaction of the ASME J. of Appl. Mech., pp.860-865, 1967.

45. MORSI S A & ALEXANDER A J (1972)
"An Investigation of Particle Trajectories in Two-Phase Flow System".
J. Fluid Mech., vol. 55, part 2, pp.193-208, 1972.

46. MURRAY J D (1965)
"On the Mathematics of Fluidization. Part 1: Fundamental Equations and Wave Propagation".
J. Fluid Mech., vol. 21, part 3, pp.465-493, 1965.

47. NIGMATULIN R I (1967)
"Equations of Hydromechanics and Compression Shock in Two-Velocity and Temperature Continuum with Phase Transformation".
IZV. AN SSSR Mekhanica Zhiclkosti i Gaza 2, no. 5, pp.33-47 (Soviet J. Fluid Mechanics).

48. PAI S I & HSICH T (1973)
"Interaction Terms in Gas-Solid Two-Phase Flows".
Z. Flugwiss, 21, pp.442-445, 1973.

49. PANTON R (1968)
"Flow Properties for the Continuum Viewpoint of a Non-Equilibrium Gas Mixture".
J. of Fluid Mechanics, vol. 31, pp. 273-303, 1968.

50. PATANKAR S V & SPALDING D B (1972)
"A Calculation Procedure for Heat, Mass and Momentum Transfer in Three-Dimensional Parabolic Flows".
International Journal of Heat and Mass Transfer 15, 1787-1806, 1972.

51. RUDINGER G (1974)
"Round Table Discussions: Modelling of Two-Phase Flow".
5th International Heat Transfer Conference, Tokyo.
Proc. in Heat Transfer, vol. VII, pp.163-168.

52. RUDINGER G (1976)
"Flow of Solid Particles in Gases".
AGARDograph No. 222, Edited by Auriol A.

53. PIVA R, SABETTA F, DI GIACINTO M (1978)
"Dusty Flows Through Baffles Inside a Duct".
Instituto di Aerodinamica, Universita Degli Studi di Roma.

54. PRATAP V S, SPALDING D B & TACHELL D G (1976)
"The NEAT Algorithm".
CHAM Ltd., Bakery House, 40, High St., Wimbledon, London, SW19, Report No. TR/20, 1976.

55. PUN W M (1975)
"Computation of Two-Dimensional Axi-Symmetrical Flows by the EASI 2 Computer Program".
CHAM Report B101/1, 1975.

56. PUN W M & SPALDING D B (1976)
"A General Computer Program for Two-Dimensional Elliptic Flows".
Imperial College, London, Mechanical Engineering Department, Heat Transfer Section Report No. HTS/76/2, 1976.

57. ROACHE J R (1972)
Computational Fluid Dynamics.
Hermosa Publication, 1972.

58. ROBERTS P H & DONELLY R J (1974)
"Superfluid Mechanics".
Annual Review of Fluid Mechanics, vol. 6, pp.179-223, 1974.

59. RUDINGER G & CHANG A (1969)
"Analysis of Non-steady Two-Phase Flow".
J. Physics of Fluids, vol. 7, pp.1747-1754, 1969.

60. RUNCHAL A K (1971)

"A Review of the Problems Associated with Numerical Instabilities".

Imperial College, London, Mechanical Engineering Department, Heat Transfer Section Report No.EF/IN/10, 1971.

61. SHARMA M P (1977)

"Numerical and Experimental Study of Gas-Particle Flows in Orifices and Venturis: Application to Flowmeter Design".

Ph.D. Thesis, Washington State University, 1977.

62. SHOOK C A & MASLIYAH J H (1974)

"Flow of a Slurry Through a Venturi Meter".

The Canadian Journal of Chemical Engineering, vol. 52, pp.228-233, April (1974)

63. SOLBRIG C W, McFADDEN J H, LYCZKOWSKI R W & HUGHES E D (1975)

"Heat Transfer and Friction Correlations Required to Describe Steam-Water Behaviour in Nuclear Safety Studies".

Paper presented at the 15th Heat Transfer Conference, August 10 - 13, San Francisco, California.

64. SOO S L (1967)

Fluid Dynamics of Multiphase Systems

Blaisdell Publishing Company, 1967.

65. SPALDING D B (1974)
"A Method for Computing Steady and Unsteady Flows Possessing Discontinuities of Density".
CHAM Ltd., Bakery House, 40, High St., Wimbledon, London, SW19, Report No. 910/2, December 1974.

66. SPALDING D B (1976 A)
"The Calculation of Free-Convection Phenomena in Gas-Liquid Mixtures".
Imperial College, London, Mechanical Engineering Department, Heat Transfer Section Report No.HTS/76/11, 1976.

67. SPALDING D B (1976)
"Basic Equations of Fluid Mechanics and Heat and Mass Transfer; Analysis of Convective Flows".
Imperial College, London, Mechanical Engineering Department, Heat Transfer Section Report No. HTS/76/6, 1976.

68. SPALDING D B (1978)
Private Communications, Concerning New Thoughts about the Inter-Phase Analyser Algorithm".

69. STREETER V L & WYLIE E B (1969)
Hydraulic Transients
McGraw-Hill Book Company, 1969.

70. STUHMILLER J H (1977)
"The Influence of Interfacial Pressure Forces on the Character of Two-Phase Model Equations". Int. J. of Multiphase Flow, vol. 3, pp.551-560, 1977.

71. VARGA R S (1962)

Matrix Iterative Analysis

Prentice-Hall International, London, 1962.

72. WALLIS G B (1969)

One-Dimensional Two-Phase Flow

McGraw-Hill Book Company, 1969.

73. WOLFSHTEIN M (1968)

"Numerical Smearing in One-Sided Difference Approximation to the Equations of Non-Viscous Flow". Imperial College, London, Mechanical Engineering Department, Heat Transfer Section Report No. HTS/68/2, 1968.

APPENDIX A

THE REDUCED PRESSURE METHOD

Body-force changes may be very large in the presence of gravity and when density variations are significant. This often introduces numerical instabilities to the solution algorithm. It is in order to mitigate such effects that the "reduced-pressure" method was derived.

In this method the pressure p is replaced by "a reduced pressure P", defined by:

$$P = p + g \int_0^Z \{\rho - \rho_d^*(Z)\} \, dZ \quad . \quad (1)$$

whereby it is presumed that the gravitational acceleration g operates in the negative-Z direction. The function $\rho_d^*(Z)$ is an arbitrary one, chosen so that the $(\rho - \rho_d^*)$ terms are small. For example, one may choose ρ_d^* as an average value taken over the r-θ planes:

$$\rho_d^* = \frac{\iint \rho_d \, r \, d\theta dr}{\iint r \, d\theta dr} \quad . \quad (2)$$

The momentum equations in the r and θ directions then contain $\frac{\partial P}{\partial r}$ and $\frac{1}{r}\frac{\partial P}{\partial \theta}$ in place of $\frac{\partial p}{\partial r}$ and $\frac{1}{r}\frac{\partial p}{\partial \theta}$; and the Z-direction equation is changed by the substitution

$$\frac{\partial p}{\partial Z} + g = \frac{\partial P}{\partial Z} + g\,(\rho - \rho_d^*) \qquad (3)$$

This change reduces the tendency of temporary errors in the calculated densities to promote numerical instability.

APPENDIX B

DERIVATION OF INDUCED GRAVITATIONAL FORCES

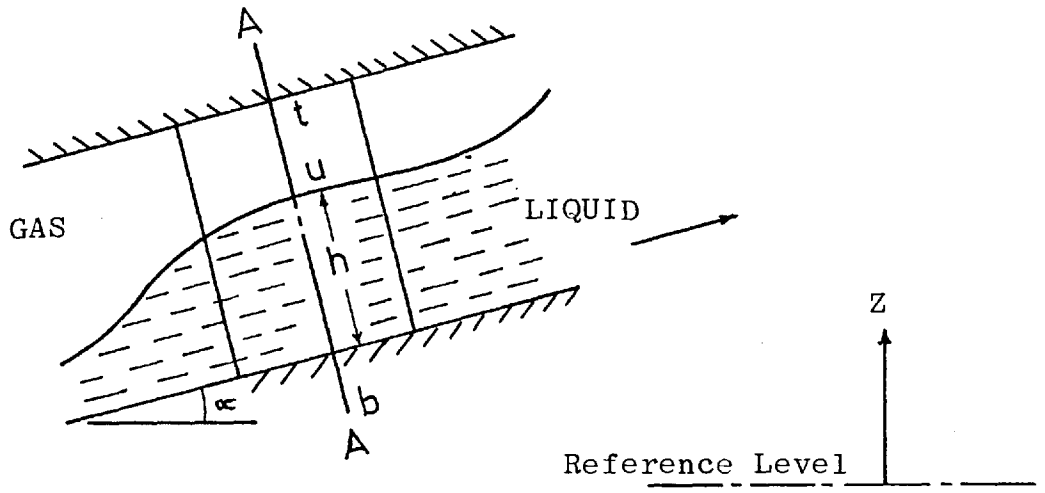


FIGURE (A-1) INCLINED CHANNEL AT AN ANGLE α

In this appendix we derive the gravity terms appearing on the right-hand side of equation (6.2); it will also be shown how, by using the reduced pressure method, these forces can be eliminated from the gas-momentum equation. Consider an inclined channel as depicted in Figure (A-1). It may be noted that the points t and b stand for the top and bottom of the channel at section A-A, while the point u represents the upper liquid surface. The vertical coordinates of these points measured from a reference level, will be referred to by Z_t, Z_b and Z_u.

Now the pressure and gravity force per unit volume acting on the liquid phase can be written as:

$$F_d = - R_d \frac{\partial p_u}{\partial y} - R_d \rho_d g \frac{\partial Z_u}{\partial y} \quad . \quad (1)$$

Similarly, the total pressure and gravity force on the gas is:

$$F_\ell = - R_\ell \frac{\partial p_t}{\partial y} - R_\ell \rho_\ell g \frac{\partial Z_t}{\partial y} \quad . \quad (2)$$

Define the reduced pressure as:

$$P = p_t + \rho_\ell g Z_t \quad . \quad (3)$$

According to the new definition of pressure, equation (2) reads:

$$F_\ell = - R_\ell \frac{\partial P}{\partial y} \quad . \quad (4)$$

The pressure at the top of the gas, p_t, and the pressure at the top of the liquid, p_u, are related hydrostatically, by:

$$p_u = p_t + g \rho_\ell (Z_t - Z_u) \quad . \quad (5)$$

The liquid equation (1) written in terms of p_t rather than p_u is:

$$F_d = - R_d \frac{\partial p_t}{\partial y} - R_d \rho_d g \frac{\partial}{\partial y} (Z_t - Z_u)$$

$$- R_s \rho_d g \frac{\partial Z_u}{\partial y} \quad , \quad (6)$$

which can be rewritten as:

$$F_d = - R_d \frac{\partial}{\partial y} (p_t + g \rho_\ell Z_t) - R_d(\rho_d - \rho_\ell) g \frac{\partial Z_u}{\partial y} \quad . \quad (7)$$

Using the definition of the reduced pressure (equation (3)) one obtains:

$$F_d = - R_d \frac{\partial P}{\partial y} - R_d (\rho_d - \rho_\ell) g \frac{\partial Z_u}{\partial y} \quad . \quad (8)$$

Further substitutions of $Z_u = Z_b + h \cos \alpha$, and $\frac{\partial Z_b}{\partial y} = \sin \alpha$ in equation (3) yields:

$$F_d = - R_d \frac{\partial P}{\partial y} - R_d (\rho_d - \rho_\ell) g \cos \alpha \frac{\partial h}{\partial y}$$

$$- R_d (\rho_d - \rho_\ell) g \sin \alpha \quad , \quad (9)$$

which represents the gravity effects caused by the interfacial and pipe line inclinations.